



VCU

Virginia Commonwealth University
VCU Scholars Compass

Theses and Dissertations

Graduate School

2013

Analyzing the functions of human polynucleotide phosphorylase (hPNPaseold-35)

Upneet K. Sokhi
Virginia Commonwealth University

Follow this and additional works at: <https://scholarscompass.vcu.edu/etd>



Part of the [Medical Genetics Commons](#)

© The Author

Downloaded from

<https://scholarscompass.vcu.edu/etd/568>

This Dissertation is brought to you for free and open access by the Graduate School at VCU Scholars Compass. It has been accepted for inclusion in Theses and Dissertations by an authorized administrator of VCU Scholars Compass. For more information, please contact libcompass@vcu.edu.

© Upneet Kaur Sokhi 2013

All Rights Reserved

ANALYZING THE FUNCTIONS OF HUMAN POLYNUCLEOTIDE PHOSPHORYLASE

(*hPNPase*^{old-35})

A dissertation submitted in partial fulfillment of the requirements for the degree of
Doctor of Philosophy at Virginia Commonwealth University.

by

UPNEET KAUR SOKHI

Master of Science, Bangalore University, Bengaluru, Karnataka, India, 2006

Advisor: Paul B. Fisher, M.Ph., Ph.D.
Professor and Chair
Department of Human and Molecular Genetics

Virginia Commonwealth University
Richmond, Virginia
October 2013

Acknowledgements

I would like to dedicate this work to my grandparents and parents. Only their belief in me and the value of education they instilled in me from a young age has brought me closer to achieving this major milestone in life and I am forever indebted to them for this. I would also like to thank my two sisters, brother and my husband Siddharth for always being there to support and encourage me throughout. I am blessed to have all of them in my life.

I would like to extend my sincere gratitude to my advisor, Dr. Paul B. Fisher for his excellent mentorship, incessant positivity and encouragement throughout my journey as a graduate student in his laboratory. I am also grateful to him for giving me the gift of independence, which allowed me to grow immensely as a researcher. I will always treasure everything I have learnt from a very accomplished advisor and feel fortunate that I was able to find a place for myself in his laboratory five and a half years ago.

I would also like to take this opportunity to thank the members of my graduate committee: Drs. Devanand Sarkar, Jolene J. Windle, Kristoffer Valerie, Michael S. Grotewiel and Paul Dent for their insightful comments and advice which were very helpful in shaping this work.

I would also like to thank Dr. Michael F. Miles for teaching me everything there is to know about analyzing microarray data for which I am very grateful. I would also like to thank Dr. Catherine I. Dumur for performing the microarray analyses presented in this work. I would like to thank Dr. Robert DeSalle for spearheading the PNPase evolution study of which I could be a part of and contribute to; Chapter 5 would not have materialized without him. I would also like to thank Dr. Rita Shiang for her helpful

critiques and suggestions. I would also like to thank all the members of the Fisher and Sarkar labs for always extending help and support when needed. Lastly, I would like to thank Dr. Gail E. Christie for giving me the opportunity to be a part of VCU by admitting me to the amazing MBG program!

Statement of Contributions

Dr. Robert DeSalle performed all the phylogenetic and bioinformatics analysis in Chapter 4, including the determination of all the dN/dS ratios and identification of the positively selected sites. He also provided the write-up for the materials and methods section and part of the results.

Dr. Michael F. Miles generated the heat maps in Figure 3.6 and also identified the myc correlating genes detailed in the results section of the section 3.4.5.

Dr. Catherine I. Dumur prepared the mRNA and probes and performed all the microarray experiments.

Dr. Manny D. Bacolod identified the TCGA correlations of the *hPNPase*^{old-35} induced genes and generated the heat map in Figure 3.17.

Table of Contents:

	Page
Acknowledgements.....	ii
Statement of contributions.....	iv
List of tables.....	x
List of figures.....	xi
Abbreviations.....	xvi
Abstract.....	xviii
Chapter	
1 Introduction.....	1
1.1 RNA degradation pathways.....	1
1.2 Exoribonucleases.....	3
1.3 PNPase.....	4
1.3.1 PNPase structure.....	5
1.3.2 PNPase, degradosome, exosome.....	8
1.4 Identification and regulation of <i>hPNPase^{old-35}</i> expression.....	9
1.5 Subcellular Localization of <i>hPNPase^{old-35}</i>	12
1.6 Functions of <i>hPNPase^{old-35}</i>	13
1.6.1 <i>hPNPase^{old-35}</i> , growth inhibition, senescence and RNA degradation.....	13
1.6.2 Molecular mechanisms of growth inhibition and senescence.....	15
1.6.3 RNA degradation by <i>hPNPase^{old-35}</i>	17
1.6.4 miRNA regulation by <i>hPNPase^{old-35}</i>	17

1.6.5 <i>hPNPase</i> ^{old-35} and inflammation.....	19
1.7 Functions of <i>hPNPase</i> ^{old-35} in mitochondria.....	21
1.7.1 <i>hPNPase</i> ^{old-35} and mitochondrial homeostasis.....	21
1.7.2 <i>hPNPase</i> and RNA import into mitochondria	22
1.7.3 Role of <i>hPNPase</i> in mtRNA processing.....	22
2 Gene Expression Signature of Human Polynucleotide Phosphorylase	
(<i>hPNPase</i>^{old-35}) in Melanoma.....	25
2.1 Abstract	25
2.2 Introduction.....	26
2.3 Materials and Methods	30
2.3.1 Cell culture.....	30
2.3.2 Expression constructs, stable cell lines and viral infections.....	30
2.3.3 RNA extraction, quality assessment and Microarray analyses.....	32
2.3.4 Statistical Analysis, IPA and functional classification of genes.....	33
2.3.5 cDNA synthesis and quantitative real-time RT-PCR (qRT-PCR).....	34
2.3.6 Protein isolation and Western blot analysis	35
2.3.7 Invasion Assay.....	36
2.3.8 Immunohistochemistry	36
2.4 Results	38
2.4.1 Melanoma cell culture model for studying <i>hPNPase</i> ^{old-35} regulated gene expression	38
2.4.2 Genetic profile of <i>hPNPase</i> ^{old-35} -knockdown melanoma cells.....	40
2.4.3 Gene expression profile of Ad. <i>hPNPase</i> ^{old-35} -infected melanoma	

cells	48
2.4.4 Identification of genes regulated by <i>hPNPase</i> ^{old-35}	53
2.4.5 <i>hPNPase</i> ^{old-35} stable knockdown in melanoma cells and invasion	66
2.5 Discussion	71
3 Analysis of global changes in gene expression induced by human	
polynucleotide phosphorylase (<i>hPNPase</i>^{old-35})	77
3.1 Abstract	77
3.2 Introduction	78
3.3 Materials and Methods	80
3.3.1 Establishing a conditional <i>hPNPase</i> ^{old-35} over-expressing	
cell line	80
3.3.2 MTT and colony formation assays	80
3.3.3 Total RNA isolation for microarray analyses	80
3.3.4 Gene Expression Microarrays	81
3.3.5 Statistical Analyses	81
3.3.6 Enrichment analysis	82
3.3.7 Analysis of TCGA Genome-wide Expression Datasets	83
3.3.8 cDNA synthesis and quantitative real-time RT-PCR (qRT-PCR)	84
3.3.9 Protein isolation and Western blot analysis	85
3.4 Results	86
3.4.1 Establishing a doxycycline-inducible <i>hPNPase</i> ^{old-35old-35} over-	
expression system	86
3.4.2 Identification of <i>hPNPase</i> ^{old-35} responsive genes	90

3.4.3	Functional categorization of <i>hPNPase</i> ^{old-35} responsive genes	93
3.4.4	TCGA correlations of <i>hPNPase</i> ^{old-35} responsive genes	104
3.4.5	Identification of Myc-correlating genes	107
3.4.6	<i>hPNPase</i> ^{old-35} overexpression in HO-1 and HeLa cells causes global changes in cell cycle-associated genes	111
3.5	Discussion	116
4	Analysis of sequence specificity for degradation by <i>hPNPase</i>^{old-35}	120
4.1	Abstract	120
4.2	Introduction	121
4.3	Materials and methods	121
4.3.1	Construction of c-myc 3'UTR deletion mutants	121
4.3.2	Colony Formation Assays	122
4.4	Results and Discussion	123
5	Evolutionary dynamics of Polynucleotide phosphorylases	127
5.1	Abstract	127
5.2	Introduction	128
5.3	Materials and Methods	132
5.3.1	Sequences and Matrix construction	132
5.3.2	Phylogenetic analysis	133
5.3.3	Detecting the Statistical imprint of skewed dN/dS ratios	133
5.3.4	Mapping Sites with dN/dS Skew Onto Secondary and Tertiary Protein Structure	134
5.4	Results	135

5.4.1 Phylogenetic relationships of PNP domains	135
5.4.2 Branch Specific Skew in dN/dS ratios.....	136
5.4.3 General Site-specific Skew in dN/dS ratios in PNP domains.....	138
5.4.4 Correlating skewed dN/dS with structural variants.....	142
5.5 Discussion	150
6 General Discussion.....	157
References	165
Vita.....	181

List of tables

	Page
Table 2.1: List of genes which are significantly altered as a result of <i>hPNPase</i> ^{old-35} stable knockdown, and are associated with cholesterol biosynthesis, according to IPA Toxicogenomic Analysis.....	44
Table 2.2: List of genes which are significantly altered as a result of <i>hPNPase</i> ^{old-35} stable knockdown, and are associated with mitochondrial dysfunction, according to IPA Toxicogenomic Analysis.....	44
Table 2.3: List of genes which are significantly altered as a result of <i>hPNPase</i> ^{old-35} overexpression, and are functionally associated with the maintenance of mitochondrial transmembrane potential, according to IPA Toxicogenomic Analysis	49
Table 2.4: List of genes which are significantly altered as a result of <i>hPNPase</i> ^{old-35} overexpression, and are associated with G2/M DNA damage checkpoint regulation, according to IPA Toxicogenomic Analysis.....	52
Table 2.5: Functional and structural categories of genes associated with <i>hPNPase</i> ^{old-35} -driven regulation	54
Table 3.1: Functional annotation of genes differentially regulated in response to <i>hPNPase</i> ^{old-35} overexpression	113
Table 5.1: Taxa used in the study. This file also contains the nucleic acid and amino acid Genbank accession numbers of sequences that were used in this study.....	131
Table 5.2: PNP domains comparison of significant dN/dS with mutagenized sites.....	146
Table 5.3: RPH Comparison of significant dN/dS with mutagenized sites.....	148
Table 5.4: KH domain comparison of significant dN/dS with mutagenized sites.....	150

List of figures

	Page
Figure 1.1: RNA decay mechanisms	3
Figure 1.2: Identification of human PNPase	5
Figure 1.3: Domain organization of PNPases from different species.....	6
Figure 1.4: Regulation of <i>hPNPase</i> ^{old-35} expression by IFN-β.....	11
Figure 1.5: Adenoviral-mediated <i>hPNPase</i> ^{old-35} overexpression causes inhibition of cellular proliferation of HO-1 cells	14
Figure 1.6: Functions of <i>hPNPase</i> ^{old-35}	24
Figure 2.1: Stable knockdown of <i>hPNPase</i> ^{old-35} using lentivirus and transient overexpression using adenovirus in HO-1 human melanoma cells.....	39
Figure 2.2: Venn diagrams representing number of genes significantly altered when <i>hPNPase</i> ^{old-35} is knocked down or overexpressed in human melanoma cells	40
Figure 2.3: Biological functions associated with genes dysregulated after <i>hPNPase</i> ^{old-35} knockdown in melanoma cells.....	41
Figure 2.4: Toxicologically related functionalities associated with genes dysregulated after <i>hPNPase</i> ^{old-35} knockdown in melanoma cells.....	42
Figure 2.5: Canonical pathways associated with genes differentially expressed when <i>hPNPase</i> ^{old-35} is knocked down in human melanoma cells	43
Figure 2.6: qRT-PCR verification of genes associated with cholesterol biosynthesis and mitochondrial dysfunction in <i>hPNPase</i> ^{old-35} silenced HO-1 cells.....	47
Figure 2.7: Biological functions associated with genes dysregulated after <i>hPNPase</i> ^{old-35} overexpression in melanoma cells.....	49
Figure 2.8: Canonical pathways associated with genes differentially expressed when <i>hPNPase</i> ^{old-35} is overexpressed in human melanoma cells.....	50
Figure 2.9: Toxicologically related functionalities associated with genes dysregulated after <i>hPNPase</i> ^{old-35} overexpression in melanoma cells	51
Figure 2.10: Network visualization of genes potentially “ <i>directly</i> ” regulated by <i>hPNPase</i> ^{old-35}	56

Figure 2.11: Network visualization of genes potentially “ <i>indirectly</i> ” regulated by <i>hPNPase</i> ^{old-35}	57
Figure 2.12: qRT-PCR verification of <i>hPNPase</i> ^{old-35} -putative “ <i>directly</i> ” regulated genes identified by microarray analyses in HO-1 melanoma cells	59
Figure 2.13: qRT-PCR verification of <i>hPNPase</i> ^{old-35} -putative “ <i>indirectly</i> ” regulated genes identified by microarray analyses in HO-1 melanoma cells	60
Figure 2.14: qRT-PCR verification of <i>hPNPase</i> ^{old-35} -putative regulated genes after <i>hPNPase</i> ^{old-35} transient silencing post 48 h	61
Figure 2.15: Stable knockdown of <i>hPNPase</i> ^{old-35} using lentivirus and transient overexpression using adenovirus in WM35 human melanoma cells	62
Figure 2.16: qRT-PCR verification of <i>hPNPase</i> ^{old-35} -putative “ <i>directly</i> ” regulated genes identified by microarray analyses in WM35 melanoma cells	63
Figure 2.17: qRT-PCR verification of <i>hPNPase</i> ^{old-35} -putative “ <i>indirectly</i> ” regulated genes identified by microarray analyses in WM35 melanoma cells	64
Fig. 2.18: qRT-PCR expression of <i>hPNPase</i> ^{old-35} following transient transfection with siRNA against <i>hPNPase</i> ^{old-35} normalized to scrambled control post 48 h in C8161 (A) and MeWo (B) melanoma cells	65
Fig. 2.19. <i>hPNPase</i> ^{old-35} knockdown and invasion of HO-1 melanoma cells	69
Fig. 2.20. qRT-PCR validation of <i>hPNPase</i> ^{old-35} and <i>EMR1</i> levels in WM35 melanoma cells following stable <i>hPNPase</i> ^{old-35} knockdown	70
Fig. 2.21. Representative images of immunohistochemistry analysis of multiple malignant melanoma tissue arrays	70
Figure 3.1: Western blots showing <i>hPNPase</i> ^{old-35} overexpression in doxycycline-inducible stable HeLa cells in a time and dose-dependent manner	87
Fig. 3.2: MTT cell viability assays. <i>hPNPase</i> ^{old-35} overexpression in doxycycline-inducible stable HeLa clones (A-D) shows a reduction in cellular growth over a period of 5 days as determined by MTT assay	88
Fig. 3.3: Colony formation assays. <i>hPNPase</i> ^{old-35} overexpression in doxycycline-inducible stable HeLa clones (A-D) shows a reduction in cellular growth as observed by reduced number of stained colonies	89
Fig. 3.4: Colony formation and MTT assays to determine cell viability of control HeLa and HeLa-RFP cells	90

Figure 3.5: Unsupervised hierarchical cluster analysis	91
Figure 3.6: Comparison of <i>hPNPase</i> ^{old-35} -induced changes in gene expression in HO-1 and HeLa cells	92
Figure 3.7: Gene Ontology (GO) terms for PNPase responsive genes corresponding to Biological process	93
Figure 3.8: Gene Ontology (GO) terms for PNPase responsive genes corresponding to Molecular functions	94
Figure 3.9: Gene Ontology (GO) terms for PNPase responsive genes corresponding to PANTHER Protein class identified by PANTHER classification system (http://www.pantherdb.org/)	95
Figure 3.10: Functional annotation of genes significantly regulated by <i>hPNPase</i> ^{old-35} represented as enrichment clusters generated by the DAVID analysis software. Cluster of 18 genes which were grouped together based on their involvement in chromosomal organization and related functions	96
Figure 3.11: Functional annotation of genes significantly regulated by <i>hPNPase</i> ^{old-35} represented as enrichment clusters generated by the DAVID analysis software. Cluster of 32 signaling molecules and cellular receptors	97
Figure 3.12: Functional annotation of genes significantly regulated by <i>hPNPase</i> ^{old-35} represented as enrichment clusters generated by the DAVID analysis software. Cluster of 15 genes grouped together based on their link to cell cycle-associated functions	98
Figure 3.13: Pathway analysis of <i>hPNPase</i> ^{old-35} responsive genes. Network associated with mitosis and involves 14 of our reported <i>hPNPase</i> ^{old-35} responsive genes	99
Figure 3.14: Pathway analysis of <i>hPNPase</i> ^{old-35} responsive genes. Network is associated with p21 signaling and involves 11 of our reported <i>hPNPase</i> ^{old-35} responsive genes	100
Figure 3.15: Real-time PCR validation of genes identified by microarray analysis	102
Figure 3.16: Real-time PCR validation of genes identified by microarray analysis following <i>hPNPase</i> ^{old-35} overexpression	103
Figure 3.17: Heat maps representing correlations of <i>hPNPase</i> ^{old-35} responsive genes with <i>hPNPase</i> ^{old-35} in different tumor types identified using TCGA datasets	106

Figure 3.18: Cluster analysis of functional enrichments for c-Myc correlating genes. Cluster of 13 genes involved in apoptosis	108
Figure 3.19: Cluster analysis of functional enrichments for c-Myc correlating genes. Cluster of 16 genes involved in cytoskeleton associated functions	109
Figure 3.20: Cluster analysis of functional enrichments for c-Myc correlating genes. Cluster of 13 genes involved in DNA repair	110
Figure 3.21: Cluster analysis of functional enrichments for c-Myc correlating genes. Cluster of 10 genes involved in mRNA processing.....	111
Figure 3.22: Genes differentially regulated in response to <i>hPNPase</i> ^{old-35} over- expression as identified by microarray analysis in HO-1 and HeLa cells.....	112
Figure 3.23: Biological functions identified by IPA corresponding to genes differentially regulated in response to <i>hPNPase</i> ^{old-35} overexpression	114
Figure 3.24: Canonical pathways identified by IPA corresponding to genes differentially regulated in response to <i>hPNPase</i> ^{old-35} overexpression.....	115
Fig. 4.1. Schematic representation of <i>c-myc</i> 3'UTR deletion constructs.....	122
Fig. 4.2. Schematic representation of the cloning strategy used for the generation of the <i>c-myc</i> 3'UTR deletion constructs	123
Fig. 4.3. Growth rescue experiment	125
Fig. 4.4. Graphical representation of colony numbers as described in Fig. 4.3	126
Figure 5.1: Schematic diagrams of PNPase (old-35) and RPH showing the various domains in these proteins.....	129
Figure 5.2: Bayesian phylogenetic tree showing the relationship of the three major domains (PNP1, PNP2 and RPH) examined in this study.....	136
Figure 5.3: Tree of animal life using plants as an outgroup showing which branches on the tree have experienced positive dN/dS skew	138
Figure 5.4: Site-specific positive dN/dS skew in the three PNP domains (PNP1, PNP2 and RPH) and the KH and S1 domain	139
Figure 5.5: Secondary structure plot indicating sites under positive selection in PNP1, PNP2 and KH/S1 (sites highlighted as green circles).....	141
Figure 5.6: Secondary structure plot indicating sites under positive selection in RNase PH (sites highlighted as green circles)	142

Figure 5.7: 3-D visualization of positively selected sites in PNP1, PNP2 and KH/S1 using the CN3D software.....	143
Figure 5.8: 3-D visualization of positively selected sites in RNasePH using the CN3D software.....	144
Figure 6.1: Flow chart depicting overall aim of project: to identify degradation targets of <i>hPNPase</i> ^{old-35}	159

Abbreviations

ADARB1	Adenosine deaminase, RNA-specific, B1
BREL	Branch-site Random Effects Likelihood
CENPA	Centromere protein A
CENPE	Centromere protein E
Cn3D	“see in 3D”
DAVID	Database for Annotation, Visualization and Integrated Discovery
dN/dS	ratio of nonsynonymous to synonymous change over time
DUSP1	Dual specificity phosphatase 1
EMR1	Egf-like module containing, mucin-like, hormone receptor-like 1
EMR2	Egf-like module containing, mucin-like, hormone receptor-like 2
ETC	Electron Transport Chain
FDR	False Discovery Rate
GLS	Glutaminase
GO	Gene Ontology
HMGCR	3-hydroxy-3-methylglutaryl-CoA reductase
HyPhy	Hypothesis testing using phylogenies
IGFBP3	Insulin-like growth factor binding protein 3
IMS	Inter membrane space
IPA	Ingenuity Pathway Analysis
LACTB2	Lactamase, beta 2
MCAM	Melanoma Cell Adhesion Molecule

MEME	Mixed Effects Model of Evolution
MKI67	Antigen identified by monoclonal antibody Ki-67
ML	Maximum Likelihood
MMDB	Molecular Modeling Database
MP	Maximum Parsimony
PANTHER	Protein ANalysis Through Evolutionary Relationships
PNPase/PNPT1	Polynucleotide phosphorylase
qRT-PCR	Quantitative Real Time Polymerase Chain Reaction
RCSB	Research Collaboratory for Structural Bioinformatics
RPH	Ribonuclease PH
ROS	Reactive Oxygen Species
RNF128	Ring finger protein 128
SYNCRIP	Synaptotagmin binding, cytoplasmic RNA interacting protein
TCGA	The Cancer Genome Atlas
UCP2	Uncoupling protein 2
VGF	VGF nerve growth factor inducible

Abstract

ANALYZING THE FUNCTIONS OF HUMAN POLYNUCLEOTIDE PHOSPHORYLASE

(*hPNPase*^{old-35})

By Upneet Kaur Sokhi, M.Sc.

A dissertation submitted in partial fulfillment of the requirements for the degree of
Doctor of Philosophy at Virginia Commonwealth University.

Virginia Commonwealth University, 2013

Major Advisor: Dr. Paul B. Fisher, M.Ph., Ph.D.
Professor and Chair, Department of Human and Molecular Genetics

RNA degradation plays a fundamental role in maintaining cellular homeostasis, along with being a part of normal regulatory mechanisms, whether it occurs as a surveillance mechanism eliminating aberrant mRNAs or during RNA processing to generate mature transcripts. 3'-5' exoribonucleases are essential mediators of RNA decay pathways, and one such evolutionarily conserved enzyme is polynucleotide phosphorylase (PNPase). The human homologue of this fascinating enzymatic protein (*hPNPase*^{old-35}) was cloned a decade ago in the context of terminal differentiation and senescence through a novel 'overlapping pathway screening' approach. Since then, significant insights have been garnered about this exoribonuclease and its repertoire of

expanding functions. *hPNPase*^{old-35} has progressed a long way from being just a 3'-5' exoribonuclease to a functionally relevant molecule implicated in a multitude of diverse and important biological effects. *hPNPase*^{old-35} plays central roles in diverse physiological processes including growth inhibition, senescence, mtRNA import, mitochondrial homeostasis, and RNA degradation, all while primarily being localized in the mitochondrial IMS (inter membrane space). *hPNPase*^{old-35} also holds immense promise as a therapeutic agent due to its ability to degrade specific miRNA (miR-221) and mRNA (c-myc) species, and this property can be exploited in treating malignancies that are characterized by upregulation of harmful miRNA or mRNA molecules. But apart from these two targets, little is known about any other targets *hPNPase*^{old-35} may degrade. Thus, the primary objective of this dissertation research was to identify targets other than c-myc or miR-221 that *hPNPase*^{old-35} could directly degrade to discover newer and biologically relevant therapeutic targets for the treatment of *hPNPase*^{old-35} – associated disease states. In order to do this we performed extensive microarray analyses following *hPNPase*^{old-35} overexpression and depletion in mammalian cell lines, and were able to identify transcripts that could be potentially regulated by *hPNPase*^{old-35} directly or indirectly. Apart from this we also analyzed the 3'UTR of c-myc in order to identify any specific sequence or secondary structural elements necessary for *hPNPase*^{old-35} mediated degradation. Lastly, we identified certain residues in *hPNPase*^{old-35} that have been under positive natural selection through evolution.

CHAPTER ONE

INTRODUCTION

Part of the work presented in this chapter has been published in *Advances in Cancer Research* 119:161-90 (2013).

1.1 RNA degradation pathways

Post-transcriptional control of gene expression occurs at multiple steps that include mRNA processing, its export from the nucleus to cytoplasm, mRNA localization, mRNA stability, translational regulation and finally mRNA decay [1]. A number of evolutionarily conserved trans-acting regulatory factors have been identified over the past years that are involved in each of these steps [2,3]. Previously, RNA degradation was thought to be a random process, but studies over the past few years have proved quite the contrary. It is a well-controlled process involving the interplay of a number of proteins working together and contributing to the maintenance of cellular homeostasis [4]. Two major pathways have been identified for eukaryotic mRNA turnover, deadenylation-dependent decay and deadenylation-independent decay [5-7]. Deadenylation-dependent decay is usually triggered by the presence of certain cis-elements in the mRNA sequence such as AU-rich elements in the 3'UTR and instability elements in the coding region [8,9]. The first step in this process is the shortening of the

poly(A) tail or deadenylation, which is brought about by certain deadenylases like the Ccr4/Pop2/NOT complex, Pan2/Pan3 or PARN [poly(A) ribonuclease]. Following this process, the mRNA can undergo 3'-5' decay by the exosome, which is a complex of 3'-5' exoribonucleases or PNPase (a phosphorolytic 3'-5' exoribonuclease), with the residual cap structure being hydrolysed by the scavenger enzyme DcpS or 5'-3' exonucleolytic digestion by an exonuclease Xrn1p after decapping by the Dcp1/Dcp2 enzyme complex [8,10]. Deadenylation-independent decay, mostly consisting of RNA surveillance mechanisms, may occur when there is a premature stop codon in the mRNA sequence (Nonsense-mediated decay or NMD) in which case 5'-3' digestion occurs after removal of the cap structure by the same enzymes discussed earlier [7,11]. In the event of an absence of a termination codon (Nonstop decay or NSD), the aberrant mRNA is recognized and degraded in a 3'-5' manner by the exosome. When there is a stall in translation elongation (No-go decay or NGD), cleavage occurs at the stall site by an endonuclease (IME1, PMR1 or RNase MRP) after which the fragments are digested by the 3' and 5' exoribonucleases [11]. These processes are summarized in Fig. 1.1.

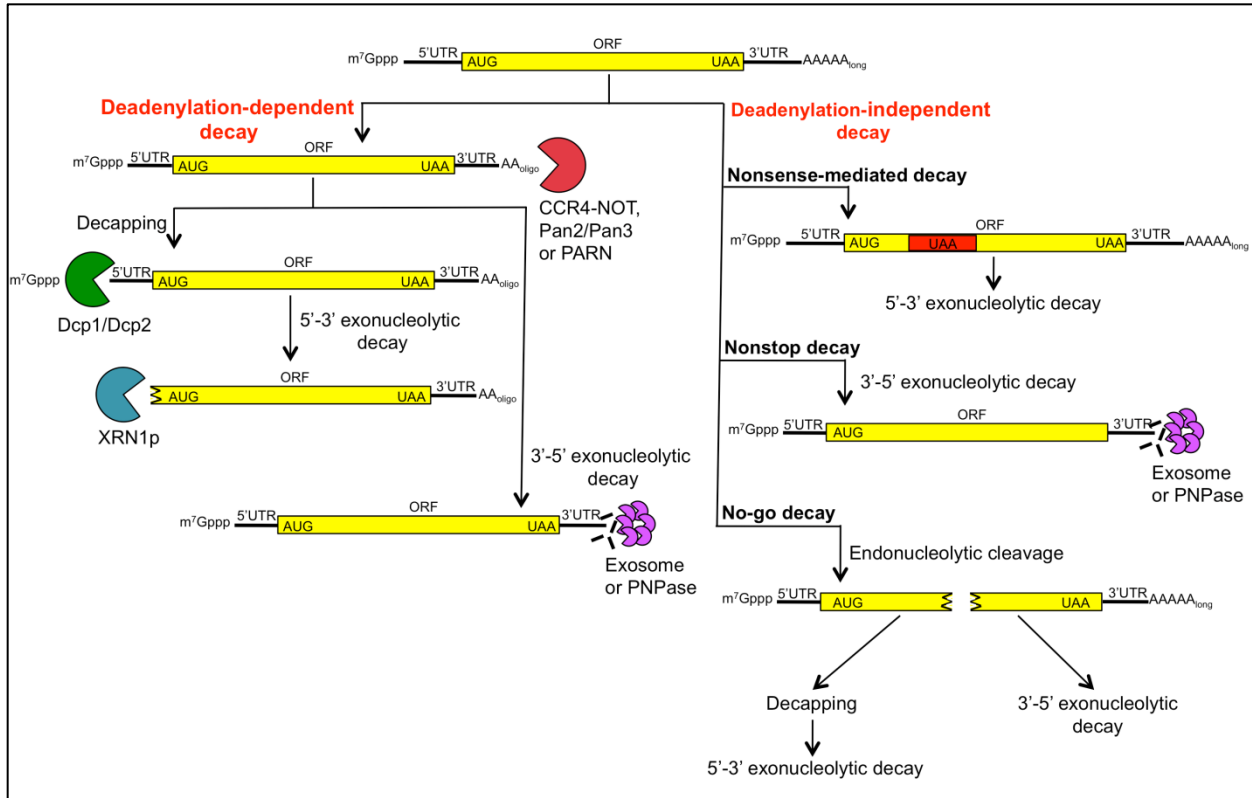


Fig. 1.1. RNA decay mechanisms. A diagrammatic representation of various RNA degradation pathways. Refer to text for details.

1.2 Exoribonucleases

Ribonucleases (RNases) are the main players involved in RNA metabolism, performing important roles in RNA maturation, RNA end-turnover and in the degradation of aberrant RNAs or species no longer required by the cell [12]. Based on their degradative properties, they are classified into exo- and endo-ribonucleases, with exoribonucleases being further classified into 5'-3' and 3'-5' exoribonucleases depending on the direction of degradation [13]. Eukaryotes possess both these classes of enzymes whereas prokaryotes like *E. coli* lack the 5'-3' exoribonuclease activity. Extensive sequence homology studies have culminated in the various exoribonucleases in all kingdoms to be grouped into the following superfamilies (with representative

examples from *E.coli* and some of their eukaryotic homologues): the RBN (RNase BN) family present only in eubacteria, the RNR (RNase II, RNase R, Rrp44, Dss I, Ssd I), DEDD (RNase D, RNase T, oligoribonuclease, Rrp6, Pan2, Rex1-4), and PDX (Rnase PH, PNPase, Rrp41-43, 45, 46, Mtr3) families present in bacteria, archaea and eukaryotes, the RRP4 (Rrp4, 40, Csl4) family present in archaea and eukaryotes and lastly the 5PX (Xrn1, Rat1) family present only in eukaryotes [14,15]. RNA degradation by most exoribonucleases occurs via hydrolytic cleavage of the 3' phosphodiester bond to generate nucleotide monophosphates, but certain members like PNPase and RNase PH do so through a phosphorolytic mechanism that utilizes inorganic phosphate to generate nucleotide diphosphates [4].

1.3 PNPase

Polynucleotide phosphorylase (PNPase) is an evolutionarily conserved phosphorolytic 3'-5' processive exoribonuclease that is present in all phyla extending from bacteria, plants, worms and flies, to mice and humans, although it is absent in fungi, trypanosomes and Archaea [13]. Studies in *E.coli* have shown that in the presence of high inorganic phosphate (Pi), this enzyme acts exclusively as an exoribonuclease, whereas in the event of low Pi, it acts as a polymerase resulting in the elongation of the poly(A) tail by adding nucleotides and generating Pi. PNPase was discovered by Severo Ochoa and Marianne Grunberg-Manago in 1955 and Ochoa received the Nobel Prize in 1959 for discovering its polymerizing activity [4,16]. The human homologue of PNPase (*hPNPase*^{old-35}) was first identified as a gene that was upregulated in terminally differentiated human melanoma cells and senescent progeroid

fibroblasts in an ‘overlapping pathway screen’ to identify differentially regulated genes in the context of terminal differentiation and senescence (Fig. 1.2) [17].

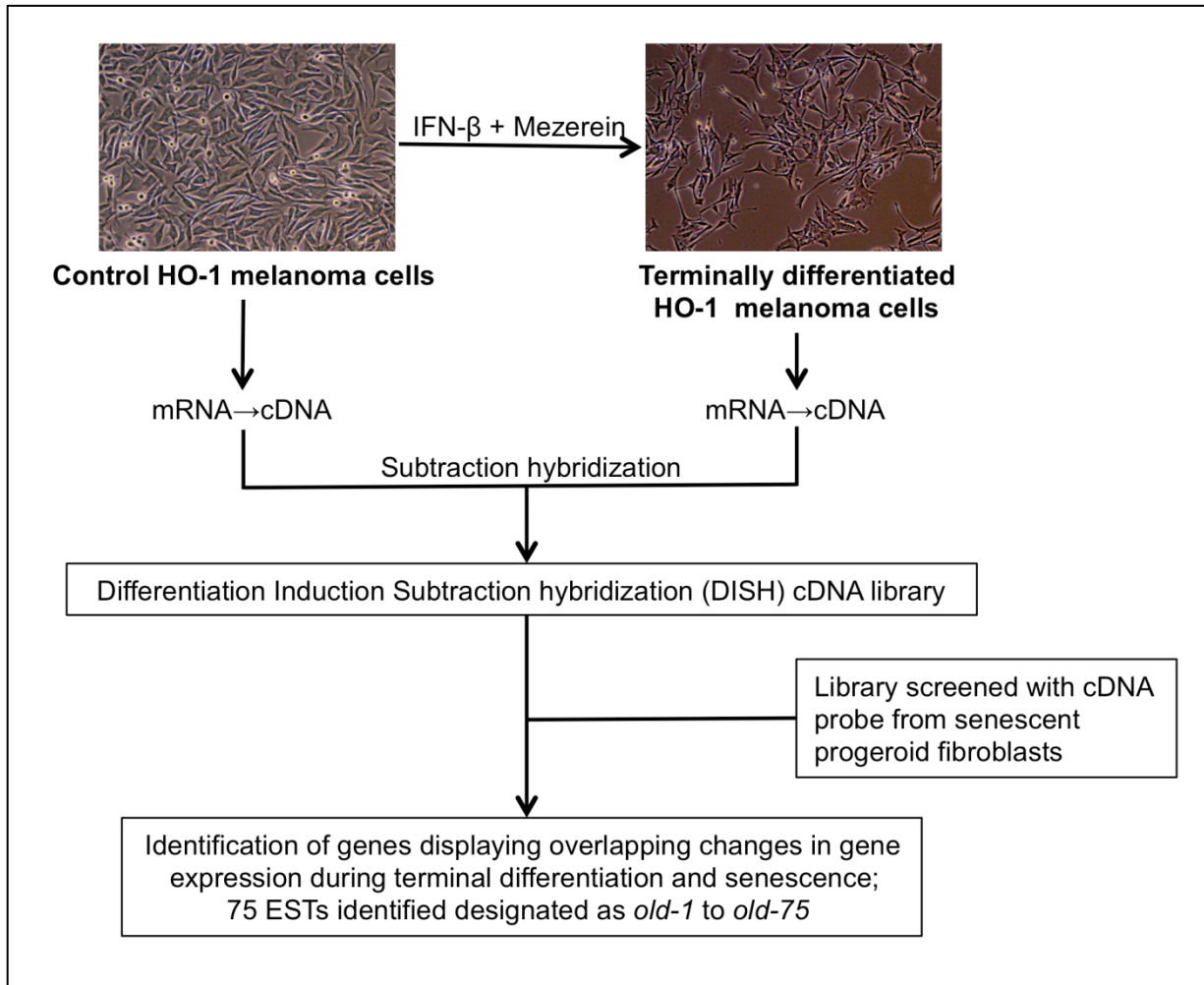


Fig. 1.2. Identification of human PNPase. Schematic representation of the overlapping pathway screen that aided in the identification of transcripts upregulated in the processes of terminal differentiation and senescence.

1.3.1 PNPase structure

PNPase from all diverse species share a classical domain structure that contains a catalytic PDX domain characteristic of all PDX family members [13,18]. Almost all PNPases are composed of five conserved structural motifs; the amino-terminal domain is composed of 2 RNase PH domains, an α -helical domain that separates the RNase

PH domains, and 2 carboxy-terminal RNA-binding domains KH (K-homology) and S1 [13,18-20] (Fig. 1.3).

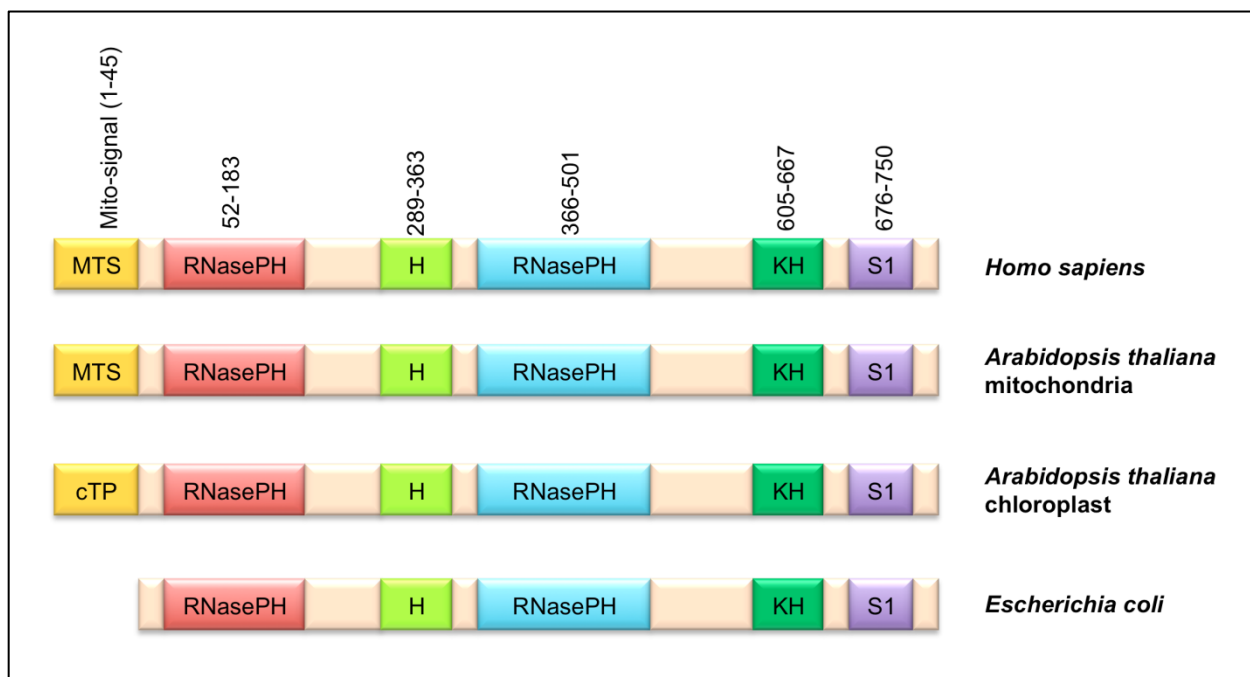


Fig. 1.3. Domain organization of PNPases from different species. PNPases from humans, plants and bacteria showing the presence of two conserved catalytic RNasePH domains and two RNA binding domains KH and S1.

In plants, PNPase is translocated to the chloroplast stroma or mitochondrial matrix by an N-terminal chloroplast-transit peptide (cTP) or a mitochondrial-targeting sequence (MTS), respectively [21]. Human PNPase (*hPNPase*^{old-35}), a 783 amino acid long ~86 kDa protein, also contains an N-terminal MTS that allows its primary location in the cell to be the mitochondria, where it assembles into a homotrimer or a dimer of two homotrimers [22,23]. PNPase from the bacterium *Streptomyces antibioticus* was the first to be crystallized; it was observed that it forms a homotrimeric doughnut shaped structure with a central channel formed by the 6 RNase PH domains containing the catalytic sites and through which a single-stranded RNA molecule can enter [20,24]. Extensive deletion and mutation studies have been done in the past decade to

understand the structural specificities of the phosphorolytic and RNA-binding properties of PNPase. The catalytic activity of the bacterial PNPase resides mainly in the second RNase PH domain, which also seems to possess RNA binding ability as demonstrated by a G454D mutation, but both domains are required for proper enzymatic activity [25]. In bacteria, deletion of the KH or S1 domain reduces the specific activity of the enzyme by ~19- or ~50-fold, respectively, whereas deleting both domains reduces the enzymatic activity to ~1% [26]. X-ray crystallography studies using *E.coli* full-length and KH/S1 truncated PNPase further elucidated that the KH and S1 domains are important for proper trimer formation apart from RNA binding along with certain conserved residues in the first RNase PH domain that are important for proper RNA binding and processive degradation [27]. In case of plants, chloroplast PNPase exists as a homo-multimer [28] and both its RNase PH domains possess phosphorolytic and polymerizing activities [21]. Mutation analysis of human PNPase showed that it possesses similar phosphorolytic properties to its homologues in different species, with both the RNase PH domains possessing equal enzymatic activity, and the presence of either one of them being sufficient for complete enzymatic activity as shown in our studies [29]. However, there are some differences in its RNA-binding affinities compared to other species of PNPases [30]. Also, human PNPase still retains enzymatic activity after deletion of both the KH and S1 domains in contrast to its bacterial homologue, which further strengthens the observation that the RNase PH domains may also play a role in RNA binding after all [29].

More recent advances in understanding the structural evolution of this interesting exoribonuclease come from the successful crystallization of an S1-domain truncated

human PNPase [31]. This study reveals a slight difference between the bacterial and human PNPases, in that the S1 domain was found to be dispensable for RNA binding and the 3 KH domains formed a pore on top of the homotrimer (formed by the 6 RNase PH domains), which in turn is solely responsible for binding RNA through its conserved GXXG motif [31]. Although this is an exciting finding, it stands in contrast to previously published reports as mentioned earlier, that the RNase PH domains also possess RNA binding ability [29]. Future studies crystallizing the full length and maybe a KH domain truncated human PNPase may provide useful insights into the workings of this intriguing protein.

1.3.2 PNPase, degradosome, exosome

Apart from existing as an individual entity in the cytoplasm, PNPase is also found as part of a multiprotein complex associated with endonuclease RNase E, the DEAD-box helicase RhlB and enolase, a glycolytic enzyme in bacteria [32-36]. This structure is called the degradosome and contains approximately 20% of the total PNPase present in the bacterial cell [37]. Yeast contains a similar multiprotein complex consisting of exoribonucleases called the exosome present in the nucleus and the cytoplasm, from which PNPase is absent [38,39]. The yeast exosome is made up of 8 exoribonucleases (Rrp6p, Rrp41-46p and Mtr3p) with some of them sharing homology with bacterial RNase PH and 3 RNA binding subunits (Rrp4p, Rrp40p and Csl4p) [40]. All of the yeast exosome subunits have human homologues, except Rrp43p and Mtr3p [19,41]. There is high structural homology between the eukaryotic exosome and homotrimeric PNPase, both looking like ring-shaped structures with a central catalytic core channel through which the RNA molecule enters for degradation [24], although recent studies have

shown that human PNPase possesses a KH pore versus a S1 pore in exosomes that facilitates RNA-binding [31].

1.4 Identification and regulation of *hPNPase^{old-35}* expression

Human PNPase is encoded by the gene *PNPT1* mapping to chromosome 2p15-2p16.1, consisting of 28 exons and spanning ~60 kb on the reverse strand [42]. It was first identified as a gene that was upregulated in senescent progeroid fibroblasts and terminally differentiated HO-1 human melanoma cells in a quest to recognize molecular mediators controlling cellular senescence and differentiation that would aid in improvement of cancer therapy [17]. Human melanoma is a well-established model for studying differentiation therapy of cancer and terminal differentiation, which can be induced by combined treatment with recombinant human fibroblast interferon (IFN)- β and protein kinase C activator mezerein (MEZ), resulting in similar phenotypic characteristics as cellular senescence. These findings formed the basis for a screening strategy intended to identify overlapping gene expression changes associated with both terminal differentiation and senescence (Fig. 2). cDNA from terminally differentiated HO-1 cells was used to generate a differentiation-induction subtraction hybridization (DISH) library, which was screened with a probe generated from the mRNA of senescent progeroid fibroblasts [17,43]. Of the 75 genes identified through this screening approach designated *old-1* to *old-75*, *old-35* was one of the identified cDNAs that showed an elevated expression associated with both terminal differentiation and senescence [17]. *old-35* exhibited substantial sequence homology to PNPase from other species and was thus identified as human polynucleotide phosphorylase or *hPNPase^{old-35}*. *hPNPase^{old-35}* is expressed in all primary tissues [17] and a *PNPT1*

knockout mouse is embryonic lethal, indicating its importance in early mammalian development [44].

Bacterial PNPase has been shown to autocontrol its own expression at the post-transcriptional level by binding and degrading part of a stem-loop structure in its own mRNA 5'-leader sequence cleaved by RNase III, subsequently resulting in mRNA instability and reduced expression [45]. On the other hand, not much is known about the transcriptional or post-transcriptional regulation of *hPNPase*^{old-35}, except that it is induced by type I interferons (IFN- α and - β) at the transcription level in both normal and cancer cells [42]. Since type I interferons are cytokines secreted by cells in response to viral infections, it could be speculated that *hPNPase*^{old-35} may play a role in the cell's antiviral response through its RNA processing function. Induction of *hPNPase*^{old-35} mRNA, which has a half-life of ~6h [42], was evident even with 1 U/ml of IFN- β and as early as 3 hrs in HO-1 cells (2000 U/ml IFN- β), demonstrating that it is an early IFN response gene [17] (Fig. 1.4).

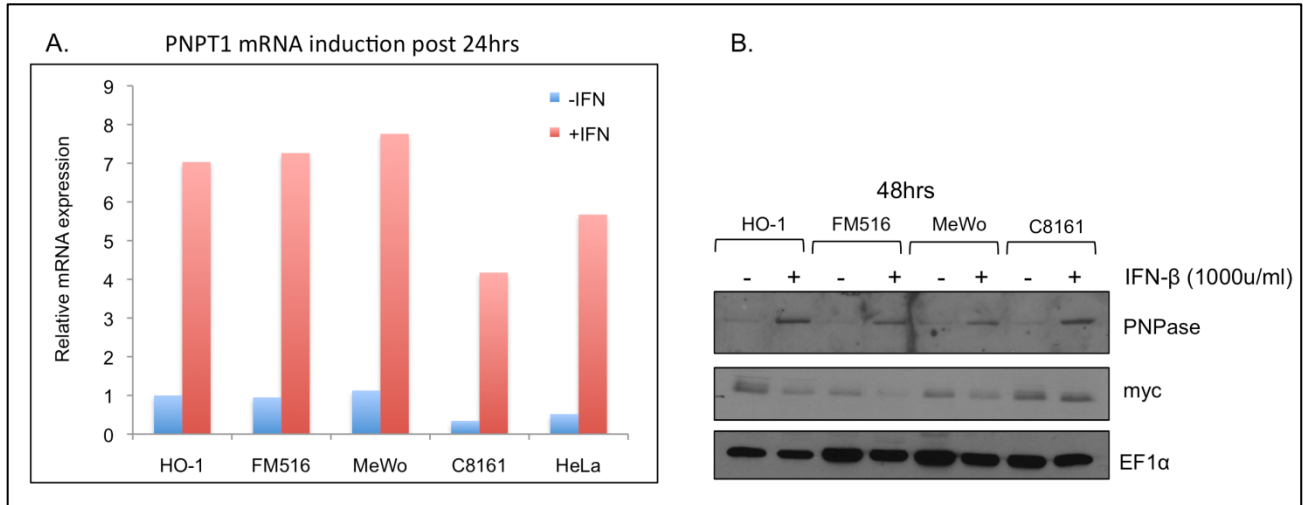


Fig. 1.4. Regulation of *hPNPase^{old-35}* expression by IFN-β. (A) Induction of *hPNPase^{old-35}* mRNA by IFN-β post 24 hours in melanoma cell lines. (B) IFN-β induces *hPNPase^{old-35}* protein resulting in downregulation of c-myc post 48hrs in melanoma cell lines.

IFN-γ and TNF-α treatment resulted in minimal or no induction, whereas poly(I)/poly(C), which induces IFN-α and -β, also stimulated *hPNPase^{old-35}* expression [17]. Promoter characterization experiments and sequence analysis resulted in the identification of an IFN-stimulated response element (ISRE) in the *hPNPase^{old-35}* promoter, to which the ISGF3 complex shows increased binding upon IFN-β treatment [42]. Mutating this site abrogated promoter induction, demonstrating that IFN-β is a transcriptional activator of *hPNPase^{old-35}* whose activation depends on the JAK/STAT signal transduction pathways [42]. *In silico* analysis of the *hPNPase^{old-35}* promoter has highlighted several additional transcription factor binding sites, but at present any connection of these regulatory elements to physiological conditions relating to *hPNPase^{old-35}* expression remains to be determined [46]. In any case, it would be relevant to determine if there are other regulatory factors controlling *hPNPase^{old-35}* expression levels and future endeavors towards achieving this goal are required to better understand *hPNPase^{old-35}* functions.

1.5 Subcellular Localization of hPNPase^{old-35}

Human PNPase possesses a mitochondrial-targeting signal (MTS) at its amino terminus. Immunofluorescence and cell fractionation studies demonstrated that endogenous and C-terminal myc-tagged hPNPase^{old-35} localizes exclusively to the mitochondria [22]. It was expected that the location was obviously mitochondrial matrix, where an enzyme like *hPNPase*^{old-35} was predicted to perform mitochondrial RNA processing analogous to its bacterial and chloroplast counterparts. However, subsequent research involving subfractionation studies, protease protection assays and carbonate extraction experiments proved that *hPNPase*^{old-35} is actually a peripheral inner membrane (IM) - bound protein located in the mitochondrial inter membrane space (IMS) [47] and is imported to this location via an *i*-AAA protease Yme1-dependent mechanism [23]. hPNPase^{old-35} first enters through the TOM complex at the outer mitochondrial membrane, and this is followed by its N-terminus extending through the TIM23 complex at the inner mitochondrial membrane into the matrix, enabling its cleavage by the matrix-processing peptidase (MPP). Yme1 localized at the inner membrane first facilitates release of the N-terminus into the IMS followed by pulling the C-terminus of hPNPase^{old-35} across the TOM complex into the IMS [23]. While these studies are quite convincing, the topic of *hPNPase*^{old-35} subcellular localization has been controversial, as our studies involving ectopic overexpression of hPNPase^{old-35} have shown that it localizes to both the mitochondria and cytoplasm. In our overexpression studies, N-terminal GFP-tagged hPNPase^{old-35} was found to localize to the cytoplasm [17], which is consistent with the findings of Chen et al [18]. This observation might be due to blockage of the N-terminal MTS, although we did not see an effect of this on the

growth inhibitory effects of hPNPase^{old-35}. C-terminal HA-tagged hPNPase^{old-35} on the other hand localizes both in the mitochondria and cytoplasm as documented in our studies. There may be shuttling mechanisms that facilitate the transport of hPNPase^{old-35} from the mitochondrial IMS to the cytoplasm, like the one suggested by Chen et al. where *hPNPase*^{old-35} migrated to the cytoplasm after mitochondrial outer membrane (OM) permeabilization [47], thus allowing it to degrade certain mRNA and miRNA species as reported previously in our studies [48,49]. Conversely physiological conditions allowing OM permeabilization or RNA import pathways could also allow RNA substrates to enter the IMS and subsequently get processed by hPNPase^{old-35} [44,50]. Recently, hPNPase^{old-35} has also been found in the nucleus of breast cancer cells exposed to ionizing radiation where it interacts with nuclear EGFR [51]. Further studies are required to establish whether this is a global or cell line and condition specific phenomena. Based on all this information it would be safe to say hPNPase^{old-35} may have distinct roles based on its specific localization in distinct cellular compartments.

1.6 Functions of *hPNPase*^{old-35}

1.6.1 *hPNPase*^{old-35}, growth inhibition, senescence and RNA degradation

As mentioned earlier, *hPNPase*^{old-35} was first identified as a gene that was upregulated in senescent progeroid fibroblasts and terminally differentiated HO-1 human melanoma cells [17]. Both senescence and terminal differentiation share certain common characteristics like irreversible growth arrest notably occurring in the G1 phase of the cell cycle, with inhibition of both DNA synthesis and telomerase activity [52-54]. To elucidate the functional link between a 3'-5' exoribonuclease like *hPNPase*^{old-35} and phenomena like senescence and terminal differentiation, replication-incompetent

adenoviral mediated *hPNPase*^{old-35}-overexpression (*Ad.hPNPase*^{old-35}) studies were performed [48]. (Fig. 1.5)

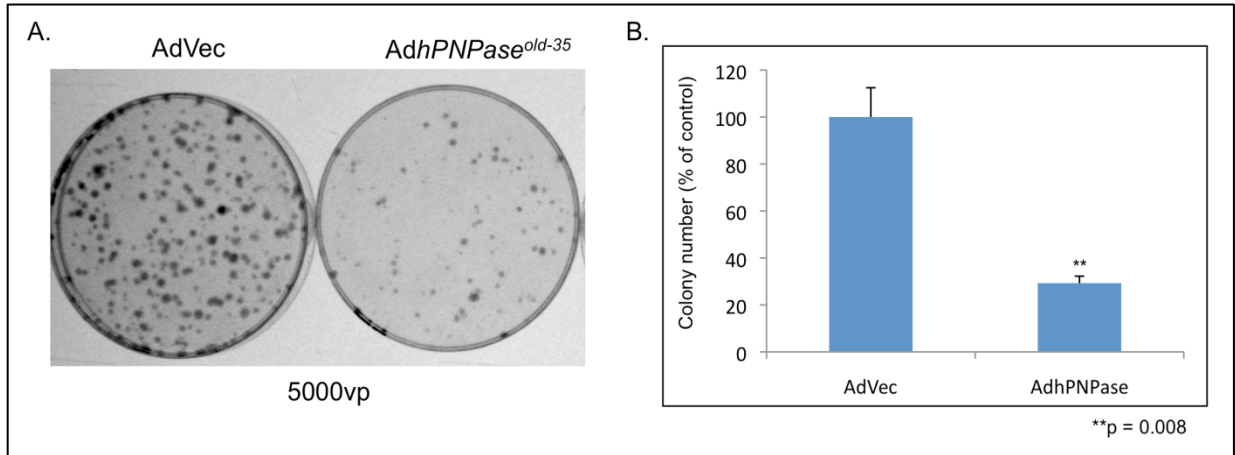


Fig. 1.5. Adenoviral-mediated *hPNPase*^{old-35} overexpression causes inhibition of cellular proliferation of HO-1 cells. (A) HO-1 cells were infected with Advec or *Ad.hPNPase*^{old-35} at an m.o.i. of 5000vp/cell. 6 hrs later, the cells were trypsinized, counted and 1000 cells were plated per 6-cm dish (in triplicate). Colony numbers were determined after 3 weeks. (B) Graphical representation of colony numbers.

It was observed that slow and sustained overexpression of *hPNPase*^{old-35} results in inhibition of growth of multiple cells types and induces a senescent-like phenotype in HO-1 human melanoma cells and normal human melanocytes, ultimately resulting in apoptosis [29,48]. The morphological features evident after about 5 days of adenoviral infection in HO-1 cells are very similar to terminally differentiated HO-1 cells treated with IFN- β and mezerein for the same period of time, which is accompanied by inhibition of telomerase activity [48]. In separate studies, normal human melanocytes stained positive for SA- β -gal, a well known biochemical marker for senescence, and morphologically resembled cells entering a senescent stage by becoming large and flattened after *Ad.hPNPase*^{old-35} infection [48]. This senescence-like phenotype could also be mediated by adenoviral overexpression of either of the 2 RNase PH domains of

hPNPase^{old-35} alone, which was confirmed by deletion studies of the full-length protein [29]. Cell cycle analysis of different cell lines infected with *Ad.hPNPase*^{old-35} showed an initial G₁/S or G₂/M arrest with inhibition of DNA synthesis followed by induction of apoptosis [48,55]. This was accompanied by gene expression changes resembling those occurring during terminal differentiation and senescence, including upregulation of *CDKI p27*^{Kip1} levels and decreases in *CDKI p21*^{CIP1/WAF-1/MDA-6} levels, both of which play significant roles in cell cycle arrest [48]. On the other hand, rapid overexpression of *hPNPase*^{old-35} rapidly promotes apoptosis without any cell-cycle changes, implying that multiple intracellular targets and signaling pathways are involved in *hPNPase*^{old-35}-mediated inhibition of cell-cycle progression and apoptosis.

1.6.2 Molecular mechanisms of growth inhibition and senescence: Interestingly, some light was shed on one of the molecular mechanisms of *hPNPase*^{old-35}-induced growth-inhibition and senescence when it was observed that *Ad.hPNPase*^{old-35} overexpression could downregulate *c-myc* mRNA and protein expression [48]. Interestingly, its expression is downregulated during both terminal differentiation of HO-1 melanoma cells and senescence. Myc is an important transcription factor that regulates numerous physiological processes like cellular growth and proliferation, metabolism and apoptosis [56]. It is one of the key mediators that play a role in transition of cells from the G₁ to S phase of the cell cycle and is known to control *p27*^{Kip1} expression by multiple mechanisms. Rescue experiments involving ectopic overexpression of *c-myc* CDS (coding sequence) significantly protected HO-1 cells from *Ad.hPNPase*^{old-35} mediated cell death, confirming that one mechanism by which *Ad.hPNPase*^{old-35} causes growth inhibition is by downregulating *c-myc* expression (Fig.

5) [48]. However, since *c-myc* overexpression provided only partial protection from *Ad.hPNPase^{old-35}*-mediated cell death, there might be other pathways involving genes that may be direct targets of *hPNPase^{old-35}* degradation, which is an interesting avenue of investigation we are currently pursuing. Interestingly, in a recent study breast cancer cells resistant to ionizing radiation had higher levels of *c-myc* mRNA. This was attributed to an inactive form of *hPNPase* which was phosphorylated at S776 in the nucleus by nEGFR-regulated DNAPK, resulting in its inability to degrade *c-myc* mRNA [51].

The mechanism by which *hPNPase^{old-35}* mediates apoptosis has also been identified and is attributed to its ability to activate double-stranded RNA (dsRNA)-dependent protein kinase (PKR) and phosphorylation of eIF-2 α . Activation of PKR results in induction of GADD153 and a decrease in the levels of the anti-apoptotic protein Bcl-xL, ultimately culminating in apoptosis [57].

Inhibition of growth by IFN- β is also characterized by downregulation of *c-myc* expression, which it is known to regulate post-transcriptionally [58,59]. *hPNPase^{old-35}* induction following IFN- β treatment has also been shown to downregulate *c-myc* mRNA and miR-221 levels, implicating its important role in IFN- β -mediated growth inhibition [49,60]. The role of *hPNPase^{old-35}* in IFN- β -mediated growth inhibition is further strengthened by the finding that transient or stable knockdown of *hPNPase^{old-35}* in melanoma cells makes them resistant to IFN- β -mediated cell death [60]. IFN- β has also been shown to reduce mitochondrial RNA levels [61], which can be another mechanism by which IFN- β -induced *hPNPase^{old-35}* plays a role in growth inhibition via its RNA degrading activity (Fig. 5) [22].

1.6.3 RNA degradation by hPNPase^{old-35}: *In vitro* mRNA degradation assays further validated that full-length hPNPase^{old-35} or either of its two RNase PH domains can specifically degrade *c-myc* mRNA, whereas other mRNAs like *c-jun*, *GAPDH* or *GADD34* are not affected (Fig. 5) [29,48]. The exact mechanism of how hPNPase^{old-35} specifically recognizes and degrades *c-myc* mRNA is still not clear, although our initial belief was that this may be mediated by a specific sequence in the 3'UTR of *c-myc* mRNA (as 3'UTRs contain various instability elements that act as important determinants of RNA turnover [62,63], as *c-myc* RNA devoid its 3'UTR was resistant to hPNPase^{old-35} degradation [48,60]. Also, no specific RNA-binding site has been described in PNPase from any other species either, which is further confounded by the fact that in *E.coli* PNPase degrades a family of CSP (Cold-shock proteins) that do not show any sequence similarity [64]. Recent advances in studies involving substrate recognition by exoribonucleases have shown that RNA secondary structural elements may be primary determining factors in RNA binding and degradation rather than primary sequence. Future studies involving bioinformatics approaches and/or deletion/mutation analysis of *c-myc* 3'UTR mRNA sequence are required to better understand the importance of secondary structural elements in *c-myc* mRNA that allow its selective degradation by hPNPase^{old-35}.

1.6.4 miRNA regulation by hPNPase^{old-35}: miRNAs are small, single-stranded, non-coding RNAs, ~19-25 nucleotides in length that bind to a specific recognition sequence in the 3'UTR of their target mRNAs by complementary base pairing ultimately resulting in their cleavage and degradation or translational repression [65]. Genes encoding miRNAs have been found to be located in intergenic regions, within introns of protein

coding genes and also within introns and exons of non-protein coding genes [66]. They are transcribed in the nucleus by RNA polymerase II or III as primary or pri-miRNA consisting of a 60-80 nucleotide long stem loop structure. Precursor or pre-miRNA is generated by cleavage of pri-miRNA by an RNase complex DROSHA/DGCR8, which is then transported to the cytoplasm by Exportin-5. Further cleavage by an RNase Dicer results in the biogenesis of a double-stranded ~22 nucleotide miRNA which finally yields the mature miRNA after unwinding and stabilization by the Argonaute proteins [65,67].

Regulation of gene expression by microRNAs was first discovered in *C. elegans* in 1993 and since then numerous miRNAs have been identified in plants and animal cells. The deregulation of miRNAs in various cancers and diseases has made them an active avenue of study that holds potential possibilities of therapeutic intervention [65]. Stemming from this interest, recently our group identified another novel mechanism by which *hPNPase*^{old-35} causes growth inhibition by playing a significant role in post-transcriptional modification of miRNA biogenesis [49,67]. In the quest to further understand *hPNPase*^{old-35} functions as an exoribonuclease, a miRNA Microarray analysis performed after *Ad.hPNPase*^{old-35} infection of melanoma cells resulted in the identification of specific miRNAs that were differentially regulated by *hPNPase*^{old-35}. Subsequent validation of downregulated miRNAs through immunoprecipitation, quantitative RT-PCR, northern blotting analysis and *in vitro* degradation assays showed that *hPNPase*^{old-35} could specifically bind and degrade certain mature miRNAs like miR-221, miR-222 and miR-106b, while having no effect on others like miR-184 and miR-let7a (Fig. 6) [49]. Also, this downregulation by *hPNPase*^{old-35} was limited to mature miRNAs only, primary and precursor miRNA were not affected, establishing a novel

hPNPase^{old-35}-mediated post-transcriptional regulatory mechanism of miRNA biogenesis. Apart from *hPNPase*^{old-35} adenoviral overexpression studies, treatment of different melanoma cell lines with IFN- β (that induces *hPNPase*^{old-35}) also resulted in downregulation of miR-221 without having an effect on miR-184 or miR-let7a, which further strengthens the authenticity of this phenomenon in a more physiological setting. On the other hand, IFN- β treatment was unable to downregulate miR-221 in melanoma cells in which *hPNPase*^{old-35} was knocked down and conversely, overexpression of miR-221 made HO-1 cells resistant to IFN- β -mediated growth arrest. Interestingly, miR-221 is a negative regulator of the *p27^{Kip1}* mRNA and accordingly this was identified as another pathway through which *hPNPase*^{old-35} suppresses growth by downregulating miR-221 resulting in a subsequent increase in *p27^{Kip1}* levels (Fig. 6) [49]. The specific binding of *hPNPase*^{old-35} to defined miRNAs can be sequence or secondary structure related, and this hypothesis needs to be further tested.

1.6.5 *hPNPase*^{old-35} and inflammation

A characteristic feature of aging is chronic inflammation, which is also a hallmark of progressive degenerative diseases like Parkinson's disease (PD), amyotrophic lateral sclerosis (ALS), atherosclerosis, Alzheimer's disease (AD) and type 2 diabetes [68,69]. Aging is a phenomenon that is studied extensively, but at this point not a lot is known about the relationship between cellular senescence and inflammation. Damage that is caused by oxidative stress plays an important role in aging-associated inflammation, which is evident in tissues collected from aged individuals or aged experimental animals in the form of oxidative damage in their DNA, protein and lipids [70,71]. One of the important generators of reactive oxygen species (ROS) in the cell is mitochondria which

cause cumulative oxidative damage over time [68]. ROS have been known to regulate activity of the transcription factor NF- κ B, which can turn on the expression of pro-inflammatory cytokines like IL-6, IL-8, RANTES and MMP-3 [72,73]. In our adenoviral overexpression studies we found that *hPNPase*^{old-35} localization in the mitochondria plays an important role in inducing ROS that leads to degradation of I κ B- α , followed by nuclear translocation of the p65 subunit of NF- κ B and increased p50/p65 NF- κ B DNA binding resulting in increased production of pro-inflammatory cytokines as mentioned earlier [74,75]. The anti-oxidant N-acetyl-L-cysteine (NAC) could inhibit all of these events linked to aging-related inflammation, but does not protect cells from *hPNPase*^{old-35}-induced growth inhibition [13,74]. Since *hPNPase*^{old-35} expression is elevated during senescence and Ad. *hPNPase*^{old-35} infection increases ROS production in the mitochondria (one possibility being that ROS could be generated as a result of mitochondrial protein turnover of *hPNPase*^{old-35}-substrates [76-78], a hypothesis that needs to be further tested), we can conclude that mitochondria-localized *hPNPase*^{old-35} plays a role in regulating the inflammatory components of senescence [74,79]. Also, given that *hPNPase*^{old-35} is an early type I IFN-responsive gene and activation of IFN-signaling pathway leading to the upregulation of IFN-regulated genes have been documented during the process of senescence [17,42,80], these findings indicate that IFN might play an important role in regulating inflammatory diseases of aging [79].

1.7 Functions of *hPNPase*^{old-35} in mitochondria

1.7.1 *hPNPase*^{old-35} and mitochondrial homeostasis: The subcellular localization of *hPNPase*^{old-35} in mitochondria has led to numerous studies aimed at trying to comprehend the role of *hPNPase*^{old-35}, if any in maintaining mitochondrial homeostasis and this has been done by classical gene knockdown and overexpression studies. The level of *hPNPase*^{old-35} knockdown seems to play a critical role in deciding the observable changes in mitochondrial physiology and function [47,50]. An ~75% reduction in *hPNPase*^{old-35} levels in HEK293T cells caused mitochondria to become filamentous and granular shaped, along with a three- to four-fold decrease in mitochondrial membrane potential ($\Delta\Psi$) and enzymatic activities of coupled respiratory complexes I and III, coupled complexes II and III, and individual complexes IV and V of the respiratory chain, accompanied by secondary changes like lactate accumulation and reduction of steady-state ATP levels [47]. Contradictory data is also available that shows no change in mitochondrial morphology or function in HeLa cells after *hPNPase*^{old-35} knockdown [76]. Recent *in vivo* data representing a more physiological setting, has confirmed a role for *hPNPase*^{old-35} in the maintenance of mitochondrial homeostasis, wherein mitochondria of liver-specific *PNPT1* knockout mice show disordered, circular and smooth cristae along with a 1.5-2 fold decrease in activity of respiratory chain complex IV and complexes II+III+IV [44].

Overexpression of *hPNPase*^{old-35} is found to cause an increase in ROS accumulation over time [74], which could be due to increased respiratory chain activity caused by mitochondrial dysfunction and implicates a role of *hPNPase*^{old-35} in mitochondrial homeostasis maintenance. An exonuclease-independent role of

hPNPase^{old-35} has also been highlighted in some studies wherein overexpressed hPNPase^{old-35} plays a role in protecting cells from oxidized forms of RNA by limiting them from the translation mechanism [81,82].

1.7.2 hPNPase and RNA import into mitochondria: Different RNA import pathways have been identified in various organisms but not much is known about the components involved [83,84]. New advances continue to be made, with one of the recent discoveries being the involvement of PNPase in regulating translocation of RNA into the mitochondria. It has been recently reported that PNPase regulates the import of nucleus-encoded small RNAs including *RNase P* RNA, *MRP* RNA, and 5S rRNA into the mitochondrial matrix by binding to specific stem-loop motifs in the imported RNAs [44,50]. Supporting this evidence is the proof that liver-specific *PNPT1* knockout mice mitochondria showed a significant reduction in the RNA component of the RNase P mtRNA complex [44]. It should also be noted that PNPase mutations that inactivate RNA processing do not affect RNA import implying that these two functions are independent of each other. How PNPase makes the decision between RNA processing versus import is still an area that requires further experimentation [44,50].

1.7.3 Role of hPNPase in mtRNA processing: Polyadenylation plays an important role in mtRNA metabolism and depending on the organism can lead to quick decay or increased stability of the transcript [85,86]. In contrast to bacteria and some eukaryotes where polyadenylation is catalyzed by poly(A) polymerases (PAPs) or PNPase, human mtRNA is polyadenylated by mitochondria-specific PAP. In order to answer the question whether hPNPase acts as a polymerase or exoribonuclease in mitochondria, it was silenced by shRNA treatment which resulted in an increase in the length of poly(A) tails

of mtRNA without having any effect on steady state levels of these mRNA species [47,76]. Another group showed that stable silencing of hPNPase had varied effects on different mt-mRNAs, and that polyadenylation of mtRNAs is performed by a polymerase distinct from both mtPAP and PNPase [87]. It is also suggested that hPNPase silencing causes ATP depletion which can alter the length of mtRNA poly(A) tails [76,87]. Other studies suggest a role for hPNPase in complex with hSUV3 (human suppressor of Var1 3) acting as degradation complex acting on double-stranded RNA in mammalian mitochondria, which hypothesizes a role for hPNPase in mitochondrial RNA degradation [78,88]. This degradation activity is suppressed by the LRPPRC/SLIRP (leucine-rich pentatricopeptide repeat motif-containing protein/ stem-loop-interacting RNA-binding protein) complex, which also promotes polyadenylation of mRNAs in the mitochondria [89]. In the light of all this information, it is clear that a lot more needs to be resolved before a clear picture of the role of hPNPase in mtRNA processing can be depicted (Fig. 1.6).

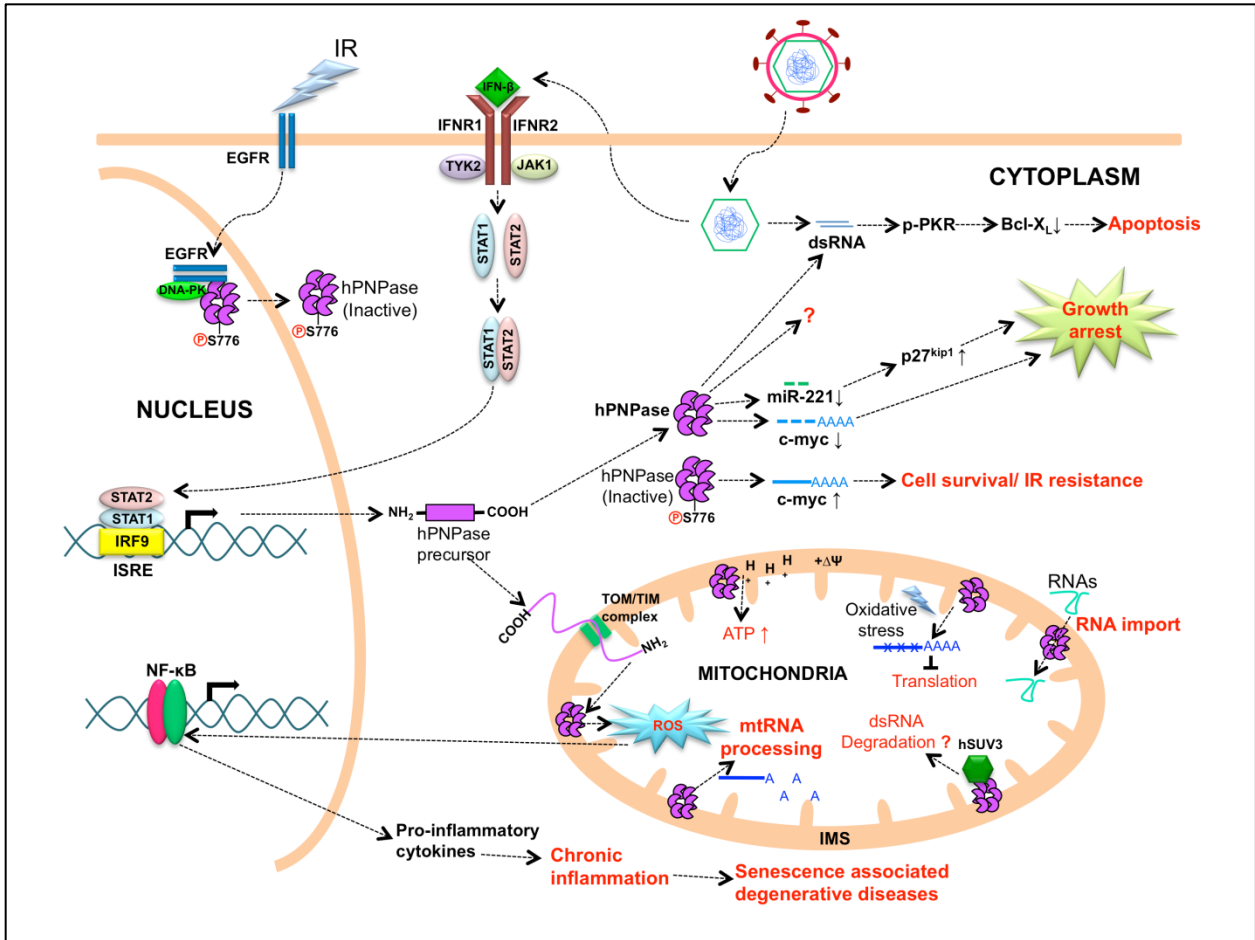


Fig. 1.6. Functions of *hPNPase^{old-35}*. *hPNPase^{old-35}* is transcriptionally induced by the JAK/STAT pathway through IFN- β produced by the cell after viral infection, exposure to tumor cells, senescence-inducing signals or terminal-differentiation promoting signals. Next, *hPNPase^{old-35}* is imported to the mitochondrial inner membrane space (IMS) by a YME- mediated mechanism or alternatively mobilized through an unknown mechanism to the cytoplasm where it causes growth arrest or apoptosis by targeting c-myc mRNA and miR-221 or activating PKR, respectively. Exposure to ionizing radiation inactivates *hPNPase^{old-35}* by an EGFR-mediated mechanism, causing c-myc mRNA upregulation and increasing radioresistance of cancer cells. In the mitochondria *hPNPase^{old-35}* maintains mitochondrial homeostasis, aids in RNA import, takes part in mtRNA processing/degradation events and increases ROS production that results in events leading to chronic inflammation.

CHAPTER TWO

Gene Expression Signature of Human Polynucleotide Phosphorylase (*hPNPase*^{old-35}) in Melanoma cells

Part of the work presented in this chapter has been published in PLoS One 8(10): e76284 (2013).

2.1 Abstract

Human Polynucleotide Phosphorylase (*hPNPase*^{old-35} or *PNPT1*) is an evolutionarily conserved 3'→5' exoribonuclease implicated in the regulation of numerous physiological processes including maintenance of mitochondrial homeostasis, mtRNA import and aging-associated inflammation. From an RNase perspective, little is known about the RNA or miRNA species it targets for degradation or whose expression it regulates, except for *c-myc* and miR-221. To further elucidate the functional implications of *hPNPase*^{old-35} in cellular physiology, we knocked-down and overexpressed *hPNPase*^{old-35} in human melanoma cells and performed gene expression analyses to identify differentially expressed transcripts. Ingenuity Pathway Analysis indicated that knockdown of *hPNPase*^{old-35} resulted in significant gene expression changes associated with mitochondrial dysfunction and cholesterol biosynthesis, whereas overexpression of *hPNPase*^{old-35} caused global changes in cell-cycle related functions. Additionally, comparative gene expression analyses between our *hPNPase*^{old-}

³⁵ knockdown and overexpression datasets allowed us to identify 77 potential “*direct*” and 61 potential “*indirect*” targets of *hPNPase*^{old-35} which formed correlated networks enriched for cell-cycle and wound healing functional association, respectively. These results provide a comprehensive database of genes responsive to *hPNPase*^{old-35} expression levels, along with the identification of new potential candidate genes offering fresh insight into cellular pathways regulated by PNPT1 which may be used in the future for possible therapeutic intervention in mitochondrial- or inflammation-associated disease phenotypes.

2.2 Introduction

Ribonucleases (RNases) are one of the central players involved in the regulation of post-transcriptional control of gene expression in both prokaryotes and eukaryotes [12,37]. They are divided into two main categories, endo- and exo-ribonucleases. Depending on the direction of degradation, exoribonucleases can be further classified as 5'→3' or 3'→5' exoribonucleases [90]. Numerous exoribonucleases identified in bacteria, Archaea and Eukarya have been placed under six major superfamilies, RBN, RNR, DEDD, PDX, RRP4 and 5PX [4,14]. Of these, the PDX family is the only one whose members use inorganic phosphate to generate nucleotide diphosphates instead of hydrolytic cleavage [14]. Polynucleotide phosphorylase (PNPase) is an evolutionarily conserved phosphorolytic 3'→5' exoribonuclease that belongs to the PDX family of proteins [4] and it plays a major role in RNA metabolism in bacteria, plants and humans. The protein encoded by this gene consists of five conserved classical domains: two RNase PH domains, a α -helical domain and two RNA binding domains KH and S1 [91]. The human homolog of this gene (*hPNPase*^{old-35}) was identified in an overlapping

pathway screen (OPS) intended to identify upregulated transcripts in terminally differentiated human melanoma cells and senescent progeroid fibroblasts [17].

Human polynucleotide phosphorylase (hPNPase^{old-35}) is encoded by the *PNPT1* gene mapping to chromosome 2p15-2p16.1 and has been characterized as a type I IFN (IFN- α/β)-inducible early response gene [17,42]. Numerous endeavors over the past decade have enriched our comprehension of the workings of this exoribonuclease. It has become increasingly clear over the years that the various physiological functions of this enzymatic protein are not restricted to a single cellular compartment, in this case the mitochondrial inter membrane space (IMS) where it is primarily located [23,47]. In the cytoplasm this protein performs a myriad of functions, which include but are not restricted to degradation of mRNA and miRNA species [48,49]. Adenoviral-mediated overexpression of hPNPase^{old-35} causes growth inhibition of normal and cancer cells characterized by morphological changes associated with senescence, G₁/S or G₂/M cell-cycle arrest and apoptosis [48,55,57,92]. The ability of hPNPase^{old-35} to selectively degrade *c-myc* mRNA through its exoribonucleolytic activity has been identified as a key molecular mechanism mediating the growth suppressive effects of hPNPase^{old-35}, since overexpression of *c-myc* could only partially rescue these effects [48]. Apart from mRNA degradation, hPNPase^{old-35} has also been identified as a direct regulator of mature miRNA species, specifically miR-221 that targets the cell cycle inhibitor p27^{Kip1} [49,67]. Both these specialized functions of hPNPase^{old-35} also implicate it as a direct mediator of IFN- β -induced growth inhibition [49,60]. Another novel function of hPNPase^{old-35} is its ability to generate double-stranded RNA (dsRNA) through a currently

unknown mechanism, which ultimately leads to apoptosis of cells due to the activation of dsRNA-dependent protein kinase (PKR) [57].

Apart from the above-mentioned cytoplasmic functions that focus on its physiological roles in the regulation of growth inhibition and senescence, numerous roles of *hPNPase*^{old-35} have been revealed that are central to its location in the mitochondria [13,67,75,93]. Overexpression of *hPNPase*^{old-35} induces reactive oxygen species (ROS) production in the mitochondria resulting in the expression of pro-inflammatory cytokines, which is a major phenomenon linking *hPNPase*^{old-35} to aging-related inflammation [74,79]. The significance of *hPNPase*^{old-35} in maintaining mitochondrial homeostasis, with a specific relevance to the electron transport chain (ETC) components, has been revealed by *hPNPase*^{old-35} knockdown studies in cell systems and also in a liver-specific knockout mouse model of *hPNPase*^{old-35} [44,47]. There are also studies providing evidence that *hPNPase*^{old-35} is a regulator of mitochondrial RNA import and plays a role in mtRNA processing [44,50,51,76,87]. Recently *hPNPase*^{old-35} has also been shown to be present in the nucleus, and is associated with nEGFR protein, which regulates the exonuclease activity of *hPNPase*^{old-35} upon exposure to ionizing radiations [75].

Most of what we know about *hPNPase*^{old-35} today has been gleaned from classical gain-of-function or loss-of-function experiments and from comparative studies performed through lessons acquired from its bacterial and plant counterparts [13,67,93]. Although these studies have been immensely valuable in illuminating the importance of *hPNPase*^{old-35} in various physiological phenomena like senescence, growth-inhibition and mitochondrial dynamics, little is known about the specific network of genes that are

involved in these processes or which might be dysregulated when *hPNPase*^{old-35} is aberrantly expressed. Moreover, when evaluating its function as an exoribonuclease, we know of only one mRNA and a single miRNA species that *hPNPase*^{old-35} can degrade directly, *c-myc* and miR-221, respectively. Such findings led to our interest in trying to identify genes or gene networks that are either potential direct degradation targets of *hPNPase*^{old-35} or regulated by *hPNPase*^{old-35}, respectively. In order to pursue this objective, we performed gene expression analysis on human melanoma cells in which *hPNPase*^{old-35} was either silenced or ectopically overexpressed. Studying the global gene expression changes associated with *hPNPase*^{old-35}-knockdown or overexpression has provided valuable new insights regarding the functions of this elusive exoribonuclease while also validating previously known information. With the help of Ingenuity Pathway Analysis (IPA) we have identified key biological functions and associated genes that are deregulated in response to aberrant expression of *hPNPase*^{old-35}. Additionally, comparative analysis of the knockdown and overexpression datasets has allowed us to identify novel genes that may be directly or indirectly regulated by *hPNPase*^{old-35}.

In summary, our present studies interrogated the global implications of *hPNPase*^{old-35} dysregulation and now provide a comprehensive database that can be further used not only to understand the biological functions of *hPNPase*^{old-35} but also to identify candidate direct degradation targets such as *c-myc* and miR-221.

2.3 Materials and methods

2.3.1 Cell culture

The human melanoma cell line HO-1 [53,95,96] was initially provided by Dr. Eliezer Huberman (Argonne National Laboratories, IL) maintained in Dulbecco's Modified Eagle Medium (DMEM; Invitrogen Life Technologies) supplemented with 10% fetal bovine serum (FBS; Sigma) and 5% penicillin/streptomycin (Gibco). The melanoma cell line WM35 [96-99], provided by Dr. Meenhard Herlyn (Wistar Institute) was maintained in MCDB153:Leibovitz's L15 (4:1) pH 7.4 supplemented with 2% FBS and CaCl₂ (1.68mM, Sigma). The *hPNPase*^{old-35}-knockdown stable cell lines were maintained in growth medium as described with the addition of 200 ng/ml (in case of HO-1 cells) or 300 ng/ml (in case of WM35 cells) of the selective antibiotic puromycin. All cell lines were maintained in a 5% CO₂ 95% O₂ humidified incubator at 37°C. 0.5%. Trypsin-EDTA (10X) solution was purchased from Gibco and 1X Dulbecco's Phosphate-Buffered Saline (DPBS) from Corning Cellgro.

2.3.2 Expression constructs, stable cell lines and viral infections

Lentiviral constructs (pGIPZ) expressing GFP were purchased from Open Biosystems. The constructs contained non-silencing short hairpin RNA (shRNA) or shRNAs against *hPNPase*^{old-35} (PNPshRNA-1: clone ID V2LHS_17644, Mature Sense: GGCAACAGGAAATTAGAAA, Mature Antisense: TTTCTAATTCCTGTTGCC; PNPshRNA-2: clone ID V2LHS_159887, Mature Sense: CAATAGGATTGGTCACCAA, Mature Antisense: TTGGTGACCAATCCTATTG). Lentiviruses encoding the different shRNAs were produced by cotransfecting the HEK-293T packaging cells with the appropriate pGIPZ constructs and the Trans-lentiviral Packaging Mix (Open

Biosystems) according to the manufacturer's protocol. The supernatants containing the lentiviral particles were harvested 48 hours after transfection, concentrated by centrifugation and frozen at -80°C as aliquots. 1ml of the above viral suspension was used to transduce 3×10^5 HO-1 human melanoma cells grown in 6-cm dishes supplemented with 10 $\mu\text{g/ml}$ polybrene. 48 hours post-transduction cells were trypsinized and replated at a low density (1:5) and complete media was added supplemented with positive selection marker puromycin to establish stable shRNA expressing single clones over a period of two weeks. Single clones isolated for PNPshRNA-1 and PNPshRNA-2 were screened to assess the level of knockdown at both the RNA and protein levels and the HO-1 clones with maximum *hPNPase*^{old-35} knockdown were used for microarray analyses (we used one of our HO-1 PNPshRNA-1 clones for this purpose).

The construction and purification of replication-incompetent adenovirus encoding *hPNPase*^{old-35} (Ad.*hPNPase*^{old-35}) has been described previously [17,48]. The empty vector Ad.*vec* was used as a control. For all adenoviral experiments, 1×10^5 cells were grown in 6-cm dishes and infected after 24 hours with Ad.*vec* or Ad.*hPNPase*^{old-35} at a final m.o.i. of 5000 vp/cell diluted in 1 ml of serum-free media. After 6 hours of infection with shaking every 15 minutes, complete media was added and cells were harvested at the required time points (e.g., 36 hours post-infection) for microarray analysis, RNA or protein isolation.

All transient transfections were performed using Lipofectamine® 2000 Transfection Reagent (Life Technologies) according to the manufacturer's protocol. RNA and protein were harvested 48hrs post-transfection for all experimental analyses.

2.3.3 RNA extraction, quality assessment and Microarray analyses

Total RNA from the *hPNPase*^{old-35}-knockdown cell line (HO-1 melanoma cells stably expressing shRNA-1 against *hPNPase*^{old-35}), HO-1 cells expressing non-silencing control shRNA, and HO-1 cells infected with *Ad.hPNPase*^{old-35} or *Ad.vec* for 36 hours was isolated from cell lysates in TRIZOL reagent (Invitrogen™ Life Technologies, Carlsbad, CA). Cell lysates were subjected to an automated extraction method using the MagMAX™-96 for Microarrays Total RNA Isolation Kit (Ambion/Invitrogen™ Life Technologies, Carlsbad, CA) on the MagMAX™ Express Magnetic Particle Processor (Applied Biosystems/Invitrogen™ LifeTechnologies, Carlsbad, CA).

Gene expression profiles were ascertained using GeneChip® Human Genome U133A 2.0 (HG-U133A 2.0) arrays (Affymetrix, Santa Clara, CA) as previously described [100]. Every chip was scanned at a high resolution, with pixelations ranging from 2.5 µm down to 0.51 µm, by the Affymetrix GeneChip® Scanner 3000 according to the GeneChip® Expression Analysis Technical Manual procedures (Affymetrix, Santa Clara, CA). After scanning, the raw intensities for every probe were stored in electronic files (in .DAT and .CEL formats) by the GeneChip® Operating Software (GCOS) (Affymetrix, Santa Clara, CA). The overall quality of each array was assessed by monitoring the 3'/5' ratios for a housekeeping gene (GAPDH) and the percentage of “Present” genes (%P); where arrays exhibiting GAPDH 3'/5' < 3.0 and %P > 40% were considered good quality arrays [100]. All experiments were done in biological triplicates. The microarray data generated for this study are available online at the Gene Expression Omnibus repository under the accession number GSE46884.

2.3.4 Statistical Analysis, IPA and functional classification of genes

The Robust Multiarray Average method (RMA) was used for normalization and generating probe set expression summaries for the gene expression assays. To identify genes significantly altered among the different conditions (i.e., *hPNPase*^{old-35} down-regulation and up-regulation), t-tests were performed for each cell type. To adjust for multiple hypothesis testing, the resulting p-values were used to obtain the false discovery rates using the q-value method. Genes were considered significant using an FDR of 5%. All analyses were performed in the R statistical environment using functions provided by the BioConductor packages [100,101].

In order to categorize biological functions related to gene expression altered by *hPNPase*^{old-35} in our microarray analyses, we used the Ingenuity Pathway Analysis (IPA, Ingenuity® Systems, <http://www.ingenuity.com>) [102,103]. Genes were considered differentially expressed if they had q-values ≤ 0.05 . The Affymetrix probe set IDs of significantly altered genes identified through the statistical analysis described above in both the *hPNPase*^{old-35}-knockdown and overexpression scenarios, along with their associated p- and q-values were uploaded into IPA and analyses performed.

The ToppFun function of the ToppGene suite of web applications [104] was used for the functional enrichment of the *hPNPase*^{old-35}-directly and indirectly regulated genes. The HGNC symbols for both the gene lists were uploaded and a FDR correction threshold of 5% was set for the subsequent functional enrichment analyses. The Gene Ontology (GO) categories (molecular function, biological process, and cellular component), biological pathway and gene and miRNA families were considered for analyses.

In order to further validate if genes regulated by alterations in *hPNPase*^{old-35} expression formed gene interaction networks, the gene symbols for the potential *hPNPase*^{old-35}-“directly” and -“indirectly” regulated genes were uploaded into GeneMANIA (<http://www.genemania.org>), a web interface for generating interactive functional association networks [105]. This resource utilizes multiple external datasets, including protein-protein interactions and published microarray datasets, to form networks of potential gene-gene interactions. The interactive functional association networks obtained were generated based on co-expression, biological pathways, predicted association, genetic interactions, physical interactions and co-localization functional association data. The networks were generated using the query-dependent automatically selected weighting method.

2.3.5 cDNA synthesis and quantitative real-time RT-PCR (qRT-PCR)

Total RNA was harvested from the *hPNPase*^{old-35}-knockdown and control stable cell lines and from the adenovirus infected HO-1 cells using the RNeasy purification kit (Qiagen). The quality and concentrations of isolated RNA samples were assessed using the NanoDrop 2000 (Thermo Scientific). 2 µg of RNA was used in a total volume of 20 µl to synthesize cDNA using the High Capacity cDNA Reverse Transcription kit (Applied Biosystems) according to the manufacturer’s instructions. Real-time quantitative PCR was conducted using the ViiA™ 7 Real-Time PCR System (Applied Biosystems) and performed in a total volume of 20 µl that contained the TaqMan Gene Expression Master Mix (Applied Biosystems), 1 µl of the cDNA template generated and the target-specific TaqMan Gene expression assays (Applied Biosystems) according to following cycle parameters: 95°C for 10 minutes followed by 40 cycles at 95°C for 15 seconds

and at 60°C for 1 minute. Each sample was run in triplicate using three biological replicates and normalized to the housekeeping gene GAPDH used as an internal control in each case. The $\Delta\Delta C_t$ method was used for comparing relative fold expression differences in the genes of interest between different test samples. Statistical significance ($P < 0.05$) was determined using two-tailed student's t-test and one-way analysis of variance ($ANOVA$) followed by Dunnett's multiple comparison test wherever required.

2.3.6 Protein isolation and Western blot analysis

Cells were harvested by centrifugation, pellets washed in PBS and subsequently lysed in ice-cold 1X cell lysis buffer (Cell Signaling) supplemented with PhosSTOP Phosphatase Inhibitor Cocktail Tablets and complete Mini Protease Inhibitor Cocktail Tablets (Roche), followed by centrifugation at 13,000 rpm for 15 minutes at 4°C. The supernatant or whole cell lysate was collected in a fresh tube and protein concentration was measured using the Bio-Rad Protein Assay Dye Reagent Concentrate (BIO-RAD). 30 μ g of total cell lysate was mixed with SDS sample buffer and heated for 5 minutes at 95°C. The proteins were separated by 8-10% SDS-PAGE gels and transferred onto nitrocellulose membranes and blocked using 5% non-fat milk supplemented with 1% bovine serum albumin (BSA) in TBS-T for 1 hour. After washing three times with TBS-T for 10 minutes each, the membranes were incubated with primary antibodies overnight at 4°C. The primary antibodies used were anti-*hPNPase*^{old-35} (chicken; 1:5000), anti-EF1 α (mouse, 1:1000). The next day membranes were washed as before and incubated with the relevant horseradish-peroxidase conjugated secondary antibodies for 1 hour at room temperature. After washing three times with TBS-T for 10 minutes each,

the proteins were detected using ECL Western Blotting detection reagent (GE Healthcare Life Sciences) and exposed to X-ray film.

2.3.7 Invasion assay

Cellular invasion was determined using a modified a Boyden chamber (BD BioCoat™ Matrigel™ Invasion Chambers (MIC) BD Biosciences, Catalog # 354480) by plating 5×10^4 HO-1 Csh or HO-1 PNPsh1 cl4/cl17 into cell well inserts in a 24-well plate provided by the manufacturer and according to the manufacturer's instructions. After an incubation of 48 hrs at 37°C in the presence of 5% CO₂ using DMEM (without serum) in both the top and bottom chambers; the number of cells that invaded through the matrigel were fixed with Solution A (fixative) for five minutes, which is a component of the Diff-Stain Kit (IMEB INC., Catalogue # K7148-2); next the wells were washed with water and the non-invading cells trapped in the matrigel layer were removed with the help of a cotton swab. The wells then were stained with Solution B (Azure stain) for 5-6 minutes and counterstained with Solution C (xanthenes dyes) for 5-6 minutes. Finally the wells were lightly washed with water, dried and observed under the microscope. Five 10X fields were chosen randomly and the average number of invaded cells were counted. The data are represented as mean \pm standard error of two independent experiments done in duplicate. Statistical significance ($P \leq 0.05$) was determined by one-way analysis of variance (_{ANOVA}) followed by Dunnett's multiple comparison test (Prism, GraphPad, San Diego, CA, USA).

2.3.8 Immunohistochemistry

The multiple malignant melanoma tissue array slides with adjacent normal skin tissue were purchased from US Biomax Inc. (Catalogue # ME241a) and

immunohistochemistry was performed. The slides were incubated at 60°C for 1 hour in a vacuum chamber, followed by de-paraffination with two changes of xylene (5 minutes each). Next the slides were rehydrated with gradient alcohol, 100%, 95%, 80% and 70% for 3 minutes each, followed by incubating in water and PBS (phosphate buffer saline) for 5 minutes each. Antigen retrieval was performed by incubating the slides in warm (95°C) Citrate-based antigen unmasking solution (Vector Laboratories, Inc., Catalogue # H-3300) in a vacuum chamber for 1 hour. Next the slides were rinsed in PBS for 5 minutes and incubated in 2% H₂O₂ in PBS for 20 minutes. The slides were then blocked with 5% goat serum in PBS-T (0.1% Tween-20 in PBS) for 1 hour at room temperature and incubated with primary antibodies (anti-hPNPase^{old-35} : chicken, 1:400; anti-EMR1: rabbit polyclonal (Origene, Catalogue # TA308395), 1:200) diluted in blocking buffer overnight at 4°C. The negative controls were also incubated in blocking buffer without any primary antibodies. The next day the slides were rinsed with PBS thrice for 5 minutes each and incubated with biotinylated secondary antibodies (anti-chicken IgG, Catalogue # BA-9010, anti-rabbit IgG, Catalogue # BA-1000, 1:500, Vector Laboratories, Inc.) diluted in 2% goat serum in PBS-T for 1 hour at room temperature. Next the slides were rinsed with PBS thrice for 5 minutes each and incubated with VECTASTAIN[®] ABC reagent (Vector Laboratories, Inc.) for 30 minutes. After this the slides were washed with PBS thrice for 5 minutes each and incubated with freshly prepared ImmPACT DAB Peroxidase Substrate (Vector Laboratories, Inc., Catalogue # SK-4105) for 1-5 minutes. The slides were rinsed with water, counterstained with Hematoxylin QS nuclear counterstain (Vector Laboratories, Inc., Catalogue # H-3404) and rinsed with water again for 5-10 minutes. The slides were then dehydrated with

gradient alcohol, 70%, 80%, 95% and 100%, each 2-3 minutes, cleaned with xylene for 5 minutes, dried and mounted with coverslip after addition of 1 drop of VectaMount™ Mounting Medium (Vector Laboratories, Inc., Catalogue #H-5000) and viewed under microscope.

2.4 Results

2.4.1 Melanoma cell culture model for studying *hPNPase*^{old-35} regulated gene expression

In order to establish stable HO-1 human melanoma cell lines in which *hPNPase*^{old-35} expression was silenced, we employed a lentiviral system to ensure efficient delivery. RNA and protein levels of *hPNPase*^{old-35} were analyzed in the different single clones that survived after puromycin selection as described. Both the shRNAs tested, PNPshRNA-1 (data shown for clone 4) and PNPshRNA-2 (data shown for clone 9), resulted in ≥80% and ~70% knockdown at the protein level as calculated by densitometric analysis (Fig. 2.1.A) relative to the scrambled control shRNA respectively. PNPshRNA-1 clone 4 was used for microarray analysis. The replication-deficient adenovirus for ectopic overexpression of *hPNPase*^{old-35} has been extensively characterized previously [17,48]. Infection of HO-1 cells was performed as previously described [17,48] and both RNA and protein were analyzed for overexpression of *hPNPase*^{old-35} (Fig. 2.1.B). RNA and protein from these cells were collected 36 h post-infection for microarray analysis and a >30 fold increase in *hPNPase*^{old-35} RNA levels and a 3 fold increase (as calculated by densitometric analysis) in *hPNPase*^{old-35} protein levels was observed in the Ad.*hPNPase*^{old-35} compared to the Ad.*Vec* treated cells.

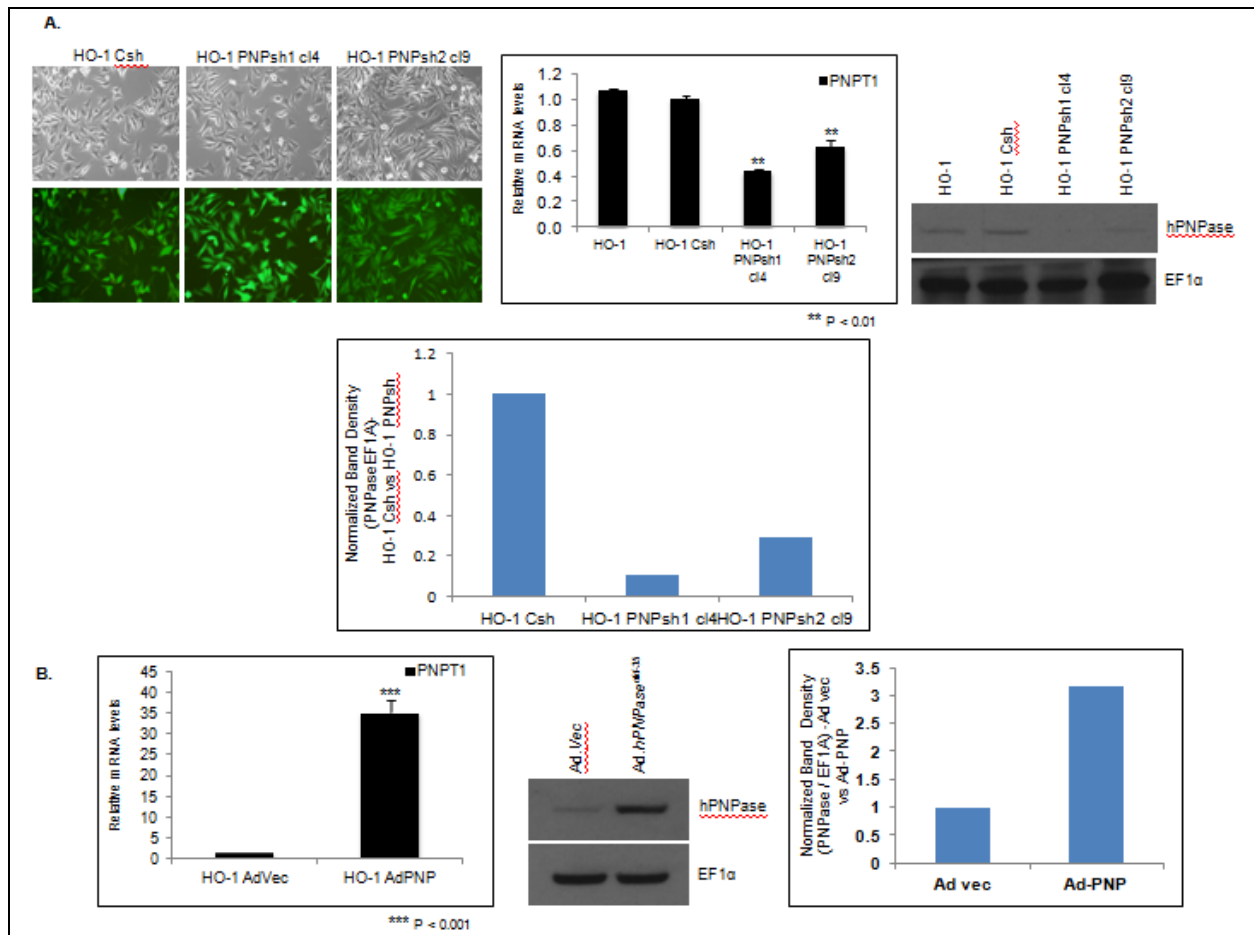


Fig. 2.1. (A) Phase contrast LM (top) and GFP fluorescent micrographs (bottom) of HO-1 melanoma cell lines following transduction with GFP expressing scrambled shRNA and *hPNPase*^{old-35} shRNA1 and 2 expressing lentiviruses and selection with puromycin. qRT-PCR expression of *hPNPase*^{old-35} normalized to control (shScramble). Mean values normalized to a GAPDH internal reference; error bars represent mean \pm S.E. of three replicate experiments, statistical significance was determined using one-way analysis of variance followed by Dunnett's multiple comparison test. Anti-*hPNPase*^{old-35} and EF1 α loading control immunoblots and densitometric analysis graphically representing protein fold decrease. (B) qRT-PCR expression of *hPNPase*^{old-35} in HO-1 cells infected with Ad.*hPNPase*^{old-35} normalized to cells infected with Ad.Vec for 36 hour. Error bars represent mean \pm S.E of three replicate experiments, statistical significance was determined using student's t-test. Immunoblot showing *hPNPase*^{old-35} overexpression compared to Ad.Vec post 36 hour of infection and densitometric analysis showing protein fold increase.

2.4.2 Genetic profile of *hPNPase*^{old-35}-knockdown melanoma cells

In order to further understand and possibly identify novel functions of *hPNPase*^{old-35}, we stably depleted it using shRNA in HO-1 human melanoma cells (Fig. 2.1.A). The ability to study changes in gene expression patterns has become a valuable technique that permits evaluation of the significance of a gene in a more global context. Microarray analysis between the *hPNPase*^{old-35} shRNA and the scrambled shRNA expressing HO-1 cells led to the identification of a total of 1025 upregulated and 1364 downregulated transcripts which were altered significantly (FDR ≤ 0.05) (Fig. 2.2.B-C).

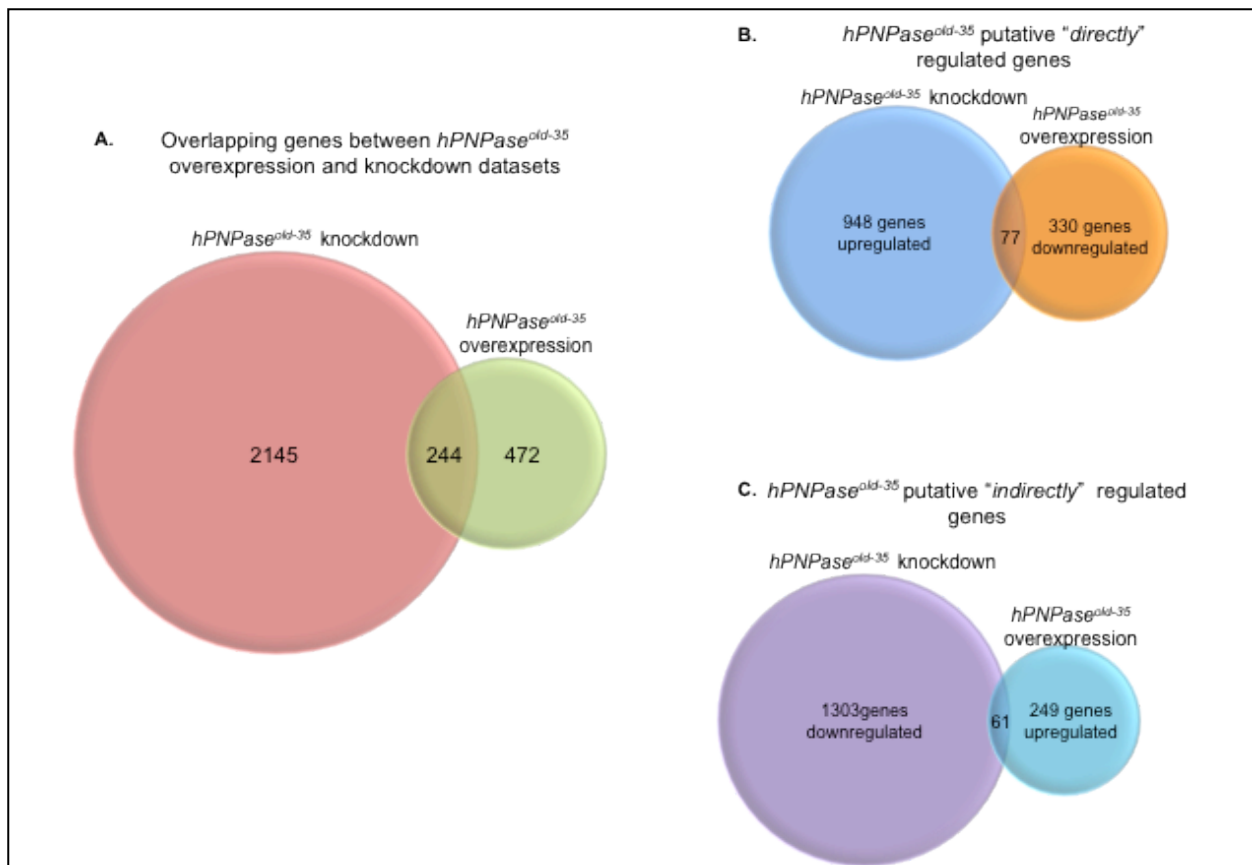
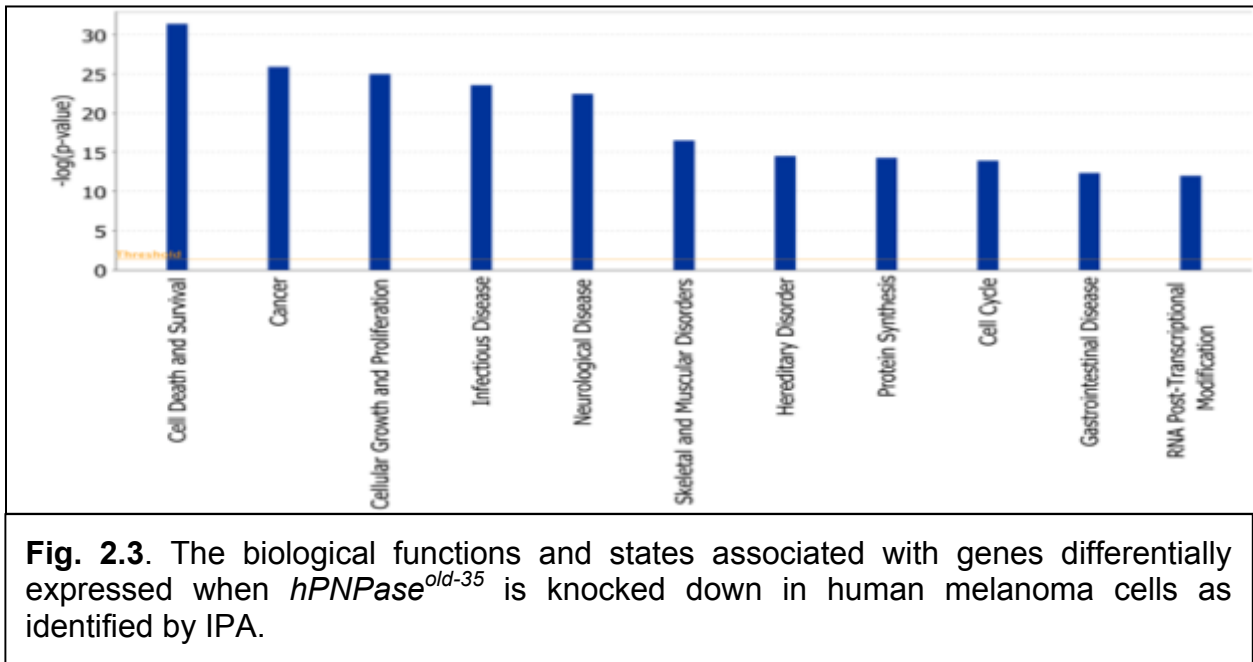


Fig. 2.2. Venn diagrams representing number of genes significantly altered when *hPNPase*^{old-35} is knocked down or overexpressed in human melanoma cells: Shown are total number of dysregulated genes (A), genes "directly" (B) and "indirectly" (C) regulated by *hPNPase*^{old-35}.

We utilized IPA to functionally categorize all the differentially expressed genes identified following *hPNPase*^{old-35} knockdown in HO-1 melanoma cells. The main molecular and cellular functions (p-values ranging from 3.92E-32 - 1.26E-03) associated with the most significantly altered genes were cell death and survival, cellular growth and proliferation, protein synthesis, cell cycle and RNA post-translational modification (Fig. 2.3, Table S1A). Based on these functional categories 25 biological gene networks were generated by IPA with a score ranging from 41 to 28 (Table S1D). IPA computes scores for each network based on p-values, which in turn indicate the likelihood of genes being found together in a network due to random chance. Higher the score, lesser the chance of the genes in a network being grouped together by random chance alone.



Apart from classifying individual genes into functional categories, IPA also predicts corresponding biological pathways that may be significantly altered, along with mechanisms related to toxicity at a more biochemical level (Fig. 2.4).

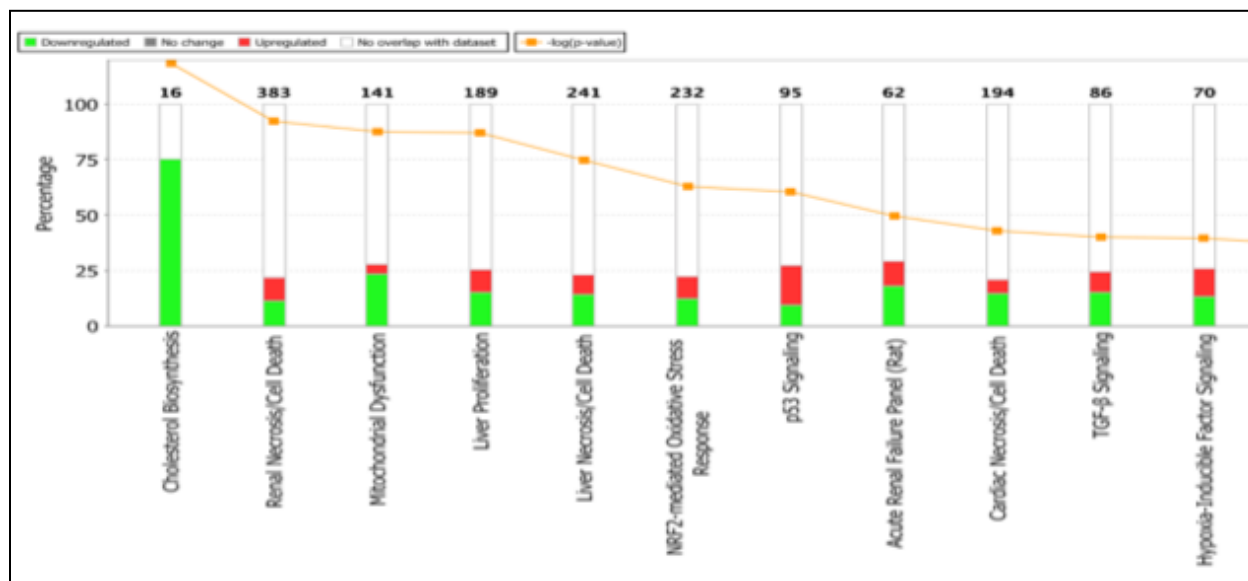


Fig. 2.4. Toxicologically related functionalities and pathways associated with genes dysregulated (proportions shown in graphs) after *hPNPase*^{old-35} knockdown in melanoma cells, as identified by IPA Toxicogenomic Analysis.

The most significant canonical pathways identified were related to EIF2 signaling, cholesterol biosynthesis, integrin signaling and mitochondrial dysfunction (Fig. 2.5, Table S1C).

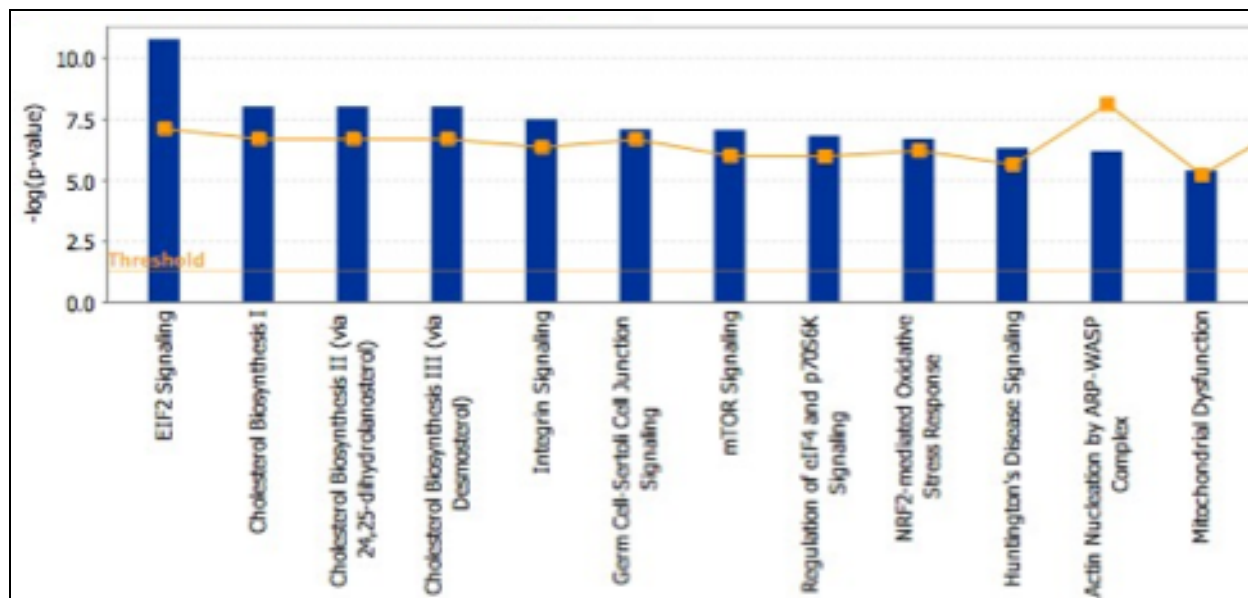


Fig. 2.5. Canonical pathways associated with genes differentially expressed when *hPNPase^{old-35}* is knocked down in human melanoma cells.

Even more fascinating was the finding that two of these biological pathways, cholesterol biosynthesis (Table 2.1) and mitochondrial dysfunction (Table 2.2), were directly correlated with predicted physiological toxicity (identified through IPA-Tox analysis) (Fig. 2.4, Table S1B). *HMGCR* (Fig. 2.6.A), *HMGCS1* and *IDI1* were the three most significantly altered genes belonging to the cholesterol biosynthesis pathway. An overall downregulation of genes belonging to the electron transport chain and some associated factors was observed, consistent with previous observations regarding the role of *hPNPase^{old-35}* in maintaining mitochondrial homeostasis [9,23]. Some of the significantly downregulated genes were *NDUFA3*, *NDUFS1*, *UQCRC1*, *COX6B1*, *COX7A1*, *ATP5C1*, *CAT* and *UCP2* (Fig. 2.6.B).

Table 2.1. List of genes which are significantly altered as a result of *hPNPase*^{old-35} stable knockdown, and are associated with cholesterol biosynthesis, according to IPA Toxicogenomic Analysis. FDR \leq 0.05 = *, FDR \leq 0.01 = **, FDR \leq 0.005 = ***.

Gene Symbol	Gene Name	Fold Change	Affymetrix ID
ACAT2	acetyl-CoA acetyltransferase 2	-1.29 *	209608_s_at
DHCR7	7-dehydrocholesterol reductase	-1.51 **	201790_s_at
EBP	emopamil binding protein (sterol isomerase)	-1.22 *	213787_s_at
FDFT1	farnesyl-diphosphate farnesyltransferase 1	-1.23 *	210950_s_at
FDPS	farnesyl diphosphate synthase	-1.17 *	201275_at
HMGCR	3-hydroxy-3-methylglutaryl-CoA reductase	-1.42 ***	202539_s_at
HMGCS1	3-hydroxy-3-methylglutaryl-CoA synthase 1 (soluble)	-1.56 ***	221750_at
IDI1	isopentenyl-diphosphate delta isomerase 1	-1.92 ***	208881_x_at
LSS	lanosterol synthase (2,3-oxidosqualene-lanosterol cyclase)	-1.29 *	202245_at
MVD	mevalonate (diphospho) decarboxylase	-1.24 *	203027_s_at
SC5DL	sterol-C5-desaturase (ERG3 delta-5-desaturase homolog, <i>S. cerevisiae</i>)-like	-1.26 *	211423_s_at
SQLE	squalene epoxidase	-1.37 **	209218_at

Table 2.2. List of genes which are significantly altered as a result of *hPNPase*^{old-35} stable knockdown, and are associated with mitochondrial dysfunction, according to IPA Toxicogenomic Analysis. FDR \leq 0.05 = *, FDR \leq 0.01 = **, FDR \leq 0.005 = ***.

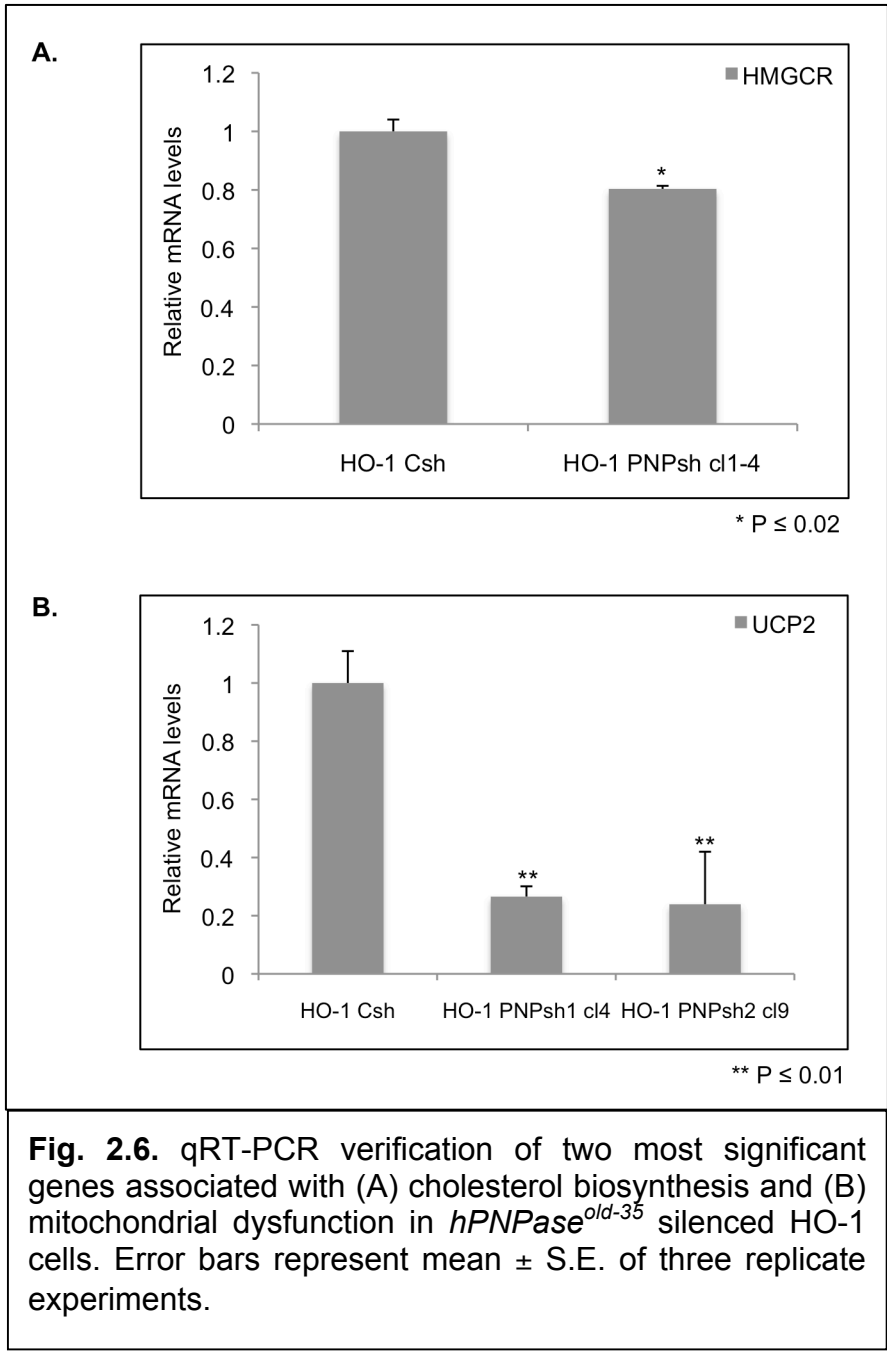
Table 2A.

ETC components	Gene symbol	Gene name	Fold change	Affymetrix ID
Complex I	NDUFA2	NADH dehydrogenase (ubiquinone) 1 alpha subcomplex, 2, 8kDa	-1.11 *	209224_s_at
	NDUFA3	NADH dehydrogenase (ubiquinone) 1 alpha subcomplex, 3, 9kDa	-1.32 ***	218563_at
	NDUFA8	NADH dehydrogenase (ubiquinone) 1 alpha subcomplex, 8, 19kDa	-1.14 *	218160_at
	NDUFA13	NADH dehydrogenase (ubiquinone) 1 alpha subcomplex, 13	1.22 **	220864_s_at
	NDUFAB1	NADH dehydrogenase (ubiquinone) 1,	-1.07 *	202077_at

	1	alpha/beta subcomplex, 1, 8kDa		
	NDUFAF1	NADH dehydrogenase (ubiquinone) complex I, assembly factor 1	-1.09 *	204125_at
	NDUFB4	NADH dehydrogenase (ubiquinone) 1 beta subcomplex, 4, 15kDa	-1.09 *	218226_s_at
	NDUFB5	NADH dehydrogenase (ubiquinone) 1 beta subcomplex, 5, 16kDa	-1.09 *	203621_at
	NDUFB7	NADH dehydrogenase (ubiquinone) 1 beta subcomplex, 7, 18kDa	1.36 **	202839_s_at
	NDUFS1	NADH dehydrogenase (ubiquinone) Fe-S protein 1, 75kDa (NADH-coenzyme Q reductase)	-1.22 ***	203039_s_at
	NDUFS2	NADH dehydrogenase (ubiquinone) Fe-S protein 2, 49kDa (NADH-coenzyme Q reductase)	-1.18 **	201966_at
	NDUFS3	NADH dehydrogenase (ubiquinone) Fe-S protein 3, 30kDa (NADH-coenzyme Q reductase)	-1.10 *	201740_at
Complex II	SDHB	succinate dehydrogenase complex, subunit B, iron sulfur (Ip)	-1.11 *	202675_at
	SDHC	succinate dehydrogenase complex, subunit C, integral membrane protein, 15kDa	-1.19 *	210131_x_at
Complex III	UQCR10	ubiquinol-cytochrome c reductase, complex III subunit X	-1.13 *	218190_s_at
	UQCR11	ubiquinol-cytochrome c reductase, complex III subunit XI	1.22 **	202090_s_at
	UQCRFS1	ubiquinol-cytochrome c reductase, Rieske iron-sulfur polypeptide 1	-1.32 ***	208909_at
Complex IV	COX6B1	cytochrome c oxidase subunit VIb polypeptide 1 (ubiquitous)	-1.31 ***	201441_at
Cytochrome c oxidase	COX7A1	cytochrome c oxidase subunit VIIa polypeptide 1 (muscle)	-1.80 ***	204570_at
	SURF1	surfeit 1	-1.17 **	204295_at
Complex V	ATP5A1	ATP synthase, H+ transporting, mitochondrial F1 complex, alpha subunit 1, cardiac muscle	-1.12 **	213738_s_at
ATP synthase	ATP5B	ATP synthase, H+ transporting, mitochondrial F1 complex, beta polypeptide	-1.10 *	201322_at
	ATP5C1	ATP synthase, H+ transporting, mitochondrial F1 complex, gamma polypeptide 1	-1.40 ***	213366_x_at

Table 2B.

Mitochondria associated factors			
Gene symbol	Gene name	Fold change	Affymetrix ID
AIFM1	apoptosis-inducing factor, mitochondrion-associated, 1	-1.11 ***	205512_s_at
APH1B	anterior pharynx defective 1 homolog B (C. elegans)	-1.37 **	221036_s_at
BACE2	beta-site APP-cleaving enzyme 2	-1.11 *	217867_x_at
CAT	catalase	-1.45 ***	201432_at
CYB5R3	cytochrome b5 reductase 3	-1.10 *	201885_s_at
GLRX2	glutaredoxin 2	-1.28 *	219933_at
GPX4	glutathione peroxidase 4	1.21 *	201106_at
GSR	glutathione reductase	-1.31 *	205770_at
HSD17B10	hydroxysteroid (17-beta) dehydrogenase 10	-1.13 *	202282_at
MAP2K4	mitogen-activated protein kinase kinase 4	1.44 *	203266_s_at
PDHA1	pyruvate dehydrogenase (lipoamide) alpha 1	-1.15 *	200980_s_at
PSEN2	presenilin 2 (Alzheimer disease 4)	-1.15 *	211373_s_at
PSENEN	presenilin enhancer 2 homolog (C. elegans)	-1.26 *	218302_at
SDHAP1	succinate dehydrogenase complex, subunit A, flavoprotein pseudogene 1	-1.19 **	222021_x_at
TRAK1	trafficking protein, kinesin binding 1	1.18 *	202080_s_at
UCP2	uncoupling protein 2 (mitochondrial, proton carrier)	-3.22 ***	208998_at



2.4.3 Gene expression profile of Ad.*hPNPase*^{old-35}-infected melanoma cells

Overexpression of *hPNPase*^{old-35} causes growth inhibition in a number of cancer types and the growth prohibitive effects have been attributed to the downregulation of c-myc RNA by *hPNPase*^{old-35}. We performed a microarray analysis of HO-1 cells infected with Ad.*hPNPase*^{old-35} (Fig. 2.1.B) and compared the gene expression changes to cells infected with Ad.*vec* to identify transcripts differentially regulated as a result of *hPNPase*^{old-35} overexpression. A total of 310 transcripts were upregulated and 407 were downregulated significantly (FDR \leq 0.05) (Fig. 2.2).

Significant gene expression changes associated with adenoviral overexpression of *hPNPase*^{old-35} could be classified into the following molecular and cellular functional categories according to IPA (p-values ranging from 7.50E-16 – 2.05E-03): cell cycle, cellular growth and proliferation, cell death and survival, DNA replication, recombination and repair and cellular development (Fig. 2.7, Table S2A). Based on these functional categories, 25 biological gene networks were generated by IPA with a score ranging from 46 to 19 (Table S2D).

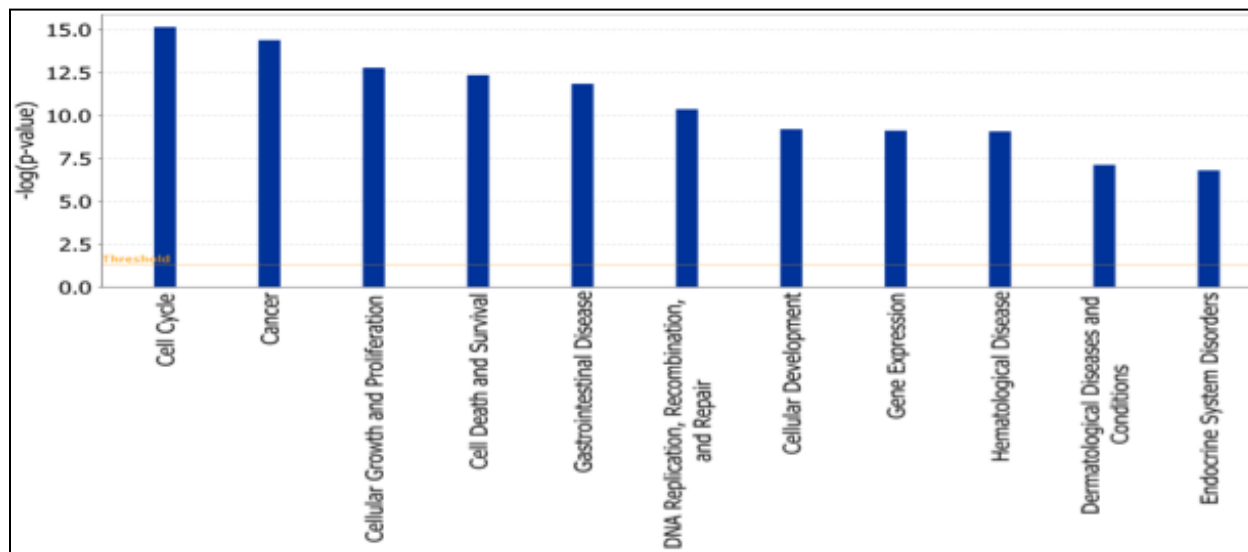


Fig. 2.7. The biological functions and states associated with genes differentially expressed when *hPNPase*^{old-35} is overexpressed in human melanoma cells, as identified by IPA.

The following are the most significant biological pathways altered when *hPNPase*^{old-35} was overexpressed: hereditary breast cancer signaling, p53 signaling, cell cycle control of chromosomal replication, IGF-1 and EIF2 signaling (Fig. 2.8, Table S2C).

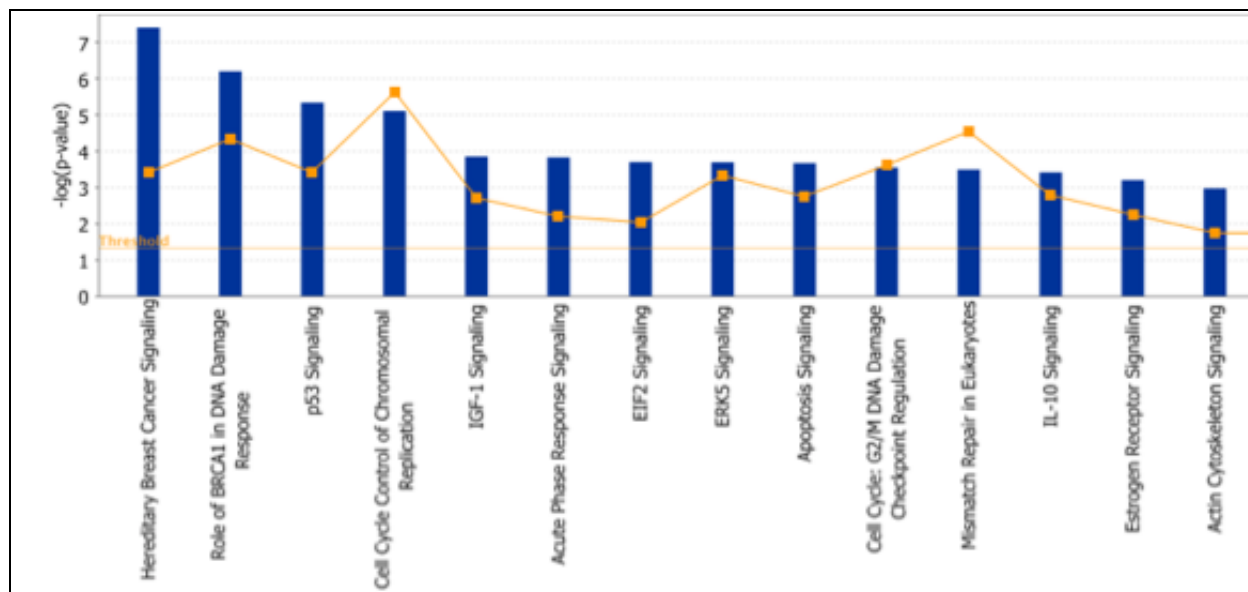


Fig. 2.8. Canonical pathways associated with genes differentially expressed when *hPNPase*^{old-35} is overexpressed in human melanoma cells.

In order to understand if these pathways were relevant to any disease phenotype, we made use of the IPA-Tox analysis which identified p53 signaling, decreases in Transmembrane Potential of Mitochondria and Mitochondrial Membrane (Table 2.3) and Cell Cycle: G2/M DNA Damage Checkpoint Regulation (Table 2.4) as some of the predicted significantly affected mechanisms (Fig. 2.9, Table S2B). The two main pathways we were interested to analyze further were the ones involved with cell cycle regulation and mitochondria, as there have been previous reports implicating a role for *hPNPase*^{old-35} in both of these cellular functions [47,93].

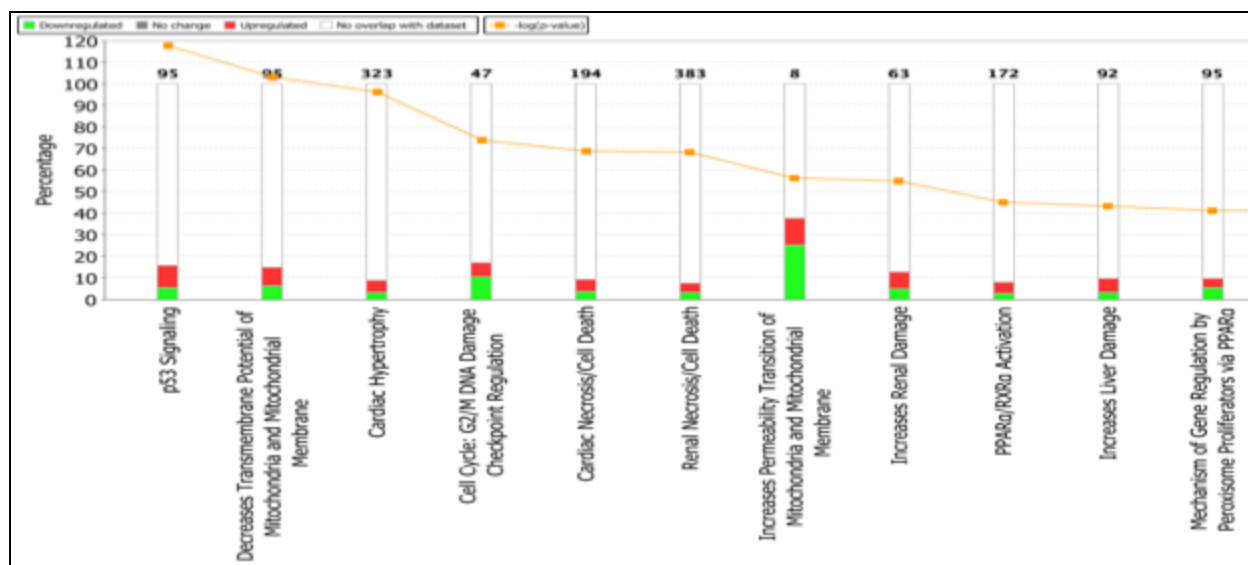


Fig. 2.9. Toxicologically related functionalities and pathways associated with genes dysregulated (proportions shown in graphs) after *hPNPase*^{old-35} overexpression in melanoma cells, as identified by IPA Toxicogenomic Analysis.

Overexpression of *hPNPase*^{old-35} causes growth inhibition, which is partially attributed to downregulation of *c-myc* [48], so it was not surprising to observe changes in gene expression related to cell cycle regulation. Some of the most significantly altered genes in this category were *CCNB2*, *CDK1*, *CHEK2* and *KAT2B*. Another interesting observation was the dysregulation of mitochondrial homeostasis, which again emphasizes a role of *hPNPase*^{old-35} in the mitochondria. These gene expression changes could be due to a direct role that *hPNPase*^{old-35} plays in the mitochondria or affects associated with growth inhibition caused by *hPNPase*^{old-35} overexpression. Some of these significantly altered genes were *FAS*, *BCL2L11* and *BIRC5* (Table 2.3).

Table 2.3. List of genes which are significantly altered as a result of *hPNPase*^{old-35} overexpression, and are functionally associated with the maintenance of mitochondrial transmembrane potential, according to IPA Toxicogenomic Analysis. FDR_≤0.05 = *, FDR_≤0.01 = **, FDR_≤0.005 = ***.

Gene Symbol	Gene Name	Fold Change	Affymetrix ID
APAF1	apoptotic peptidase activating factor 1	1.113**	211553_x_at
BARD1	BRCA1 associated RING domain 1	-1.414**	205345_at
BCL2L11	BCL2-like 11 (apoptosis facilitator)	1.351**	222343_at
BIRC5	baculoviral IAP repeat containing 5	-1.312**	202094_at
BNIP3	BCL2/adenovirus E1B 19kDa interacting protein 3	-1.280**	201848_s_at
CD47	CD47 molecule	1.148**	213857_s_at
CHEK2	checkpoint kinase 2	-1.387**	210416_s_at
CHMP5	charged multivesicular body protein 5	1.715**	218085_at
FAS	Fas (TNF receptor superfamily, member 6)	1.450**	204781_s_at
IFI6	interferon, alpha-inducible protein 6	1.345**	204415_at
NFKB1	nuclear factor of kappa light polypeptide gene enhancer in B-cells 1	-1.404**	209239_at
SLC25A14	solute carrier family 25 (mitochondrial carrier, brain), member 14	-1.155**	204587_at
SOD2	superoxide dismutase 2, mitochondrial	1.384**	216841_s_at
TGM2	transglutaminase 2 (C polypeptide, protein-glutamine-gamma-glutamyltransferase)	1.423**	201042_at

Table 2.4. List of genes which are significantly altered as a result of *hPNPase*^{old-35} overexpression, and are associated with G2/M DNA damage checkpoint regulation, according to IPA Toxicogenomic Analysis. FDR \leq 0.05 = *, FDR \leq 0.01 = **, FDR \leq 0.005 = ***.

Gene Symbol	Gene Name	Fold Change	Affymetrix ID
BRCA1	breast cancer 1, early onset	-1.235**	211851_x_at
CCNB2	cyclin B2	-1.217**	202705_at
CDK1	cyclin-dependent kinase 1	-1.496**	203214_x_at
CHEK2	checkpoint kinase 2	-1.387**	210416_s_at
KAT2B	K(lysine) acetyltransferase 2B	1.520**	203845_at
SKP1/SKP1P2	S-phase kinase-associated protein 1	1.173**	207974_s_at
YWHAB	tyrosine 3-monooxygenase/tryptophan 5-monooxygenase activation protein, beta polypeptide	-1.139**	217717_s_at
YWHAZ	tyrosine 3-monooxygenase/tryptophan 5-monooxygenase activation protein, zeta polypeptide	1.332**	200639_s_at

2.4.4 Identification of genes regulated by *hPNPase*^{old-35}

Bearing in mind that *hPNPase*^{old-35} is functionally an exoribonuclease, there could be two major mechanisms through which it could modulate gene expression; it could either degrade target genes directly (“*direct regulation*”) or it could degrade miRNAs (or mRNAs for other regulatory proteins) that in turn are regulators of certain genes (“*indirect regulation*”). Since we had gene expression patterns corresponding to both *hPNPase*^{old-35} overexpression and knockdown, we employed stringent criteria to identify genes that could be directly or indirectly regulated by *hPNPase*^{old-35}. Instead of making the obvious choice of selecting genes that were inversely related to the expression of *hPNPase*^{old-35} in either microarray dataset, we performed an overlapping screen with the help of the online tool VENNY [106] in order to identify transcripts whose expressions

changed inversely in both the datasets. This comparison resulted in the identification of 77 potential *hPNPase^{old-35}*-directly regulated genes that were up-regulated when *hPNPase^{old-35}* was depleted and down-regulated when *hPNPase^{old-35}* was overexpressed (Fig. 2.2.B; Table S3A, B). A second set of 61 transcripts that were downregulated when *hPNPase^{old-35}* was depleted by shRNA and up-regulated when *hPNPase^{old-35}* was overexpressed were also taken in consideration as potential *hPNPase^{old-35}*-indirectly regulated genes (Fig. 2.2.C; Table S3C, D). All the genes in these lists were significant with q-values ≤ 0.05 .

In order to place the *hPNPase^{old-35}*-regulated genes into functional categories, we made use of the ToppFun function of the ToppGene suite of web applications. A summary of the GO categories with the maximum number of genes and the most significant p-values is provided in Table 2.5.

Table 2.5. Functional and structural categories of genes associated with *hPNPase^{old-35}*-driven regulation.

Functional category	Source	p-value	no. of genes
“Directly” regulated genes			
RNA binding	GO: Molecular Function	6.21E-05	13/894
Chromosome organization	GO: Biological Process	1.28E-06	19/751
Cell cycle	GO: Biological Process	1.28E-06	25/1460
Chromosome	GO: Cellular Component	1.46E-10	21/671
Mitotic Prometaphase pathway	MSigDB	3.62E-02	6/92
“Indirectly” regulated genes			
Response to wounding	GO: Biological Process	5.43E-03	16/1168
Vacuole	GO: Cellular Component	4.74E-03	9/424
Integral to plasma membrane	GO: Cellular Component	4.81E-02	13/1328
CD molecules	Gene Family (genenames.org)	3.45E-04	5/276
miR-124a	MicroRNA (PicTar)	4.04E-02	11/626

The *hPNPase*^{old-35}-directly regulated genes represent significant enrichment related to RNA binding, chromosome organization and cell cycle associated (*CENPE*, *MKI67*, *POLD3*, *MCM4*) functions (Table S4A). To determine how the *hPNPase*^{old-35}-regulated genes might interact with each other, gene symbols were uploaded into GeneMANIA. The directly-regulated genes form a densely correlated network with overlapping functional categories akin to organelle fission, chromosome segregation and DNA strand elongation as predicted by the gene functional analysis (Fig. 2.10). There was an over-representation of genes related to cellular response to wounding (*TGM2*, *SDC2*, *MCAM*), genes belonging to the CD family of cell surface receptors (*DDR1*, *JAG1*, *CD164*, *MCAM*, *CD47*), and miR-124a predicted targets (*SLC7A8*, *JAG1*, *SDC2*, *CADM1*, *RNF128*) in the *hPNPase*^{old-35}-indirectly regulated genes dataset (Table S4B). These probe sets also form a network cluster comprised mainly of co-expressed genes (Fig. 2.11). The inter-gene correlations between probe sets defined as being potentially directly or indirectly regulated by *hPNPase*^{old-35} were largely based on publically available co-expression association data.

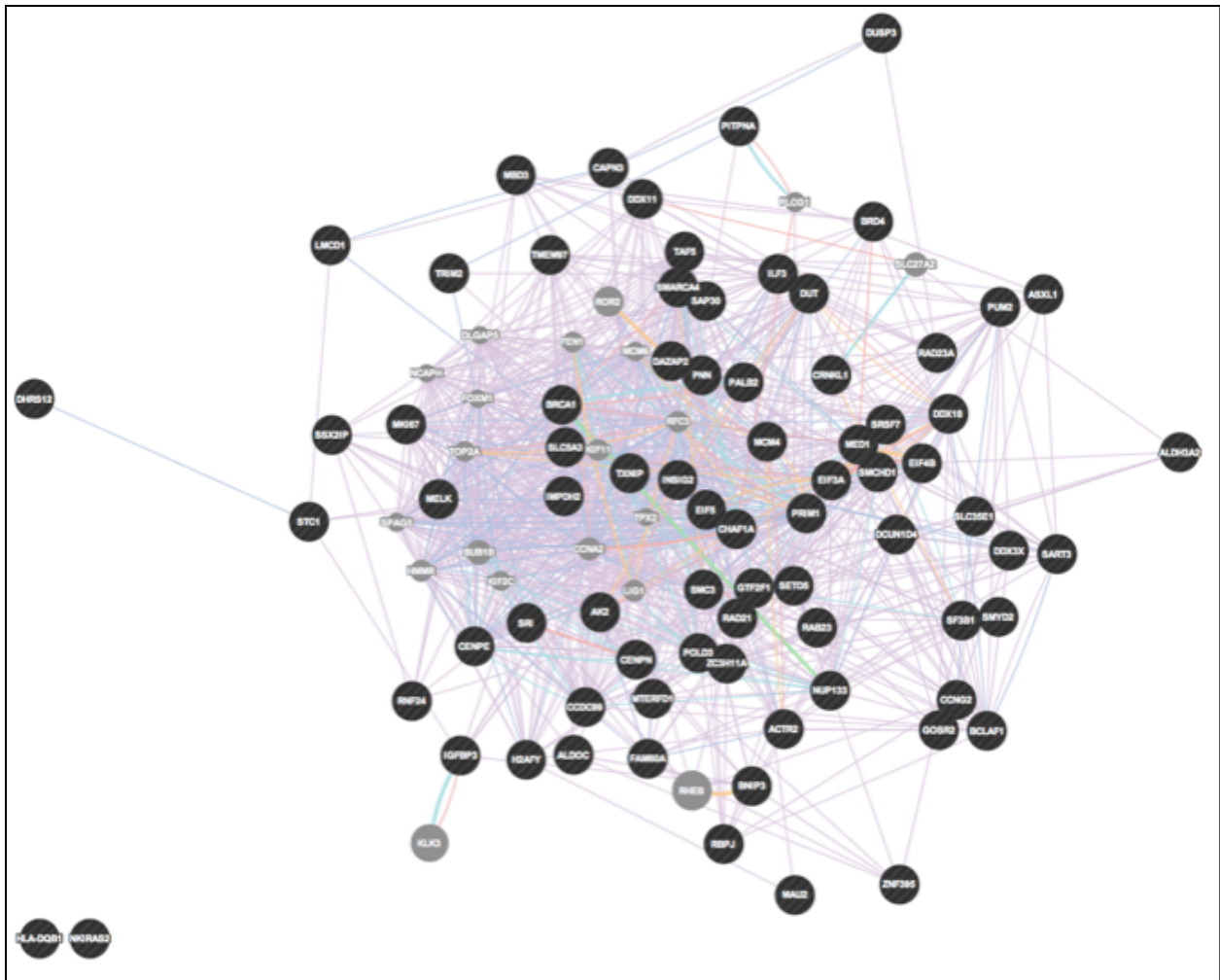


Fig. 2.10. Network visualization of genes potentially “*directly*” regulated by *hPNPase*^{old-35}.

correlation with *hPNPase*^{old-35} expression in the HO-1 melanoma cell line as shown in Figs. 2.12 and 2.13 (putative “direct target”: *CENPE*, *MKI67*; putative “indirect targets”: *VGF*, *RNF128*). *CENPE* and *MKI67* were chosen for validation as they were also identified in an overlapping screen we performed between *hPNPase*^{old-35}-knockdown cells and a doxycycline inducible *hPNPase*^{old-35} overexpression system in HeLa cells (Chapter 3) and showed a 20-40% increase upon *hPNPase*^{old-35} knockdown and >40% decrease following *hPNPase*^{old-35} overexpression at the RNA level. *VGF* and *RNF128* were chosen as they showed the maximum fold change in the *hPNPase*^{old-35}-knockdown cells and showed >40-80% decrease by qRT-PCR following *hPNPase*^{old-35} knockdown and ~20-50% increase following *hPNPase*^{old-35} overexpression. Statistical analysis determined using one-way analysis of variance followed by Dunnett’s multiple comparison test in case of *hPNPase*^{old-35} knockdown samples and by a two tailed student’s t-test in case of *hPNPase*^{old-35} overexpression samples, where *= P< 0.05, **= P< 0.01 and ***=P< 0.001.

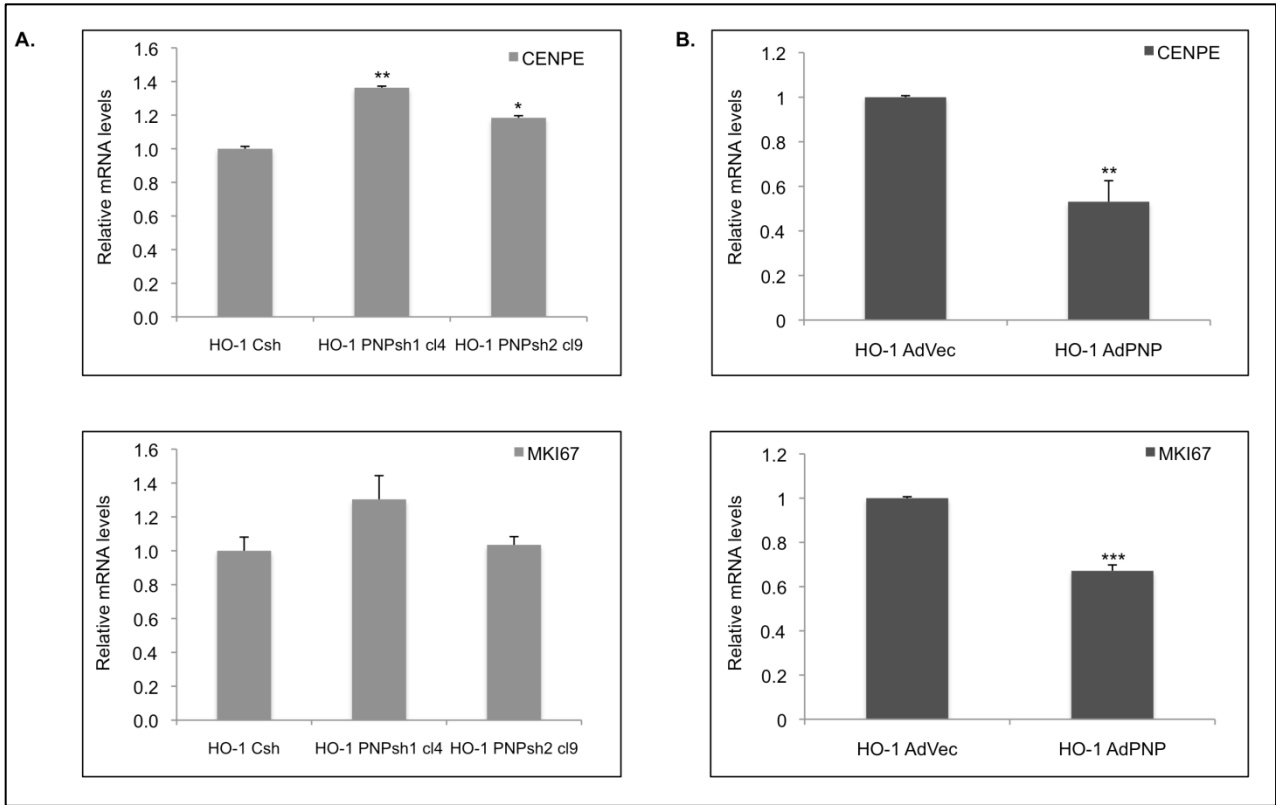


Fig. 2.12. qRT-PCR verification of *hPNPase*^{old-35}-putative “directly” regulated genes identified by microarray analyses in response to *hPNPase*^{old-35} (A) knockdown or (B) overexpression in HO-1 melanoma cells. Error bars represent mean ± S.E. error of three replicate experiments.

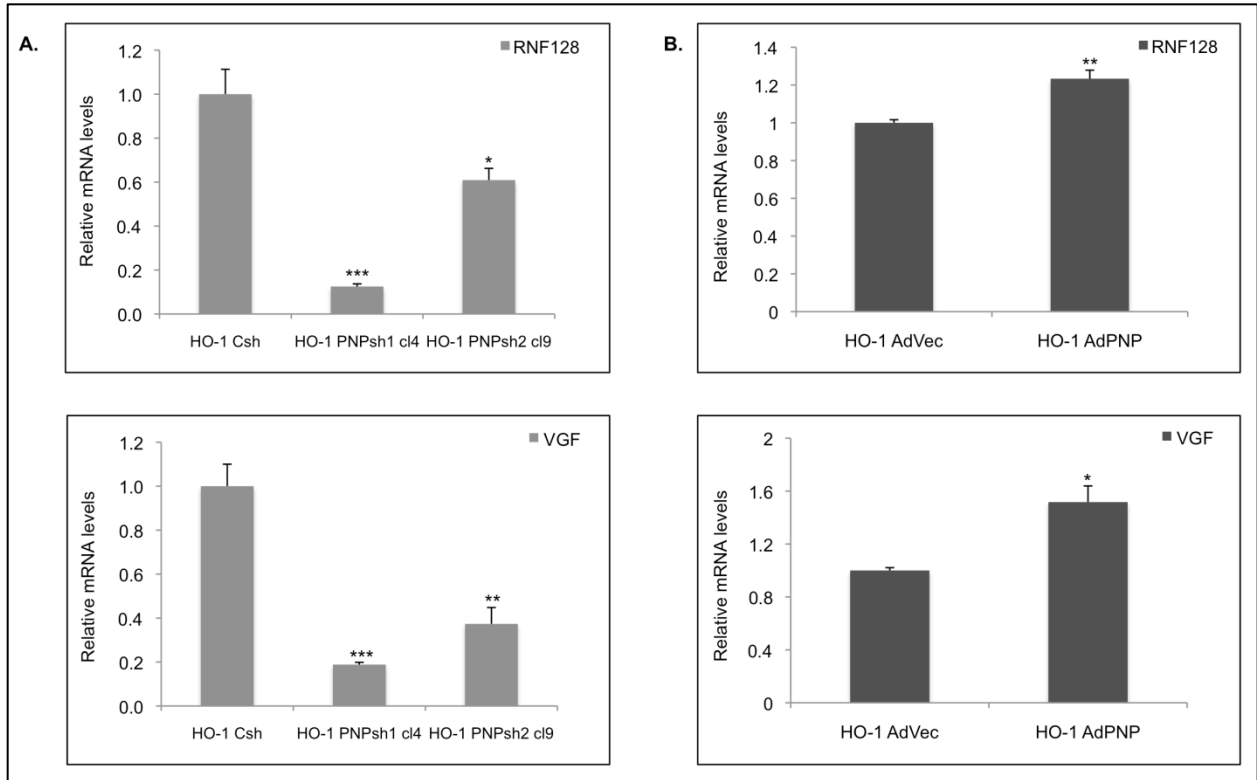


Fig. 2.13. qRT-PCR verification of *hPNPase*^{old-35}-putative “indirectly” regulated genes identified by microarray analyses in response to *hPNPase*^{old-35} (A) knockdown or (B) overexpression in HO-1 melanoma cells. Error bars represent mean ± S.E. of three replicate experiments.

Transient knockdown of *hPNPase*^{old-35} using siRNA also showed the inverse correlation of *hPNPase*^{old-35} expression with potential direct targets *CENPE*, *MKI67* (qRT-PCR validation showed a ~20% increase in both) and indirect targets *VGF*, *MCAM* (qRT-PCR validation showed a ~20% decrease in both) (Figure 2.14). Statistical analysis determined using a two tailed student’s t-test, where *= P< 0.05, **= P< 0.01 and ***=P< 0.001.

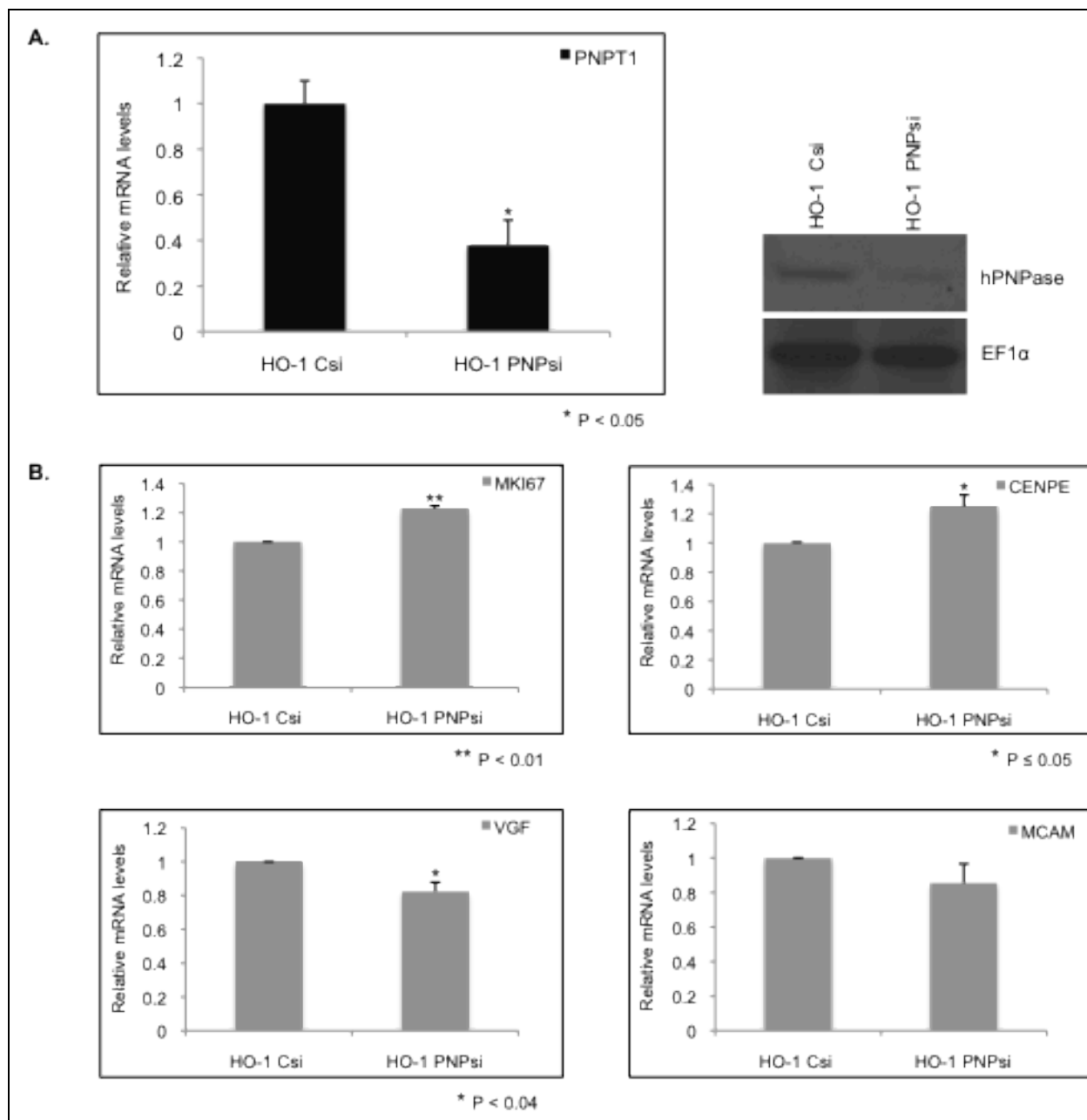


Fig. 2.14. (A) qRT-PCR expression of *hPNPase*^{old-35} following transient transfection with siRNA against *hPNPase*^{old-35} normalized to scrambled control post 48 hour. Immunoblot showing *hPNPase*^{old-35} levels after siRNA transfection. (B) qRT-PCR verification of *hPNPase*^{old-35}-putative (i) “directly” and (ii) “indirectly” regulated genes after *hPNPase*^{old-35} transient silencing post 48 h. Error bars represent mean ± S.E. of two replicate experiments.

The expression changes of four putative *hPNPase*^{old-35}-directly and indirectly regulated genes were also validated using another melanoma cell line WM35 (Figs. 2.15-17). *MKI67* and *CENPE* showed a 1.2 and 1.5 fold increase at the RNA level following *hPNPase*^{old-35} knockdown respectively. Following *hPNPase*^{old-35} overexpression in WM35 cells, *MKI67* and *CENPE* levels reduced 30 and 20% respectively. Both *VGF* and *MCAM* RNA levels reduced 20% upon *hPNPase*^{old-35} knockdown. Overexpression of *hPNPase*^{old-35} resulted in a 1.2 and 1.4 fold increases in *MCAM* and *VGF* RNA levels. Statistical significance was determined using a two-tailed student's t-test.

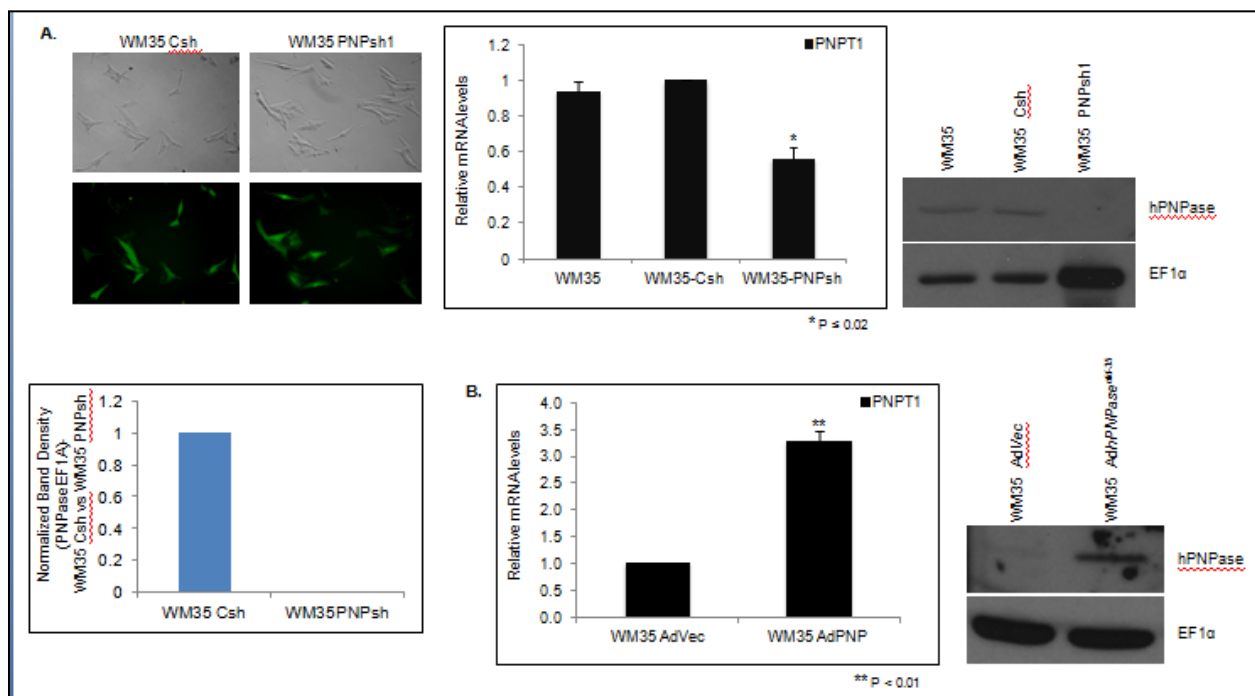


Fig. 2.15. (A) Phase contrast LM (top) and GFP fluorescent micrographs (bottom) of WM35 melanoma cells following transduction with GFP expressing scrambled shRNA and *hPNPase^{old-35}* shRNA1 expressing lentiviruses and selection with puromycin. qRT-PCR expression of *hPNPase^{old-35}* (*hPNPase^{old-35}* knockdown) normalized to control (shScramble). Mean values normalized to a GAPDH internal reference; error bars represent mean \pm S.E. of three replicate experiments. Anti-*hPNPase^{old-35}* and EF1 α loading control immunoblots. (B) qRT-PCR expression of *hPNPase^{old-35}* in WM35 cells infected with Ad.*hPNPase^{old-35}* normalized to cells infected with Ad.Vec for 36 hour. Immunoblot showing *hPNPase^{old-35}* overexpression compared to Ad.Vec post 36 hour of infection. Error bars represent mean \pm S.E. of three replicate experiments. * $P < 0.02$, ** $P < 0.01$.

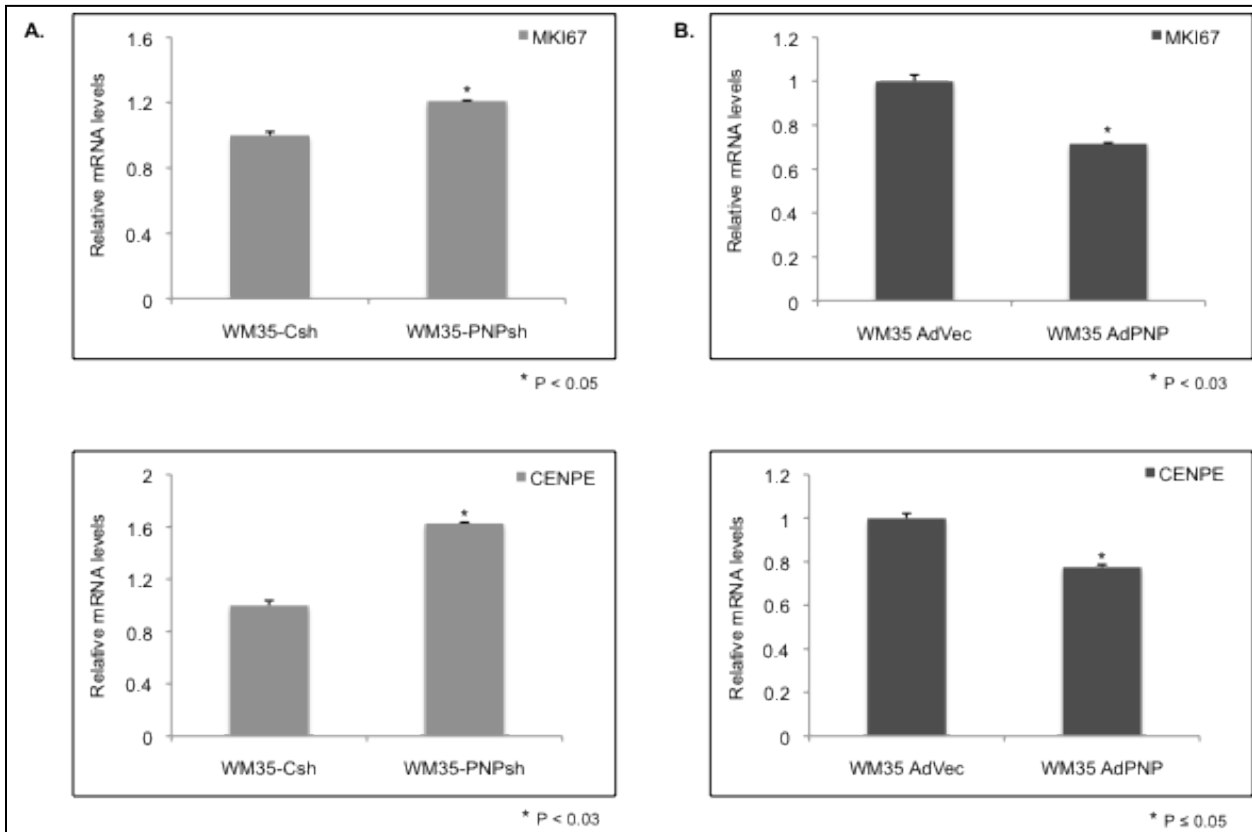


Fig. 2.16. qRT-PCR verification of *hPNPase^{old-35}*-putative "directly" regulated genes identified by microarray analyses in response to *hPNPase^{old-35}* (A) knockdown or (B) overexpression in WM35 melanoma cells. Error bars represent mean \pm S.E. of two replicate experiments done in triplicate.

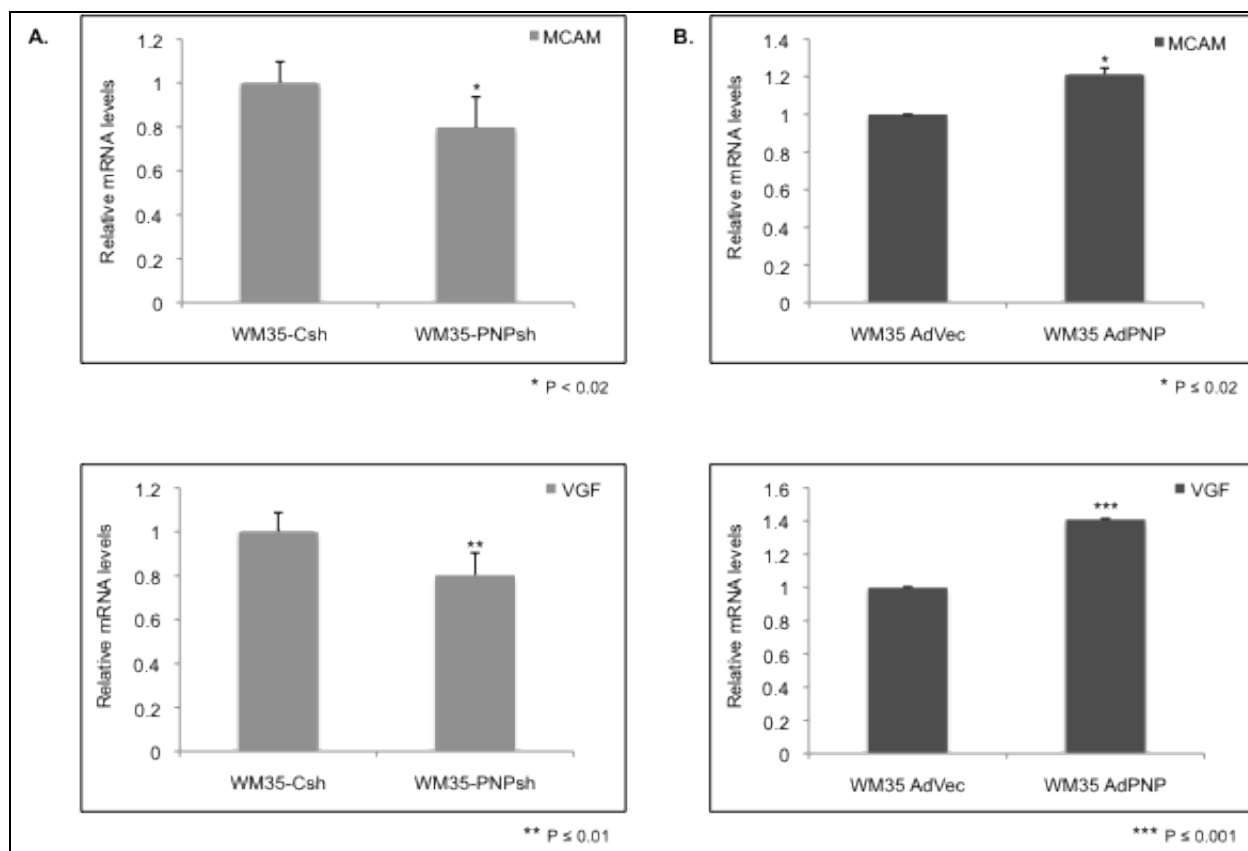


Fig. 2.17. qRT-PCR verification of *hPNPase*^{old-35}-putative “indirectly” regulated genes identified by microarray analyses in response to *hPNPase*^{old-35} (A) knockdown or (B) overexpression in WM35 melanoma cells. Error bars represent mean ± S.E. of two replicate experiments done in triplicate.

Finally, some of the *hPNPase*^{old-35} direct and indirect targets were validated by qRT-PCR in two additional melanoma cell lines (C8161 and MeWo) following transient knockdown of *hPNPase*^{old-35} in order to show that the decrease or increase in transcript levels was not due to indirect effects of stable knockdown. Direct target *CENPE* showed a ~1.2 fold increase in C8161 and MeWo cells both; *MKI67* showed a 1.2 fold increase in C8161 cells at the RNA level. Levels of indirect targets *MCAM* and *RNF128* decreased 40 and 50% in C8161 cells and 10 and 20% in MeWo melanoma cells.

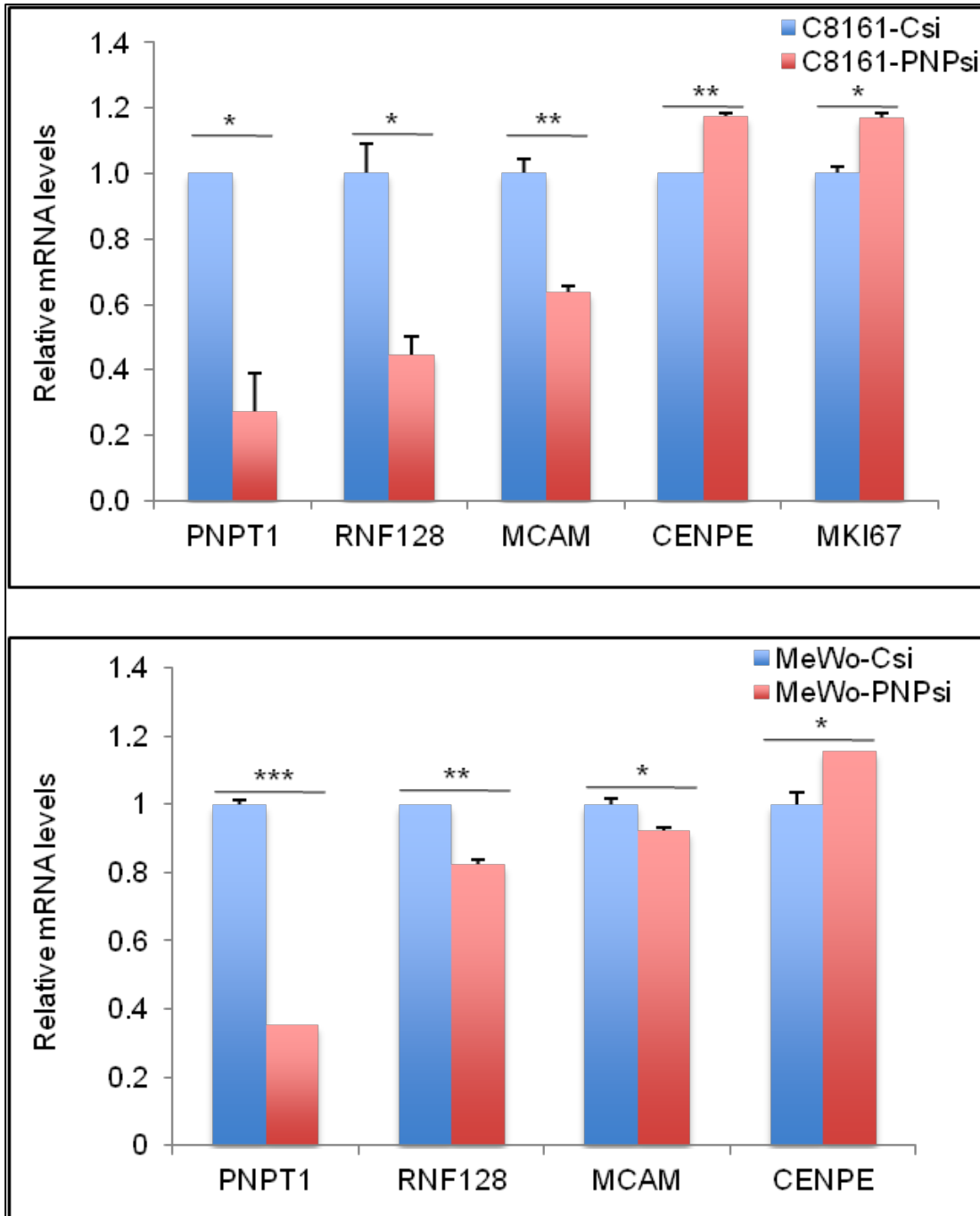


Fig. 2.18. qRT-PCR expression of *hPNPase^{old-35}* following transient transfection with siRNA against *hPNPase^{old-35}* normalized to scrambled control post 48 h in C8161 (A) and MeWo (B) melanoma cells. Error bars represent mean \pm S.E. of two replicate experiments. Statistical significance determined using two-tailed student's t-test, * $P < 0.05$, ** $P < 0.01$, *** $P < 0.001$.

2.4.5 *hPNPase*^{old-35} stable knockdown in melanoma cells and invasion

Analysis of the microarray results following *hPNPase*^{old-35} stable knockdown in HO-1 melanoma cells revealed gene expression changes in numerous genes associated with cellular invasion. Thus we decided to analyze any effect that stable knockdown of *hPNPase*^{old-35} may have on cellular invasion using matrigel based Boyden chambers. We observed that stable knockdown of *hPNPase*^{old-35} in HO-1 melanoma cells resulted in a ~2-3 fold increase in *in vitro* invasion in two *hPNPase*^{old-35} knockdown clones we tested (Figure 2.19A). Next we checked the relative mRNA levels of a few of the genes that maybe related to cellular invasion based on our knowledge of current literature. We observed a ~6-10 fold increase in the levels of *EMR1* (egf-like module containing, mucin-like, hormone receptor-like 1; a gene that was the most upregulated (3 fold) transcript in our *hPNPase*^{old-35} knockdown microarray results), a ~2 fold increase in *MMP2* (matrix metalloproteinase 2) , *FN1* (fibronectin 1) and *CADM3* (cell adhesion molecule 3) (Figure 2.19B). *MMP2* and *FN1* are well-studied proteins that have been known to be involved in the invasion-related functions of numerous cancer cell types, and currently we believe that the slight increase we observe in their levels could be an indirect effect (could be miRNA related) of *hPNPase*^{old-35} knockdown rather than a direct effect mediated by *hPNPase*^{old-35} degradation of these transcripts. On the other hand, there are no known reports relating *EMR1* or *CADM3* to invasion, but we were interested to pursue them, as they are cell surface receptors and could potentially play a role in cell-cell signaling events. There are some studies where the homologues of *EMR1*, *EMR2* and 3, have been associated with poor prognosis and an invasive phenotype in glioblastoma. Thus we decided to check *EMR1* levels in another

melanoma cell line, WM35 following stable *hPNPase*^{old-35} knockdown, but we did not observe an increase in its levels, instead we observed a decrease (Figure 2.20). Thus at the current moment we believe that *EMR1* is probably an indirect target of *hPNPase*^{old-35} whose levels may probably be regulated by certain miRNA species and the modest increase in invasion we observe following *hPNPase*^{old-35} knockdown in HO-1 melanoma cells may be attributed to the cumulative upregulation of cellular invasion related genes like *EMR1*, *MMP2*, *FN1*. Future studies in additional melanoma cell lines would be required and levels of other invasion related genes (levels of other *EMR1* homologues like *EMR2* and *3* may also be checked) or miRNAs would need to be determined in order to evaluate the mechanism behind the increase in cellular invasion observed following stable *hPNPase*^{old-35} knockdown.

Since we saw an increase in *EMR1* levels upon *hPNPase*^{old-35} knockdown at least in HO-1 melanoma cells, we were still interested to pursue this molecule further and see if there was any correlation between *EMR1* and *hPNPase*^{old-35} levels in tumor versus normal tissue samples to analyze if there was any potential biological significance of this hypothesized indirect effect of *hPNPase*^{old-35} knockdown on *EMR1* levels. In order to do this we purchased multiple melanoma tissue array slides with tissue sections from normal and different tumor stages and performed immunohistochemistry (IHC) with *hPNPase*^{old-35} and *EMR1* specific antibodies. Visual observation of the stained IHC slides showed that *EMR1* levels seem to increase and *hPNPase*^{old-35} levels decrease with tumor stage (Stage II-IV) (Figure 2.21). Also the adjacent normal tissue sections seem to have higher levels of *hPNPase*^{old-35} and lower levels of *EMR1* compared to their tumor counterparts. From this preliminary result we

can conclude that there seems to be an inverse correlation between $hPNPase^{old-35}$ and $EMR1$ levels, which may or may not be due to $hPNPase^{old-35}$ direct or indirect regulation. Future studies would be required to further explore this premise and as suggested earlier, identification of $hPNPase^{old-35}$ –degradable miRNA species regulating $EMR1$ may allow recognition of therapeutic opportunities for cancers with high levels of $EMR1$.

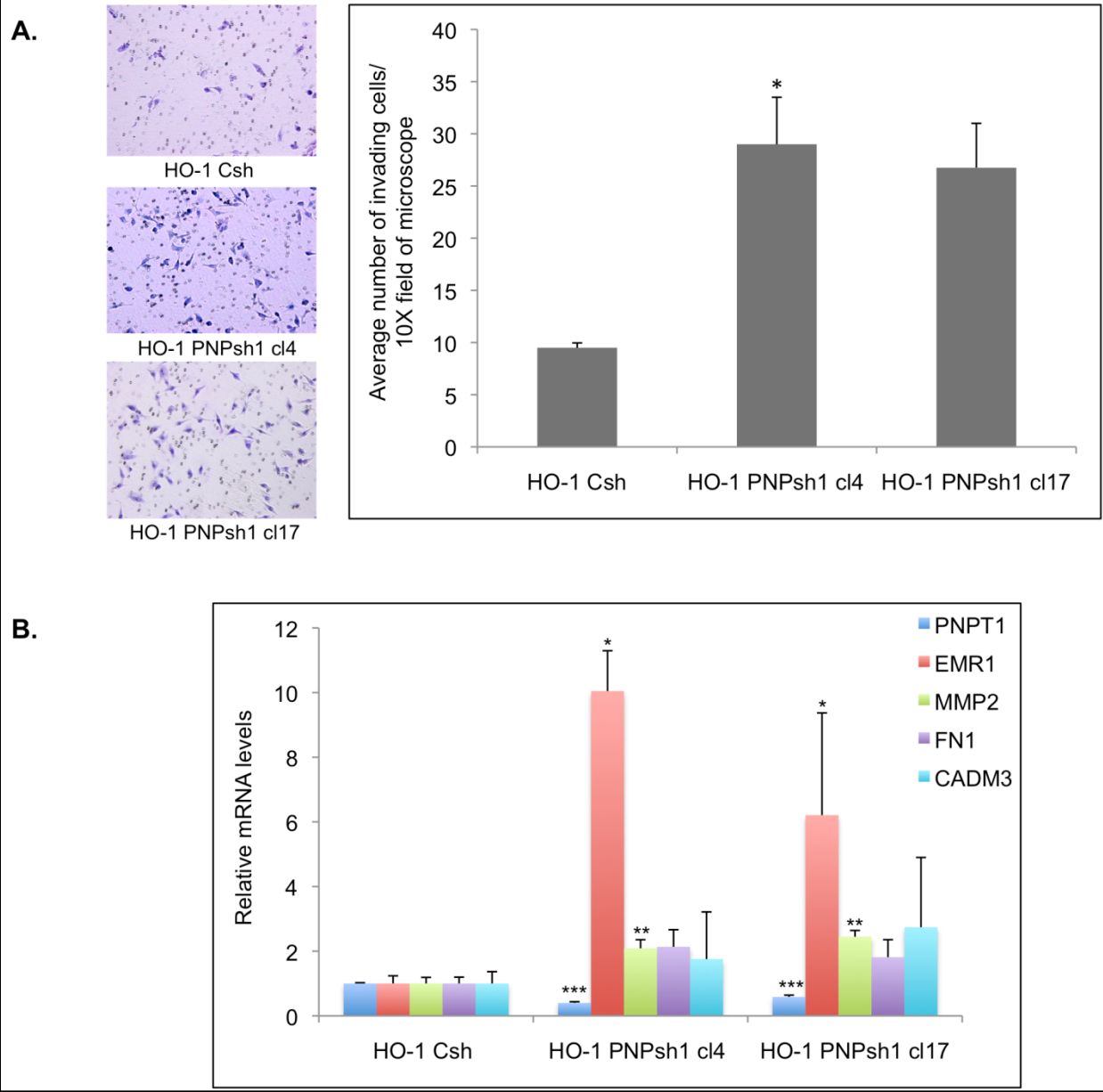


Fig. 2.19. *hPNPase^{old-35}* knockdown and invasion of HO-1 melanoma cells (A) Invasion assay images and graphical representation of invasion assay results of scrambled shRNA control and *hPNPase^{old-35}* shRNA stably transduced HO-1 melanoma cells. Error bars represent mean \pm standard error of two independent experiments done in duplicate. (B) qRT-PCR validation of invasion related genes identified in microarray results. Error bars represent mean \pm standard error of three independent experiments done in triplicate. Statistical significance was determined using a one-way analysis of variance followed by Dunnett's multiple comparison test. * $P < 0.05$, ** $P < 0.01$, *** $P < 0.001$.

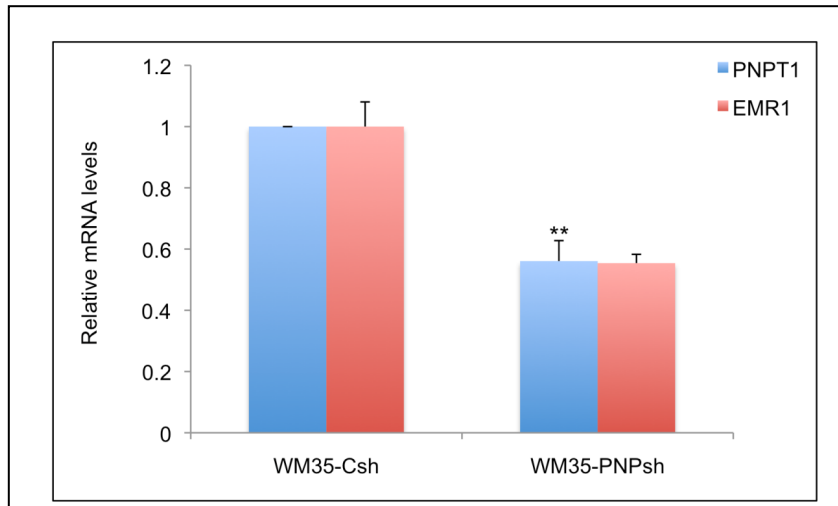


Fig. 2.20. qRT-PCR validation of *hPNPase^{old-35}* and *EMR1* levels in WM35 melanoma cells following stable *hPNPase^{old-35}* knockdown. Error bars represent mean \pm standard error of two independent experiments done in triplicate. **P<0.01.

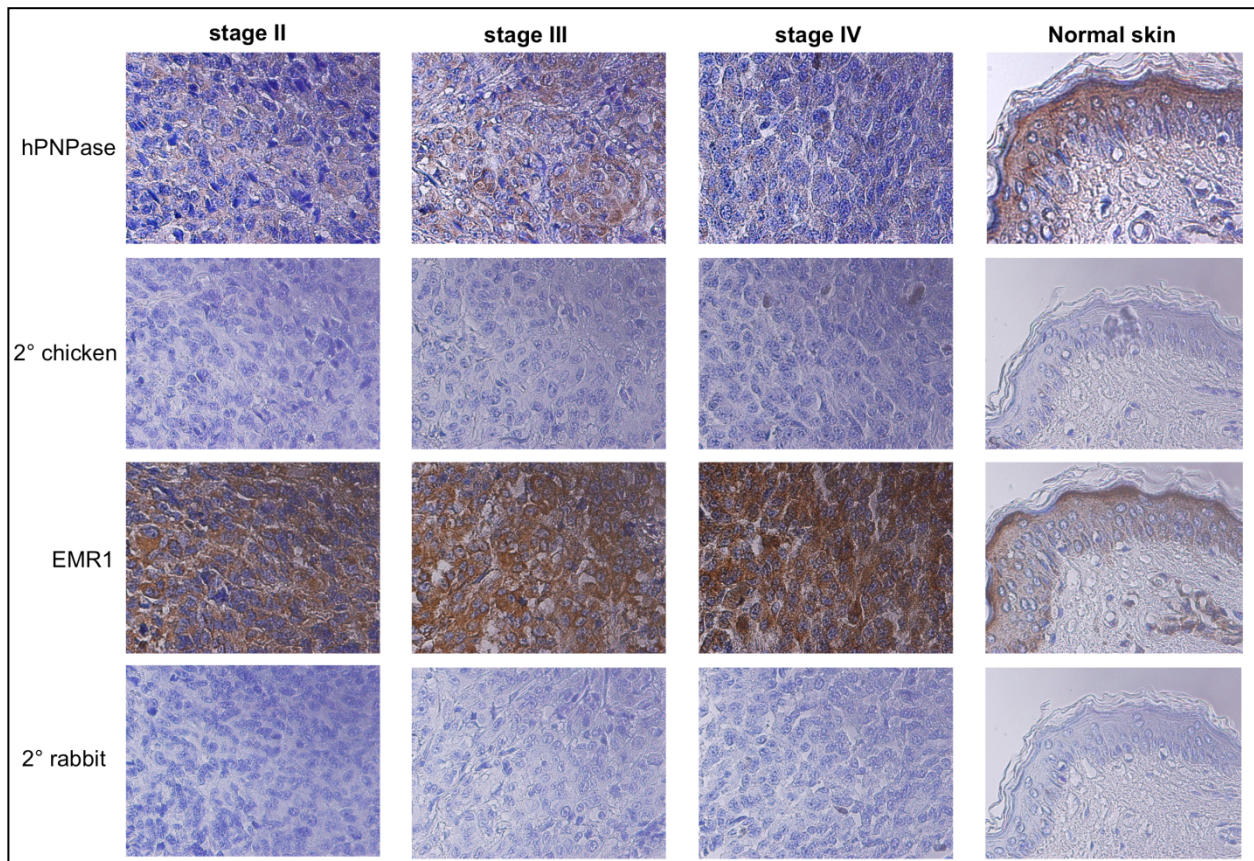


Fig. 2.21. Representative images of immunohistochemistry analysis of multiple malignant melanoma tissue arrays.

2.5 Discussion

Numerous studies performed over the past decade have utilized the RNAi methodology to evaluate the functions of *hPNPase*^{old-35}. Most of these studies concentrated on studying the role of *hPNPase*^{old-35} in reference to its mitochondrial location with special emphasis on mtRNA processing, maintenance of mitochondrial homeostasis and more recently its role in mitochondrial RNA import [44,47,50,51,76,87]. In other studies, overexpression of *hPNPase*^{old-35} has been shown to cause growth inhibition attributed to downregulation of c-myc and miR-221 by its exoribonuclease activity in the cytosol [48,49]. In this study we have incorporated both these classic genetic approaches of gene knockdown and overexpression to further understand *hPNPase*^{old-35} functions on a more comprehensive level. This is the first attempt of its kind aimed at studying global gene expression changes resulting from *hPNPase*^{old-35} knockdown or overexpression in order to identify unique genes regulated by *hPNPase*^{old-35}. In this manuscript we focus on the analysis of gene expression patterns of the most relevant biological pathways of *hPNPase*^{old-35} potential functions.

Our results show that stable knockdown of *hPNPase*^{old-35} in melanoma cells affects mitochondrial function and cholesterol biosynthesis. Other groups have previously reported the importance of *hPNPase*^{old-35} in the maintenance of mitochondrial homeostasis through knockdown and liver specific knockout experiments where they showed a deregulation of the various respiratory complexes in the Electron Transport Chain (ETC) following *hPNPase*^{old-35} silencing [44,47]. These results further strengthen those findings. In this study we report novel genes (Table 2.2) that encode for proteins constituting the various ETC respiratory complexes, which were differentially expressed

in our *hPNPase*^{old-35} knockdown melanoma cells. Some mitochondrial accessory factors were also affected and one of them *UCP2* [107], which is a mitochondrial anion transporter that plays a role in energy dissipation and maintenance of mitochondrial membrane potential was downregulated ~3-fold (Fig. 2.6.B). The exact mechanism of how *hPNPase*^{old-35} regulates these genes remains to be elucidated and the possibilities may be numerous ranging from RNA degradation, miRNA regulation or RNA import. Moreover, recently mutations in *hPNPase*^{old-35} have also been identified that impair respiratory-chain activity [108]. The ETC genes identified in this study identify the specific genes affected by *hPNPase*^{old-35} that maybe causative for mitochondrial dysfunction. Further studies aimed at understanding the functional implications of the identified genes may provide valuable insight to the physiological role of *hPNPase*^{old-35} in mitochondrial diseases and discovering suitable therapeutic options.

We also identified genes belonging to the cholesterol biosynthesis pathway that were significantly downregulated with depletion of *hPNPase*^{old-35}. This is a novel and potentially biologically important result since association of *hPNPase*^{old-35} with this pathway has not been previously reported. Mitochondrial dynamics have been linked to steroid biosynthesis and the gene expression changes we observed pertaining to cholesterol biosynthesis could be a consequence of mitochondrial dysfunction, or vice versa. Additionally, since this analysis was performed in a stable cell line in which *hPNPase*^{old-35} was silenced, certain compensatory changes could be acquired over time as opposed to primary effects of gene knockdown. On the other hand *hPNPase*^{old-35} could indeed directly regulate the RNA levels of these genes or alter their expression by regulating upstream transcriptional control elements. *SREBF2* is one such transcription

factor that was found to be downregulated 1.3-fold in our microarray analyses which regulates the expression of *HMGCR* (Fig. 2.6.A), *HMGCS1* and *IDI1*. Further studies to address and evaluate these possibilities would be required to assess the relevance of *hPNPase*^{old-35} in this context.

Previous studies have shown that adenoviral overexpression of *hPNPase*^{old-35} induces growth suppression and a senescence-like phenotype [17,48]. Our present analyses show that the majority of genes differentially expressed as a result of adenoviral overexpression of *hPNPase*^{old-35} compared to the empty vector control (Ad.Vec) belong to cell cycle, cellular assembly and organization categories. Biological pathways likely affected as a consequence of the gene expression changes included cell cycle control of chromosomal replication. Key genes down-regulated more than 1.5-fold in this category belonged to the mini-chromosome maintenance complex (*MCM2*, *MCM4-7*) that is essential for eukaryotic DNA replication. Important regulators of G2/M DNA damage checkpoint control; *CCNB2*, *CHEK2* and *CDK1* were also downregulated. The gene expression changes of these cell-cycle regulators may contribute towards tipping the balance in the cell in the direction of growth inhibition. Also, changes in gene expression were identified in apoptosis regulatory molecules. *FAS*, *BIK* and *BCL2L11* (pro-apoptotic) expression was increased and *BIRC5* (anti-apoptotic) levels were reduced significantly, which may have played a role in decreasing the transmembrane potential of the mitochondrial membrane observed upon *hPNPase*^{old-35} overexpression in the IPA analyses, an important phenomenon implicated in apoptosis [109]. These findings provide new information regarding the cell-cycle associated implications of *hPNPase*^{old-35} overexpression and provide targets for further studies. These findings are

also supported by previous studies; where it was shown that terminal differentiation (which shares overlapping characteristics with cellular senescence) of HO-1 melanoma cells caused by combination treatment with IFN- β plus the protein kinase C activator mezerein resulted in global gene expression reductions of cell-cycle associated genes [110,111]. *hPNPase*^{old-35} is a Type I-IFN inducible early response gene [42]; thus it was not surprising that we observed a similar pattern of gene expression changes in our present study involving *hPNPase*^{old-35} overexpression. The candidate genes identified may also provide insight regarding the role of *hPNPase*^{old-35} in aging-associated inflammation [74,79]. Some of the potentially biologically significant genes in this category were *CAPN3*, *BIRC5*, *TRIM2*, *CENPF*, *FN1*, *BCL6* and *GMNN*. This premise needs further attention, as it is evident that the cell-cycle changes associated with *hPNPase*^{old-35} overexpression are diverse and complex. Also, c-myc is a key regulator of cell-cycle progression, which is targeted by *hPNPase*^{old-35} for degradation. Bearing this in mind, in the present study we chose an earlier time point of 36 hours, before changes in the *c-myc* transcript levels were evident, to study Ad.*hPNPase*^{old-35} associated gene expression changes. Even so, in order to identify genes directly targeted by *hPNPase*^{old-35} irrespective of *c-myc* status we plan to study the effects of *hPNPase*^{old-35} overexpression in a *c-myc* null background [112,113].

To identify additional genes regulated by *hPNPase*^{old-35}, we ascertained transcripts in our two separate datasets (i.e. *hPNPase*^{old-35} knockdown and overexpression) whose expression inversely correlated with *hPNPase*^{old-35}. This novel strategy helped us detect 77 potential “*directly*” (mRNA degraded by *hPNPase*^{old-35}) and 61 potential “*indirectly*” (miRNAs targeting these transcripts degraded by *hPNPase*^{old-35})

regulated transcripts. Although in this study we have concentrated on this small list of genes identified through the overlapping approach between our *hPNPase*^{old-35} depleted and overexpression datasets, future studies would be required to analyze the remaining genes whose expression is also regulated by *hPNPase*^{old-35} but do not fall in this list (Figs. 2.2.B-C). Most of these potential “*direct*” targets were genes implicated in cell-cycle associated functions and two of them have been validated by qRT-PCR; *CENPE* (Centromere protein E) which is involved in mitotic checkpoint control [114,115] and *MKI67* (antigen identified by monoclonal antibody Ki-67), a known cellular proliferation marker implicated in rRNA synthesis [116-118]. Since most of the genes thought to be “*directly*” regulated belong to a closely associated network of cell cycle regulatory functions, at this point it is difficult to say whether these gene expression changes represent global effects of *hPNPase*^{old-35} deregulation caused by key upstream regulators or if they are genes that are directly targeted by *hPNPase*^{old-35} for degradation. Future studies using *in vitro* mRNA degradation assays will help answer these questions. Among the “*indirectly*” regulated targets, a fraction of genes were identified that had conserved sites for miR-124a (Table S4). We validated one of these genes by qRT-PCR; *RNF128* (ring finger protein 128) an E3 ubiquitin ligase that is involved in the regulation of cytokine gene transcription [119]. Another potential indirect target we validated was *VGF* (VGF nerve growth factor inducible), which encodes a neuro-endocrine polypeptide implicated in a vast array of biological phenomena that include energy metabolism and inflammation [120-122]. Identification and subsequent validation of miRNAs targeting the genes we identified would aid in clarifying the role of

hPNPase^{old-35}, if any, in the context of the relevant biological processes these genes are implicated in and would further allow appropriate therapeutic intervention.

In summation, this study has produced a novel genetic and genomic analysis of the functional implications for alterations in PNPT1 gene expression. Our analysis has identified a limited set of candidate genes for direct regulation by *hPNPase*^{old-35}. Such genes could provide novel targets for intervention in *hPNPase*^{old-35}-related disease states. Furthermore, this work has generated a comprehensive database of *hPNPase*^{old-35}-responsive genes that are potentially relevant to the mechanisms of global cellular functions affected by this important regulatory molecule.

CHAPTER THREE

Analysis of global changes in gene expression induced by human polynucleotide phosphorylase (*hPNPase*^{old-35})

3.1 Abstract

In an attempt to identify gene expression changes induced by human polynucleotide phosphorylase (*hPNPase*^{old-35}) we performed genes expression analysis of HeLa cells in which *hPNPase*^{old-35} was overexpressed and compared these changes to HO-1 melanoma cells in which stably knocked down *hPNPase*^{old-35}. We identified 90 transcripts following this analysis which positively or negatively correlated with *hPNPase* expression and most of which were associated with cell communication, cell cycle and chromosomal organization gene ontology categories. Some of these genes were also identified in four TCGA (The Cancer Genome Atlas) datasets we screened, colon adenocarcinoma (COAD), skin cutaneous melanoma (SKCM), ovarian serous cyst adenocarcinoma (OV), and prostate adenocarcinoma (PRAD), with expressions correlating with *hPNPase*^{old-35} as we identified in our microarray analysis. Further analysis comparing the gene expression changes between Ad.*hPNPase*^{old-35} infected HO-1 melanoma cells and HeLa cells overexpressing *hPNPase*^{old-35} under the control of a doxycycline-inducible promoter, revealed global changes in genes involved in cell cycle and mitosis. This study provides further evidence that *hPNPase*^{old-35} is associated

with global changes in cell cycle-associated genes.

3.2 Introduction

Human polynucleotide phosphorylase, an evolutionarily conserved 3'-5' exoribonuclease, has been implicated in numerous cellular functions over the past decade since its discovery as an upregulated transcript in terminally differentiated melanoma cells and senescent fibroblasts [17]. Some of the major findings relating to this interesting enzymatic protein revolve around its ability to cause growth suppression of cancer cells as a result of *c-myc* mRNA degradation and more recently due to its post-transcriptional regulation of miR-221 [48,49]. It is also implicated in the generation of reactive oxygen species leading to chronic inflammation, suggesting a probable role for this enzyme in senescence associated degenerative diseases [74,75]. Apart from this *hPNPase*^{old-35} plays a major role in the maintenance of cellular homeostasis, imports RNA into the mitochondria, mediates mtRNA processing and is part of a complex that is responsible for mtRNA decay [44,47,50,76,87,88]. Although these findings are a major step forward in delineating the functional roles this enzyme plays in cellular physiology, not a lot is known about the molecular targets of *hPNPase*^{old-35} from an enzymatic perspective apart from *c-myc* and miR-221 and its processing activities in the mitochondria.

Thus, to further our quest in trying to unravel the molecular targets involved in the biological processes *hPNPase*^{old-35} regulates which would ultimately help in the identification of therapeutic targets, we decided to perform gene expression analysis of melanoma cell lines following gain or loss of function of *hPNPase*^{old-35}. Pertaining to this, we provide extensive details in Chapter 2, where we have attempted to unravel the

global implications of *hPNPase*^{old-35} deregulation using melanoma as a model system. We have been able to identify transcripts that may be direct or indirect targets of *hPNPase*^{old-35}, while also showing and reinforcing the fact that *hPNPase*^{old-35} regulates mitochondrial homeostasis and cell cycle associated pathways.

As an extension of Chapter 2 we wanted to explore the possibility of whether similar effects would be observed in a system other than melanoma. In order to do this we performed microarray analysis in HeLa cells to evaluate the gene expression changes occurring as a result of *hPNPase*^{old-35} overexpression, which would help us answer whether the changes we observed in the HO-1 cells were a more global phenomana or a cell type specific effect. Also, to attain overexpression levels of *hPNPase*^{old-35} that were more physiologically relevant we made use of a doxycycline-inducible overexpression system. To identify *hPNPase*^{old-35} induced or repressed genes, we overlapped these microarray results with the *hPNPase*^{old-35} knockdown data we reported in Chapter 2. Secondly, we explored the TCGA database to identify in vivo tissue correlations of the genes we identified with *hPNPase*^{old-35} expression levels which provides additional validation for our current findings. Finally, we also compared the gene expression changes occurring as a result of *hPNPase*^{old-35} overexpression in HeLa cells and the *Ad.hPNPase*^{old-35} infected HO-1 cells we described in Chapter 2 to understand the global implications of *hPNPase*^{old-35} upregulation. This study provides further proof of the global impact of *hPNPase*^{old-35} on cell cycle events and the identified targets provide us with additional information, which may be used for the recognition of possible therapeutic targets for *hPNPase*^{old-35} associated diseases.

3.3 Materials and methods

3.3.1 Establishing a conditional *hPNPase*^{old-35old-35} over-expressing cell line

The full-length cDNA of *hPNPase*^{old-35old-35} with a C-terminal HA tag was cloned into a modified version of the Tet-On pTRIPZ vector (Open Biosystems, provided by Dr. Kristoffer Valerie) to permit inducible expression of the gene in the presence of doxycycline. HeLa-Tet-On cell lines were established by transfecting HeLa cells (Lipofectamine 2000, Invitrogen) with the pTRIPZ -*hPNPase*^{old-35old-35} plasmid (sequence was verified before use) and stable clones were selected with the help of puromycin (2 µg/ml) supplemented media. The expression of *hPNPase*^{old-35old-35} in the different clones was tested after inducing with doxycycline by Western blotting analysis.

3.3.2 MTT and colony formation assays

Dox-inducible HeLa cell clones 5, 6, 7 and 27 were seeded in 96-well plates (in quadruplicates) at a density of 1000 cells per well and difference in cellular viability between the dox-induced and uninduced controls was monitored by 3-(4,5-dimethylthiazol-2-yl)-2,5-diphenyl tetrazolium bromide (MTT) staining over a period of 5 days. The same cells were also seeded in 6-cm plates at a density of 1000 cells per plate and doxycycline was added. Colonies in the dox-treated and untreated plates (done in triplicates) were counted after 2 weeks by treating with Giemsa stain. Normal HeLa cells and pTRIPZ-RFP HeLa cells (with and without dox) were used as additional controls in both of the above experiments.

3.3.3 Total RNA isolation for microarray analyses

Total RNA from the *hPNPase*^{old-35old-35} knockdown and control cell lines (HO-1 melanoma cells stably expressing shRNA for *hPNPase*^{old-35old-35} and scrambled control

shRNA) and the *hPNPase*^{old-35old-35} conditionally over-expressing doxycycline treated and untreated control cell lines (HeLa cells stably transfected with pTRIPZ-*hPNPase*^{old-35old-35} induced with doxycycline for 24 hrs and uninduced cells as control) was isolated from cell lysates in TRIZOL reagent (Invitrogen™ Life Technologies, Carlsbad, CA). Cell lysates were subjected to an automated extraction method using the MagMAX™-96 for Microarrays Total RNA Isolation Kit (Ambion/Invitrogen™ Life Technologies, Carlsbad, CA) on the MagMAX™ Express Magnetic Particle Processor (Applied Biosystems/Invitrogen™ Life Technologies, Carlsbad, CA).

3.3.4 Gene Expression Microarrays

Gene expression profiles were ascertained using GeneChip® Human Genome U133A 2.0 (HG-U133A 2.0) arrays (Affymetrix, Santa Clara, CA) as previously described [100]. Every chip was scanned at a high resolution, with pixelations ranging from 2.5 µm down to 0.51 µm, by the Affymetrix GeneChip® Scanner 3000 according to the GeneChip® Expression Analysis Technical Manual procedures (Affymetrix, Santa Clara, CA). After scanning, the raw intensities for every probe were stored in electronic files (in .DAT and .CEL formats) by the GeneChip® Operating Software (GCOS) (Affymetrix, Santa Clara, CA). The overall quality of each array was assessed by monitoring the 3'/5' ratios for a housekeeping gene (GAPDH) and the percentage of “Present” genes (%P); where arrays exhibiting GAPDH 3'/5' < 3.0 and %P > 40% were considered good quality arrays. All experiments were done in biological triplicates.

3.3.5 Statistical Analyses

The Robust Multiarray Average method (RMA) was used for normalization and obtaining probe set expression summaries for the gene expression assays. These

values were then used to identify genes significantly altered among the different conditions (i.e., *hPNPase*^{old-35old-35} up- and down-regulation), and analyzed for significance across replicate experiments with the help of TM4-MeV (MultiExperiment Viewer) analysis software by using a permutation method performed with the Significance Analysis of Microarray (SAM) program from Stanford University [Stanford, CA]. Once the program reported the list of ranked genes whose expression changed in the opposite direction in the two datasets, the “delta value” was adjusted to a stringent false discovery rate (FDR) of 5%. Cluster analysis was done using the Cluster and TreeView programs 4. Genes reported by SAM were analyzed by hierarchical clustering with average linkage grouping.

In order to identify transcripts whose expression negatively or positively correlated with the expression of c-myc, we employed a Pearson correlation coefficient of 0.01 and statistical significance of the identified genes was set at p-value cutoff of 0.05 using standard t-test.

3.3.6 Enrichment analysis

The Protein ANalysis THrough Evolutionary Relationships (PANTHER) resource was used to identify Gene Ontology (GO) categories and generate pie charts for the *hPNPase*^{old-35} responsive genes (www.pantherdb.org) [123-125]. PANTHER can categorize genes based on their molecular functions, biological processes and protein classes with the help of available literature and evolutionary relationships.

Functional annotation cluster analysis was done using the Database for Annotation, Visualization and Integrated Discovery (DAVID) for the Gene ontology-based functional enrichment of the gene lists, using their respective gene symbols [126-128]. This kind of

analysis allows us to group functionally related genes together, which in turn provides a global view of altered biological networks.

The MetaCore™ (GeneGo Inc. USA) bioinformatics software was used in order to gain a deeper understanding of the plausible molecular networks or biological pathways the *hPNPase*^{old-35} responsive might be involved in [129,130]. The build network tool assigns pathway significance based upon the number of genes represented within a pathway and the direction of change.

The comparison analysis tool in the IPA (Ingenuity Pathway Analysis) software was used to evaluate the common biological processes and canonical pathways between the doxycycline-inducible HeLa *hPNPase*^{old-35} overexpression system and the Ad.*hPNPase*^{old-35} infected HO-1 cells.

3.3.7 Analysis of TCGA Genome-wide Expression Datasets

The processed, Illumina Hi Seq 2000-generated TCGA (The Cancer Genome Atlas) genome-wide expression datasets for colon adenocarcinoma (COAD), skin cutaneous melanoma (SKCM), OV (ovarian serous cystadenocarcinoma) and PRAD (prostate adenocarcinoma) were obtained through the UCSC Cancer Genomics Browser (<https://genome-cancer.ucsc.edu/>) (Goldman M et al, 2013). The sample breakdown for each dataset is as follows: COAD (193 primary, tumors, 18 solid tissue normal), SKCM (241 metastatic, samples, 43 primary tumors), OV (262 primary tumors, 4 recurrent tumors), PRAD (176 primary tumors, 44 solid tissue normals). In addition, the UCSC pan cancer (PANCAN) dataset (Cline MS et al., 2013), which resulted from merging (and normalization) of all of the 22 TCGA genome wide expression (Illumina Hi Seq 2000) cancer cohorts (including COAD, OV, PRAD, and SKCM) with a combined

total of 6040 samples (4982 primary tumors, 271 metastatic, 27 recurrent tumors, 173 peripheral blood, 587 solid tissue normals), was downloaded from the same website and subsequently analyzed. The primary objective of the analyses was to examine the possible transcriptional correlations between hPNPase (PNPT1) and genes identified through the cell line-based experiments. Through the use of the Gene-E program (Broad Institute, Cambridge, MA) and the JMP 10 Pro statistical software (SAS, Cary, NC), the correlations between hPNPase expression levels and those of other genes of interest were examined by calculation of Pearson correlation coefficients and generation of heat maps.

3.3.8 cDNA synthesis and quantitative real-time RT-PCR (qRT-PCR)

Total RNA was harvested using the RNeasy purification kit (Qiagen). The quality and concentrations of isolated RNA samples were assessed using the NanoDrop 2000 (Thermo Scientific). 2 µg of RNA was used in a total volume of 20 µl to synthesize cDNA using the High Capacity cDNA Reverse Transcription kit (Applied Biosystems) according to the manufacturer's instructions. Real-time quantitative PCR was conducted using the ViiA™ 7 Real-Time PCR System (Applied Biosystems) and performed in a total volume of 20 µl that contained the TaqMan Gene Expression Master Mix (Applied Biosystems), 1 µl of the cDNA template generated and the target-specific TaqMan Gene expression assays (Applied Biosystems) according to following cycle parameters: 95°C for 10 minutes followed by 40 cycles at 95°C for 15 seconds and at 60°C for 1 minute. Each sample was run in triplicate using three biological replicates and normalized to the housekeeping gene GAPDH used as an internal control in each case. The $\Delta\Delta C_t$ method

was used for comparing relative fold expression differences in the genes of interest between different test samples.

3.3.9 Protein isolation and Western blot analysis

Cells were harvested by centrifugation, pellets washed in PBS and subsequently lysed in ice-cold 1X cell lysis buffer (Cell Signaling) supplemented with PhosSTOP Phosphatase Inhibitor Cocktail Tablets and complete Mini Protease Inhibitor Cocktail Tablets (Roche), followed by centrifugation at 13,000 rpm for 15 minutes at 4°C. The supernatant or whole cell lysate was collected in a fresh tube and protein concentration was measured using the Bio-Rad Protein Assay Dye Reagent Concentrate (BIO-RAD). 30 µg of total cell lysate was mixed with SDS sample buffer and heated for 5 minutes at 95°C. The proteins were separated by 8-10% SDS-PAGE gels and transferred onto nitrocellulose membranes and blocked using 5% non-fat milk supplemented with 1% bovine serum albumin (BSA) in TBS-T for 1 hour. After washing three times with TBS-T for 10 minutes each, the membranes were incubated with primary antibodies overnight at 4°C. The primary antibodies used were anti-HA (mouse, 1:1000), anti-*hPNPase*^{old-35old-35} (chicken; 1:5000), anti-EF1α (mouse, 1:1000). The next day membranes were washed as before and incubated with the relevant horseradish-peroxidase conjugated secondary antibodies for 1 hour at room temperature. After washing three times with TBS-T for 10 minutes each, the proteins were detected using ECL Western Blotting detection reagent (GE Healthcare Life Sciences) and exposed to X-ray film.

3.4 Results

3.4.1 Establishing a doxycycline-inducible *hPNPase*^{old-35} over-expression system

The stable clones selected were evaluated for *hPNPase*^{old-35} expression by Western blotting. Figure 3.1 represents the results obtained for clones 5, 6, 7 and 27, where protein expression was checked at different time points and with increasing doses of doxycycline separately. Clone 5 showed better responses to different doses and temporal expression than the other clones and was thus selected for microarray analysis.

Previous studies have established a role for *hPNPase*^{old-35} in the processes of growth inhibition, where it was overexpressed by means of a replication-deficient adenovirus. In order to corroborate these results in the present overexpression system, MTT cell viability assays and colony formation assays were performed. Doxycycline treated clones 5 and 6 showed a slower growth rate (~40% less) as compared to their untreated counterparts as measured by MTT reagent (Figure 3.2) and reduced number of colonies (~50% less colonies) (Figure 3.3), when *hPNPase*^{old-35} was overexpressed as compared to clones 7 and 27 (Figures 3.3 and 3.4). The control HeLa cells and the empty pTRIPZ vector HeLa clones did not show any significant difference in growth with or without the presence of doxycycline (Figure 3.4).

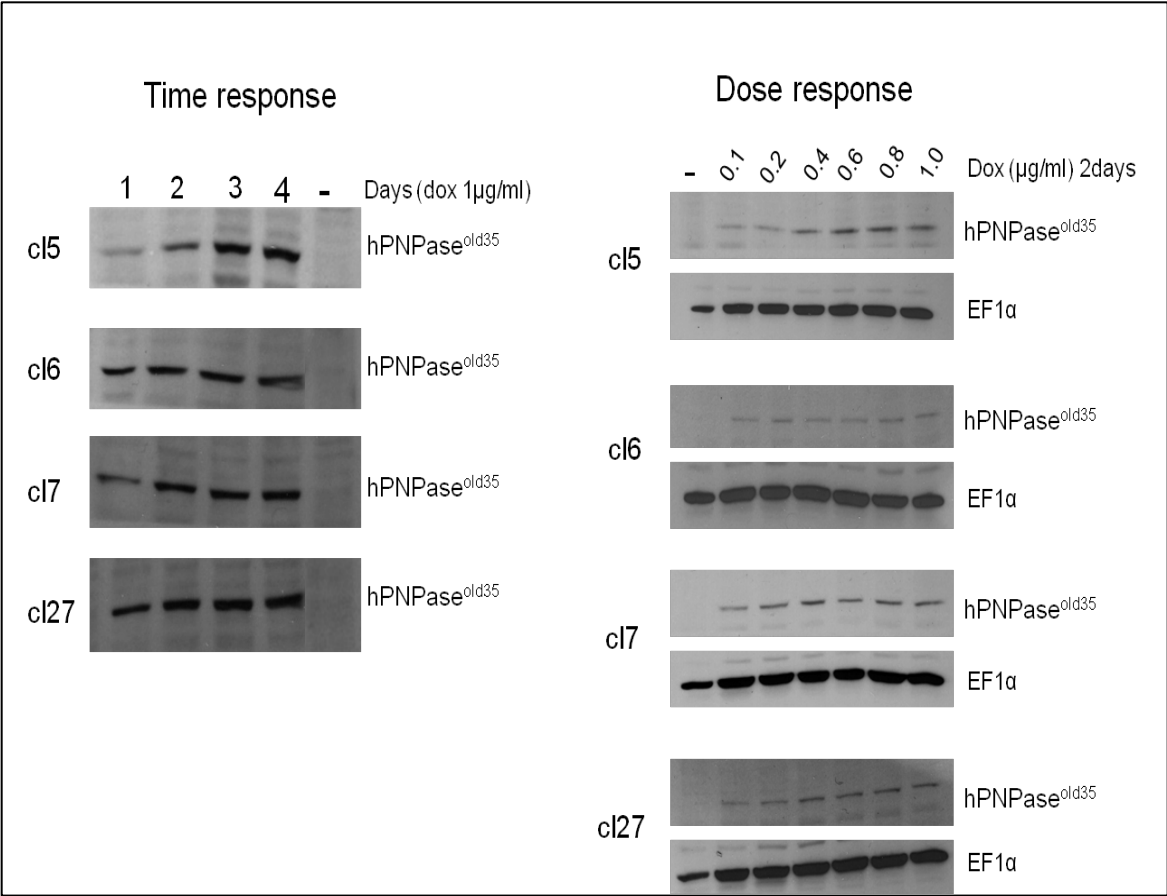


Fig. 3.1. Western blots showing hPNPase^{old-35} overexpression in doxycycline-inducible stable HeLa cells in a time and dose-dependent manner.

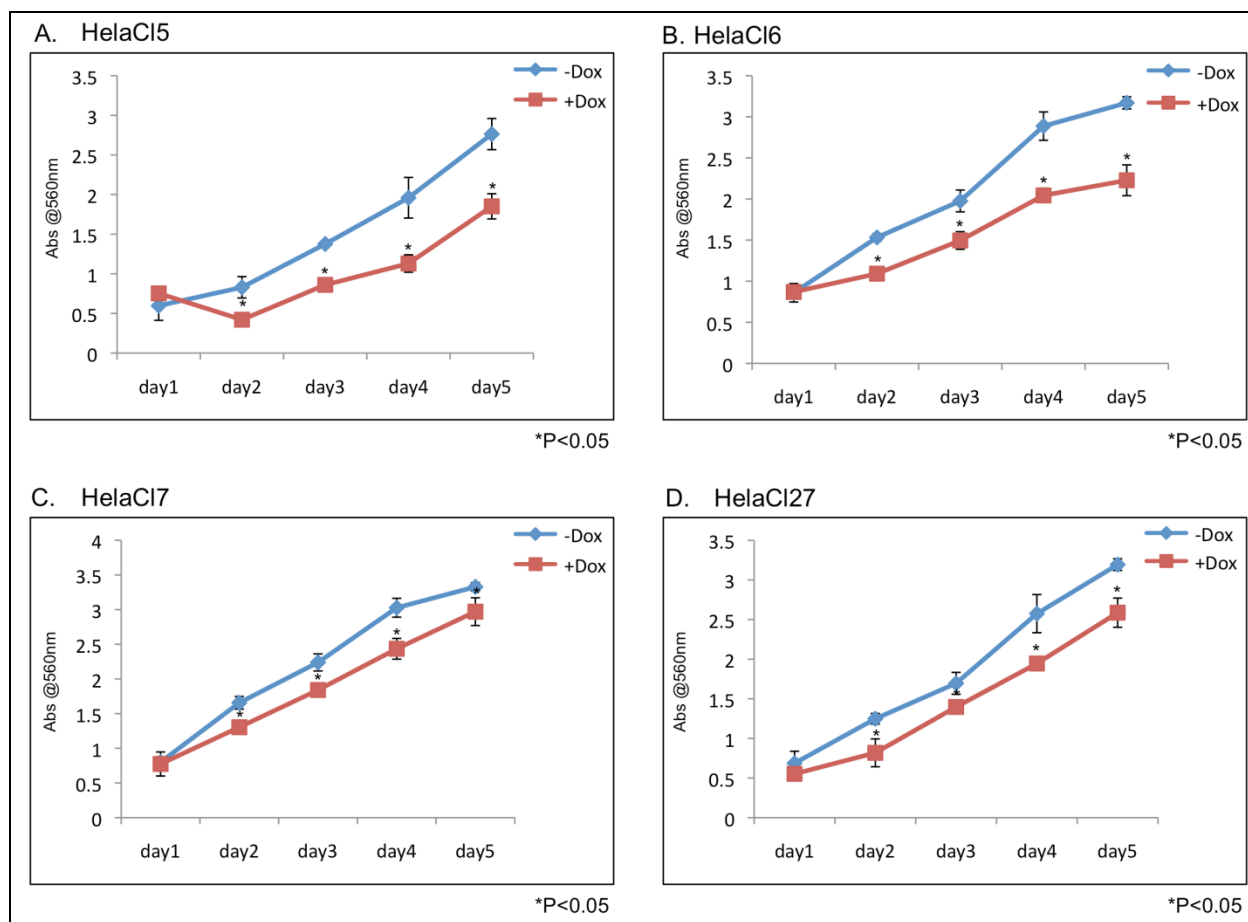


Fig. 3.2. MTT cell viability assays. hPNPase^{old-35} overexpression in doxycycline-inducible stable HeLa clones (A-D) shows a reduction in cellular growth over a period of 5 days as determined by MTT assay. Error bars represent mean \pm standard error of one experiment done in quintuplicate, statistical significance determined by two-tailed student's t-test, *P<0.05.

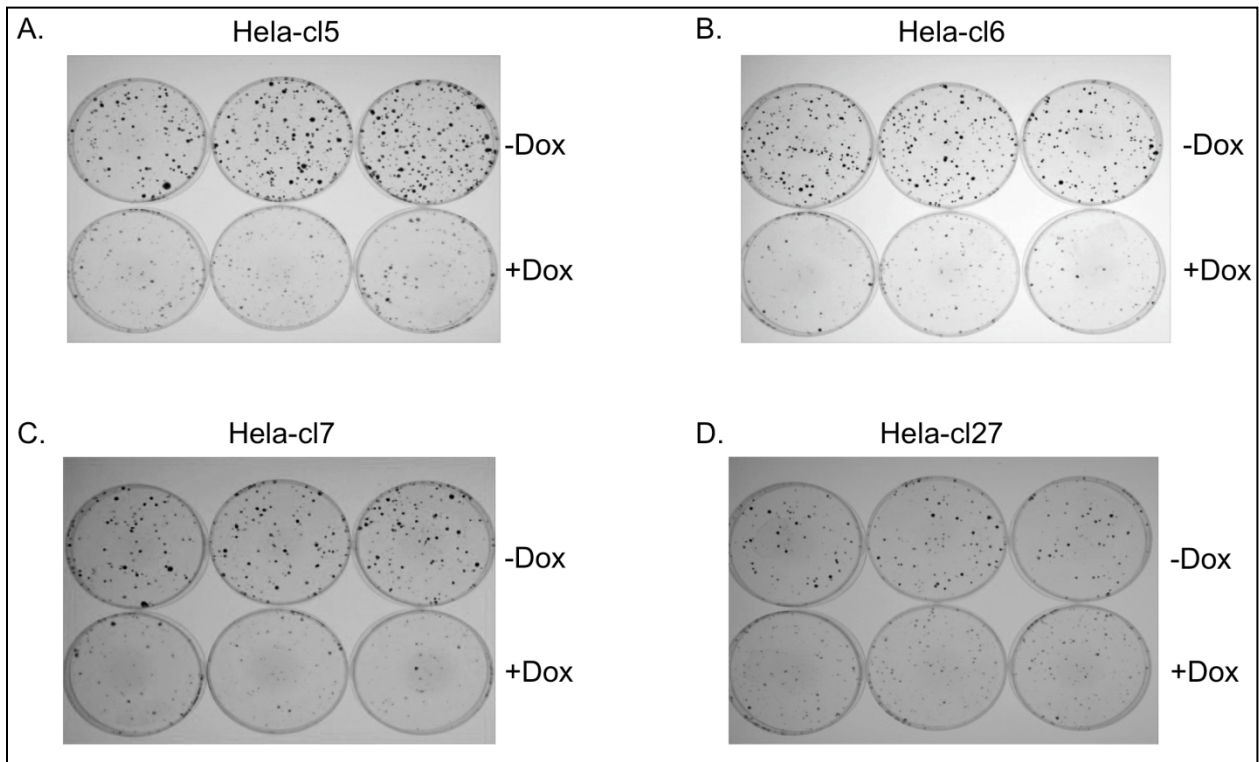


Fig. 3.3. Colony formation assays. hPNPase^{old-35} overexpression in doxycycline-inducible stable HeLa clones (A-D) shows a reduction in cellular growth as observed by reduced number of stained colonies.

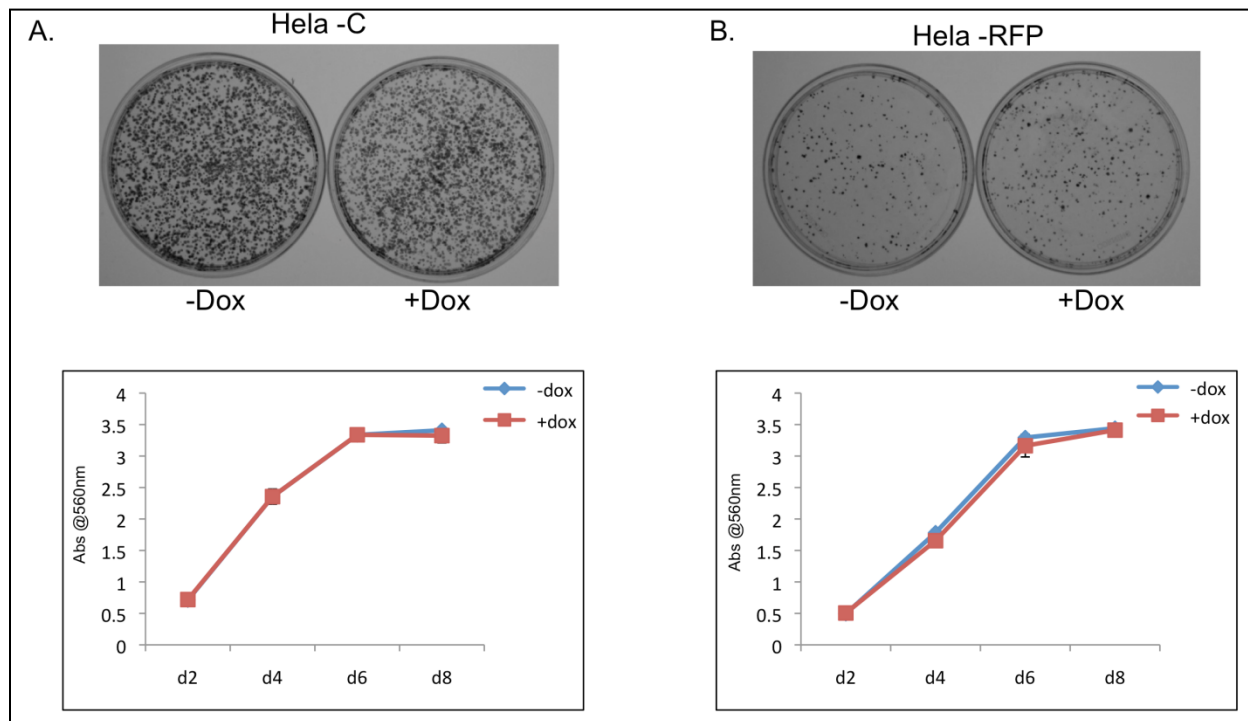


Fig. 3.4. Colony formation and MTT assays to determine cell viability of control HeLa and HeLa-RFP cells. Error bars represent mean \pm standard error of one experiment done in quintuplicate.

3.4.2 Identification of *hPNPase^{old-35}* responsive genes

To explore the effects of *hPNPase^{old-35}* on the global regulation of gene expression, we conducted cDNA microarray analyses using HeLa cells stably transfected with a doxycycline-inducible *hPNPase^{old-35}* expression vector to attain physiologically relevant levels of *hPNPase^{old-35}* overexpression and HO-1 melanoma cells in which *hPNPase^{old-35}* expression was stably knocked down using shRNA (described in detail in Chapter 2). Unsupervised hierarchical cluster analyses revealed that the six HeLa and six HO-1 arrays cluster with their respective class (Figure 3.5), which implies that the microarray results are robust and can differentiate between the cell types.

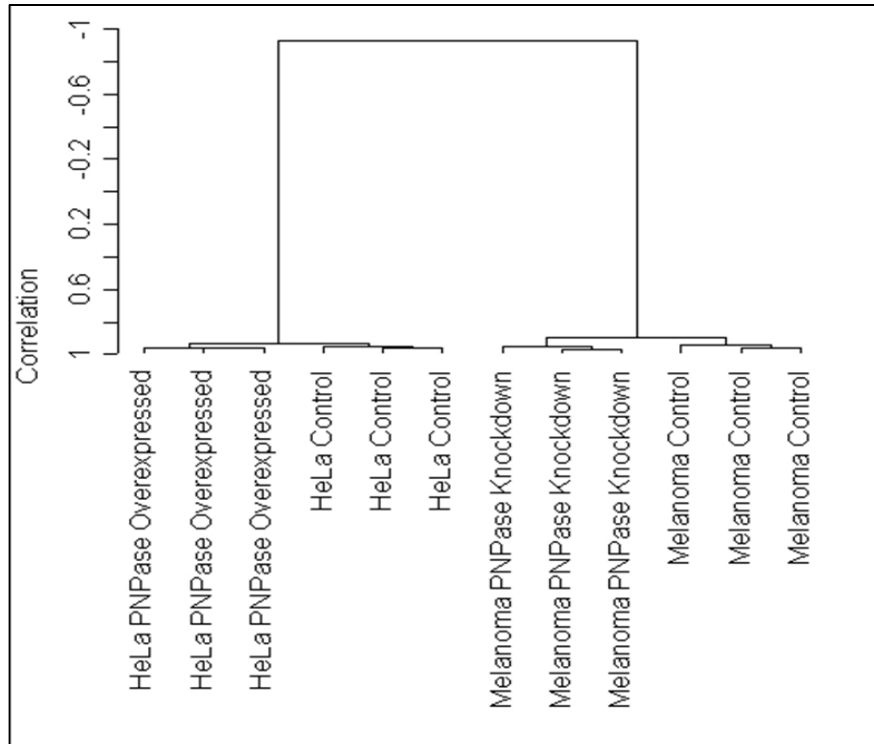


Fig. 3.5. Unsupervised hierarchical cluster analysis. Unsupervised cluster dendrogram using centered correlation and average linkage, based on 22,227 probe sets for the 12-array dataset.

A comparative analysis between the two datasets with the help of TM4-MeV analysis software allowed the identification of 90 transcripts whose expression was inversely affected in both datasets significantly. Out of these 90 transcripts, the expression of 62 transcripts correlated positively with $hPNPase^{old-35}$ (Figure 3.6.A) and the expression of 28 transcripts anti-correlated or negatively correlated with $hPNPase^{old-35}$ (Figure 3.6.B). Some genes are represented on the microarray by multiple probe sets and thus were identified more than once (as evident in Figure 3.6). Apart from providing an additional internal control, this finding also increases confidence in the identification of certain genes as being responsive to $hPNPase^{old-35}$ levels.

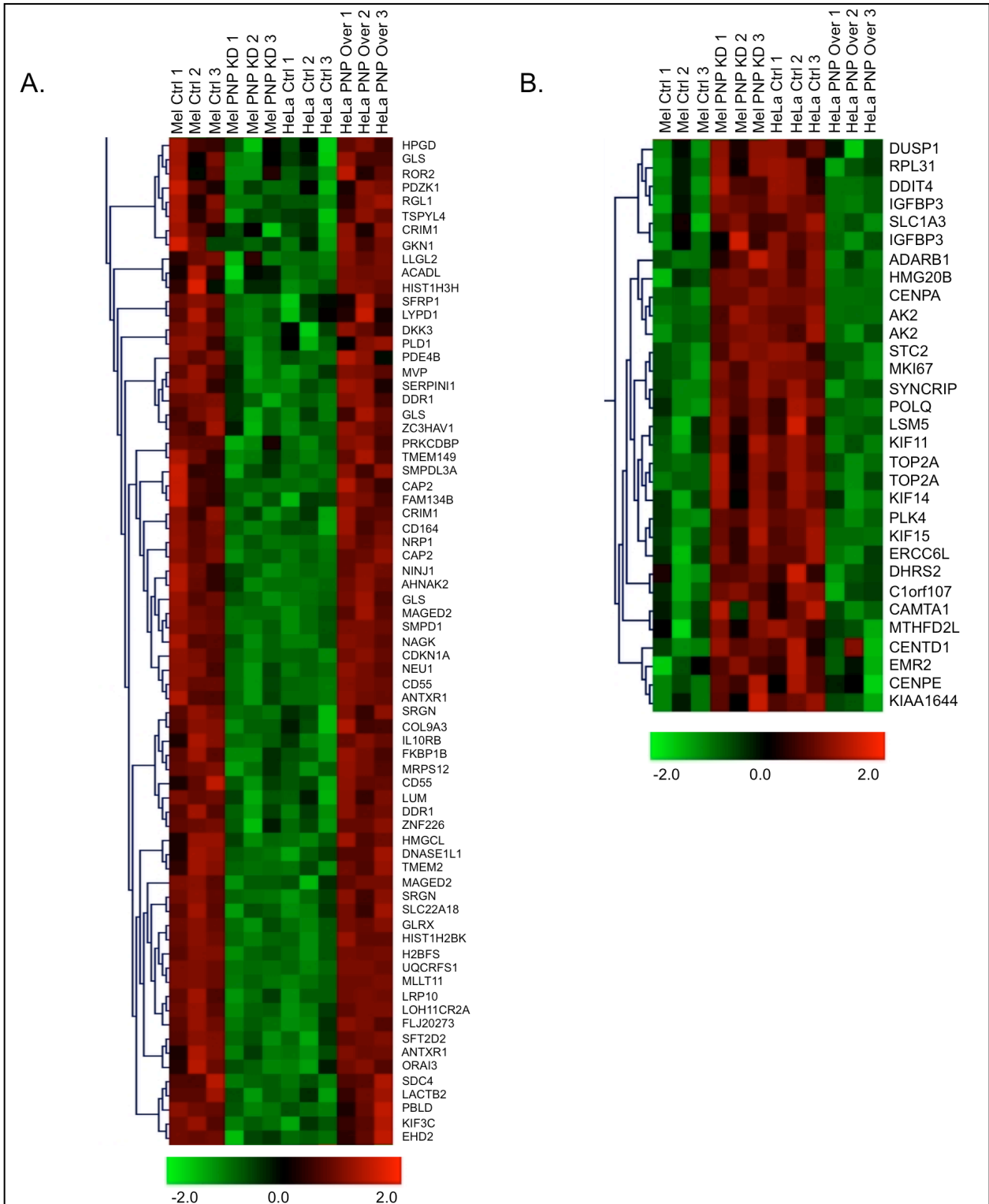


Fig. 3.6. Comparison of *hPNPase*^{old-35}-induced changes in gene expression in HO-1 and HeLa cells. Hierarchical clustering of *hPNPase*^{old-35} positively (A) and negatively (B) correlating genes as identified by microarray analysis.

3.4.3 Functional categorization of *hPNPase*^{old-35} responsive genes

The *hPNPase*^{old-35} responsive genes were arranged into various biological processes, molecular functions and protein classes using the Gene Ontology (GO) categories available through the PANTHER database and its tools. These functional categories are represented in Figure 3.7 where the pie charts include categories with at least five genes. GO analysis of the biological processes (12 identified in total) involving the *hPNPase*^{old-35} responsive genes we report here showed that the major categories in this case belonged to cellular (18.5%) and metabolic processes (17.6%). The genes involved in cellular processes belonged majorly to cell communication (36.4%), cell cycle (19.5%) and cell adhesion (16.9%) sub-categories.

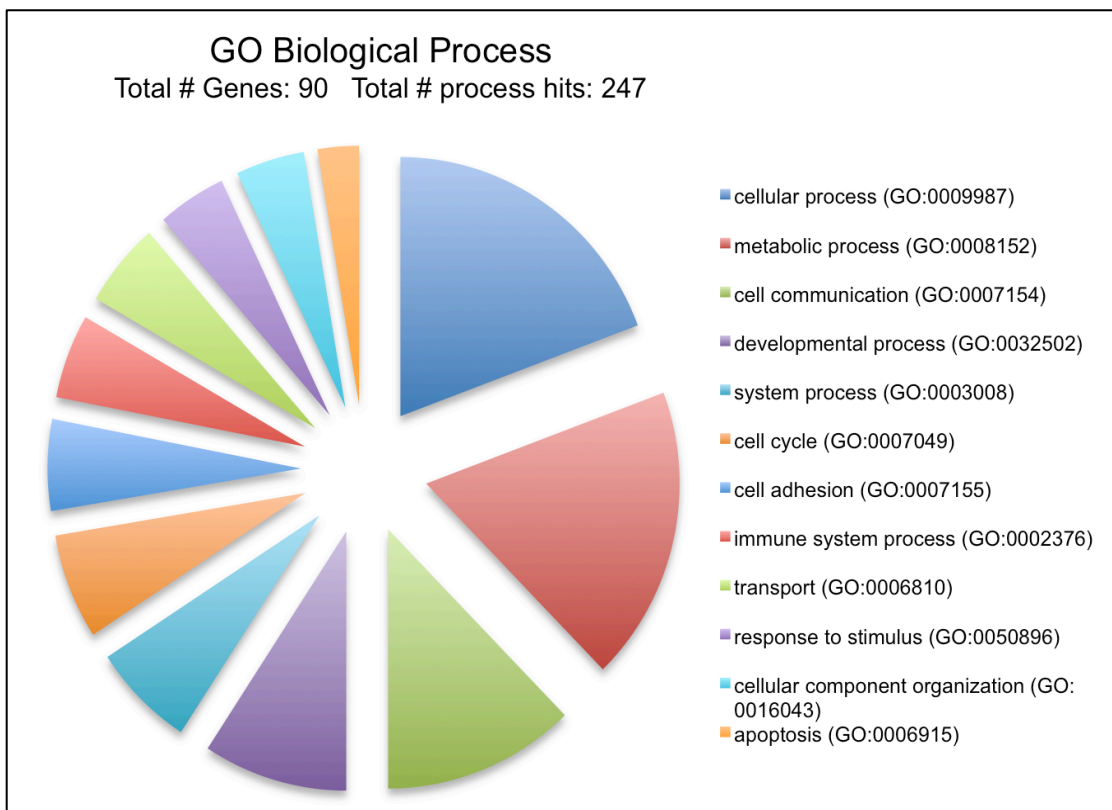


Fig. 3.7. Gene Ontology (GO) terms for PNPase responsive genes. GO analysis corresponding to Biological process

The genes involved with metabolic processes belonged majorly to primary metabolic processes (86%), which in turn comprised of nucleic acid (38.3%), protein (34%), lipid (14.9%), amino acid (8.5%) and carbohydrate metabolism (4.3%). The major molecular functions the *hPNPase^{old-35}* responsive genes were attributed to were catalytic activity (29.2%, mainly hydrolases, oxidoreductases and transferases) and binding (28.3%, mainly protein and nucleic acid binding) (Figure 3.8).

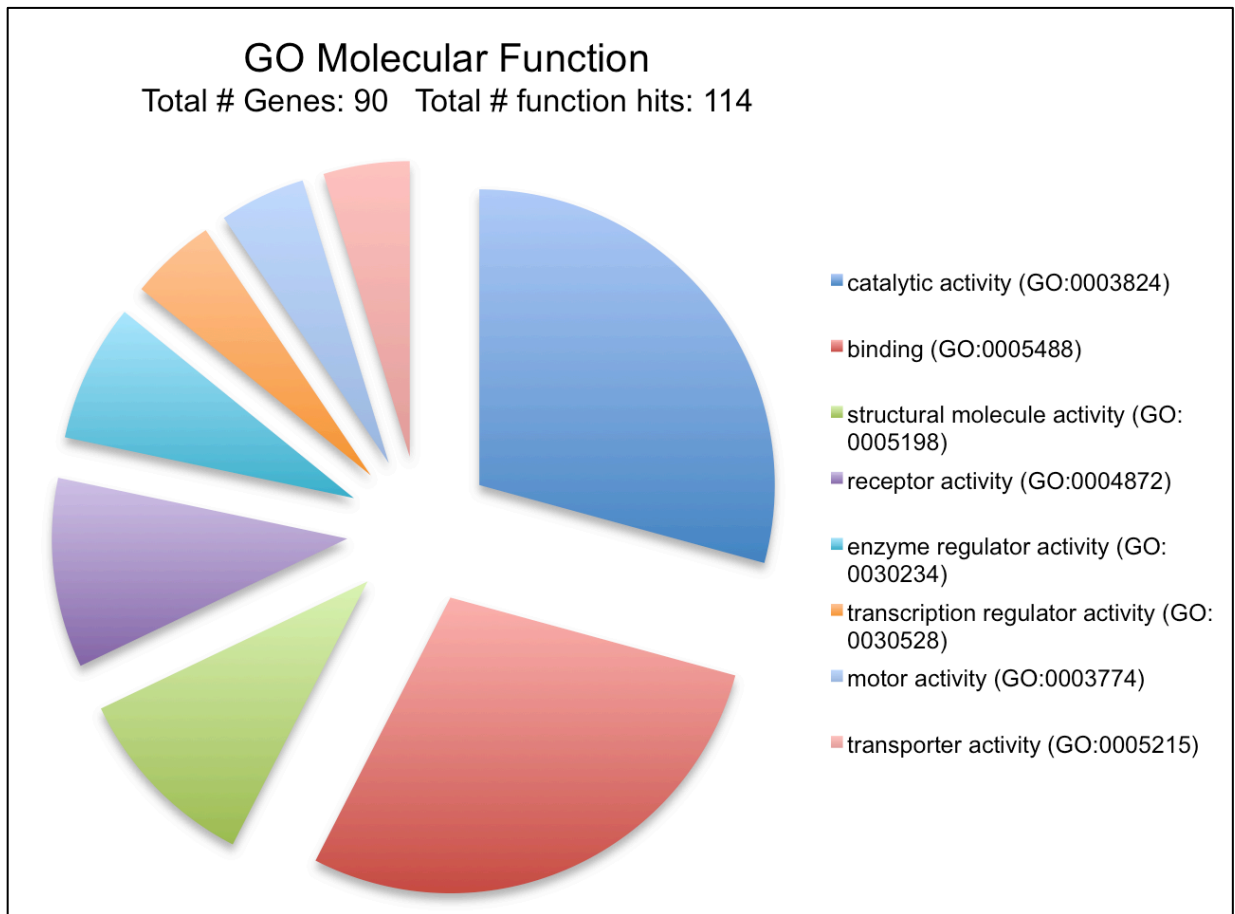


Fig. 3.8. Gene Ontology (GO) terms for PNPase responsive genes. GO analysis corresponding to Molecular functions.

The top protein function categories the *hPNPase*^{old-35} responsive genes belonged to were; hydrolases (12.4%), nucleic acid binding (10%) and receptors (8.5%) (Figure 3.9).

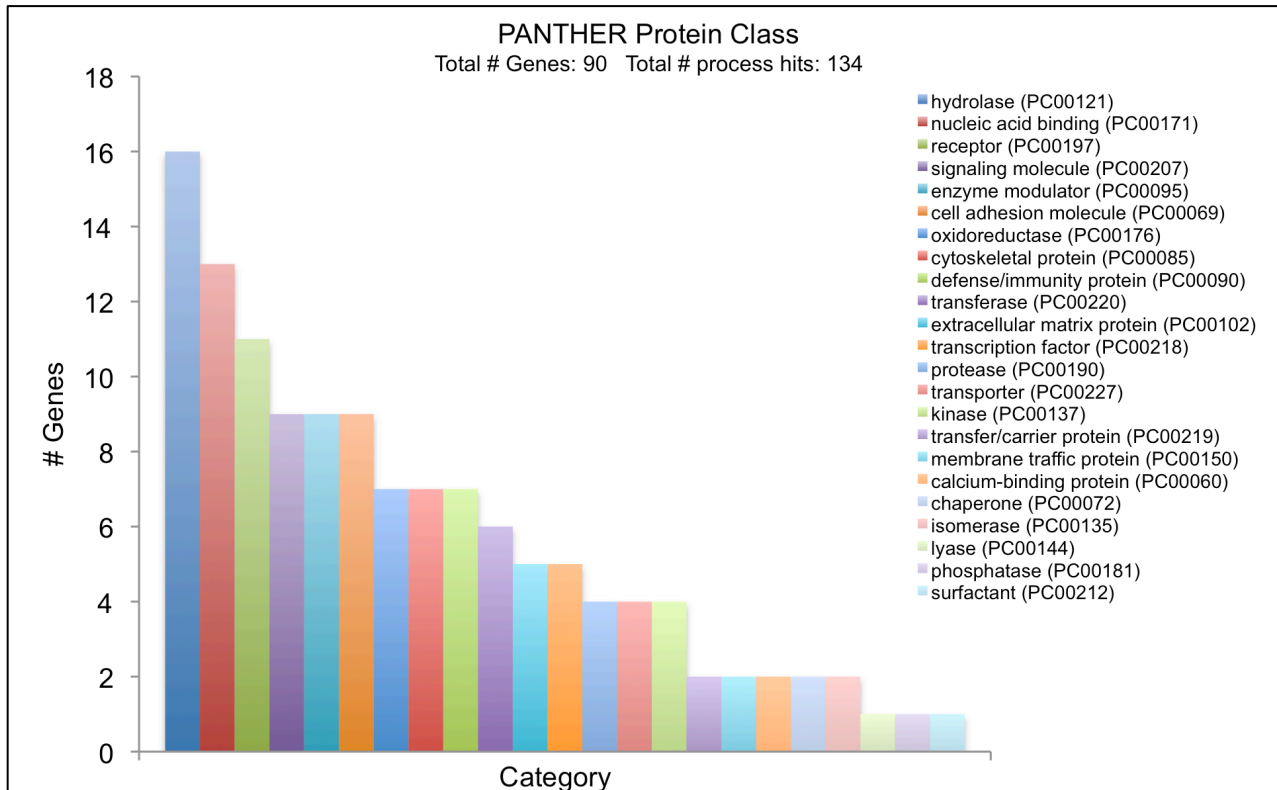


Fig. 3.9. Gene Ontology (GO) terms for PNPase responsive genes corresponding to PANTHER Protein class identified by PANTHER classification system (<http://www.pantherdb.org/>).

Functional annotation clustering by DAVID resulted in the identification of 32 clusters of related genes, with the highest enrichment score being 1.91. The most significantly enriched gene clusters along with their GO categories are represented in Figures 3.10-3.12 and relate to chromosomal organization (score=1.91, 18 genes: *HIST1H2BK*, *HIST1H3H*, *H2BFS*, *CENPA*, *TSPYL4*, *CENPE*, *TOP2A*, *HMG20B*, *ERCC6L*, *SYNCRIP*, *KIF14*, *MKI67*, *ZNF226*, *DNASE1L1*, *POLQ*, *KIF15*, *CDKN1A*, *PLK4*) (Figure 3.10), signaling molecules (score=1.67, 32 genes: *AK2*, *GLRX*, *UQCRFS1*, *TMEM2*,

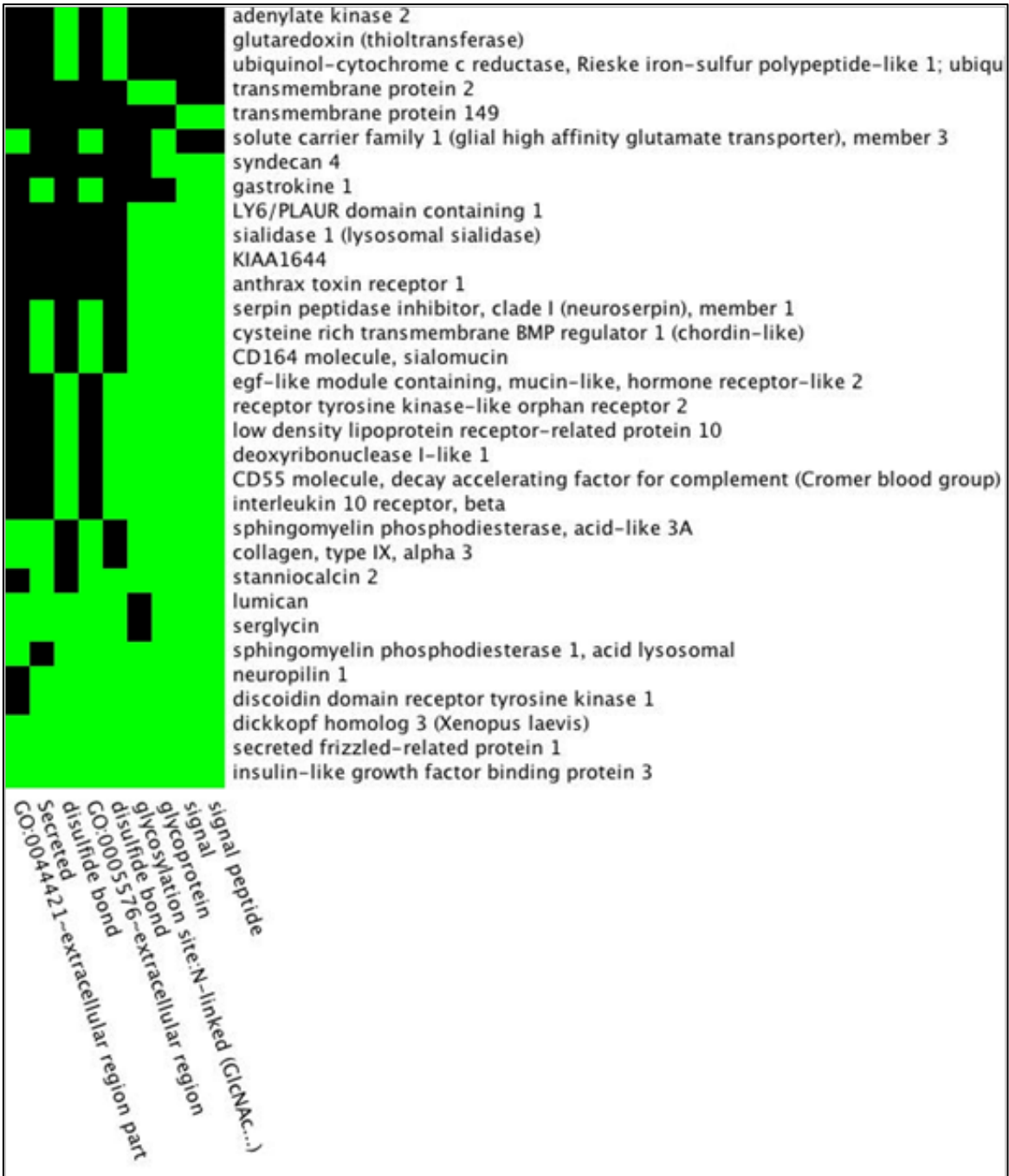


Fig. 3.11. Functional annotation of genes significantly regulated by *hPNPase*^{old-35} represented as enrichment clusters generated by the DAVID analysis software. Cluster of 32 signaling molecules and cellular receptors. Green - corresponding gene-term association positively reported in DAVID; black - corresponding gene-term association not reported yet in DAVID.

³⁵ responsive genes, with STAT1 and p21 appearing as major regulatory proteins in this pathway.

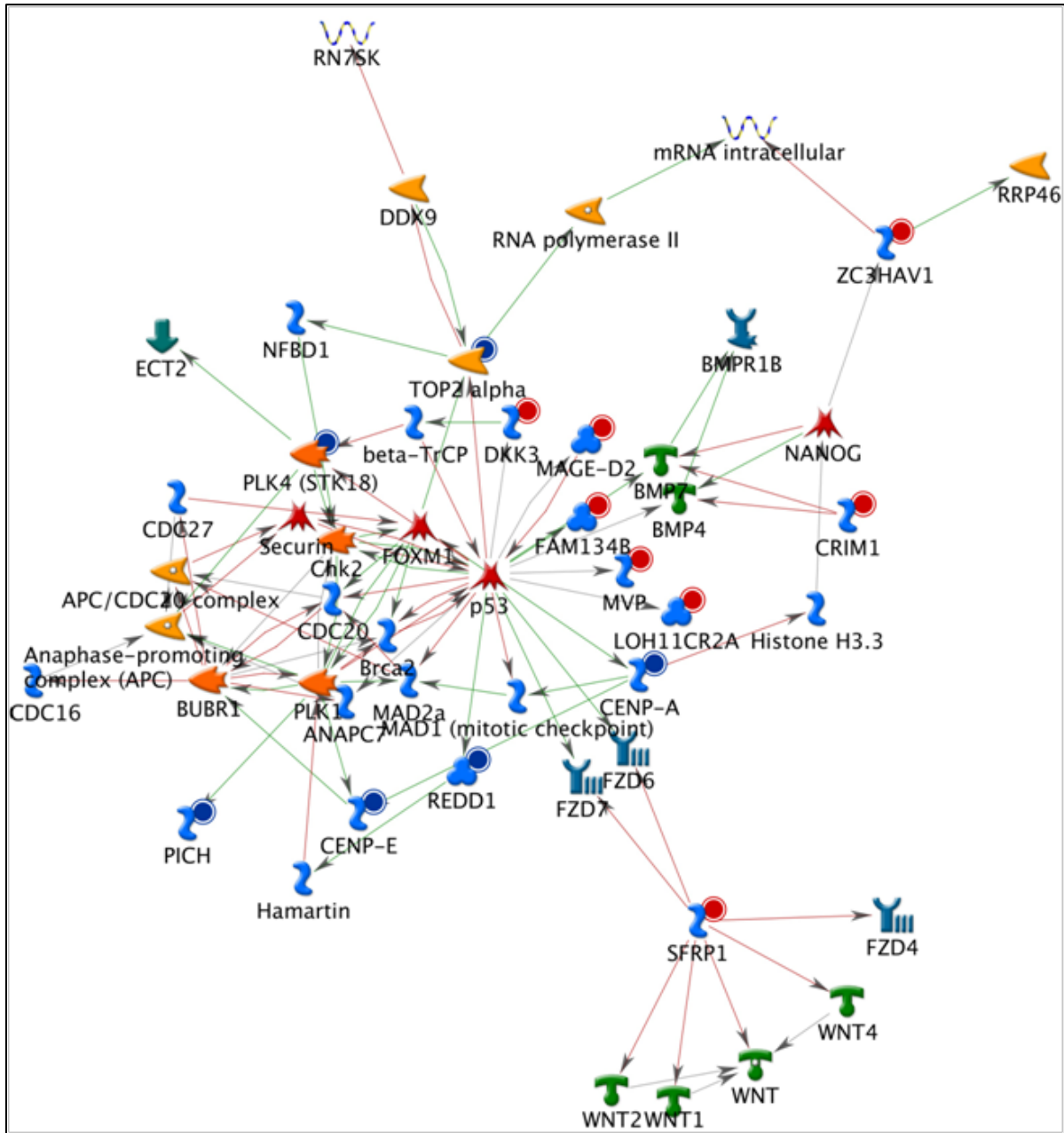


Fig. 3.13. Pathway analysis of *hPNPase*^{old-35} responsive genes. Network associated with mitosis and involves 14 of our reported *hPNPase*^{old-35} responsive genes.

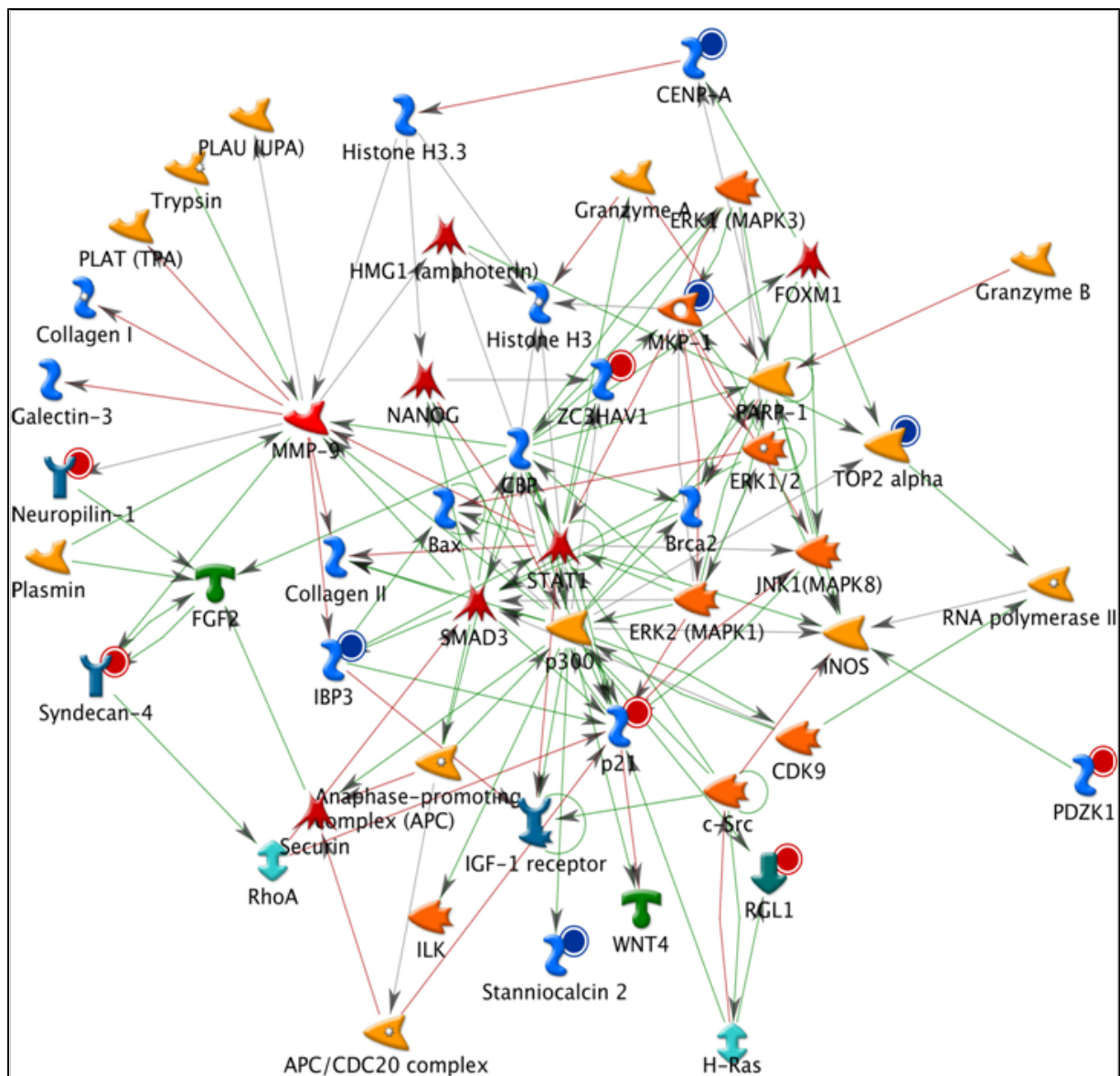


Fig. 3.14. Pathway analysis of *hPNPase*^{old-35} responsive genes. Network associated with p21 signaling and involves 11 of our reported *hPNPase*^{old-35} responsive genes.

- | | | | | |
|-------------------------|----------------------------|-----------------|-----------------|--------|
| Generic binding protein | Generic binding protein | Metalloprotease | Protein | GTPase |
| Generic enzyme | Generic receptor | Generic kinase | Regulators | |
| Transcription factor | Receptor (Enzyme activity) | GPCR | Receptor ligand | |

Representative genes in the two networks such as *CENPA* and *CENPE* are validated by qRT-PCR, which are downregulated in response to *hPNPase^{old-35}* overexpression (Figures 3.15 and 3.16). *hPNPase^{old-35}* stable knockdown in HO-1 and WM35 melanoma cells resulted in a ~1.2 fold increase in *SYNCRIP* and a ~1.2-1.6 fold increase in *CENPA* potential direct target levels as determined by qRT-PCR (Figure 3.15A-B). Transient knockdown of *hPNPase^{old-35}* also resulted in a 1.4 fold increase in *SYNCRIP* and a ~2 fold increase in *CENPA* RNA levels in HeLa cells (Figure 3.15C), validating that this is not a cell line specific effect, nor an indirect effect due to stable knockdown. Plasmid mediated overexpression of *hPNPase^{old-35}* in HO-1 melanoma cells resulted in a 20% and 30% reduction in *SYNCRIP* and *CENPA* RNA levels respectively (Figure 3.15D). Figure 3.16A shows a graphical representation of the fold decrease in the RNA levels of *CENPA*, *CENPE* and *MKI67* following adenoviral mediated overexpression of *hPNPase^{old-35}* in HO-1 and WM35 melanoma cells in comparison to their respective fold changes as obtained in the microarray results. Adenoviral mediated overexpression of *hPNPase^{old-35}* in three different melanoma cell lines (HO-1, WM35 and MeWo) all resulted in ~40% reduction in *CENPA* levels (Figure 3.16B).

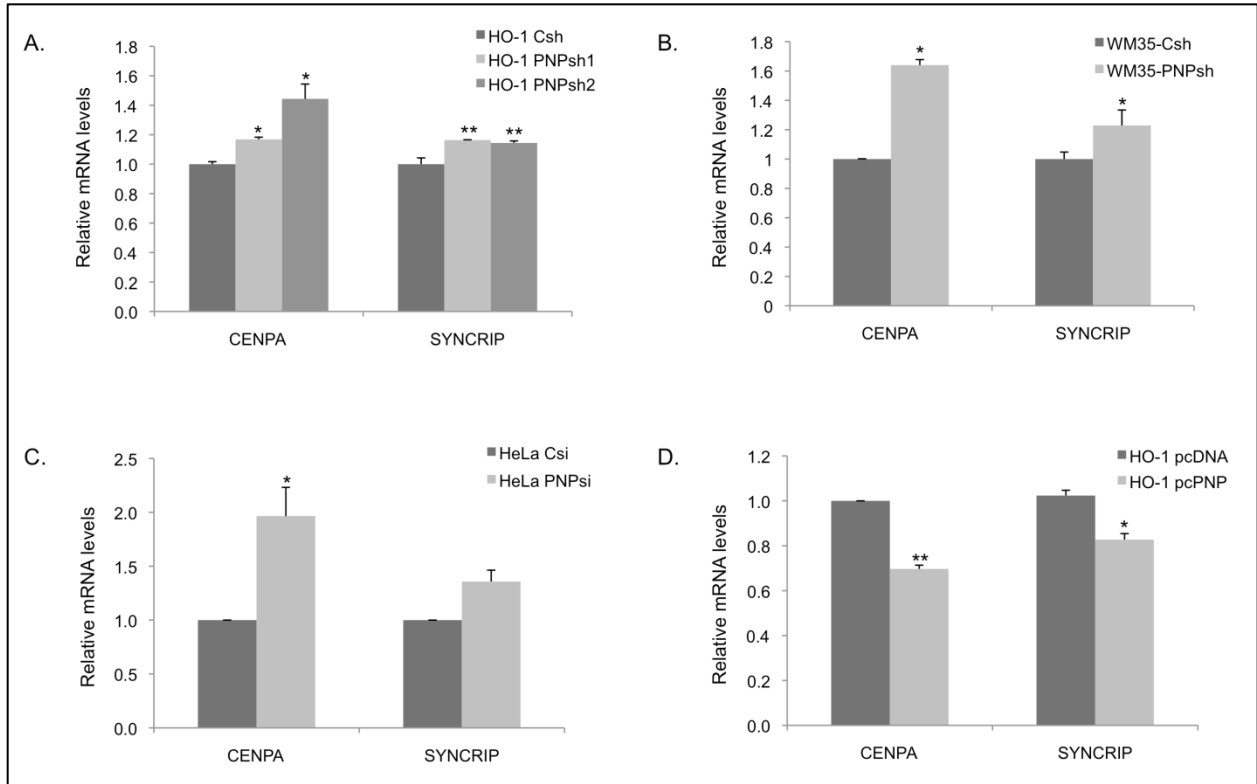


Fig. 3.15. Real-time PCR validation of genes identified by microarray analysis. (A) *hPNPase*^{old-35}-stable knockdown HO-1 cells, (B) *hPNPase*^{old-35}-stable knockdown WM35 cells, (C) HeLa cells transiently transfected with siRNA against *hPNPase*^{old-35} and (D) HO-1 cells transfected with pcDNA3.1- *hPNPase*^{old-35}. Error bars represent mean \pm S.E. of three independent experiments done in triplicate, statistical significance was determined by a one-way analysis of variance followed by Dunnett's multiple comparison test and a two-tailed student's t-test, *P<0.05, **P<0.01, ***P<0.001.

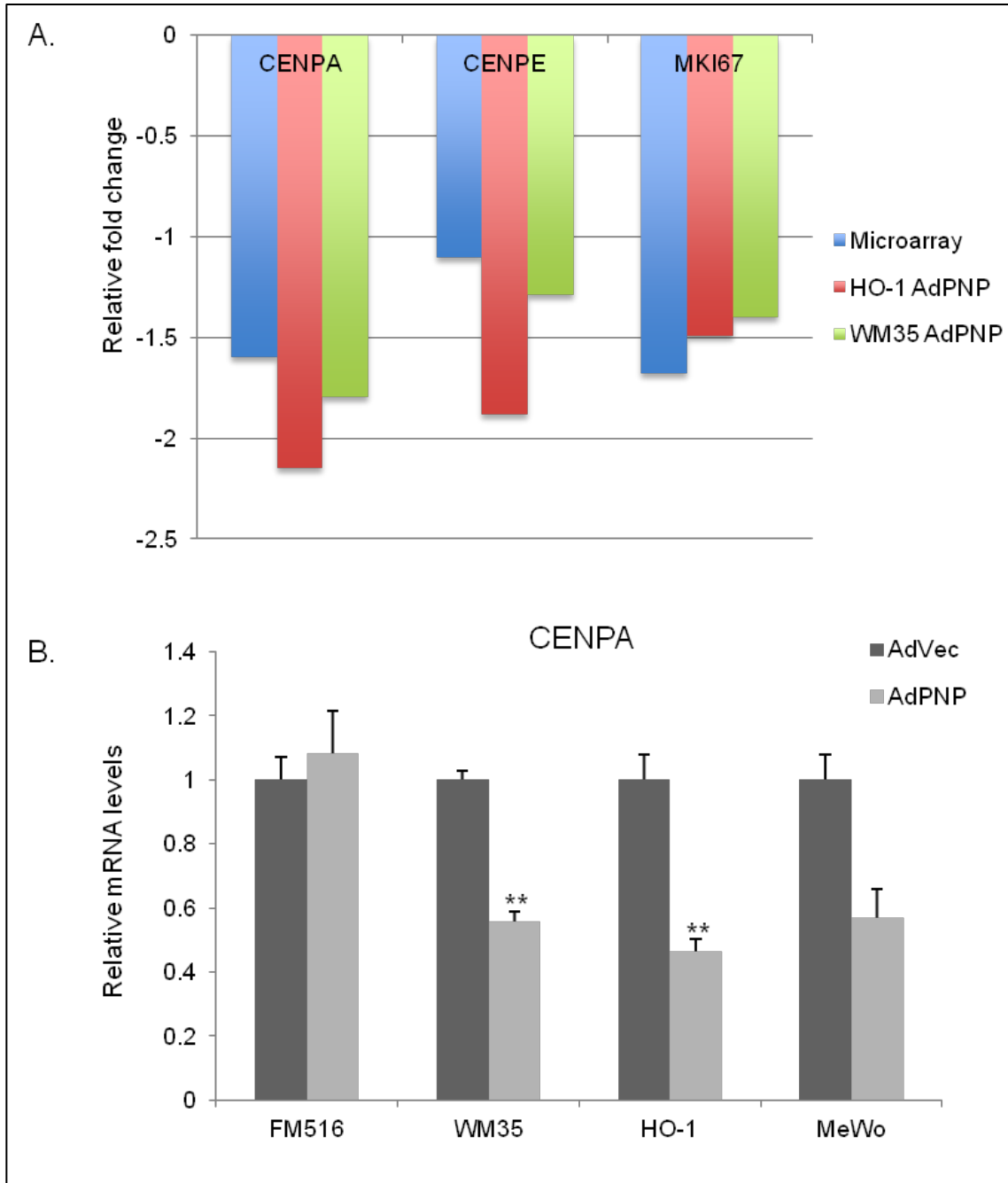


Fig. 3.16. Real-time PCR validation of genes identified by microarray analysis following *Ad.hPNPase^{old-35}*-mediated overexpression. Error bars represent mean \pm S.E. of three replicate experiments. Statistical significance was determined by two-tailed student's t-test, * $P < 0.05$, ** $P < 0.01$.

3.4.4 TCGA correlations of $hPNPase^{old-35}$ responsive genes

The Cancer genome atlas (TCGA) database is an enormous repository of gene expression data from various normal and cancer tissue types. In order to evaluate the in vivo implications of the $hPNPase^{old-35}$ responsive genes we identified, we decided to investigate their potential correlation with $hPNPase^{old-35}$ in various TCGA datasets. The genes identified as positively or negatively correlating with $hPNPase^{old-35}$ expression in different cancer types are represented in the heat maps shown in Figure 3.17. Prior to heat map generation, each gene expression value (at log, base 2 scale) for every sample was transformed by subtracting the average expression across all samples in a given dataset. As shown in Figure 3.17, the samples in the TCGA OV, COAD, SKCM, and PRAD cohorts were arranged in order of increasing $hPNPase^{old-35}$ expression level, going from green to red. One gene that stood out is *DUSP1*. As the $hPNPase^{old-35}$ expression of OV, COAD, SKCM, and PRAD samples increased, *DUSP1* level decreased (also indicated by negative Pearson correlation coefficients). The Pearson correlation coefficient (r) between $hPNPase^{old-35}$ and *DUSP1* registered at -0.362. This r value was 221st lowest (99th percentile) among the 20500 genes whose expression was related to $hPNPase^{old-35}$. As the heat maps indicate, opposite expression trends (compared to $hPNPase^{old-35}$) were observed for the genes *KI1644* (OV, COAD, PRAD), *ADARB1* (OV, COAD), *HMG20B* (COAD), *IGFBP3* (COAD, PRAD), *DDIT4* (COAD, PRAD), *EMR2* (COAD, SKCM), *SLC1A3* (COAD, PRAD), and *DHRS2* (PRAD). In contrast, the expression levels of the genes *GLS* (COAD, SKCM, PRAD), *LACTB2* (COAD, SKCM, PRAD), *MRPS12* (COAD), *NEU1* (COAD), *CD164* (SKCM), *FKBP1B*

(OV), *KIF3C* (OV), and *SFT2D2* (PRAD) exhibited positive correlation with *hPNPase*^{old-}

35 .

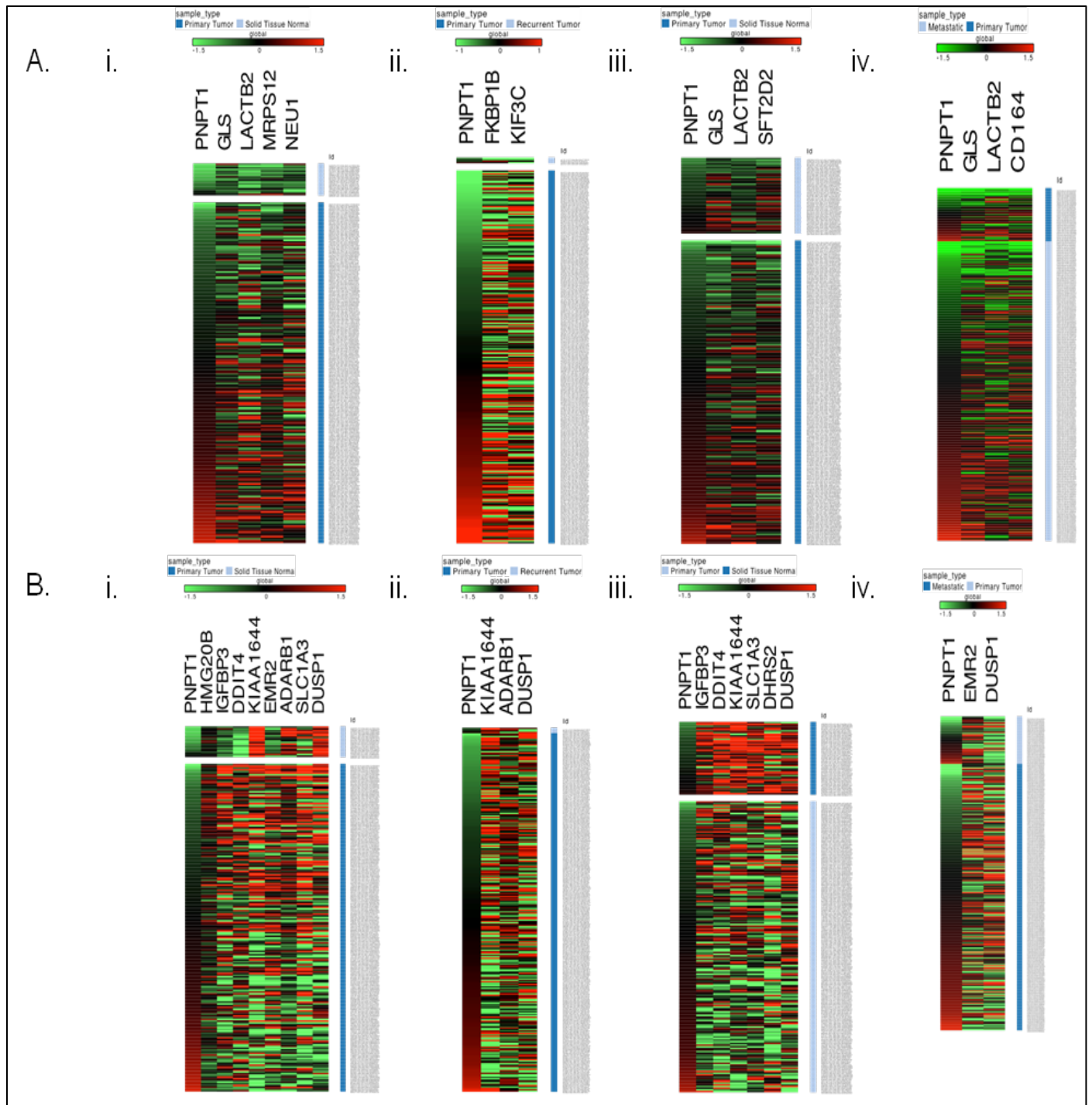


Fig. 3.17. Heat maps representing correlations of $hPNPase^{old-35}$ responsive genes with $hPNPase^{old-35}$ in different tumor types identified using TCGA datasets. (A) $hPNPase^{old-35}$ positively and (B) $hPNPase^{old-35}$ negatively correlating genes in (i) colon adenocarcinoma (COAD), (ii) ovarian serous cyst adenocarcinoma (OV), (iii) prostate adenocarcinoma (PRAD), and (iv) skin cutaneous melanoma (SKCM).

3.4.5 Identification of Myc-correlating genes

c-MYC mRNA has been previously shown to be regulated by *hPNPase*^{old-35} at the post-transcriptional level. Since c-myc is an essential cell cycle regulator and also a transcription factor implicated in the regulation of expression of numerous genes, we were interested to identify if genes differentially regulated by *hPNPase*^{old-35} following its gain or loss of function were in any way under c-myc transcriptional control. Thus, in order to dissect the potential role of myc in the regulation of *hPNPase*^{old-35} responsive genes, we identified genes in our two datasets (*hPNPase*^{old-35} knockdown and overexpression) whose expression correlated with c-myc expression. 31 genes were identified with expression negatively correlating with c-myc and 29 with expression positively correlating with c-myc. We further grouped the 60 c-myc correlating genes into biological categories using the functional annotation cluster analysis tool in DAVID, which resulted in the identification of 26 gene enrichment clusters with the highest enrichment score being 2.02. Some of the functional categories identified were apoptosis (Figure 3.18), DNA repair (Figure 3.19), cytoskeleton (Figure 3.21) and mRNA processing (Figure 3.22). 11 of c-myc correlating genes identified were also among the *hPNPase*^{old-35} regulated genes we report here. Of these eleven genes, the expression of *DHRS2*, *LSM5*, *STC2*, *TOP2A* positively correlated with c-myc and *IL10RB*, *LOH11CR2A*, *MLLT11*, *MRPS12*, *NEU1*, *SMPD1*, *UQCRFS1* negatively correlated with c-myc.

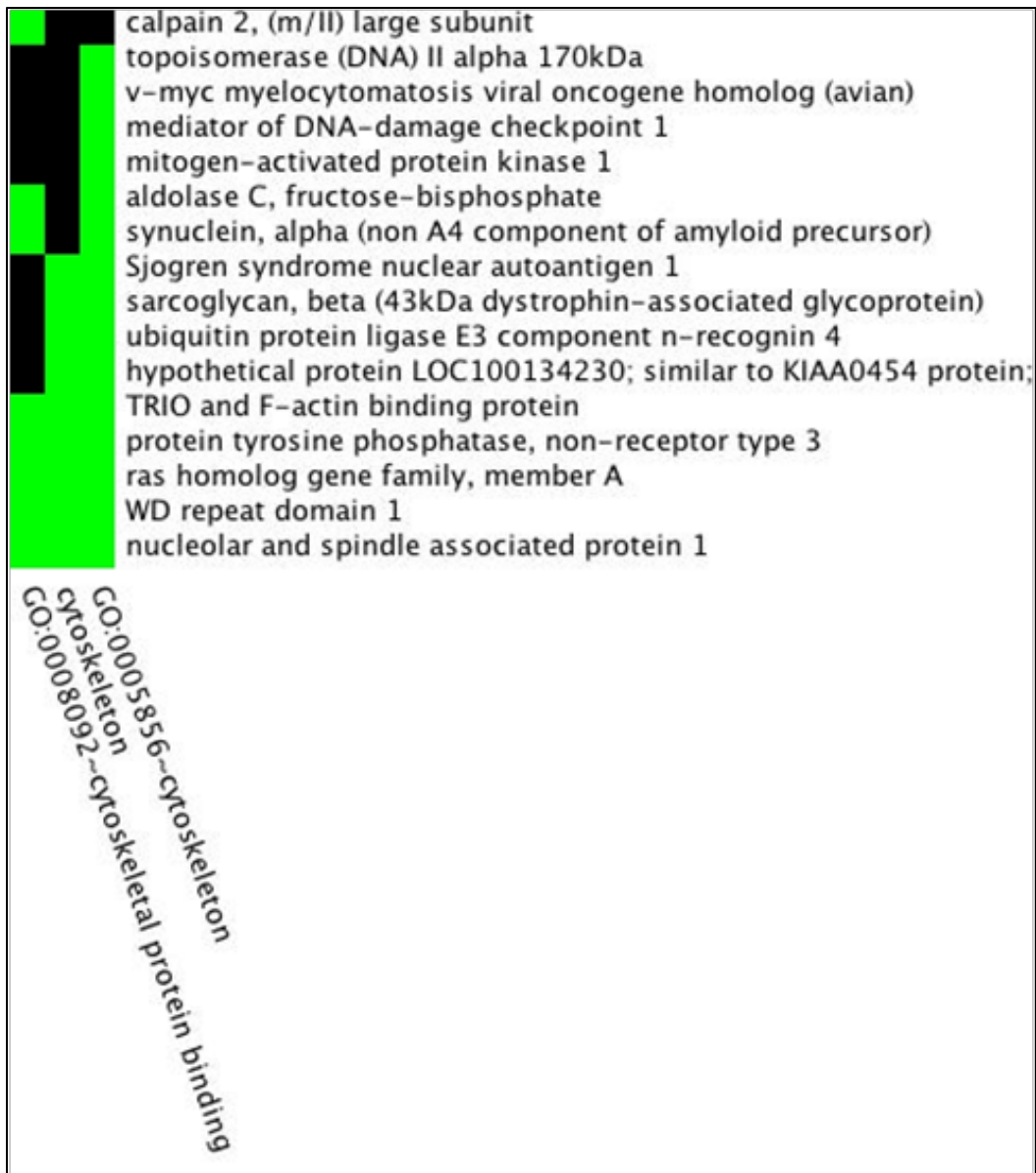


Fig. 3.19. Cluster analysis of functional enrichments for c-Myc correlating genes. Cluster of 16 genes involved in cytoskeleton associated functions. Green - corresponding gene-term association positively reported in DAVID; black - corresponding gene-term association not reported yet in DAVID.

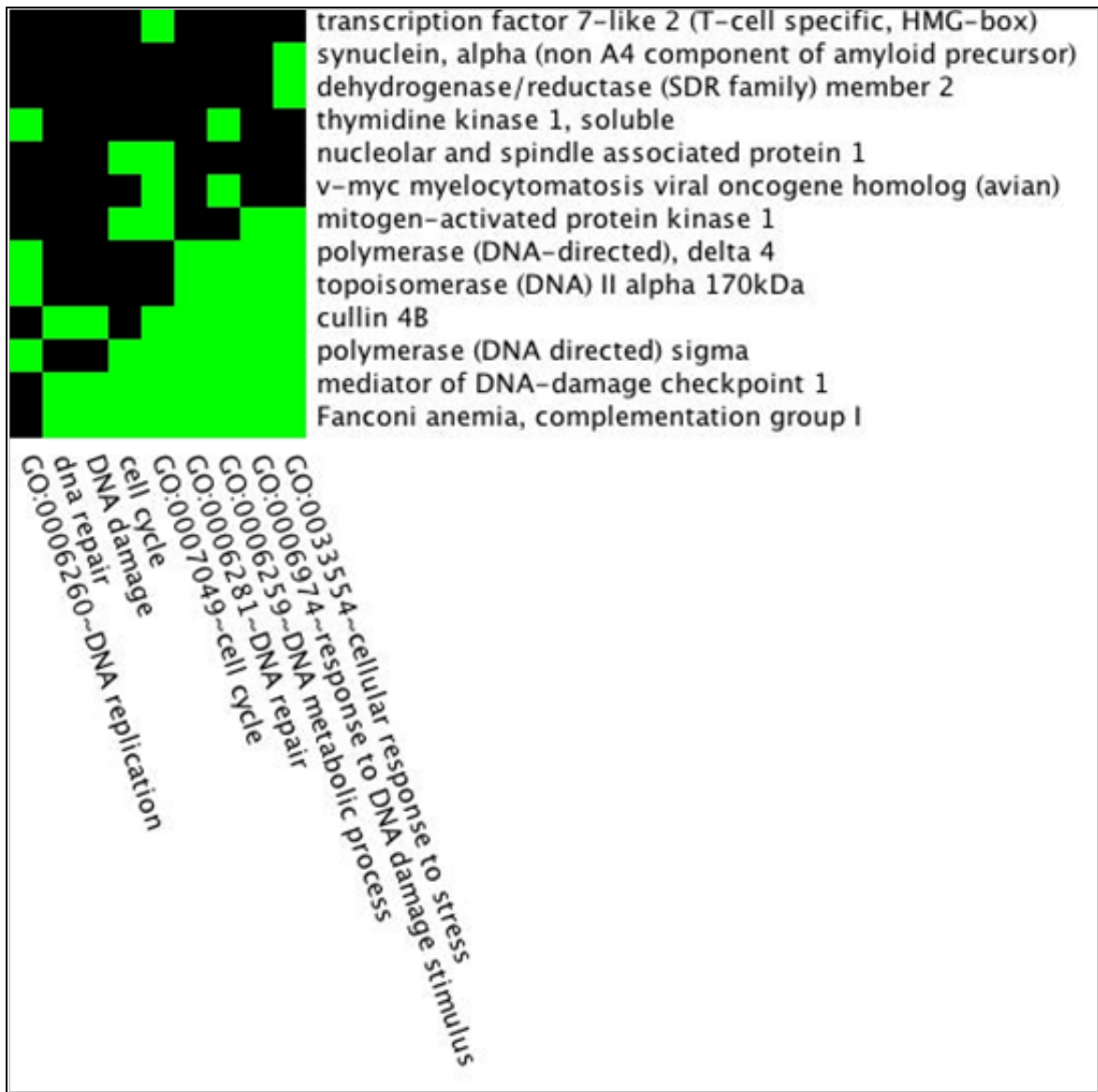


Fig. 3.20. Cluster analysis of functional enrichments for c-Myc correlating genes. Cluster of 13 genes involved in DNA repair. Green - corresponding gene-term association positively reported in DAVID; black - corresponding gene-term association not reported yet in DAVID.

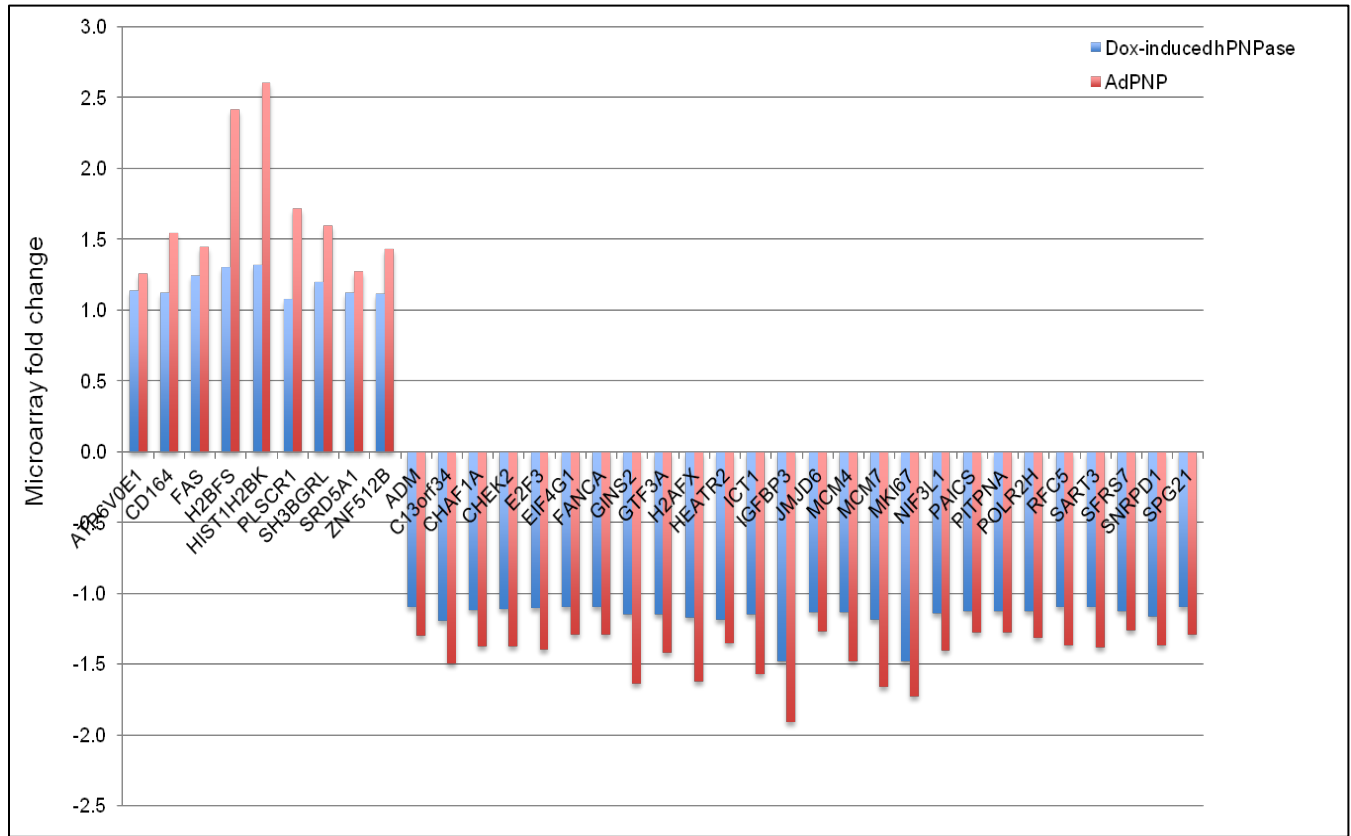


Fig. 3.22. Genes differentially regulated in response to *hPNPase*^{old-35} overexpression as identified by microarray analysis in HO-1 and HeLa cells.

Overall, there were 31 upregulated and 74 downregulated overlapping transcripts in both studies. In order to classify these genes into biological categories, we made use of the ToppGene suite of web applications (Table 3.1). The most significant overrepresented categories were cell cycle, mitosis and DNA metabolism associated functions.

Table 3.1. Functional annotation of genes differentially regulated in response to *hPNPase^{old-35}* overexpression by ToppGene suite.

Functional category	Source	p-value	no. of genes
RNA binding	GO: Molecular Function	1.90E-02	16/857
Cell Cycle phase	GO: Biological Process	5.81E-11	30/864
Mitotic Cell Cycle	GO: Biological Process	1.31E-08	26/785
DNA metabolic process	GO: Biological Process	9.19E-07	25/879
Chromosome	GO: Cellular Component	3.89E-08	21/641
Nucleoplasm	GO: Cellular Component	6.32E-06	28/1483
Genes involved in cell cycle, Mitotic pathway	MSigDB	2.61E-04	14/306

We also compared the top biological functions (Figure 3.23) and canonical pathways (Figure 3.24) associated with all the differentially regulated transcripts in both systems to further understand the global implications of *hPNPase^{old-35}* overexpression. The most significant biological processes identified by IPA (Ingenuity Pathway Analysis) were majorly associated with cell cycle-associated functions. More interestingly, most of the canonical pathways identified in both overexpression systems were also associated with cell cycle regulatory functions.

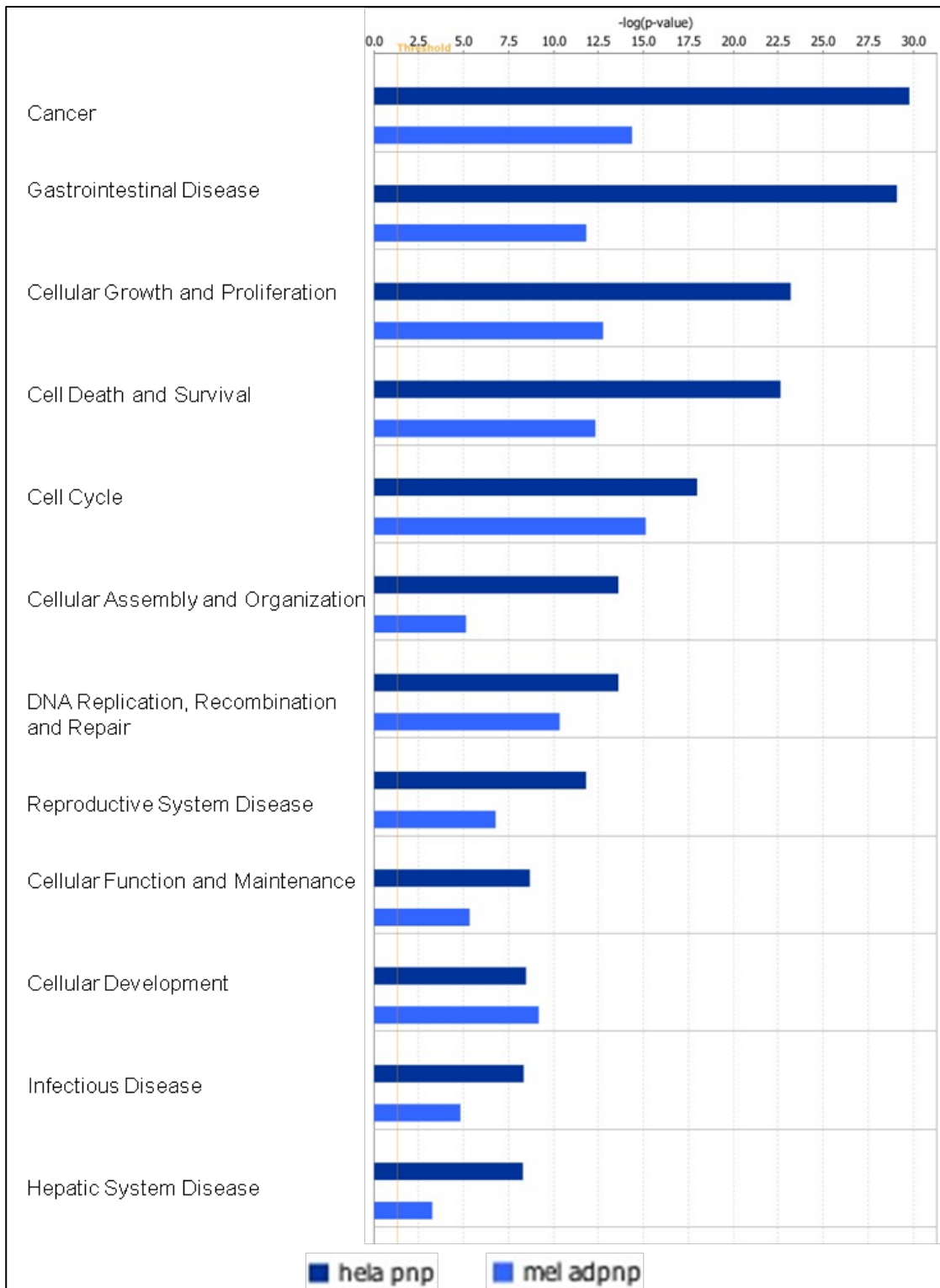


Fig. 3.23. Biological functions identified by IPA corresponding to genes differentially regulated in response to $hPNPase^{old-35}$ overexpression. Hela pnp = dox-inducible $hPNPase^{old-35}$ overexpression, mel adpnp = Ad. $hPNPase^{old-35}$ -mediated overexpression.

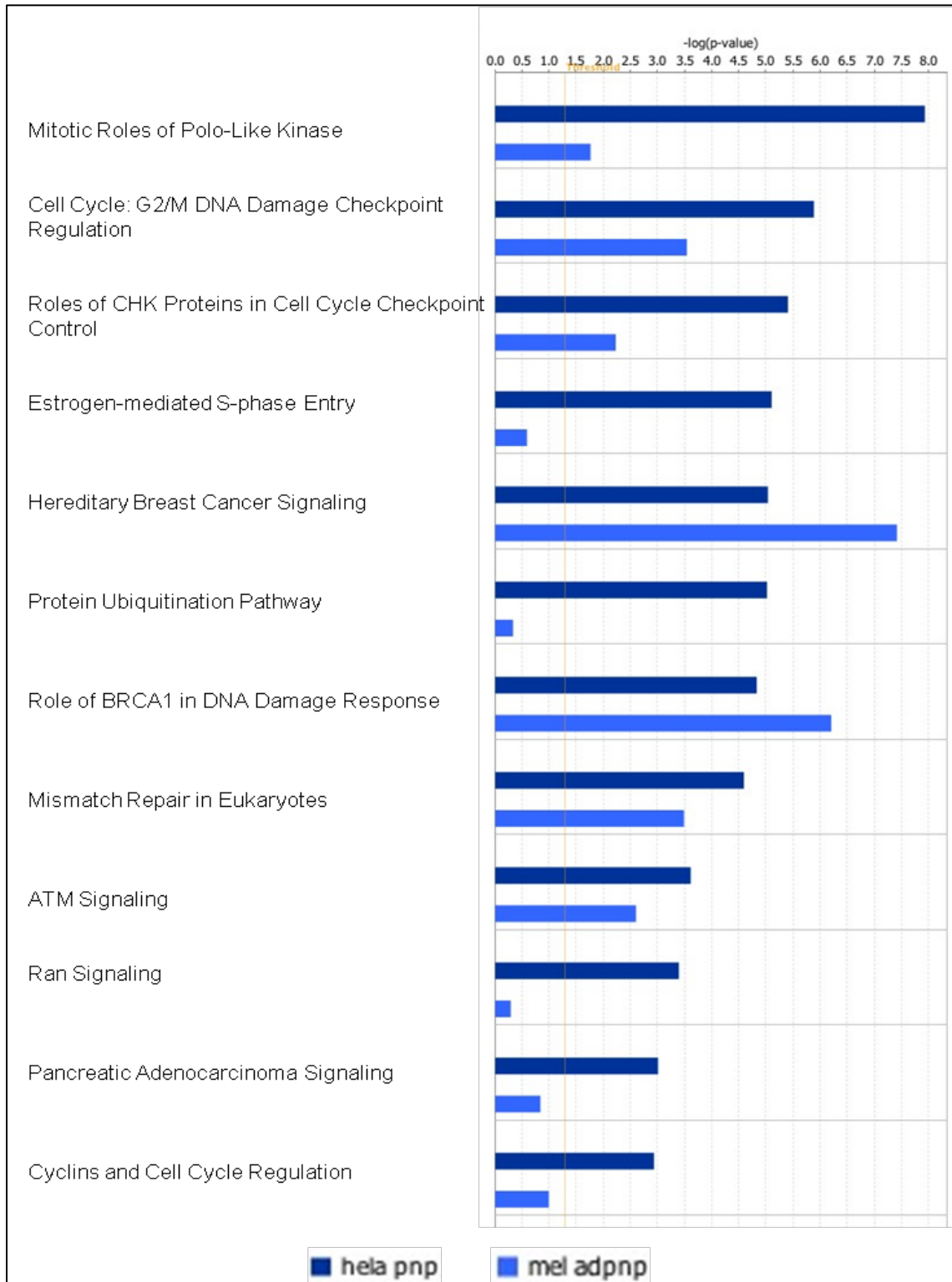


Fig. 3.24. Canonical Pathways identified by IPA corresponding to genes differentially regulated in response to *hPNPase*^{old-35} overexpression. HeLa pnp = dox-inducible *hPNPase*^{old-35} overexpression, mel adpnp = Ad.*hPNPase*^{old-35}-mediated overexpression.

3.5 Discussion

In the present study, we have attempted to further unravel the global gene expression patterns involved with *hPNPase*^{old-35} gain or loss-of-function. We compared the gene expression changes resulting from *hPNPase*^{old-35} knockdown and overexpression in two different cells lines and identified overlapping genes. In the current analysis we identified 62 *hPNPase*^{old-35} induced and 28 *hPNPase*^{old-35} repressed genes. Gene ontology analysis of these *hPNPase*^{old-35} induced and repressed transcripts revealed that a number of them are involved in cell cycle, chromosomal organization and cellular signaling. We obtained similar evidence in Chapter 2, where we showed that overexpression of *hPNPase*^{old-35} cause's global deregulation in cell cycle-associated genes. Our overlapping analysis helped us to identify genes like *KIF3C* [133] and *CDKN1A* [135], which are transcripts upregulated during growth arrest, also induced by *hPNPase*^{old-35}. Also, a number of genes involved in cellular growth and proliferation were found to be downregulated like *CENPA*, *CENPE*, *PLK4*, *TO2PA*, and *POLQ*, transcripts repressed by *hPNPase*^{old-35}. Further support for this premise was obtained when we attempted to identify any particular network the *hPNPase*^{old-35} correlating genes interacted in. We were able to identify two networks relating to mitosis/cell cycle and p21 (a known regulator of growth arrest and cellular senescence) regulation. From this it can be concluded that *hPNPase*^{old-35} plays a role in cell cycle-associated functions, but future studies would be required in order to gain more mechanistic insights of this regulation.

Interestingly, some of these genes are common between the overlapping genes we identified in Chapter 2, *MKI67* (a cellular proliferation marker) and *CENPE*

(Centromere protein E), which are repressed or negatively correlate with *hPNPase*^{old-35} expression and are important for cellular proliferation. In a way this is a further validation of the fact that the expression of these transcripts is in some way regulated by *hPNPase*^{old-35}. Another centomeric protein, which is also repressed, *CENPA* (Centromere protein A), was identified in this analysis. This finding could be of potential importance, as *CENPA* is reported to be a prognostic marker for ER-positive breast cancer [134] and lung adenocarcinoma [135] and could be a potential therapeutic target for treatment of cancer and other *hPNPase*^{old-35} associated diseases. Future studies would be required to further explore this avenue. More interestingly, some of the *hPNPase*^{old-35} correlated genes we report here were also found to correlate with *hPNPase*^{old-35} expression in four TCGA normal and cancer tissue datasets we analyzed. Some of the transcripts identified may provide promising therapeutic leads in terms of treatment options for certain cancers while harnessing on *hPNPase*^{old-35}'s anti-proliferative properties. Among these candidates are *DUSP1*, implicated in promotion of angiogenesis and metastasis of non-small-cell-lung cancer [136]; *ADARB1*, reported to be upregulated in numerous carcinomas [137-139]; *EMR2*, associated with poor prognosis in glioblastoma [140]. Although identification of these transcripts provides valuable future options for treatment of cancer and possible other diseases, the mechanism of *hPNPase*^{old-35} regulation of these genes would need to be elucidated, i.e. are they directly degraded by *hPNPase*^{old-35} (*hPNPase*^{old-35} repressed genes) or do specific miRNAs control their expression which in turn *hPNPase*^{old-35} regulates (*hPNPase*^{old-35} induced genes).

c-myc is a transcription factor involved in the regulation of numerous cellular

processes including but not restricted to apoptosis, cell cycle and metabolism, and most of the c-myc correlated genes we report here are associated with apoptosis, cell cycle, mRNA processing and DNA repair gene ontology categories. c-myc mRNA is also targeted by *hPNPase*^{old-35} for exoribonucleolytic degradation, thus arises the complexity in our analyses of *hPNPase*^{old-35} regulated gene expression changes. To this end we performed our microarray analyses at an early timepoint of 24 hrs following *hPNPase*^{old-35} overexpression, before c-myc levels started to deplete, but a small change of -1.4 fold was still evident in our microarray analyses following *hPNPase*^{old-35} overexpression. Thus, we wanted to confirm if there were transcripts we identified as being *hPNPase*^{old-35} regulated that were also c-myc target genes. A search of the Myc target gene database (<http://www.mycncancer.org>) involving the 11 c-myc correlated/*hPNPase*^{old-35} responsive transcripts did not reveal any report of the direct regulation of these genes by c-myc transcription factor. Thus, at this time we cannot claim that the expression correlation of these transcripts with c-myc means that they are its targets. Future studies involving a search of c-myc binding sites in the promoter region of these transcripts may provide concrete information regarding this premise. Until then it would be safe to proclaim that gene expression changes induced by *hPNPase*^{old-35} may involve numerous other regulatory factors causing global changes in cell cycle-associated functions, apart from *hPNPase*^{old-35}'s direct degradation of mRNA and miRNA species.

Finally, we compared the gene expression profiles of two different cell lines in which we overexpressed *hPNPase*^{old-35} using two different mechanisms, a doxycycline-inducible expression vector and an adenoviral vector. We not only observed 105

overlapping genes between both systems, but interestingly almost all these genes were associated with cell cycle, mitosis and chromosomal functions as identified by gene ontology categories. Apart from the overlapping genes, comparative pathway analysis of both the *hPNPase*^{old-35} overexpression datasets revealed that the most significant affected pathways were related to cellular growth and proliferation. Since there was such a strong correlation of this gene list with cell cycle associated functions we wanted to evaluate whether any of these genes were targets of c-myc transcription activation or repression. A search for these genes in the c-myc target database mentioned earlier revealed that 28 of these genes were predicted targets of c-myc. Out of these 28 genes, four of the downregulated genes (*E2F3*, *PTMA*, *DDX18* and *TFRC*) were also identified by ToppGene suite as validated targets of c-myc transcriptional activation (Table 1). Thus, at this time we can say that overexpression of *hPNPase*^{old-35} may be associated with global regulation of cell cycle associated functions, as evidence is provided by the global deregulation of numerous genes involved in these events, although some of these changes could be associated with c-myc downregulation. In the event of *hPNPase*^{old-35} overexpression, upregulation of pro-apoptotic molecules like *FAS* and downregulation of genes essential for cellular proliferation like *E2F3*, *MCM4*, *MCM7* and *EIF4G1* may tip the balance towards growth arrest. Whether *hPNPase*^{old-35} directly degrades these transcripts (*in vitro* degradation assays would provide the ultimate proof for this hypothesis) or whether these are downstream events of a few preliminary events (like downregulation of c-myc eventually resulting in the cascade of events leading to growth inhibition) remains to be answered in the future studies performed in a c-myc-null background.

CHAPTER FOUR

Analysis of sequence specificity for degradation by hPNPase^{old-35}

4.1 Abstract

Previous studies have established that *c-myc* mRNA is a direct degradation target of hPNPase^{old-35}. Over-expression of *c-myc* devoid its 3'UTR partially but not completely protects HO-1 cells from the growth-inhibitory effects of *Ad.hPNPase*^{old-35} infection. Other RNA species like *c-jun* and *GADD34* are not degraded, suggesting that *c-myc* mRNA is a very specific target of hPNPase^{old-35} degradation. This may be due to the presence of specific sequence or secondary structural elements in the 3'UTR of *c-myc* mRNA. The primary aim of this study is to address this question.

4.2 Introduction

One of the molecular mechanisms elucidated responsible for the growth inhibitory properties of *hPNPase*^{old-35} in cancer cells was found to be selective degradation of *c-myc* mRNA [48]. This has been proven by in vitro mRNA degradation assays also, where *hPNPase*^{old-35} could specifically degrade *c-myc* mRNA, but not other mRNAs such as *c-jun*, *GAPDH* or *GADD34* [29,48]. Specific RNA cis elements have been identified which affect the stability and/or translation of given subsets of mRNAs. Within the 3'UTR, the most commonly found cis elements determinants of mRNA turnover and translation are AU rich elements (AREs). The 3'UTR of *c-myc* mRNA has four such instability elements. It would be important to understand whether the presence of these ARE elements provides a specific sequence identification element or secondary structure that allows its degradation by *hPNPase*^{old-35}. Also, further sequence/secondary structure homology searches identifying similar mRNA species would be helpful in finding other *hPNPase*^{old-35} target genes.

4.3 Materials and Methods

4.3.1 Construction of *c-myc* 3'UTR deletion mutants

In order to evaluate the importance of each of the four AU rich elements in the 3'UTR of *c-myc* mRNA and the role they may play in degradation by *hPNPase*^{old-35}, five sequential deletion constructs including the coding sequence and parts of the 3'UTR of *c-myc* were constructed (M1-M5). The specific 3'UTR deletion fragments were PCR amplified with specific primers using a human cDNA clone (ORIGENE) as template and subcloned into pGEM-Teasy vector (Promega). Subsequently, the fragments were digested with the help of EcoRI and XbaI restriction endonucleases and religated into

pcDNA 3.1/Hygro (+) expression vector. The sequences of all the constructs were verified before transfection. A diagrammatic representation of the deletion constructs M1-M5 is provided in Figure 4.1.

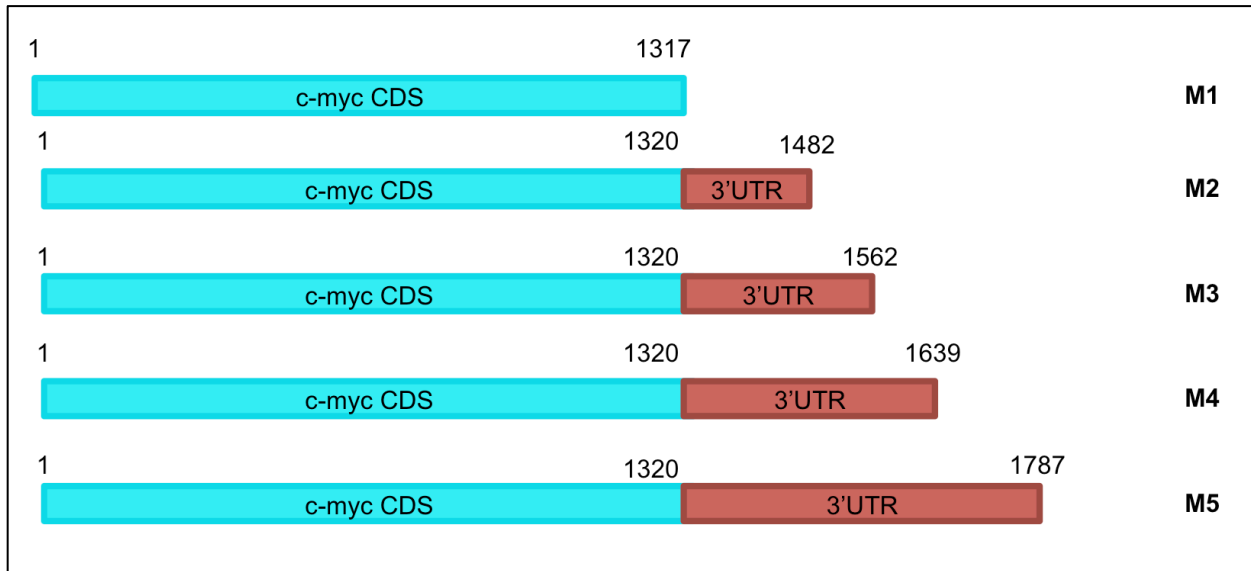


Fig. 4.1. Schematic representation of *c-myc* 3'UTR deletion constructs.

4.3.2 Colony Formation Assays

HO-1 cells were plated at a density of 2×10^5 cells/6-cm dish and 24 h later were transfected with 4 μ g of either empty vector or plasmids M1-M5 using LipofectamineTM 2000 (Invitrogen) transfection reagent according to the protocol from the manufacturer. After 36 h, the cells were infected with Ad.Vec or Ad.hPNPase^{old-35} at a multiplicity of infection (m.o.i.) of 5000vp/cell; 6 h later, the cells were trypsinized and counted and 10^3 cells were plated in 6-cm dishes in triplicate. Colonies were visualized by Giemsa staining and counted after 3 weeks.

regions in the 3'UTR of *c-myc* mRNA that could be required for degradation by hPNPase^{old-35}. In order to evaluate this hypothesis, HO-1 cells were transfected with the five 3'UTR deletion constructs (M1-M5), infected with Ad.hPNPase^{old-35} and the growth of cells was analyzed by colony formation assays after a period of 3 weeks (Figure 4.3). We observed that growth suppression caused by adenoviral-mediated hPNPase^{old-35} overexpression could be partially rescued by c-myc-3'UTR deletion constructs M1 (28%, offers most protection as it is completely devoid of the 3'UTR), M2 (23%), and M3 (17%) (Figure 4.4). Transfection with M4 resulted in >80% growth inhibition in conjunction with Ad.hPNPase^{old-35} infection and M5 transfection resulted in only a ~10% rescue in growth followed by Ad.hPNPase^{old-35} infection as compared to constructs M1-M3, as shown in Figure 4.4. Based on these preliminary results we can presume that the region between 1562 and 1787bps (sequence present in constructs M4, M5 and deleted from constructs M1-M3) in the 3'UTR sequence of c-myc could possess recognition sequences or secondary structure elements necessary for hPNPase^{old-35} mediated degradation thus eliminating the growth protection rendered by constructs M1-M3 (which do not possess the specific sequence region and are protected from hPNPase^{old-35} degradation). Also, since M5, which has the complete 3' UTR, provided more protection than M4 (which has region 1639-1787 deleted), it can be presumed that the specificity of degradation by hPNPase^{old-35} is most likely dependent on secondary structural elements rather than primary sequence alone. These results would need to be further validated as although done in technical triplicates, these results are based on one biological experiment. Future experiments involving *in vitro* transcription of these deletion fragments followed by hPNPase^{old-35} *in vitro* degradation assays would need to

be performed to analyze whether fragments M1-M3 are indeed protected from hPNPase^{old-35} degradation and whether fragments M4, M5 are degraded by hPNPase^{old-}

35

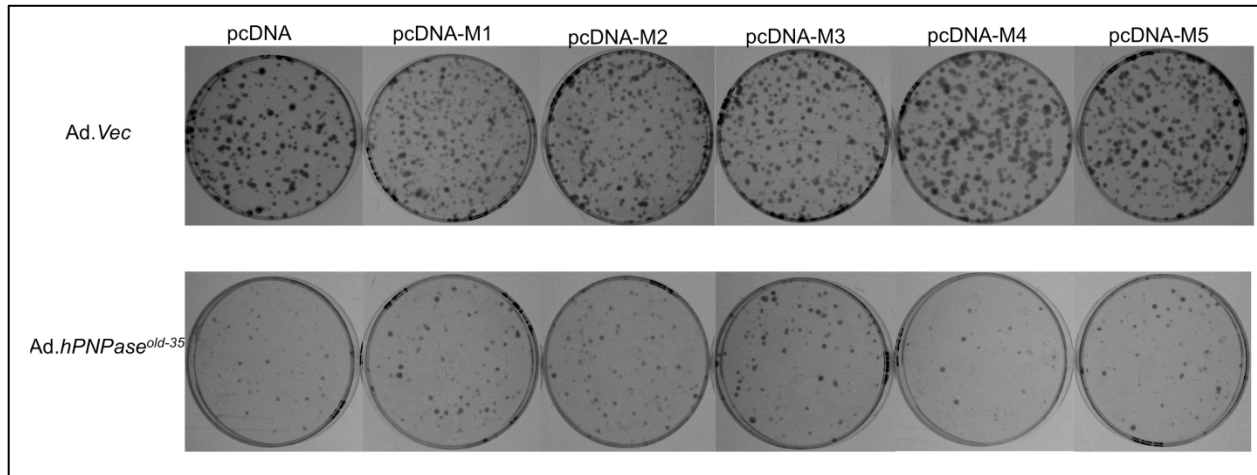


Fig. 4.3. Growth rescue experiment. HO-1 cells were plated at a density of 2×10^5 cells/6-cm dish and 24 h later were transfected with 4 μ g of either empty vector or *c-myc* 3'UTR deletion constructs M1-M5. After 36 h, the cells were infected with Ad.Vec or Ad.hPNPase^{old-35} at a multiplicity of infection (m.o.i.) of 5000vp/cell; 6 h later, the cells were trypsinized and counted and 10^3 cells were plated in 6-cm dishes in triplicate. Colonies were visualized by Giemsa staining and counted after 3 weeks.

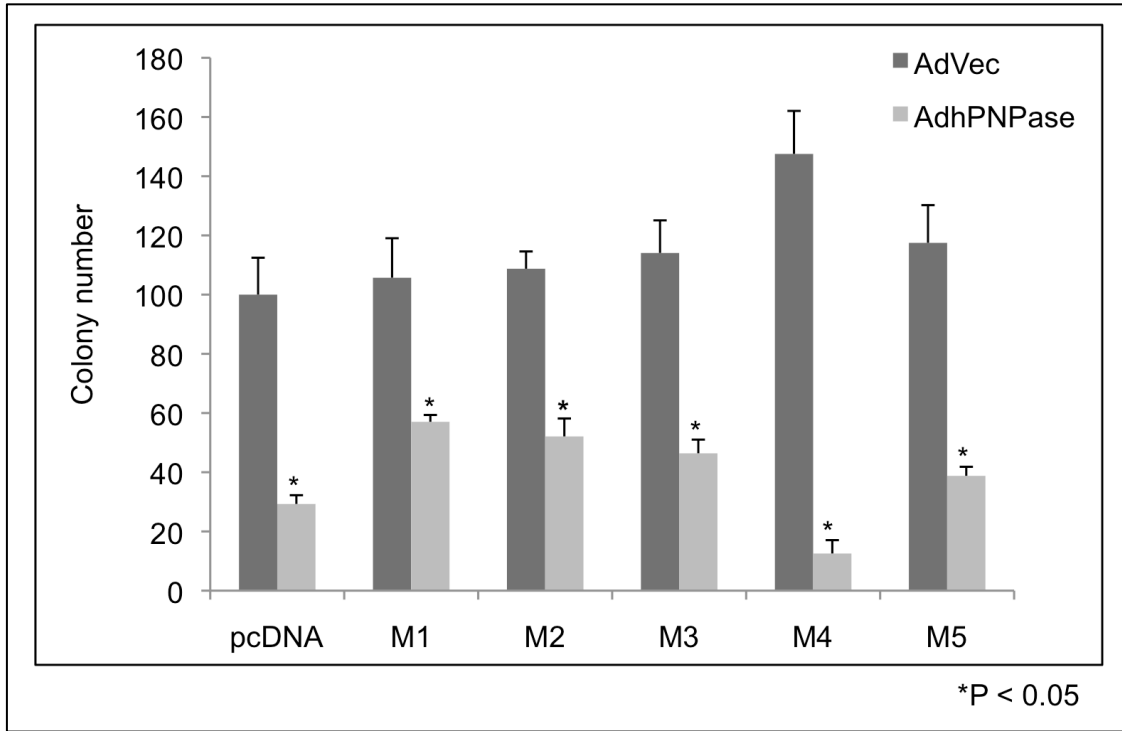


Fig. 4.4. Graphical representation of colony numbers as described in Fig. 4.3. The data represent mean \pm standard error of one experiment done in triplicate, statistical significance was determined by two-tailed student's t-test, *P<0.05.

CHAPTER FIVE

Evolutionary dynamics of Polynucleotide phosphorylases

Part of the work presented in this chapter has been submitted for publication in *Molecular Phylogenetics and Evolution* (2013).

5.1 Abstract

Polynucleotide phosphorylase (PNPase) is an evolutionarily conserved 3'→5' phosphate-dependent exoribonuclease belonging to the PDX family of proteins. It consists of two catalytic RNase PH domains (PNP1 and PNP2), an α -helical domain and two RNA-binding domains. The PNP1 and PNP2 domain share substantial sequence and structural homology with RNase PH (RPH), which is another PDX family member found in all the three major kingdoms of life, suggesting that these three domains originated from a common ancestor. Phylogenetic analysis (based on the PNPase /RNase PH sequence information for 43 vertebrate taxa) shows that PNP2 and RPH are sister taxa which arose through duplication of the ancestral PNP1 domain. Also, all three domains (PNP1, PNP2 and RPH), along with the KH and S1 domains have undergone significant and directional sequence change, as determined by branch and site-specific dN/dS analyses. In general, codons that show dN/dS ratios that are significantly greater than 1.0 are outside the ordered regions (α -helices and β -sheets) of these protein domains. In addition, sites that have been selected for mutagenesis in

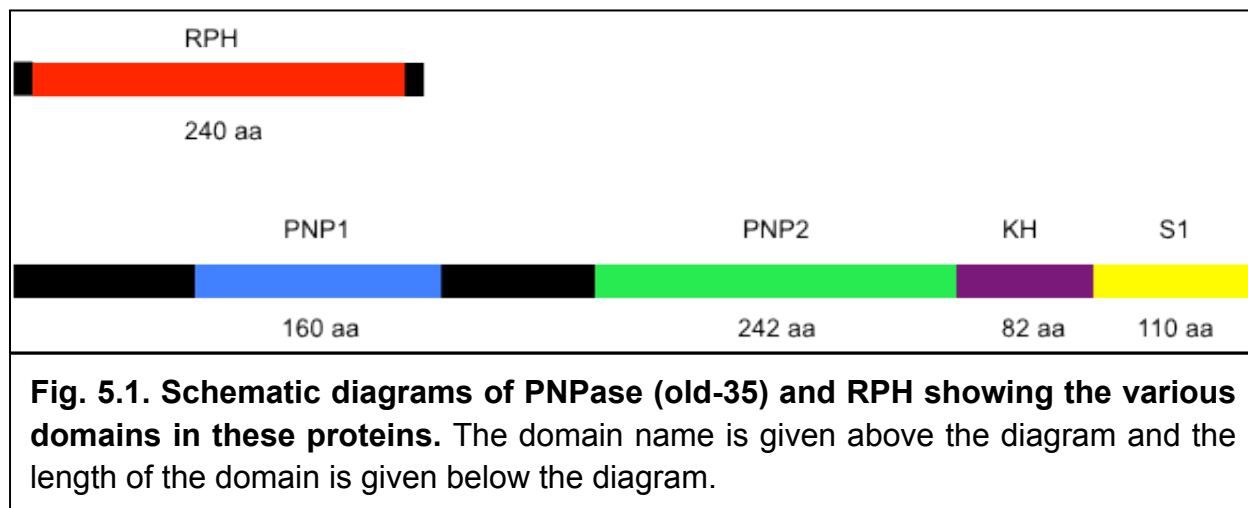
these proteins lie embedded in regions where there is a preponderance of codons with dN/dS values that are not significantly different from 0.0. Overall, this report is an attempt to further our understanding of the evolutionary history of these three protein domains, and define the evolutionary events that led to their refinement in the vertebrate lineage leading to mammals.

5.2 Introduction

RNA metabolism plays a significant role in the post-transcriptional control of gene expression in both prokaryotic and eukaryotic organisms [12]. Key players involved in the decay and processing of various RNA species are a special class of enzymatic proteins called ribonucleases (RNases) [37,141]. Based on their degradative functions, RNases are divided into endo- and exo-ribonucleases [13,93]. One such exoribonuclease is polynucleotide phosphorylase (PNPase), which is an ancient enzyme that has been evolutionarily conserved in all the kingdoms of life, although it is absent in Archaea and certain single cell eukaryotes [91]. Functionally, it is a 3'→5' phosphorolytic exoribonuclease belonging to the PDX family of proteins [4,14]. The PDX family includes RNase PH, another phosphate-dependent exoribonuclease. Considered the simplest member of the PDX family, RNase PH was first identified in *E.coli* [28,142], and its orthologues are found in all kingdoms [91]. The main difference between RNase PH and PNPase is that *in vivo*, RNase PH is involved in the processing of tRNA precursors and in the digestion of structured RNA in bacteria [142,143], whereas PNPase mainly plays a role in mRNA degradation [16,48].

Sequence alignment shows that PNPases from various kingdoms share a classical domain structure consisting of: two N-terminal RNase PH domains (containing

the PDX catalytic sites, designated PNP1 and PNP2), an α -helical domain between PNP1 and PNP2, and the RNA-binding domains KH (K-homology) and S1 domain located at the C-terminal (Figure 5.1) [13,18,19].



Both RNase PH and PNPase form ring-like structure (hexameric and homotrimeric respectively) with a central channel in its active form. The level of structural and sequence similarity between the PDX domains in PNPase and RNase PH raises the possibility that these domains may have originated from a common ancestor (in the most recent common ancestor of life; MRCA) via gene duplication events [91,93].

Previously, our primary focus has been to analyze how the three PDX domains (PNP1, PNP2 and RPH) have evolved in the tree of life. However, recent structural and phylogenetic information on these domains has made possible the examination of the evolutionary dynamics of their function. One common tool that is used to examine functional significance of proteins over evolutionary time is to characterize the impact of natural selection on sequence change. The methodology for statistically assessing

patterns of natural selection in a phylogenetic context on a residue by residue basis, as well as on a branch by branch basis in a phylogeny are well developed [144-147]. They are based on corrected assessment of the ratio of nonsynonymous to synonymous substitutions over evolutionary time. The null hypothesis in such studies is the situation where the nonsynonymous to synonymous changes are equal in abundance. A statistically significant overabundance of nonsynonymous change relative to synonymous change is usually taken as an indication of positive natural selection. And a significant lack of nonsynonymous change to synonymous change has been taken as evidence for negative or purifying selection by researchers.

These approaches have been criticized on statistical grounds [148] and on the grounds that statistical demonstration of selection is only the first step in understanding natural selection on proteins. In other words, once natural selection has been suggested by statistical methods it should also be tested in a functional or biochemical context [148,149].

Here, we use the well known functional and structural characteristics of the PNP and RPH domains to examine the validity of statistically determined measures of natural selection. Several sites in PNPases have been mutagenized and the functional significance of those mutations has been well characterized. In addition, sequence integrity is an invariable factor [148], but recent advances in structural biology show that secondary structure is equally important in not only determining the functionality but also in dictating the rates of site-specific evolution of proteins [150]. These residues under natural selection (positive or negative) may occur in ordered (α -helices and β -sheets) or disordered (random coils and turns) regions [151]. However, from our

analyses of PNP1, PNP2 and RPH sequences from 43 eukaryotic taxa (Table 5.1), we can infer that the residues with dN/dS measures greater than 1 are almost entirely found outside of α -helices and β -sheets. Finally, through phylogenetic analysis, we have been able to discern the possible time course of evolution and molecular events when PNPase (PNP1, PNP2, KH and S1) and RPH domains might have been under positive natural selection among vertebrates.

Table 5.1. Taxa used in the study

Deuterostome		
	Mammals	Primates
		Homo
		Pan_
		Papio
		Macaca
		Nomascus
		Otolemur
		Calithrix
		Saimiri
	Carnivora	Felis
		Canis
		Ailuropoda
	Rodentia	Cricetulus
		Mus
		Rattus
		Cavia
		Oryctolagus
		Sus
		Bos
		Equus
		Loxodonta
	Marsupials	Monodelphis
		Sarcophilus
		Ornithorhy
	Lizards/Birds	Gallus
		Taeniopygia
		Anolis
	Amphibia	Xenopus
	Fish	Takifugu

		Danio
		Oreochromis
Other deuterostome		
		Branchiostoma
Protostome		
	Insect	Drosophila
		Tribolium
	Nematode	C.elegans
	Worm	Brugia
	Lower Metazoa	Amphimedon
		Trichoplax
		Nematostella
Plant		Arabidopsis
		Physcomytrella
		Selaginella

5.3 Materials and Methods

5.3.1 Sequences and Matrix construction

PNPase and RNase PH sequences were obtained from Genbank using a taxonomic sampling strategy to cover the eukaryotic tree of life. Only PNPase and RNase PH sequences from fully sequenced and accurately annotated eukaryotic genomes were used. A list of the taxa used in this study is given in Table 5.1. Codon sequences were obtained in all cases and accession numbers for the sequences are given in Table 5.1. Sequences were aligned in TranslatorX [152] a program that aligns codons using amino acids as a guide. For the various analyses in this paper we generated several different phylogenetic matrices that were used in tree building and natural selection detection programs. The first kind of matrix we generated was a taxonomic based matrix with the 43 taxa we list in Table 5.1. This matrix consists of full-length PNP sequences concatenated with RNase PH sequences for the same 43 taxa in a NEXUS formatted matrix. The different regions of the PNPase genes and the RPH

gene (Figure 5.1) were then partitioned using NEXUS commands in the NEXUS matrix. The root of this matrix was established using the three plant taxa (Arabidopsis, Selaginella and Physcomytrella) as outgroups.

The second kind of matrix combined PNP1, PNP2 and RPH domains from all 43 taxa used in this study. This matrix was constructed using a separate alignment procedure from the taxonomic-based matrix. In addition two RNase II genes (one from human and the other from Trichoplax) were used to root trees for this latter matrix.

5.3.2 Phylogenetic analysis

Phylogenetic trees were constructed using parsimony, maximum likelihood and Bayesian approaches [153]. The model used was a GTR with invariants rates and gamma distribution (estimated from the data set). 100 bootstrap replicates were performed when bootstrapping (either MP or ML) [154]. Bayesian analysis was performed using 1 million generations of simulation and the model described above. For the selection analyses we used a predetermined tree topology based on the well-accepted taxonomy of the organisms in the study [155].

5.3.3 Detecting the Statistical imprint of skewed dN/dS ratios

For the selection analyses we used a predetermined tree topology based on the well-accepted taxonomy of the organisms in the study [146]. Two tests were used to detect statistically significant patterns of skewed dN/dS ratios. The first test determines the branches in the accepted phylogeny where statistically significant departure from neutral evolution occurs. The BREL (Branch-site Random Effects Likelihood) test in the HyPhy [156] package was used on the three domains for the taxon based matrices

(PNP1, PNP2 and RPH) separately. In addition, the BREL option was also used to analyze branch specific natural selection in the matrix with all three-domain sequences as terminals. The default settings and the accepted tree topology were used in these tests [157,158].

The second test implemented the MEME (Mixed Effects Model of Evolution) [159] option in DataMonkey, the web version of HyPhy [157,159]. This option uses mixed model approaches to detect departure from neutrality at individual codons. This latter test was performed individually on each of the three domains – PNP1, PNP2 and RPH.

5.3.4 Mapping Sites with dN/dS Skew Onto Secondary and Tertiary Protein Structure

The NIH-NCBI Structure Summary MMDB (<http://www.ncbi.nlm.nih.gov/Structure/MMDB/mmdb.shtml>) was used to map residues onto the tertiary structure of PNPase and RNasePH proteins. The CN3D software (<http://www.ncbi.nlm.nih.gov/Structure/CN3D/cn3d.shtml>) was used to visualize tertiary structure. This program allows for the selection of residues previously determined as under positive natural selection using the “Select Columns” option. Once these residues are selected their position in the three dimensional model of the protein are marked by yellow “slivers”. The CN3D structures presented are for the trimeric conformation of the protein.

The secondary structure of these two proteins was mapped using the RCSB-PDB web browser (<http://www.rcsb.org/pdb/home/home.do>) using the “Sequence”

pulldown menu. This web browser produces a linear model of the proteins with regions corresponding to alpha helices, beta sheets and other critical secondary structures marked on the sequence. For obtaining both the tertiary and secondary structures of these proteins the human sequence was used as a guide.

5.4 Results

5.4.1 Phylogenetic relationships of PNP domains

The matrix with domains as terminals yielded a tree where the different PNP domains are monophyletic with respect to one another (Figure 5.2). In addition, the root of the Bayesian domain tree indicates that PNP1, PNP2 and RPH cannot be determined. However, both maximum parsimony and maximum likelihood recover a tree wherein PNP2 and RPH are sister taxa (root at arrow in Figure 5.2), as previously reported by Leszczyniecka et al., (2004) [91]. This rooting indicates that the PNP1 domain appeared first in the genomes of the common ancestor of all life, and that PNP2 and RPH arose as the result of subsequent duplication events. This rooting lacked robustness since the out-groups (human and trichoplax RNase II) are quite distant from the in-group domains. Large out-group distances can result in random rooting [160] on the in-group and this may explain why the Bayesian analysis fails to recover a more resolved root for the domain tree.

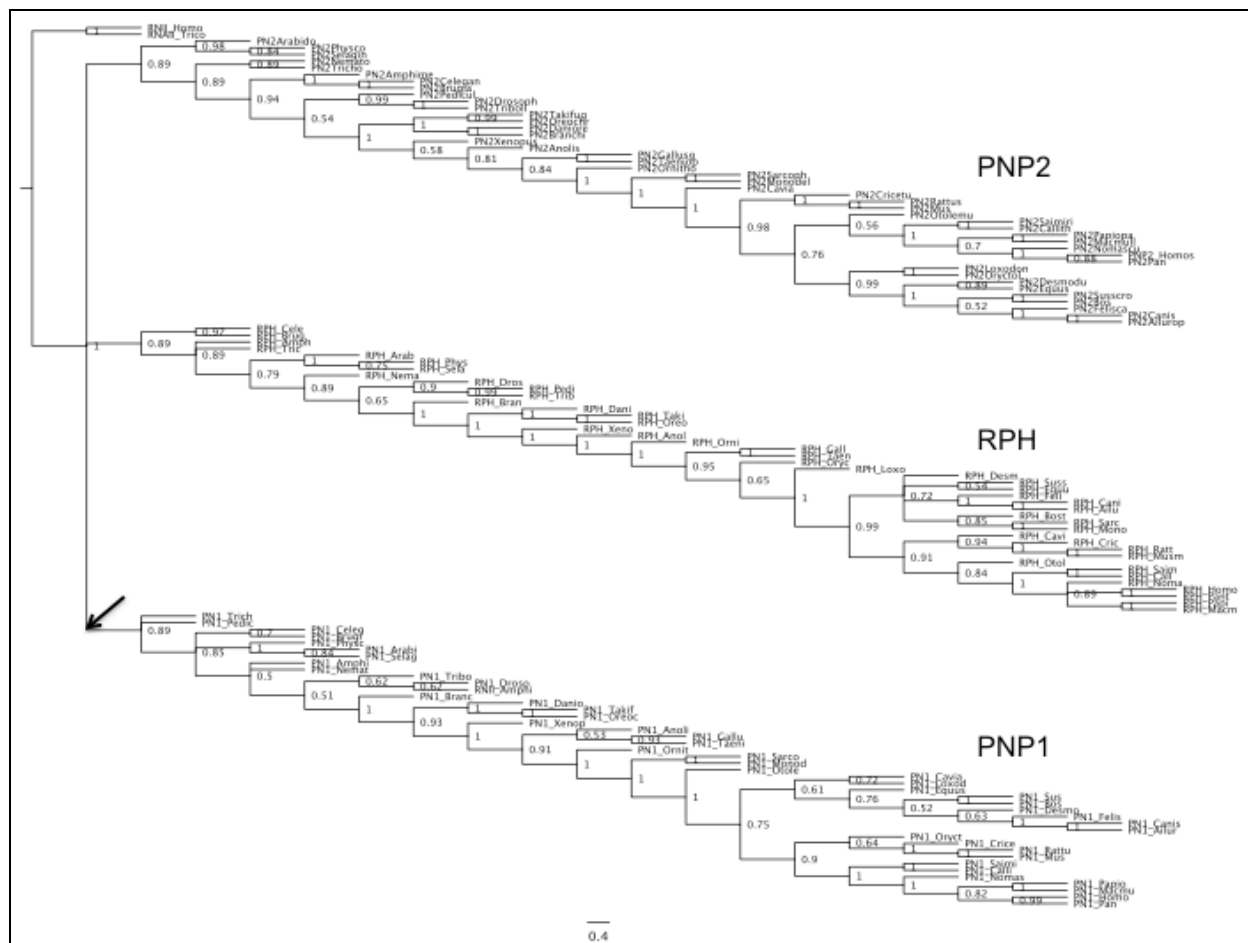


Fig. 5.2. Bayesian phylogenetic tree showing the relationship of the three major domains (PNP1, PNP2 and RPH) examined in this study.

5.4.2 Branch Specific Skew in dN/dS ratios

The BREL test in HyPhy detected several branches in the backbone of the vertebrate phylogeny leading to mammals that show significant departure from a dN/dS ratio of 1.0 (Figure 5.3). Specifically all of the seven branches in the tree in Figure 5.3, leading to mammals from the common ancestor of *Branchiostoma* and true vertebrates show a shift in intensity of this skew. Of these seven branches, three are impacted by skewed ratios in PNP1, two in PNP2 and three in RPH. There are only two other

regions of the tree where two of the genes exhibit skew of this ratio. One region involves the lineage leading to protostomes (i.e. insects and nematodes), and the other, the lineage leading to *Bos* and *Sus* (bovids and pigs). These results suggest a major shift in sequence dynamics and subsequent stabilization of the evolution of these protein domains as vertebrates, fish and mammals evolved.

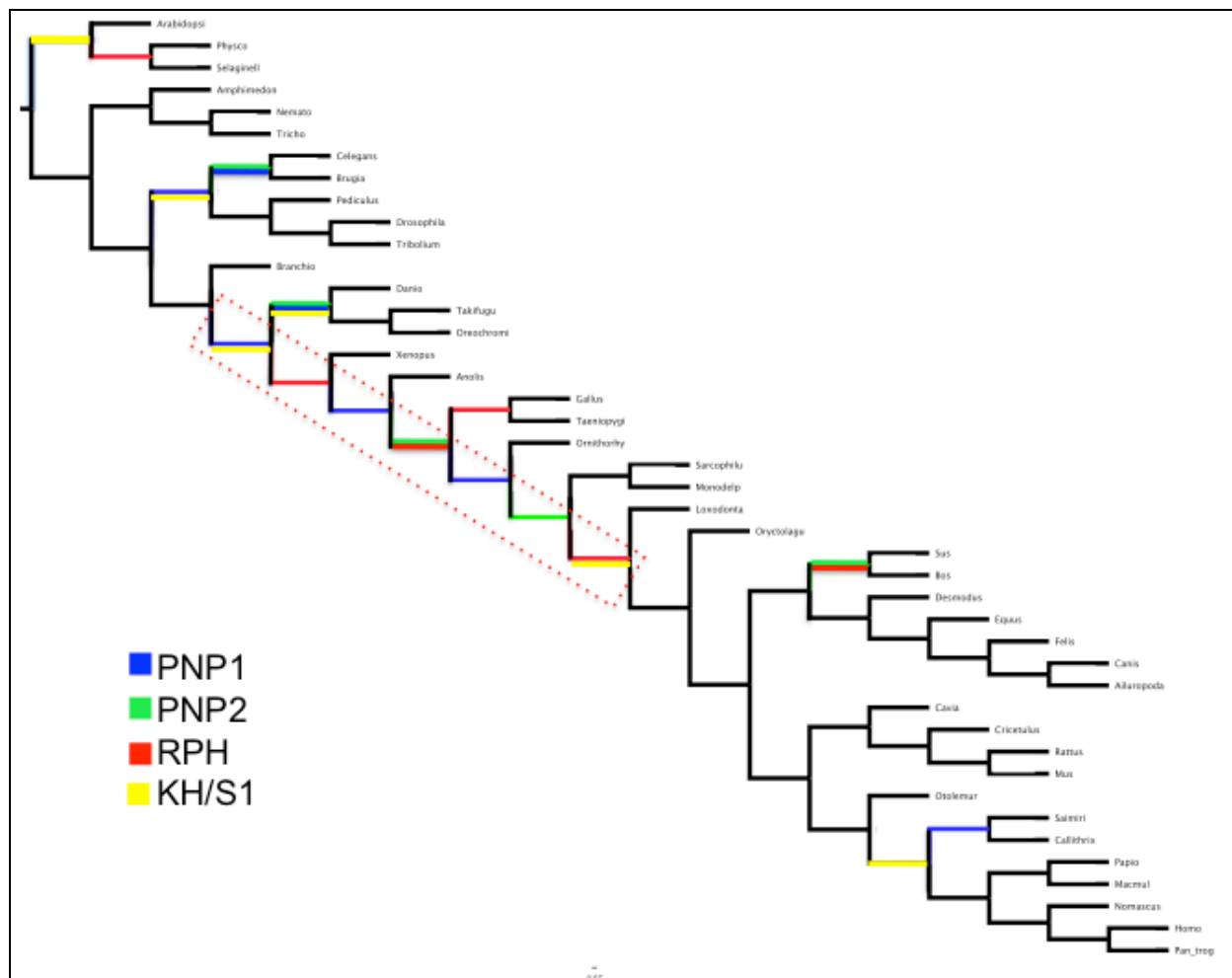


Fig. 5.3. Tree of animal life using plants as an outgroup showing which branches on the tree have experienced positive dN/dS skew. The domains that are under selection are shown in colors and the nodes where positive skew exists are colored accordingly for the different domains. The dotted lined box indicate the region of the backbone in the tree leading from primitive vertebrates to mammals where positive dN/dS skew has occurred in the four domain regions we examined.

5.4.3 General Site-specific Skew in dN/dS ratios in PNP domains

The MEME analyses of PNP1, PNP2, RPH and the KH domains (Figure 5.4A) indicate that the sites experiencing positive dN/dS skew are generally outside of α -helices and β -sheets (Figure 5.4B). Surprisingly, RPH appears to have twice as many sites that are positively skewed compared to PNP1 or PNP2 (Figure 5.4B).

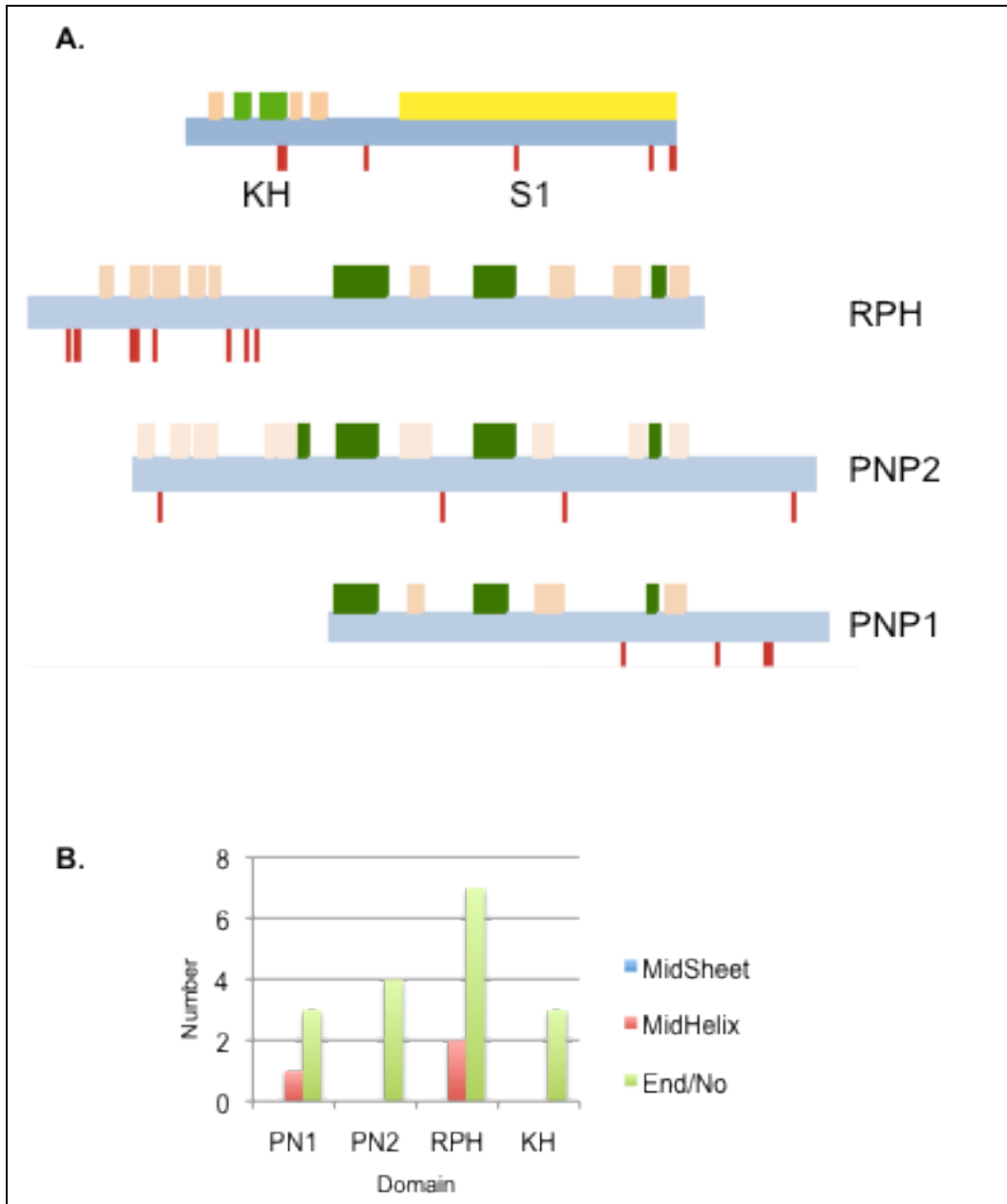


Fig. 5.4. Site-specific positive dN/dS skew in the three PNP domains (PNP1, PNP2 and RPH) and the KH and S1 domain. (A) The cartoons show the location of α -helices (green), β -sheets (tan), and the S1 region (yellow). Also indicated are the specific locations of sites that have skewed dN/dS ratios (red lines). (B) Bar chart showing the number of sites in beta-sheets and alpha helices under positive skewed dN/dS. The green bars show the number of sites that are either not in sheets and helices or on the very edge of a sheet or helix. The red bars show the number of sites that have positive skewed dN/dS that are squarely within alpha helices. There were no sites positive skew found squarely in beta sheets.

All of the RPH sites that show positive skew are in the N-terminus of the protein. In contrast, the sites with positive dN/dS ratios in the PNP domains are oftentimes in the C-terminus, which might impact how the helices and β -sheets in the domains make turns. The S1 domain consists primarily of β -sheets with four skewed sites at the C-terminus, outside of the sheets (Figure 5.4). In total, 17 sites in all of these domains with positively skewed dN/dS ratios are either outside of sheets and helices or in the first residue of a sheet or helix. Only three sites with positive skew lie squarely within alpha helices, and none within the beta sheets. Secondary structure plots indicating sites experiencing positive dN/dS skew in PNP1, PNP2, KH/S1 and RNase PH are provided in Figures 5.5 and 5.6.

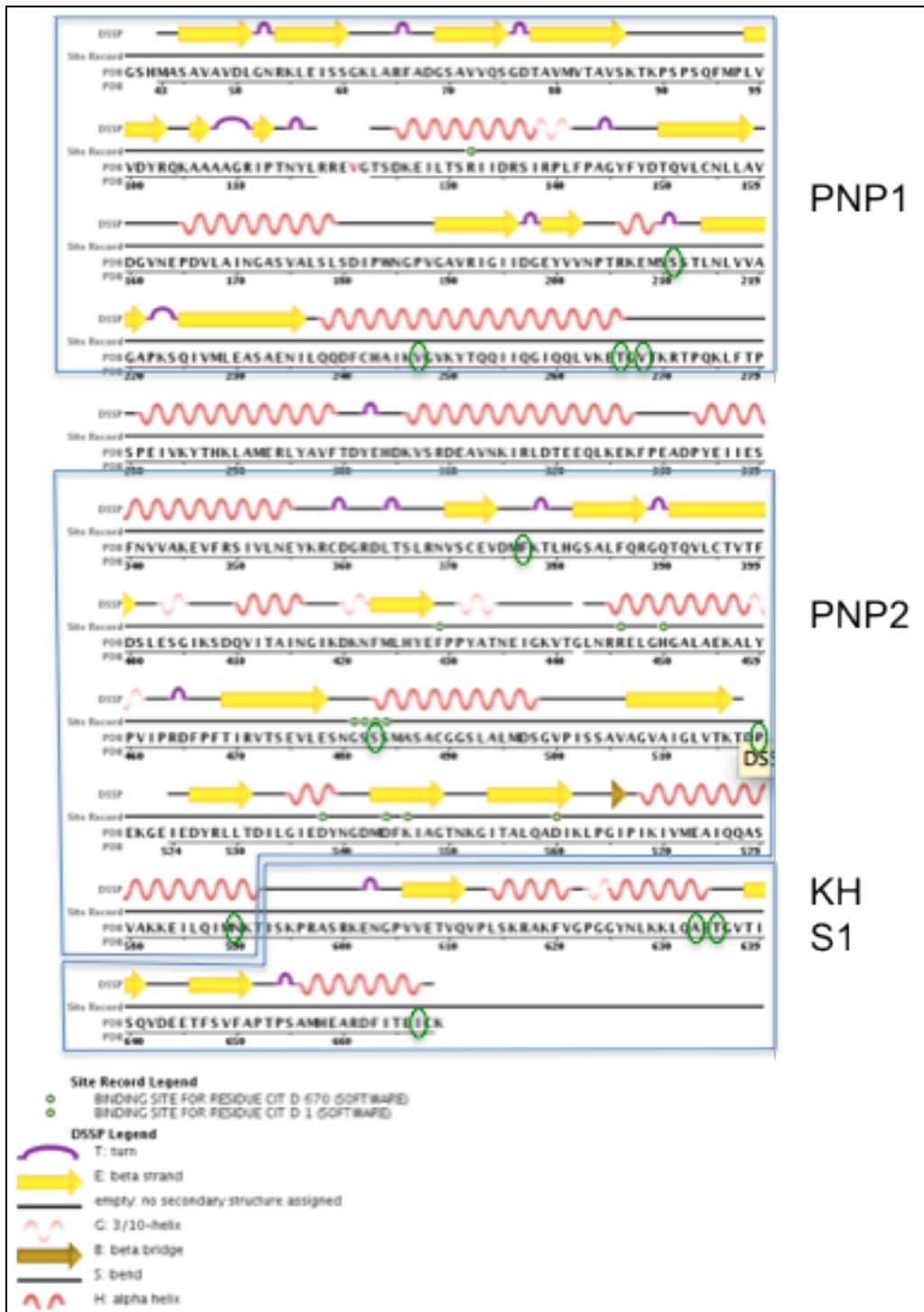


Fig. 5.5. Secondary structure plot indicating sites under positive selection in PNP1, PNP2 and KH/S1 (sites highlighted as green circles).

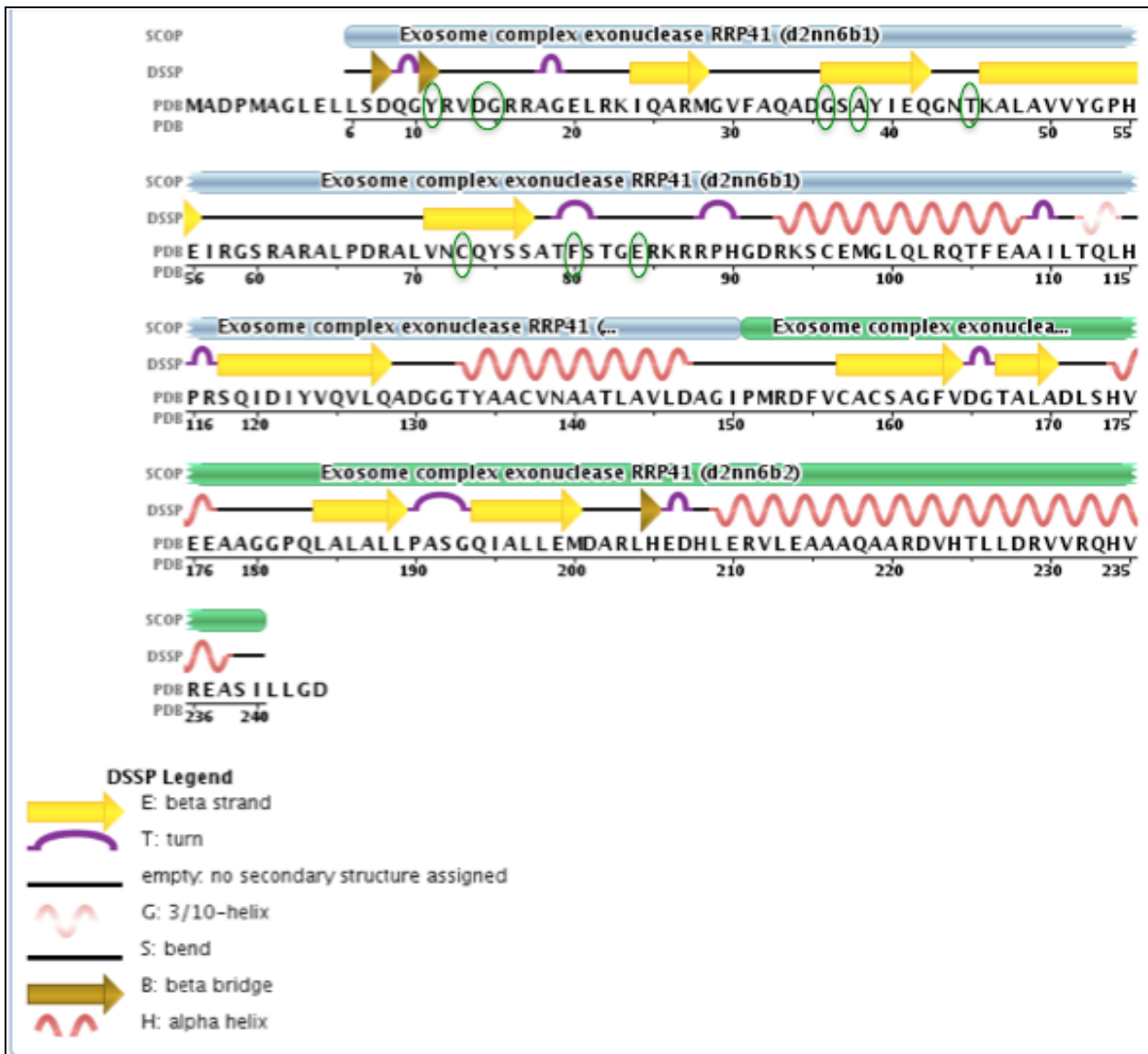


Fig. 5.6. Secondary structure plot indicating sites under positive selection in RNase PH (sites highlighted as green circles).

5.4.4 Correlating skewed dN/dS with structural variants

The locations of residues with significant $dN/dS > 1.0$, relative to the protein's three-dimensional structure were visualized through the use of the CN3D software. Most of the skewed sites (yellow linings) in the PNP1, PNP2, and KH/S1 domains of PNPase (Figure 5.7), as well RNase PH (Figure 5.8) are either outside or at the edges of ordered secondary structures.

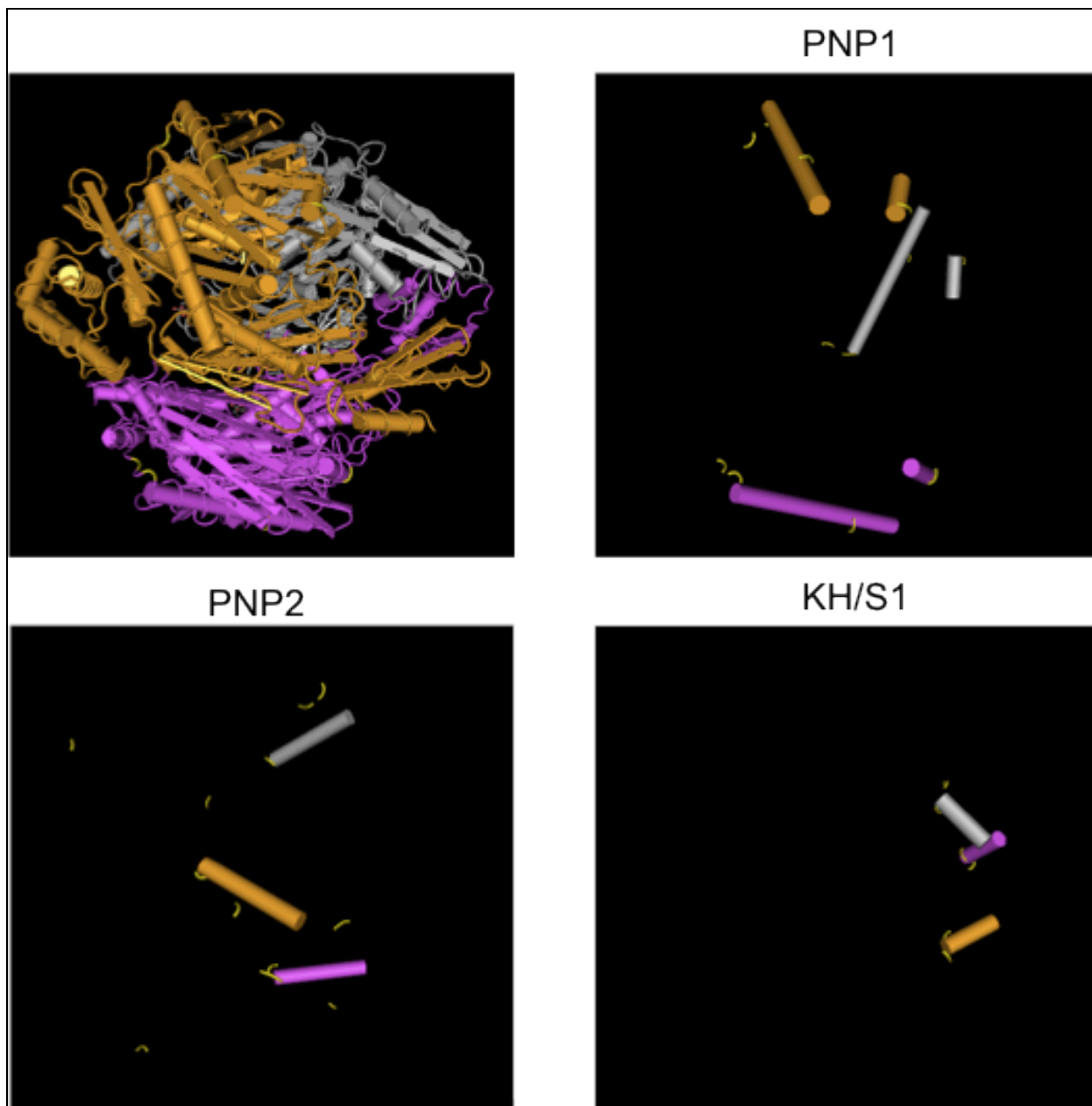
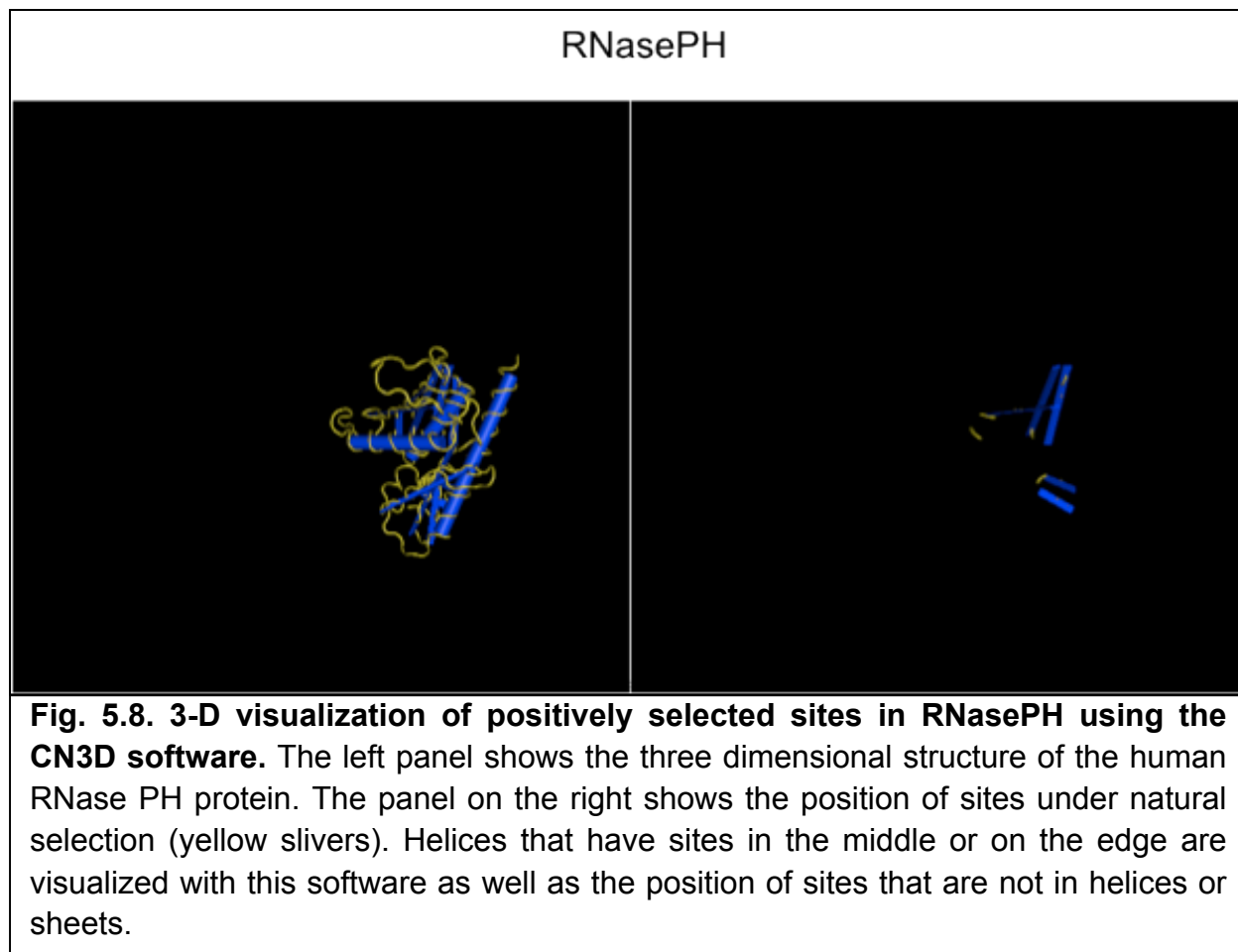


Fig. 5.7. 3-D visualization of positively selected sites in PNP1, PNP2 and KH/S1 using the CN3D software. The upper left panel shows the three dimensional crystal structure of the human PNPase^{old-35} protein. Each of the subsequent panels shows the position of sites under natural selection (yellow slivers). Helices that have sites in the middle or on the edge are visualized with this software as well as the position of sites that are not in helices or sheets.



Next we compared the positions of residues that cause known structural variation via mutagenesis with their dN/dS ratios. Because the functional significance of the mutagenized residues is known this comparison allows us to examine possible correlations of significant dN/dS values with function. Since most of the mutagenized sites were chosen to disrupt function, we do not expect a direct correlation of significantly skewed dN/dS ratios with mutagenized site. In fact, we hypothesize that mutagenized sites disrupting function should be under intense purifying selection, and have no significant dN/dS ratios. For the most part this is what we observe, and in addition, it appears that many of the sites chosen for mutagenesis are embedded in

regions of these domains that show dN/dS ratios that are not significantly different from 0.0 (an indication of strong negative or purifying selection). There are some exceptions.

PNPase domains: Table 5.2 lists the residues in PNP domains that have been mutagenized and the functional significance of the variation along with the sites detected in this study with statistically significant dN/dS ratios > 1.0. The only extreme overlap of positively skewed dN/dS ratio with a site mutagenized that alters function is S483 a dN/dS > 1.0 site which is a binding site for Citrate D 670 located near the active site. This significant dN/dS site is right next to the S484 mutagenesis site, which abrogates polymerization and degradation activities of hPNPase. The juxtaposition of these two sites is interesting and it could be hypothesized that the S483 dN/dS site might have been involved in the evolution of this function. P519 a site that has a dN/dS ratio > 1.0 is also the position of a somatic mutation (P519T) found in hPNPase that was identified through the COSMIC (<http://cancer.sanger.ac.uk/cosmic>) database. This site is not observed as a mutated site in human populations with any significant frequency, but it could be hypothesized that this site is important for a derived hPNPase function in normal human or primate tissues and this function may be disrupted after the mutation found in a cancer patient (P519T). This might be a very interesting residue to work with in the future and would have to be validated in future *in vitro* experiments. Since this residue is solvent exposed, it could be a site required for interaction with other proteins, a premise that would also need further verification.

Table 5.2. PNP domains comparison of significant dN/dS with mutagenized sites.

Domain	Conserved residues	dN/dS residues	Function affected	Ref.
PNP1 or 2	wt		pol ++ / deg ++	[30,44]
PNP1	D135G	14 X 12	pol - / deg -	[30,44]
PNP1	n	S211	?	
PNP1	n	V247	?	
PNP1	n	T266	?	
PNP1	n	V268	?	
PNP2	n	F377	?	
PNP2	Q387R	9 x 16	Blocks trimer formation, mtRNA import, mt translation	[161]
PNP2	R445E	19 XX 12	pol +++ / deg +	[30,44]
PNP2	R446E	18 XX 11	pol +++ / deg +	[30,44]
PNP2	E475G	17 X 7	Blocks trimer formation	[108]
PNP2	S484A	S483	pol - deg -	[30,44]
PNP2	D538A	15 X 5 X 26	pol + / deg +	[30,44]
PNP2	D544G	15 X 5 X 26	pol +++ / deg +	[30,44]
PNP2	n	P519	?	Somatic mutation (COSMIC database)

PNP2	n	N590	?	
------	---	------	---	--

Red lettering = mutagenized sites and green lettering positively skewed dN/dS sites. Green shading = two codons adjacent to each other R445 and R446. Blue shading marks two codons within six codons of each other D538 and D544. The notation for dN/dS for conserved mutagenized sites is nXm, where X indicates the position of a mutagenized codon and n indicates the number of residues toward the amino end of the protein that have dN/dS = 0.0, and m indicates the number of residues toward the carboxy end of the protein that have dN/dS = 0.0

RPH domain: The sites with dN/dS > 1.0 at the amino terminal of this domain are interspersed with several sites that have been altered by mutagenesis (Table 5.3). The first 22 or so residues appear to be very important in maintaining the structural integrity of the domain and both mutagenized and skewed dN/dS sites exist here. This result could point to the importance of this region in maintaining the structural integrity of the domain. The remainder of the residues in this domain behaves, as we would predict. Any mutagenized residue appears to be embedded in long stretches of sites with dN/dS ratios not significantly different from 0.0, indicating a strong tendency toward conservation of sequences and of function. Any sites showing positively skewed dN/dS > 1.0 are outside of these highly conserved regions.

Table 5.3. RPH Comparison of significant dN/dS with mutagenized sites.

Conserved residues	dN/dS residues	Function	Ref.
R12	Y11	structural	[162]
D14	D14	structural	[162]
R16	G15	structural	[162]
R22	5 X 5	structural	[162]
n	G36	?	
n	A38	?	
n	T45	?	
R61	11 X 10	RNA-binding (RNA entry site)	[162,163]
A62	12 X 9	RNA-binding (RNA entry site)	[162,163]
n	C73	?	
n	F80	?	
n	E84	?	
R93	3 XX 3 X 12	RNA-binding (RNA exit site)	[162,163]
K94	3 XX 3 X 12	RNA-binding (RNA entry site)	[162,163]
E97	3 XX 3 X 12	RNA-binding	[162]
D130	22 X 3 X 40	phosphate- binding	[162]
T133	22 X 3 X 40	phosphate- binding	[162]

D171	40 X 4 XX 31	catalytic	[162]
E176	40 X 4 XX 31	catalytic	[162]
E177	40 X 4 XX 31	catalytic	[162]

Red lettering = mutagenized sites and green lettering positively skewed dN/dS sites. Green shading two codons adjacent to each other. Different shading indicates sites that are in close adjacency to one another. The notation for dN/dS for conserved mutagenized sites is nXm, where X indicates the position of a mutagenized codon and n indicates the number of residues toward the amino end of the protein that have dN/dS = 0.0, and m indicates the number of residues toward the carboxy end of the protein that have dN/dS = 0.0

KH domain: Two residues in the KH domain identified as having positively skewed dN/dS ratios, T635 and I667, are highly conserved [31], and located around the pore of the trimeric protein near residue G622 (Table 5.4) which has been shown to be important for RNA binding [31]. Again these may be positions that show strong positive selection because of recent acquisition of function. In addition, two other sites might be involved in trimer formation - S211 and A633. It could be that these are important for trimer formation or RNA binding as suggested by their location and evolutionary conservation, but this again would need to be tested by extensive mutation analysis and biochemical assays.

Table 5.4. KH domain comparison of significant dN/dS with mutagenized sites.

Domain	Conserved residues	dN/dS residues	Function	Ref.
KH/S1	G622D	10 X 10	RNA binding lost	[31]
KH/S1	n	A633	?	
KH/S1	n	T635	pore of the trimeric protein	
KH/S1	n	I667	pore of the trimeric protein	

Red lettering = mutagenized sites and green lettering positively skewed dN/dS sites. The notation for dN/dS for conserved mutagenized sites is nXm, where X indicates the position of a mutagenized codon and n indicates the number of residues toward the amino end of the protein that have dN/dS = 0.0, and m indicates the number of residues toward the carboxy end of the protein that have dN/dS = 0.0

5.5 Discussion

There are two evolutionarily conserved members of the PDX family of proteins: RNase PH and PNPase. The RNase PH protein is the simplest 3'→5' phosphorolytic exoribonuclease which can be considered as a prototype of the PDX family of proteins [4,14]. Within PNPase are the catalytic domains PNP1 and PNP2, which share significant sequence similarity with RNase PH. The evolutionary origin of RNase PH can be traced in a straightforward manner because it exists in bacteria, and has orthologues in Archaea and Eukarya. Its ubiquitous phylogenetic distribution exemplifies the functional importance of this ribonuclease. In contrast, PNPase is absent in all Archaea and single cell eukaryotes such as yeast [13,91,93]. The prevalent phylogenetic distribution of these proteins and sequence similarity between them raises the

possibility that the PDX domains of PNPase (PNP1 and PNP2) and RNase PH arose via gene duplication events from a common origin (i.e. the most recent common ancestor; MRCA) [91,93]. The current study attempts to address where in the phylogenetic history did major sequence changes appear that might have shaped the important functions of these domains.

Domain evolution in PNPases: Phylogenetic analysis performed in this study, using sequences of RNase PH, PNP1 and PNP2 domains from 43 eukaryotic taxa, confirms a previous finding that PNP2 and RPH are more closely related to each other (i.e. sister taxa), with PNP1 having diverged from the PDX domain family earlier in evolution [91,93]. The rooting of parsimony and likelihood trees specifies PNP1 as the domain that appeared in the genomes of the Most Recent Common Ancestor (MRCA) of life. This is consistent with the PNP1 “first” hypothesis being the most parsimonious and likely scenario. This being the case, it seems safe to assume that PNP2 and RNase PH arose as a result of duplication events. If RNase PH emerged only during later stages of evolution, it is important that we explain the presence of its orthologues in all kingdoms of life, while PNPase is absent in all Archaea and a number of other organisms. There are two likely explanations. First, the terminally duplicated RNase PH domain could have been transferred to Archaea by horizontal gene transfer (HGT) via the common Eukaryote ancestor. Second, the full-length PNPase might have been lost in the Archaeal lineage. The “node height test” predicted that the lineage extinction of PNPase in Archaea is the more acceptable sequence of events, which occurred during the evolution of these domains [91,164]. In any case, the series of events or the kinds of

selective pressure that may have factored in this evolutionary process are still under speculation.

Branch Specific Sequence Skew: For PNPase and RNase PH, a deeper understanding of the process of sequence change during their evolution, may translate to better insights regarding the proteins' conserved (and evolved) functionalities. Using the Branch-site Random Effects Likelihood (BREL) and Mixed Effects Model of Evolution (MEME) analytical tools, we were able to identify previously unknown branch- and site-specific departures from $dN/dS=1.0$ related to the PNP1, PNP2, KH, S1 and RPH domains [158,159]. When a codon has a dN/dS ratio that is statistically significantly greater than 1.0 we call this positive skew. BREL analyses led to the detection of lineage specific positive skew relating to all the five domains during vertebrate evolution. The advantage of this approach is its ability to infer episodic skew events on branches in a phylogeny. Moreover, this tool helped us identify the three branches of the phylogeny of animals exhibiting a significant positive skew in dN/dS . The first branch is the lineage leading to Protostomes (the lineage that is sister to the large clade that vertebrates belong to) where both PNP1 and KH/S1 show positive skew once. The second region comprises seven branches in the vertebrate phylogenetic tree leading to mammals from the common ancestor of *Branchiostoma*, with all of them exhibiting significant positive skew in one or more of the domains of PNPase and RNasePH. The third branch is the lineage leading to Bovids where both PNP2 and RPH show positive skew once. As pointed out earlier, the inference we can draw from these findings is that all four protein domains PNP1, PNP2, RPH and KH/S1 experienced positive skew during sequence evolution leading to the vertebrates, after

which the analysis suggests stabilization of the domains leading to higher mammals. While we cannot at this point in time claim that natural selection was at work in molding these domains in the common ancestor of the vertebrates, we can point to the fact that some highly skewed sequence change occurred in the lineage leading to vertebrates.

Domain Region Specific Sequence Skew: Results of MEME analyses indicate that the sites with positive dN/dS skew in the PNP1, PNP2 and RPH domains are mostly located outside α -helices and β -sheets or in other words are in disordered regions of the domains. In the N-terminal region of the PNP1 protein domain, only two out of ten sites showing skew are located within β -sheets. These observations are actually consistent with recent reports that amino acids located in the disordered regions (e.g., random coils and turns) of protein secondary structure are more likely to be under positive selective pressure, relative to residues in the more structurally conserved regions like α -helices and β -sheets [150,151]. More specifically, Nilsson and colleagues [150], upon their examination of the molecular evolution of 3746 genes across 64 strains of budding yeast (*S. cerevisiae*, *S. paradoxus*), concluded that there is a significantly higher degree of positive Darwinian selection in intrinsically disordered regions compared to alpha helix, beta sheet or tertiary structures.

In their analysis of 26 protein families, Brown and co-workers concluded that disordered regions in proteins generally have faster rates of evolution [165]. These observations are possibly related to the roles disordered regions play in the protein's functionality. As Mittag et al explained [166], higher mutation rates in disordered regions may have been allowed during evolution because sequential modifications within these regions did not pose severe consequences on protein stability and functionalities.

Moreover, the disordered regions provide protein flexibility necessary for recognition of other molecules (such as other proteins and RNAs). This is especially applicable for proteins such as PNPase and RNase PH, whose target molecules can have a varying range of secondary and tertiary structures. For PNPase and RNase PH, the need to adapt to its target molecules is very crucial since the target molecules themselves are evolving (i.e., mutating) as they adapt to new environment and species physiology.

Another interesting observation in our study is the higher incidence of dN/dS positive skew in the N-terminus of RPH compared to those of the PNP1 and PNP2. In the C-termini of the domains, the opposite was evident. The N- and C-termini of proteins encompass important binding motifs, and it is possible that the termini regions of these domains, as they diverged during evolution, required different structural modifications for the different molecules (e.g., helicases or other ribonucleases) they interact with. Overall, RPH has twice as many positively skewed sites as PNP1 or PNP2. In other words, RPH has undergone more changes at the molecular level than either PNPase domain. One possible interpretation is that RPH is evolutionarily more malleable than the PNPase domains. This perhaps explains the emergence of RPH orthologues in all kingdoms of life, after it had diverged from the linked PNP domains early on during organismal evolution [91,93].

Positive skew in codons was also detected in the structurally more complex KH domain (at numerous positions in α -helices), as well as the S1 domain (at four positions in the β -sheets at the C-terminus). These events were likely structural refinements that subsequently aided PNPases in higher organisms as it necessitated them binding to

newer mRNA and miRNA species. A prime example of this is the human PNPase which has high specificity for binding and degrading *c-myc* mRNA and miR-221 [48,49,67,93].

Correlating positive dN/dS skew with mutagenized sites: There is a direct correlation between sites chosen for mutagenesis and the loss of function of the PNPase and RNasePH proteins and an inverse correlation of these sites with positive dN/dS skew. In general, sites that are important for the function of these proteins as determined by mutagenesis studies appear to be embedded in regions of the protein with dN/dS values that are not significantly different from 0.0. This result suggests that sites adjacent to those currently chosen for mutagenesis studies might also be appropriate candidates for mutagenesis to study the function of these proteins. There are two major exceptions to this general trend. The first concerns a region of the PNP2 domain where two serine (S) residues are adjacent to each other. One serine (S484) has been mutagenized and has been shown to be near a binding site for Citrate D 670 located near the active site of the protein. A site directly adjacent to site S484 (S483) has positive sequence skew, indicating that this region of PNP2 has some interesting sequence evolution dynamics involved with it. The second departure from the general inverse relationship of positive skew with mutagenized sites is at the amino terminus of the RNasePH domain, where a six amino acid stretch (Y11, R12, D14, G15, R16) has three residues important for structure of the protein and three residues with positive dN/dS skew.

In summary, we present a study that analyzed the molecular events, which have occurred during the course of evolution of two important RNA degrading enzymes. We attempted to explain why some regions of the proteins are biased towards positive dN/dS skew. We have exercised caution in not calling these codons with positive skew as sites under positive natural selection and in calling codons chosen for mutagenesis as sites under purifying selection. We do however suggest that the sites we have identified in this study as skewed are sites that are good candidates for examining the dynamics of the activity of these proteins. We also suggest that previous choice of sites for mutagenesis chosen on the basis of extreme conservation, have settled on codons in regions where surrounding codons have extremely low dN/dS ratios that are for the most part not significantly different from 0.0. This result suggests that sites adjacent to those currently in use for mutagenesis studies could be used to expand the repertoire of tools for studying the functionality of these proteins.

CHAPTER SIX

General Discussion

Human polynucleotide phosphorylase (*hPNPase*^{old-35}) is an evolutionarily conserved 3'-5' exoribonuclease [13,91,93]. It has been implicated to play a role in numerous cellular functions, like growth arrest, apoptosis, senescence associated degenerative diseases, hearing loss, inflammation, mtRNA import, maintenance of mitochondrial homeostasis, mtRNA processing and decay. Most of its functions in the mitochondria are associated with cellular maintenance and routine RNA processing activities [13,67,93]. As an exoribonuclease in the cytoplasm it has been found to degrade c-myc mRNA and miR-221 [48,49], which ultimately leads to apoptosis of cancer cells. Apart from these two mRNA and miRNA species not much is known about the degradation targets of *hPNPase*^{old-35}. These functions of *hPNPase*^{old-35} have been extensively described in Chapter 1.

The overall aim of this project was to identify degradation targets of *hPNPase*^{old-35} other than c-myc and miR-221 and also to further understand the role of *hPNPase*^{old-35} in the maintenance of cellular homeostasis and this premise has been extensively dealt with in Chapters 2 and 3. Identification of *hPNPase*^{old-35} targets would help in not

only furthering our understanding of this protein, but may also provide novel therapeutic targets for treatment of cancer and other *hPNPase*^{old-35}-associated diseases. Another aspect of this project was to evaluate the evolutionary history of *hPNPase*^{old-35} in comparison with another RNA degrading enzyme RNasePH, with special focus on the prediction of functionally important residues under natural selection, mutating which would hamper the enzymatic activity or RNA binding ability of these proteins. In the current work (Figure 6.1), we were able to (i) identify *hPNPase*^{old-35}- “directly” and “indirectly” regulated genes in two different overlapping analyses; (ii) demonstrate that *hPNPase*^{old-35} stable knockdown causes global changes in mitochondrial respiratory complex and associated genes; (iii) show that *hPNPase*^{old-35} overexpression causes global changes in cell cycle associated genes; (iv) identify amino acid sites under positive natural selection in *hPNPase*^{old-35} which could be of potential importance in mediating its catalytic activity and RNA binding ability.

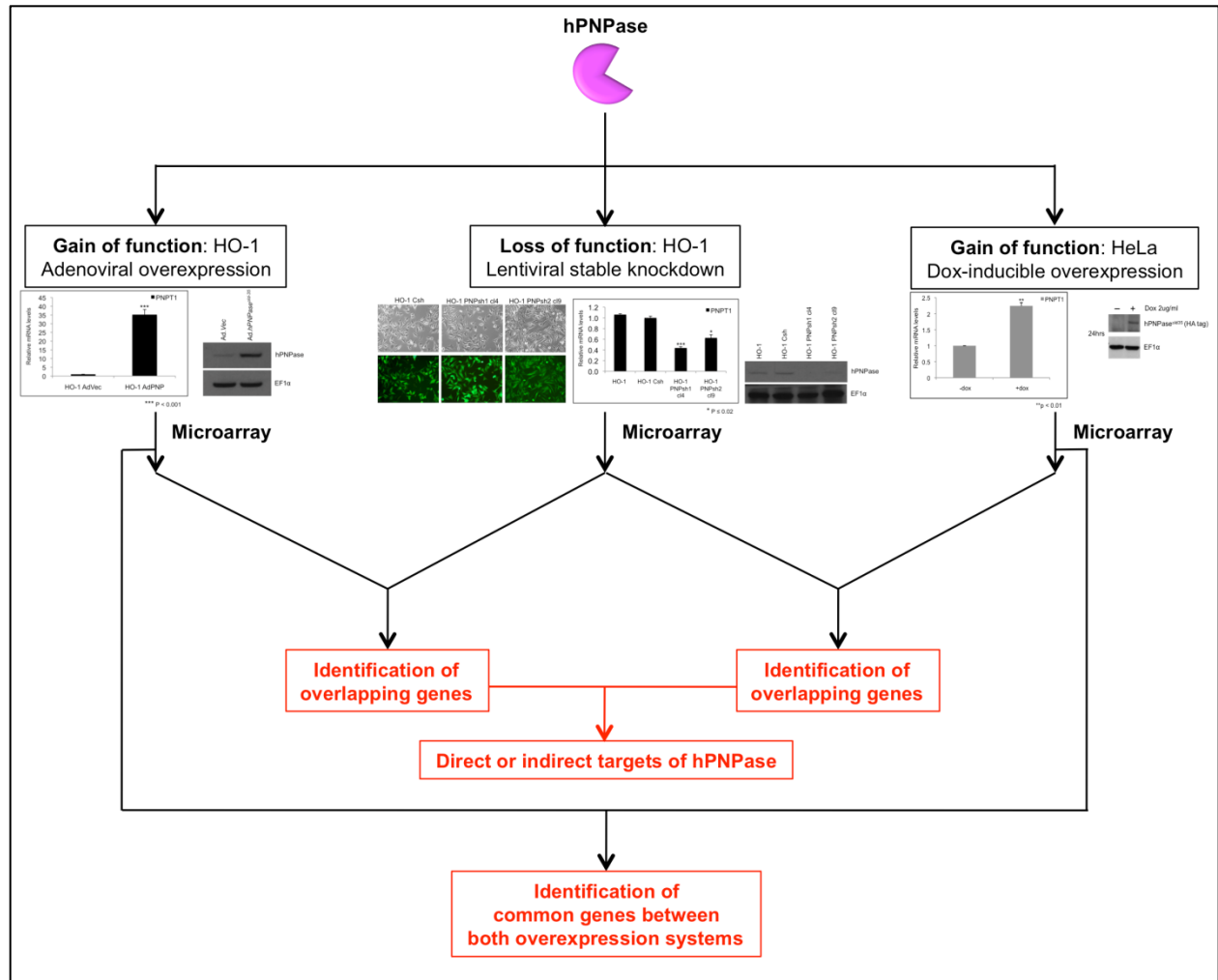


Fig. 6.1. Flow chart depicting overall aim of project: to identify degradation targets of *hPNPase^{old-35}*.

In order to identify direct degradation targets of *hPNPase^{old-35}*, we performed microarray analysis on cell lines in which *hPNPase^{old-35}* was overexpressed and knocked down. In Chapter 2 we used melanoma as a model system to answer these questions. We were able to identify a number of candidate genes through our overlapping analysis which could be potential direct or indirect targets of *hPNPase^{old-35}* and were also able to validate the already known involvement of *hPNPase^{old-35}* in biological processes like mitochondrial respiration and cell cycle arrest with the help of

pathway analyses tools in IPA (Ingenuity Pathway Analysis). We identified 77 potential direct targets and validated certain genes like *CENPE* and *MKI67*, which are important for cellular growth and proliferation as being repressed by *hPNPase*^{old-35} by transient knockdown and overexpression of *hPNPase*^{old-35}. Future experiments would involve verifying the exact mechanism by which *hPNPase*^{old-35} regulates these genes. *In vitro* RNA degradation assays would be able to validate if *hPNPase*^{old-35} actually degrades these transcripts. Other mechanisms of regulation could be more complex and may involve *hPNPase*^{old-35}-regulated miRNA species targeting genes (like certain transcription factors), which in turn control the expression of the aforementioned identified transcripts. To pursue this particular avenue, an analysis of the promoter regions of the identified direct targets would provide precise knowledge of the transcription factor (TF) binding elements. If the regulation of the identified targets by a specific TF has not been reported yet, reporter based assays can be performed to validate regulation. Finally, a search using the numerous miRNA databases (e.g. miRBase or TargetScan) can help identify any predicted or validated miRNAs that target our TF of interest, and even further through RNA degradation assays we can validate if *hPNPase*^{old-35} regulates that particular miRNA. A similar approach could be used to validate the mechanism of *hPNPase*^{old-35}-regulation of the potential indirect targets identified like *VGF*, *RNF128* and *MCAM*, which could probably be regulated by miRNAs targeted by *hPNPase*^{old-35}. In this case we would need to identify miRNA binding sites in these transcripts by scanning the aforementioned miRNA prediction databases, then functionally prove that the specific miRNA targets the specific gene by overexpression or knockdown of the miRNA and finally investigate if *hPNPase*^{old-35} regulates it. Of

particular interest here is the gene *MCAM*, which is a cell surface receptor associated with poor prognosis of melanoma and other cancers [167,168]. *hPNPase^{old-35}* knockdown causes the downregulation of this gene, identifying the mechanism of *hPNPase^{old-35}*-regulation of *MCAM* (probably via miRNA) may provide valuable therapeutic opportunities for melanoma treatment [169]. In the same context, *VGF* (usually only expressed in nerve cells or neuroendocrine cells) could be promising candidate too, which is upregulated in lung cancer [170].

In Chapter 3, we extended to identify possible *hPNPase^{old-35}* induced or repressed genes by performing a similar microarray experiment in HeLa cells following *hPNPase^{old-35}* overexpression using a doxycycline-inducible expression vector. The purpose of this additional microarray was to gain perspective relating to *hPNPase^{old-35}* functions in a system other than melanoma and eventually, comparison of two *hPNPase^{old-35}* datasets in two different cell lines may provide a more global perspective of *hPNPase^{old-35}* associated gene expression changes. First, in order to identify *hPNPase^{old-35}* induced or repressed genes, we performed a similar overlapping screen that we performed in Chapter 2. We used the same melanoma *hPNPase^{old-35}* knockdown dataset we used in Chapter 2, but this time we overlapped it with our HeLa *hPNPase^{old-35}* dataset rather than with the melanoma. In this analysis we identified 28 repressed and 62 *hPNPase^{old-35}*-induced transcripts. Of special interest here was the identification of two *hPNPase^{old-35}*-repressed genes *CENPE* and *MKI67*, which we also identified in our melanoma screen. Future experiments would be required to confirm their direct degradation by *hPNPase^{old-35}* or whether they are downstream/indirect effects of the downregulation of a key TF like c-myc, which can be validated by myc-

knockdown experiments. Another interesting *hPNPase*^{old-35} –repressed gene identified here was *CENPA*, which was downregulated in three melanoma cell lines upon Ad. *hPNPase*^{old-35} infection, but levels of which did not change significantly in an immortalized normal human melanocyte cell line FM516 in preliminary experiments. *CENPA* is associated with poor prognosis in breast cancer [134], and thus could prove to be a potential therapeutic target once we could figure out the mechanism of *hPNPase*^{old-35} –regulation of this gene, which seems to be indirect as levels of *CENPA* did not change in immortalized normal cells. We were also able to identify significant similar correlations of *hPNPase*^{old-35} expression with a number of the identified induced and repressed genes in four TCGA datasets we analyzed: colon adenocarcinoma (COAD), skin cutaneous melanoma (SKCM), ovarian serous cyst adenocarcinoma (OV), and prostate adenocarcinoma (PRAD). Some of the interesting candidates in this category were *DUSP1*, *ADARB1* and *EMR2*, all of which negatively correlate with *hPNPase*^{old-35} expression and are upregulated in different cancers [136-140]. As explained earlier as in the case of *CENPE*, *MKI67*, *VGF*, *MCAM* and *CENPA*, once the mechanistic details of the regulation of these genes by *hPNPase*^{old-35} are identified, they could lead to the discovery of promising therapeutic interventions.

We also compared the gene expression profiles of melanoma and HeLa cells in which *hPNPase*^{old-35} was overexpressed, and as detailed in Chapter 3, apart from the fact that almost all the 105 common dysregulated genes identified belonged to cell cycle-associated gene ontology categories, some of them were also identified as possible transcriptional targets of c-myc. Therefore, although this analysis provided us with a gene expression signature of *hPNPase*^{old-35} induced growth arrest, unless we can

prove otherwise (through RNA degradation assays), it would be difficult to say at this point whether they are direct targets of *hPNPase*^{old-35} or dysregulated due to changes in c-myc levels. In order to pursue this avenue further, validation of these genes in a myc-null background would be helpful, which would confirm whether dysregulation of these genes is caused by *hPNPase*^{old-35} or c-myc.

An alternative approach to validate the directly degraded targets of *hPNPase*^{old-35} identified in Chapters 2 and 3 would be to compare the 3'UTR sequence or secondary structure of c-myc (a direct degradation target of *hPNPase*^{old-35}) with the 3'UTR of these transcripts and recognize any common elements between them. This may also shed some light on the conundrum of what is/are the specificity element/s that allows recognition and subsequent degradation by *hPNPase*^{old-35}, a premise dealt with in Chapter 4. Also, since *Ad.hPNPase*^{old-35} infection causes growth arrest of cancer cells resulting from degradation of c-myc mRNA with an intact 3'UTR, rescue experiments involving 3'UTR deletion mutants of c-myc may also help to delineate the region which may be required for *hPNPase*^{old-35} recognition and degradation.

In Chapter 5, we set out to identify the residues under natural selection in the different domains of *hPNPase*^{old-35} (PNP1, PNP2, KH and S1) and another closely related exoribonuclease RNasePH that may be important for their enzymatic activity or RNA binding ability. The other purpose behind this was that maybe such an evolutionary analysis would help us identify exactly where in evolutionary history did or did not *hPNPase*^{old-35} acquire any specificities towards the recognition of certain mRNA species (like c-myc) versus others. The results provided in Chapter 5 offer in depth insights into the sequence evolution of *hPNPase*^{old-35} in the vertebrate lineage leading to

mammals. The residues under positive selection that we identified (extensively described in Chapter 5) could or could not be involved in the trimer formation, degradative or binding activities of hPNPase^{old-35} and RNasePH. Future work involving mutation analyses of these sites followed by functional RNA degradation or binding assays would confirm the importance of these residues in those functions. The eventual importance of this work lies in understanding the biochemical importance of these residues, information that provide useful in treating disease states where these may be mutated or inactivated.

Throughout the course of this dissertation I have tried to explore and understand the functional implications of *hPNPase*^{old-35} (Figure 6.1). Although our studies have led to numerous conclusions as detailed in Chapters 2-5, there still remain a number of unanswered questions that have been discussed in the current chapter. Also, a lot remains unanswered regarding the biological consequences of hPNPase in normal versus cancer cells, and animal models with either conditional overexpression or knockdown of hPNPase will be extremely useful. These models will prove helpful in understanding the various physiological processes hPNPase is a part of, like mtRNA import, and will also facilitate studies relating to viral infection, mitochondrial dysfunction and aging allowing the future development of suitable therapeutics.

References

References

1. Halbeisen, R. E., Galgano, A., Scherrer, T., & Gerber, A. P. (2008). Post-transcriptional gene regulation: From genome-wide studies to principles. *Cellular and Molecular Life Sciences*, 65(5), 798-813.
2. Audic, Y., & Hartley, R. (2004). Post-transcriptional regulation in cancer. *Biology of the Cell*, 96(7), 479-498.
3. Glisovic, T., Bachorik, J., Yong, J., & Dreyfuss, G. (2008). RNA-binding proteins and post-transcriptional gene regulation. *FEBS Letters*, 582(14), 1977-1986.
4. Andrade, J., Pobre, V., Silva, I., Domingues, S., & Arraiano, C. (2009). The role of 3'-5' exoribonucleases in RNA degradation. *Prog Mol Biol Transl Sci*, 85, 187-229.
5. Newbury, S. F. (2006). Control of mRNA stability in eukaryotes. *Biochemical Society Transactions*, 34(1), 30-34.
6. Parker, R., & Song, H. (2004). The enzymes and control of eukaryotic mRNA turnover. *Nature Structural Molecular Biology*, 11(2), 121-127.
7. Shyu, A., Wilkinson, M., & van Hoof, A. (2008). Messenger RNA regulation: To translate or to degrade. *EMBO Journal*, 27(3), 471-481.
8. Garneau, N., Wilusz, J., & Wilusz, C. (2007). The highways and byways of mRNA decay. *Nature Reviews.Molecular Cell Biology*, 8(2), 113-126.
9. Hollams, E., Giles, K., Thomson, A., & Leedman, P. (2002). MRNA stability and the control of gene expression: Implications for human disease. *Neurochemical Research*, 27(10), 957-980.
10. Meyer, S., Temme, C., & Wahle, E. (2004). Messenger RNA turnover in eukaryotes: Pathways and enzymes. *Critical Reviews in Biochemistry and Molecular Biology*, 39(4), 197-216.
11. Doma, M., & Parker, R. (2007). RNA quality control in eukaryotes. *Cell*, 131(4), 660-668.
12. Arraiano C, Andrade J, Domingues S, Guinote I, Malecki M, Matos R, et al. (2010). The critical role of RNA processing and degradation in the control of gene expression. *FEMS Microbiology Reviews*, 34(5), 883-923.
13. Sarkar, D., & Fisher, P. B. (2006). Polynucleotide phosphorylase: An evolutionary conserved gene with an expanding repertoire of functions. *Pharmacology Therapeutics*, 112(1), 243-263.

14. Ibrahim, H., Wilusz, J., & Wilusz, C. (2008). RNA recognition by 3'-to-5' exonucleases: The substrate perspective. *Biochimica Et Biophysica Acta*, 1779(4), 256-265.
15. Zuo, Y., & Deutscher, M. P. (2001). Exoribonuclease superfamilies: Structural analysis and phylogenetic distribution. *Nucleic Acids Research*, 29(5), 1017-1026.
16. Grunberg-Manago, M., Ortiz, P.J., & Ochoa, S. (1955). Enzymatic synthesis of nucleic acidlike polynucleotides. *Science*, 122(3176), 907-910.
17. Leszczyniecka, M., Kang, D., Sarkar, D., Su, Z., Holmes, M., Valerie, K., et al. (2002). Identification and cloning of human polynucleotide phosphorylase, hPNPase old-35, in the context of terminal differentiation and cellular senescence. *Proceedings of the National Academy of Sciences of the United States of America*, 99(26), 16636-16641.
18. Chen, H., Koehler, C., & Teitell, M. (2007). Human polynucleotide phosphorylase: Location matters. *Trends in Cell Biology*, 17(12), 600-608.
19. Raijmakers, R., Egberts, W., van Venrooij, W., & Pruijn, G. J. M. (2002). Protein-protein interactions between human exosome components support the assembly of RNase PH-type subunits into a six-membered PNPase-like ring. *Journal of Molecular Biology*, 323(4), 653-663.
20. Symmons, M. F., Jones, G. H., & Luisi, B. F. (2000). A duplicated fold is the structural basis for polynucleotide phosphorylase catalytic activity, processivity, and regulation. *Structure*, 8(11), 1215-1226.
21. Yehudai Resheff, S., Portnoy, V., Yogev, S., Adir, N., & Schuster, G. (2003). Domain analysis of the chloroplast polynucleotide phosphorylase reveals discrete functions in RNA degradation, polyadenylation, and sequence homology with exosome proteins. *Plant Cell*, 15(9), 2003-2019.
22. Piwowarski, J., Grzechnik, P., Dziembowski, A., Dmochowska, A., Minczuk, M., & Stepień, P. (2003). Human polynucleotide phosphorylase, hPNPase, is localized in mitochondria. *Journal of Molecular Biology*, 329(5), 853-857.
23. Rainey, R., Glavin, J., Chen, H., French, S., Teitell, M., & Koehler, C. (2006). A new function in translocation for the mitochondrial i-AAA protease Yme1: Import of polynucleotide phosphorylase into the intermembrane space. *Molecular and Cellular Biology*, 26(22), 8488-8497.
24. Symmons, M., Williams, M., Luisi, B., Jones, G., & Carpousis, A. (2002). Running rings around RNA: A superfamily of phosphate-dependent RNases. *Trends in Biochemical Sciences*, 27(1), 11-18.

25. Jarrige, A., Brchemier-Baey, D., Mathy, N., Duch, O., & Portier, C. (2002). Mutational analysis of polynucleotide phosphorylase from escherichia coli. *Journal of Molecular Biology*, 321(3), 397-409.
26. Stickney, L., Hankins, J., Miao, X., & Mackie, G. (2005). Function of the conserved S1 and KH domains in polynucleotide phosphorylase. *Journal of Bacteriology*, 187(21), 7214-7221.
27. Shi, Z., Yang, W., Lin Chao, S., Chak, K., & Yuan, H. (2008). Crystal structure of escherichia coli PNPase: Central channel residues are involved in processive RNA degradation. *RNA*, 14(11), 2361-2371.
28. Baginsky, S., Shteiman Kotler, A., Liveanu, V., Yehudai Resheff, S., Bellaoui, M., Settlege, R. E., et al. (2001). Chloroplast PNPase exists as a homo-multimer enzyme complex that is distinct from the escherichia coli degradosome. *RNA*, 7(10), 1464-1475.
29. Sarkar, D., Park, E., Emdad, L., Randolph, A., Valerie, K., & Fisher, P. B. (2005). Defining the domains of human polynucleotide phosphorylase (hPNPaseOLD-35) mediating cellular senescence. *Molecular and Cellular Biology*, 25(16), 7333-7343.
30. Portnoy, V., Palnizky, G., Yehudai Resheff, S., Glaser, F., & Schuster, G. (2008). Analysis of the human polynucleotide phosphorylase (PNPase) reveals differences in RNA binding and response to phosphate compared to its bacterial and chloroplast counterparts. *RNA*, 14(2), 297-309.
31. Lin, C., Wang, Y., Yang, W., Hsiao, Y., & Yuan, H. (2012). Crystal structure of human polynucleotide phosphorylase: Insights into its domain function in RNA binding and degradation. *Nucleic Acids Research*, 40(9), 4146-4157.
32. Carpousis, A. J., Van Houwe, G., Ehretsmann, C., & Krisch, H. M. (1994). Copurification of E. coli RNAase E and PNPase: Evidence for a specific association between two enzymes important in RNA processing and degradation. *Cell*, 76(5), 889-900.
33. Carpousis, A. J. (2002). The escherichia coli RNA degradosome: Structure, function and relationship in other ribonucleolytic multienzyme complexes. *Biochemical Society Transactions*, 30(2), 150-155.
34. Miczak, A., Kaberdin, V. R., Wei, C. L., & Lin Chao, S. (1996). Proteins associated with RNase E in a multicomponent ribonucleolytic complex. *Proceedings of the National Academy of Sciences of the United States of America*, 93(9), 3865-3869.
35. Py, B., Causton, H., Mudd, E. A., & Higgins, C. F. (1994). A protein complex mediating mRNA degradation in escherichia coli. *Molecular Microbiology*, 14(4), 717-729.

36. Py, B., Higgins, C. F., Krisch, H. M., & Carpousis, A. J. (1996). A DEAD-box RNA helicase in the escherichia coli RNA degradosome. *Nature*, *381*(6578), 169-172.
37. Deutscher M P, Li Z (2001) Exoribonucleases and their multiple roles in RNA metabolism. *Prog Nucleic Acid Res Mol Biol*, *66*, 67-105.
38. Min, J. J., & Zassenhaus, H. P. (1991). Characterization of a novel NTP-dependent 3' exoribonuclease from yeast mitochondria. *SAAS Bulletin, Biochemistry and Biotechnology*, *4*, 1-5.
39. Mitchell, P., Petfalski, E., Shevchenko, A., Mann, M., & Tollervey, D. (1997). The exosome: A conserved eukaryotic RNA processing complex containing multiple 3'→5' exoribonucleases. *Cell*, *91*(4), 457-466.
40. Houseley, J., LaCava, J., & Tollervey, D. (2006). RNA-quality control by the exosome. *Nature Reviews.Molecular Cell Biology*, *7*(7), 529-539.
41. Fritz, D., Bergman, N., Kilpatrick, W., Wilusz, C., & Wilusz, J. (2004). Messenger RNA decay in mammalian cells: The exonuclease perspective. *Cell Biochemistry and Biophysics*, *41*(2), 265-278.
42. Leszczyniecka, M., Su, Z., Kang, D., Sarkar, D., & Fisher, P. B. (2003). Expression regulation and genomic organization of human polynucleotide phosphorylase, hPNPase(old-35), a type I interferon inducible early response gene. *Gene*, *316*, 143-156.
43. Huang, F., Adelman, J., Jiang, H., Goldstein, N. I., & Fisher, P. B. (1999). Identification and temporal expression pattern of genes modulated during irreversible growth arrest and terminal differentiation in human melanoma cells. *Oncogene*, *18*(23), 3546-3552.
44. Wang, G., Chen, H., Oktay, Y., Zhang, J., Allen, E., Smith, G., et al. (2010). PNPASE regulates RNA import into mitochondria. *Cell*, *142*(3), 456-467.
45. Jarrige, A. C., Mathy, N., & Portier, C. (2001). PNPase autocontrols its expression by degrading a double-stranded structure in the pnp mRNA leader. *EMBO Journal*, *20*(23), 6845-6855.
46. Gewartowski, K., Tomecki, R., Muchowski, L., Dmochow Ska, A., Dzwonek, A., Malecki, M., et al. (2006). Up-regulation of human PNPase mRNA by beta-interferon has no effect on protein level in melanoma cell lines. *Acta Biochimica Polonica*, *53*(1), 179-188.
47. Chen, H., Rainey, R., Balatoni, C., Dawson, D., Troke, J., Wasiak, S., et al. (2006). Mammalian polynucleotide phosphorylase is an intermembrane space RNase that

maintains mitochondrial homeostasis. *Molecular and Cellular Biology*, 26(22), 8475-8487.

48. Sarkar, D., Leszczyniecka, M., Kang, D., Lebedeva, I. V., Valerie, K., Dhar, S., et al. (2003). Down-regulation of myc as a potential target for growth arrest induced by human polynucleotide phosphorylase (hPNPaseold-35) in human melanoma cells. *Journal of Biological Chemistry*, 278(27), 24542-24551.

49. Das, S., Sokhi, U., Bhutia, S., Azab, B., Su, Z., Sarkar, D., et al. (2010). Human polynucleotide phosphorylase selectively and preferentially degrades microRNA-221 in human melanoma cells. *Proceedings of the National Academy of Sciences of the United States of America*, 107(26), 11948-11953.

50. Wang, G., Shimada, E., Koehler, C., & Teitell, M. (2011). PNPASE and RNA trafficking into mitochondria. *Biochimica Et Biophysica Acta*,

51. Yu, Y., Chou, R., Wu, C., Wang, Y., Chang, W., Tseng, Y., et al. (2012). Nuclear EGFR suppresses ribonuclease activity of polynucleotide phosphorylase through DNAPK-mediated phosphorylation at serine 776. *Journal of Biological Chemistry*, 287(37), 31015-31026.

52. Campisi, J. (1992). Gene expression in quiescent and senescent fibroblasts. *Annals of the New York Academy of Sciences*, 663, 195-201.

53. Fisher, P. B., Prignoli, D. R., Hermo, H., Weinstein, I. B., & Pestka, S. (1985). Effects of combined treatment with interferon and mezerein on melanogenesis and growth in human melanoma cells. *Journal of Interferon Research*, 5(1), 11-22.

54. Hayflick, L. (1976). The cell biology of human aging. *The New England Journal of Medicine*, 295(23), 1302-1308.

55. Van Maerken, T., Sarkar, D., Speleman, F., Dent, P., Weiss, W., & Fisher, P. B. (2009). Adenovirus-mediated hPNPase(old-35) gene transfer as a therapeutic strategy for neuroblastoma. *Journal of Cellular Physiology*, 219(3), 707-715.

56. Dang, C. V. (1999). c-myc target genes involved in cell growth, apoptosis, and metabolism. *Molecular and Cellular Biology*, 19(1), 1-11.

57. Sarkar, D., Park, E., Barber, G., & Fisher, P. B. (2007). Activation of double-stranded RNA dependent protein kinase, a new pathway by which human polynucleotide phosphorylase (hPNPase(old-35)) induces apoptosis. *Cancer Research*, 67(17), 7948-7953.

58. Dani, C., Mechti, N., Piechaczyk, M., Lebleu, B., Jeanteur, P., & Blanchard, J. M. (1985). Increased rate of degradation of c-myc mRNA in interferon-treated daudi cells.

Proceedings of the National Academy of Sciences of the United States of America, 82(15), 4896-4899.

59. Knight, E., Anton, E. D., Fahey, D., Friedland, B. K., & Jonak, G. J. (1985). Interferon regulates c-myc gene expression in daudi cells at the post-transcriptional level. *Proceedings of the National Academy of Sciences of the United States of America*, 82(4), 1151-1154.

60. Sarkar, D., Park, E. S., & Fisher, P. B. (2006). Defining the mechanism by which IFN-beta downregulates c-myc expression in human melanoma cells: Pivotal role for human polynucleotide phosphorylase (hPNPaseold-35). *Cell Death and Differentiation*, 13(9), 1541-1553.

61. Shan, B., Vazquez, E., & Lewis, J. A. (1990). Interferon selectively inhibits the expression of mitochondrial genes: A novel pathway for interferon-mediated responses. *EMBO Journal*, 9(13), 4307-4314.

62. López de Silanes, I., Quesada, M., & Esteller, M. (2007). Aberrant regulation of messenger RNA 3'-untranslated region in human cancer. *Cellular Oncology*, 29(1), 1-17.

63. Pesole, G., Mignone, F., Gissi, C., Grillo, G., Licciulli, F., & Liuni, S. (2001). Structural and functional features of eukaryotic mRNA untranslated regions. *Gene*, 276(1-2), 73-81.

64. Yamanaka, K., & Inouye, M. (2001). Selective mRNA degradation by polynucleotide phosphorylase in cold shock adaptation in escherichia coli. *Journal of Bacteriology*, 183(9), 2808-2816.

65. Sun, W., Julie Li, Y., Huang, H., Shyy, J. Y., & Chien, S. (2010). microRNA: A master regulator of cellular processes for bioengineering systems. *Annual Review of Biomedical Engineering*, 12, 1-27.

66. Cai, Y., Yu, X., Hu, S., & Yu, J. (2009). A brief review on the mechanisms of miRNA regulation. *Genomics, Proteomics Bioinformatics*, 7(4), 147-154.

67. Das, S. K., Bhutia, S. K., Sokhi, U. K., Dash, R., Azab, B., Sarkar, D., et al. (2011). Human polynucleotide phosphorylase (hPNPase(old-35)): An evolutionary conserved gene with an expanding repertoire of RNA degradation functions. *Oncogene*, 30(15), 1733-1743.

68. Finkel, T., & Holbrook, N. J. (2000). Oxidants, oxidative stress and the biology of ageing. *Nature*, 408(6809), 239-247.

69. Kiecolt Glaser, J., Preacher, K., MacCallum, R., Atkinson, C., Malarkey, W., & Glaser, R. (2003). Chronic stress and age-related increases in the proinflammatory

cytokine IL-6. *Proceedings of the National Academy of Sciences of the United States of America*, 100(15), 9090-9095.

70. Chen, Q. M. (2000). Replicative senescence and oxidant-induced premature senescence. beyond the control of cell cycle checkpoints. *Annals of the New York Academy of Sciences*, 908, 111-125.

71. Harman, D. (1956). Aging: A theory based on free radical and radiation chemistry. *Journal of Gerontology*, 11(3), 298-300.

72. Barnes, P. J., & Karin, M. (1997). Nuclear factor-kappaB: A pivotal transcription factor in chronic inflammatory diseases. *The New England Journal of Medicine*, 336(15), 1066-1071.

73. Schreck, R., Albermann, K., & Baeuerle, P. A. (1992). Nuclear factor kappa B: An oxidative stress-responsive transcription factor of eukaryotic cells (a review). *Free Radical Research Communications*, 17(4), 221-237.

74. Sarkar, D., Lebedeva, I. V., Emdad, L., Kang, D.C., Baldwin, A., & Fisher, P. B. (2004). Human polynucleotide phosphorylase (hPNPaseold-35): A potential link between aging and inflammation. *Cancer Research*, 64(20), 7473-7478.

75. Sarkar, D., & Fisher, P. B. (2006). Human polynucleotide phosphorylase (hPNPase old-35): An RNA degradation enzyme with pleiotrophic biological effects. *Cell Cycle*, 5(10), 1080-1084.

76. Nagaike, T., Suzuki, T., Katoh, T., & Ueda, T. (2005). Human mitochondrial mRNAs are stabilized with polyadenylation regulated by mitochondria-specific poly(A) polymerase and polynucleotide phosphorylase. *Journal of Biological Chemistry*, 280(20), 19721-19727.

77. Nagaike, T., Suzuki, T., & Ueda, T. (2008). Polyadenylation in mammalian mitochondria: Insights from recent studies. *Biochimica Et Biophysica Acta*, 1779(4), 266-269.

78. Wang, D., Shu, Z., Lieser, S., Chen, P., & Lee, W. (2009). Human mitochondrial SUV3 and polynucleotide phosphorylase form a 330-kDa heteropentamer to cooperatively degrade double-stranded RNA with a 3'-to-5' directionality. *Journal of Biological Chemistry*, 284(31), 20812-20821.

79. Sarkar, D., & Fisher, P. B. (2006). Molecular mechanisms of aging-associated inflammation. *Cancer Letters*, 236(1), 13-23.

80. Tahara, H., Kamada, K., Sato, E., Tsuyama, N., Kim, J. K., Hara, E., et al. (1995). Increase in expression levels of interferon-inducible genes in senescent human diploid

fibroblasts and in SV40-transformed human fibroblasts with extended lifespan. *Oncogene*, 11(6), 1125-1132.

81. Hayakawa, H., & Sekiguchi, M. (2006). Human polynucleotide phosphorylase protein in response to oxidative stress. *Biochemistry*, 45(21), 6749-6755.

82. Wu, J., & Li, Z. (2008). Human polynucleotide phosphorylase reduces oxidative RNA damage and protects HeLa cell against oxidative stress. *Biochemical and Biophysical Research Communications*, 372(2), 288-292.

83. Mukherjee, S., Basu, S., Home, P., Dhar, G., & Adhya, S. (2007). Necessary and sufficient factors for the import of transfer RNA into the kinetoplast mitochondrion. *EMBO Reports*, 8(6), 589-595.

84. Tarassov, I., Entelis, N., & Martin, R. P. (1995). An intact protein translocating machinery is required for mitochondrial import of a yeast cytoplasmic tRNA. *Journal of Molecular Biology*, 245(4), 315-323.

85. Gagliardi, D., & Leaver, C. J. (1999). Polyadenylation accelerates the degradation of the mitochondrial mRNA associated with cytoplasmic male sterility in sunflower. *EMBO Journal*, 18(13), 3757-3766.

86. Temperley, R., Seneca, S., Tonska, K., Bartnik, E., Bindoff, L., Lightowers, R., et al. (2003). Investigation of a pathogenic mtDNA microdeletion reveals a translation-dependent deadenylation decay pathway in human mitochondria. *Human Molecular Genetics*, 12(18), 2341-2348.

87. Slomovic, S., & Schuster, G. (2008). Stable PNPase RNAi silencing: Its effect on the processing and adenylation of human mitochondrial RNA. *RNA*, 14(2), 310-323.

88. Szczesny, R., Borowski, L., Brzezniak, L., Dmochowska, A., Gewartowski, K., Bartnik, E., et al. (2010). Human mitochondrial RNA turnover caught in flagranti: Involvement of hSuv3p helicase in RNA surveillance. *Nucleic Acids Research*, 38(1), 279-298.

89. Chujo, T., Ohira, T., Sakaguchi, Y., Goshima, N., Nomura, N., Nagao, A., et al. (2012). LRPPRC/SLIRP suppresses PNPase-mediated mRNA decay and promotes polyadenylation in human mitochondria. *Nucleic Acids Research*, 40(16), 8033-8047.

90. Deutscher MP (1993) Ribonuclease multiplicity, diversity, and complexity. *J Biol Chem*, 268, 13011-13014.

91. Leszczyniecka M, DeSalle R, Kang DC, Fisher PB (2004) The origin of polynucleotide phosphorylase domains. *Mol Phylogenet Evol*, 31(1), 123-130.

92. Chan I, Lebedeva IV, Su ZZ, Sarkar D, Valerie K, Fisher PB (2008) Progression elevated gene-3 promoter (PEG-Prom) confers cancer cell selectivity to human polynucleotide phosphorylase (hPNPaseold-35)-mediated growth suppression. *J Cell Physiol*, 215, 401-409.
93. Sokhi UK, Das SK, Dasgupta S, Emdad L, Shiang R, DeSalle R, Sarkar S, Fisher PB (2013). Human polynucleotide phosphorylase (hPNPaseold-35): should I eat you or not- that is the question? *Advances in Cancer Research*, 119, 161-190.
94. Giovanella BC, Stehlin JS, Williams LJ Jr (1974) Heterotransplantation of human malignant tumors in "nude" thymusless mice. II. Malignant tumors induced by injection of cell cultures derived from human solid tumors. *J Natl Cancer Inst*, 52(3), 921-30.
95. Huberman E, Heckman C, Langenbach R (1979) Stimulation of differentiated functions in human melanoma cells by tumor-promoting agents and dimethyl sulfoxide. *Cancer Res*, 39, 2618-2624.
96. Herlyn M, Thurin J, Balaban G, Bennicelli JL, Herlyn D, Elder DE, Bondi E, Guerry D, Nowell P, Clark WH, Koprowski H (1985) Characteristics of cultured human melanocytes isolated from different stages of tumor progression. *Cancer Res* 45: 5670-5676.
97. Balaban G, Herlyn M, Guerry D IV, Bartolo R, Koprowski H, Clark WH, Nowell PC (1984) Cytogenetics of human malignant melanoma and premalignant lesions. *Cancer Genet Cytogenet* 11: 429-439.
98. Li G, Schaidler H, Satyamoorthy K, Hanakawa Y, Hashimoto K, Herlyn M (2001) Downregulation of E-cadherin and Desmoglein 1 by autocrine hepatocyte growth factor during melanoma development. *Oncogene* 20(56):8125-35.
99. Jiang H, Lin J, Su ZZ, Herlyn M, Kerbel RS, Weissman BE, Welch DR, Fisher PB (1995) The melanoma differentiation-associated gene mda-6, which encodes the cyclin-dependent kinase inhibitor p21, is differentially expressed during growth, differentiation and progression in human melanoma cells. *Oncogene* 10(9):1855-64.
100. Dumur CI, Ladd AC, Wright HV, et al. (2009) Genes involved in radiation therapy response in head and neck cancers. *Laryngoscope* 119: 91-101.
101. Gentleman R, Carey V, Bates D, et al. (2004) Bioconductor: open software development for computational biology and bioinformatics. *Genome Biology* 5: R80.
102. Gatta V, Drago D, Fincati K, Valenti MT, Dalle Carbonare L, Sensi SL, Zatta P (2011) Microarray analysis on human neuroblastoma cells exposed to aluminum, $\beta(1-42)$ -amyloid or the $\beta(1-42)$ -amyloid aluminum complex. *PLoS One* 6(1): e15965.

103. Redmond LC, Dumur CI, Archer KJ, Haar JL, Lloyd JA (2008) Identification of erythroid-enriched gene expression in the mouse embryonic yolk sac using microdissected cells. *Developmental Dynamics* 237: 436-446.
104. Chen J, Bardes EE, Aronow BJ, Jegga AG (2009) ToppGene Suite for gene list enrichment analysis and candidate gene prioritization. *Nucleic Acids Res* 37: W305-W311.
105. Warde-Farley D, Donaldson SL, Comes O, et al. (2010) The GeneMANIA prediction server: biological network integration for gene prioritization and predicting gene function. *Nucleic Acids Research* 38: W214-W220.
106. Oliveros, J.C. (2007) VENNY. An interactive tool for comparing lists with Venn Diagrams. <http://bioinfogp.cnb.csic.es/tools/venny/index.html>.
107. Arsenijevic D, Onuma H, Pecqueur C, Raimbault S, Manning BS, Miroux B, Couplan E, Alves-Guerra MC, Gubern M, Surwit R, Bouillaud F, Richard D, Collins S, Ricquier D (2000) Disruption of the uncoupling protein-2 gene in mice reveals a role in immunity and reactive oxygen species production. *Nat Genet* 26(4): 435-439.
108. Vedrenne, V., Gowher, A., De Lonlay, P., Nitschke, P., Serre, V., Boddaert, N., et al. (2012). Mutation in PNPT1, which Encodes a Polyribonucleotide Nucleotidyltransferase, Impairs RNA Import into Mitochondria and Causes Respiratory-Chain Deficiency. *Am J Hum Genet*, 91(5):912-918.
109. Gottlieb E, Armour SM, Harris MH, Thompson CB (2003) Mitochondrial membrane potential regulates matrix configuration and cytochrome c release during apoptosis. *Cell Death Differ* 10(6): 709-717.
110. Huynh KM, Kim G, Kim D, et al. (2009) Gene expression analysis of terminal differentiation of human melanoma cells highlights global reductions in cell cycle-associated genes. *Gene* 433: 32-39.
111. Staudt MR, DePass AL, Sarkar D, Fisher PB (2009) Model cell culture system for defining the molecular and biochemical events mediating terminal differentiation of human melanoma cells. *J Cell Physiol* 218: 304-314.
112. Obaya MM, Mateyak MK, Obaya AJ, Adachi S, Sedivy JM (1997) Phenotypes of c-Myc-deficient rat fibroblasts isolated by targeted homologous recombination; Phenotypes of c-Myc-deficient rat fibroblasts isolated by targeted homologous recombination. *Cell Growth Differ* 8(10): 1039-1048.
113. Bush A, Mateyak M, Dugan K, Obaya A, Adachi S, Sedivy J, Cole M (1998) c-myc null cells misregulate cad and gadd45 but not other proposed c-Myc targets. *Genes Dev* 12(24): 3797-3802.

114. Yen TJ, Compton DA, et al. (1991) CENP-E, a novel human centromere-associated protein required for progression from metaphase to anaphase. *EMBO J* 10(5): 1245-1254.
115. Tanudji M, Shoemaker J, L'Italien L, Russell L, Chin G, Schebye XM (2004) Gene silencing of CENP-E by small interfering RNA in HeLa cells leads to missegregation of chromosomes after a mitotic delay. *Mol Biol Cell* 15(8): 3771-3781.
116. Scholzen T, Gerdes J (2000) The Ki-67 protein: From the known and the unknown. *J Cell Physiol* 182: 311-322.
117. Bullwinkel J, Baron-Lühr B, Lüdemann A, Wohlenberg C, Gerdes J, Scholzen T (2006) Ki-67 protein is associated with ribosomal RNA transcription in quiescent and proliferating cells. *J Cell Physiol* 206: 624-635.
118. Rahmzadeh R, Hüttmann G, Gerdes J, Scholzen T (2007) Chromophore-assisted light inactivation of pKi-67 leads to inhibition of ribosomal RNA synthesis. *Cell Prolif* 40(3): 422-430.
119. Anandasabapathy N, Ford GS, Bloom D, et al. (2003) GRAIL: An E3 Ubiquitin Ligase that Inhibits Cytokine Gene Transcription Is Expressed in Anergic CD4+ T Cells. *Immunity* 18: 535-547.
120. Hahm S, Mizuno TM, Wu TJ, et al. (1999) Targeted Deletion of the Vgf Gene Indicates that the Encoded Secretory Peptide Precursor Plays a Novel Role in the Regulation of Energy Balance. *Neuron* 23: 537-548.
121. Rizzi R, Bartolomucci A, Moles A, et al. (2008) The VGF-derived peptide TLQP-21: A new modulatory peptide for inflammatory pain. *Neurosci Lett* 441: 129-133.
122. Ferri G, Noli B, Brancia C, D'Amato F, Cocco C (2011) VGF: An inducible gene product, precursor of a diverse array of neuro-endocrine peptides and tissue-specific disease biomarkers. *J Chem Neuroanat* 42: 249-261.
123. Huaiyu Mi, Anushya Muruganujan and Paul D. Thomas (2012) PANTHER in 2013: modeling the evolution of gene function, and other gene attributes, in the context of phylogenetic trees. *Nucl Acids Res*, doi: 10.1093/nar/gks1118
124. Huaiyu Mi, Anushya Muruganujan, John T Casagrande and Paul D Thomas (2013) Large-scale gene function analysis with the PANTHER classification system. *Nature Protocols* 8, 1551 – 1566.
125. Hitomi J, Christofferson DE, Ng A, Yao J, Degterev A, Xavier RJ, Yuan J (2008) Identification of a molecular signaling network that regulates a cellular necrotic cell death pathway. *Cell*, 135(7):1311-23.

126. Huang da W, Sherman BT, Tan Q, Collins JR, Alvord WG, Roayaei J, Stephens R, Baseler MW, Lane HC, Lempicki RA (2007) The DAVID Gene Functional Classification Tool: a novel biological module-centric algorithm to functionally analyze large gene lists. *Genome Biol*, 8(9):R183.
127. Babenko O, Golubov A, Ilnytskyy Y, Kovalchuk I, Metz GA (2012) Genomic and epigenomic responses to chronic stress involve miRNA-mediated programming. *PLoS One*, 7(1), e29441.
128. Hanaoka M, Ito M, Droma Y, Ushiki A, Kitaguchi Y, Yasuo M, Kubo K (2012) Comparison of gene expression profiling between lung fibrotic and emphysematous tissues sampled from patients with combined pulmonary fibrosis and emphysema. *Fibrogenesis Tissue Repair*, 5(1):17.
129. Hellman U, Mörner S, Engström-Laurent A, Samuel JL, Waldenström A (2010) Temporal correlation between transcriptional changes and increased synthesis of hyaluronan in experimental cardiac hypertrophy. *Genomics*, 96(2), 73-81.
130. Malaney P, Pathak RR, Xue B, Uversky VN, Davé V (2013) Intrinsic Disorder in PTEN and its Interactome Confers Structural Plasticity and Functional Versatility. *Sci Rep*, 3:2035.
131. Goldman M, Craft B, Swatloski T, Ellrott K, Cline M, Diekhans M, Ma S, Wilks C, Stuart J, Haussler D, Zhu J (2013) The UCSC Cancer Genomics Browser: update 2013. *Nucleic Acids Res*. 41:D949-54.
132. Cabibbo A, Consalez GG, Sardella M, Sitia R, Rubartelli A. (1998) Changes in gene expression during the growth arrest of HepG2 hepatoma cells induced by reducing agents or TGFbeta1. *Oncogene*. 16 (22):2935-43.
133. Harper JW, Adami GR, Wei N, Keyomarsi K, Elledge SJ (1993). "The p21 Cdk-interacting protein Cip1 is a potent inhibitor of G1 cyclin-dependent kinases". *Cell* **75** (4): 805–16.
134. McGovern SL, Qi Y, Pusztai L, Symmans WF, Buchholz TA. (2012) Centromere protein-A, an essential centromere protein, is a prognostic marker for relapse in estrogen receptor-positive breast cancer. *Breast Cancer Res*. 14(3):R72.
135. Toh SH, Prathipati P, Motakis E, Kwoh CK, Yenamandra SP, Kuznetsov VA. (2011) A robust tool for discriminative analysis and feature selection in paired samples impacts the identification of the genes essential for reprogramming lung tissue to adenocarcinoma. *BMC Genomics*. 12 Suppl 3:S24.
136. Moncho-Amor V, Ibañez de Cáceres I, Bandres E, Martínez-Poveda B, Orgaz JL, Sánchez-Pérez I, Zazo S, Rovira A, Albanell J, Jiménez B, Rojo F, Belda-Iniesta C,

García-Foncillas J, Perona R. (2011) DUSP1/MKP1 promotes angiogenesis, invasion and metastasis in non-small-cell lung cancer. *Oncogene*. 30(6):668-78.

137. Flanagan JM, Funes JM, Henderson S, Wild L, Carey N, Boshoff C. (2009) Genomics screen in transformed stem cells reveals RNASEH2A, PPAP2C, and ADARB1 as putative anticancer drug targets. *Mol Cancer Ther*. 8(1):249-60.

138. Shaikhibrahim Z, Lindstrot A, Ochsenfahrt J, Fuchs K, Wernert N. (2013) Epigenetics-related genes in prostate cancer: expression profile in prostate cancer tissues, androgen-sensitive and -insensitive cell lines. *Int J Mol Med*. 31(1):21-5.

139. Valles I, Pajares MJ, Segura V, Guruceaga E, Gomez-Roman J, Blanco D, Tamura A, Montuenga LM, Pio R. (2012) Identification of novel deregulated RNA metabolism-related genes in non-small cell lung cancer. *PLoS One*. 7(8):e42086.

140. Rutkowski MJ, Sughrue ME, Kane AJ, Kim JM, Bloch O, Parsa AT. (2011) Epidermal growth factor module-containing mucin-like receptor 2 is a newly identified adhesion G protein-coupled receptor associated with poor overall survival and an invasive phenotype in glioblastoma. *J Neurooncol*. 105(2):165-71.

141. Deutscher MP. 1993. Promiscuous exoribonucleases of escherichia coli. *J Bacteriol* 175(15): 4577-4583.

142. Deutscher MP, Marshall GT, Cudny H. 1988. RNase PH: An escherichia coli phosphate-dependent nuclease distinct from polynucleotide phosphorylase. *Proc Natl Acad Sci U S A* 85(13): 4710-4714.

143. Jain C. 2012. Novel role for RNase PH in the degradation of structured RNA. *J Bacteriol* 194(15): 3883-90.

144. dos Reis M, Inoue J, Hasegawa M, Asher RJ, Donoghue PC, Yang Z. 2012. Phylogenomic datasets provide both precision and accuracy in estimating the timescale of placental mammal phylogeny. *Proc Biol Sci* 279(1742): 3491-3500.

145. Murphy WJ, Eizirik E, Johnson WE, Zhang YP, Ryder OA, O'Brien SJ. 2001. Molecular phylogenetics and the origins of placental mammals. *Nature* 409(6820): 614-618.

146. O'Leary MA, Bloch JI, Flynn JJ, et al. (23 co-authors). 2013. The placental mammal ancestor and the post-K-Pg radiation of placentals. *Science* 339(6120): 662-667.

147. Pentony MM, Winters P, Penfold-Brown D, Drew K, Narechania A, DeSalle R, Bonneau R, Purugganan MD. 2012. The plant proteome folding project: Structure and positive selection in plant protein families. *Genome Biology and Evolution* 4(3): 360-371.

148. Hughes AL. 2008. The origin of adaptive phenotypes. *Proc Natl Acad Sci U S A* 105(36): 13193-13194
149. Dean AM and Thornton JW. 2007. Mechanistic approaches to the study of evolution: The functional synthesis. *Nat Rev Genet* 8(9): 675-688.
150. Nilsson J, Grahn M, Wright AP. 2011. Proteome-wide evidence for enhanced positive Darwinian selection within intrinsically disordered regions in proteins. *Genome Biology* 12(7): R65.
151. Ridout KE, Dixon CJ, Filatov DA. 2010. Positive selection differs between protein secondary structure elements in drosophila. *Genome Biology and Evolution* 2: 166-179.
152. Abascal F, Zardoya R, Telford MJ. 2010. TranslatorX: Multiple alignment of nucleotide sequences guided by amino acid translations. *Nucleic Acids Research* 38: W7-W13.
153. Huelsenbeck JP and Ronquist F. 2001. MRBAYES: Bayesian inference of phylogenetic trees; bioinformatics. *Bioinformatics* 17(8): 754-755.
154. Stamatakis A, Hoover P, Rougemont J. 2008. A rapid bootstrap algorithm for the RAxML web servers. *Systematic Biology* 57(5): 758-771.
155. Ronquist F and Huelsenbeck JP. 2003. MrBayes 3: Bayesian phylogenetic inference under mixed models; bioinformatics. *Bioinformatics* 19(12): 1572-1574.
156. Pond SL, Frost SD, Muse SV. 2005. HyPhy: Hypothesis testing using phylogenies. *Bioinformatics* 21(5): 676-679.
157. Delport W, Poon AF, Frost SD, Kosakovsky Pond SL. 2010. Datamonkey 2010: A suite of phylogenetic analysis tools for evolutionary biology. *Bioinformatics* 26(19): 2455-2457.
158. Kosakovsky Pond SL, Murrell B, Fourment M, Frost SD, Delport W, Scheffler K. 2011. A random effects branch-site model for detecting episodic diversifying selection. *Molecular Biology and Evolution* 28(11): 3033-3043.
159. Murrell B, Wertheim JO, Moola S, Weighill T, Scheffler K, Kosakovsky Pond SL. 2012. Detecting individual sites subject to episodic diversifying selection. *PLoS Genetics* 8(7): e1002764.
160. Wheeler WC. 1990. Nucleic Acid Sequence Phylogeny and Random Outgroups. *Cladistics* 6(4): 363-367.

161. von Ameln, S., Wang, G., Boulouiz, R., Rutherford, M. A., Smith, G. M., Li, Y., et al. (2012). Mutation in PNPT1, Encoding Mitochondrial-RNA-Import Protein PNPase, Causes Hereditary Hearing Loss. *Am J Hum Genet*, 91(5):919-927.
162. Lorentzen E and Conti E. 2005. Structural basis of 3' end RNA recognition and exoribonucleolytic cleavage by an exosome RNase PH core. *Molecular cell* 20(3): 473-481.
163. Bonneau F, Basquin J, Ebert J, Lorentzen E, Conti E. 2009. The yeast exosome functions as a macromolecular cage to channel RNA substrates for degradation. *Cell* 139(3): 547-559.
164. Almeida, F.C., Leszczyniecka, M., Fisher, P.B., & DeSalle R. (2008). Examining ancient inter-domain horizontal gene transfer. *Evol Bioinform* 4, 109-119.
165. Brown CJ, Takayama S, Campen AM, Vise P, Marshall TW, Oldfield CJ, Williams CJ, Dunker AK. 2002. Evolutionary rate heterogeneity in proteins with long disordered regions. *J Mol Evol* 55(1): 104-110.
166. Mittag T, Kay LE, Forman-Kay JD. 2010. Protein dynamics and conformational disorder in molecular recognition. *Journal of Molecular Recognition* 23(2): 105-116.
167. Zhang X, Wang Z, Kang Y, Li X, Ma X, Ma L. (2013) MCAM expression is associated with poor prognosis in non-small cell lung cancer. *Clin Transl Oncol*.
168. Wu Z, Wu Z, Li J, Yang X, Wang Y, Yu Y, Ye J, Xu C, Qin W, Zhang Z. (2012) MCAM is a novel metastasis marker and regulates spreading, apoptosis and invasion of ovarian cancer cells. *Tumour Biol*. 33(5):1619-28.
169. Wang HF, Chen H, Ma MW, Wang JA, Tang TT, Ni LS, Yu JL, Li YZ, Bai BX. (2013) miR-573 regulates melanoma progression by targeting the melanoma cell adhesion molecule. *Oncol Rep*. 30(1):520-6.
170. Matsumoto T, Kawashima Y, Nagashio R, Kageyama T, Kodera Y, Jiang SX, Okayasu I, Kameya T, Sato Y. (2009) A new possible lung cancer marker: VGF detection from the conditioned medium of pulmonary large cell neuroendocrine carcinoma-derived cells using secretome analysis. *Int J Biol Markers*. 24(4):282-5.

VITA

Upneet Kaur Sokhi

PHONE: (804) 332-7843 · EMAIL: upneet8@gmail.com, sokhiuk@vcu.edu;

Personal information

Date of Birth: November 17th 1980

Place of Birth: Jamshedpur

Citizenship: India

Sex: Female

Education

Ph.D. Virginia Commonwealth University, Richmond, VA, December 2013.
Molecular Biology and Genetics

M.Sc. Bangalore University, Bengaluru, Karantaka, India, May, 2006.
Biotechnology

B.Sc. Bangalore University, Bengaluru, Karantaka, India, May, 2004.
Biotechnology

Awards and Honors

Roscoe D. Hughes Fellowship for an outstanding graduate student, 2011, Department of Human and Molecular Genetics, VCU.

Certificate for academic achievement awarded by The Honor Society of Phi Kappa Phi, 2008.

Publications

1. Global changes in gene expression induced by human polynucleotide phosphorylase (*hPNPase^{old-35}*). **Sokhi UK**, Bacolod MD, Emdad L, Das SK, Dumur CI, Miles MF, Sarkar D, Fisher PB. (In preparation)
2. Sequential adaptive refinement of PNPases by natural selection in the vertebrate lineage leading to mammals. **Sokhi UK**, DeSalle R, Bacolod MD, Das SK, Dasgupta S, Sarkar D, Fisher PB. (Submitted to Molecular Phylogenetics and Evolution)
3. Identification of genes potentially regulated by human polynucleotide phosphorylase (*hPNPase^{old-35}*) using melanoma as a model. **Sokhi UK**, Bacolod MD, Dasgupta S, Emdad L, Das SK, Dumur CI, Miles MF, Sarkar D, Fisher PB. PLoS One. 2013;8(10):e76284.
4. Combining Histone deacetylase inhibitors with MDA-7/IL-24 enhances killing of renal carcinoma cells. Hamed H, Das SK, **Sokhi UK**, Park M, Cruickshanks N, Archer K, Ogretmen B, Grant S, Sarkar S, Fisher PB, Dent P. Cancer Biology and Therapy. 2013;14(11).
5. Human polynucleotide phosphorylase (*hPNPase^{old-35}*): should I eat you or not- that is the question? **Sokhi UK**, Das SK, Dasgupta S, Emdad L, Shiang R, DeSalle R, Sarkar D, Fisher PB. Advances in Cancer Research. 2013;19:161-90.
6. Raf kinase inhibitor RKIP inhibits MDA-9/syntenin-mediated metastasis in melanoma. Das SK, Bhutia SK, **Sokhi UK**, Azab B, Su ZZ, Boukerche H, Anwar T, Moen EL, Chatterjee D, Pellecchia M, Sarkar D, Fisher PB. Cancer Res. 2012;72(23):6217-26.
7. SH3GL2 is frequently deleted in non-small cell lung cancer and downregulates tumor growth by modulating EGFR signaling. Dasgupta S, Jang JS, Shao C, Mukhopadhyay ND, **Sokhi UK**, Das SK, Brait M, Talbot C, Yung RC, Begum S, Westra WH, Hoque MO, Yang P, Yi JE, Lam S, Gazdar AF, Fisher PB, Jen J, Sidransky D. J Mol Med (Berl). 2013;91(3):381-93
8. Selected approaches for rational drug design and high throughput screening to identify anti-cancer molecules. Hedvat M, Emdad L, Das SK, Kim K, Dasgupta S, Thomas S, Hu B, Zhu S, Dash R, Quinn BA, Oyesanya RA, Kegelman TP, **Sokhi UK**, Sarkar S, Erdogan E, Menezes ME, Bhoopathi P, Wang XY, Pomper MG, Wei J, Wu B, Stebbins JL, Diaz PW, Reed JC, Pellecchia M, Sarkar D, Fisher PB. Anticancer Agents Med Chem. 2012;12(9):1143-55.
9. MDA-9/syntenin: a positive gatekeeper of melanoma metastasis. Das SK, Bhutia SK, Kegelman TP, Peachy L, Oyesanya RA, Dasgupta S, **Sokhi UK**, Azab B, Dash R, Quinn BA, Kim K, Barral PM, Su ZZ, Boukerche H, Sarkar D, Fisher PB. Front Biosci. 2012;17:1-15.
10. Developing an effective gene therapy for prostate cancer: New technologies with potential to translate from the laboratory into the clinic. Dash R, Azab B, Shen XN, **Sokhi**

UK, Sarkar S, Su ZZ, Wang XY, Claudio PP, Dent P, Dmitriev IP, Curiel DT, Grant S, Sarkar D, Fisher PB. *Discov Med*. 2011;11(56):46-56.

11. Human polynucleotide phosphorylase (hPNPase(old-35)): an evolutionary conserved gene with an expanding repertoire of RNA degradation functions. Das SK, Bhutia SK, **Sokhi UK**, Dash R, Azab B, Sarkar D, Fisher PB. *Oncogene*. 2011;30(15):1733-43.
12. Melanoma differentiation associated gene-7/interleukin-24 potently induces apoptosis in human myeloid leukemia cells through a process regulated by endoplasmic reticulum stress. Rahmani M, Mayo M, Dash R, **Sokhi UK**, Dmitriev IP, Sarkar D, Dent P, Curiel DT, Fisher PB, Grant S. *Mol Pharmacol*. 2010;78(6):1096-104.
13. Human polynucleotide phosphorylase selectively and preferentially degrades microRNA-221 in human melanoma cells. Das SK, **Sokhi UK**, Bhutia SK, Azab B, Su ZZ, Sarkar D, Fisher PB. *Proc Natl Acad Sci U S A*. 2010;107(26):11948-53.